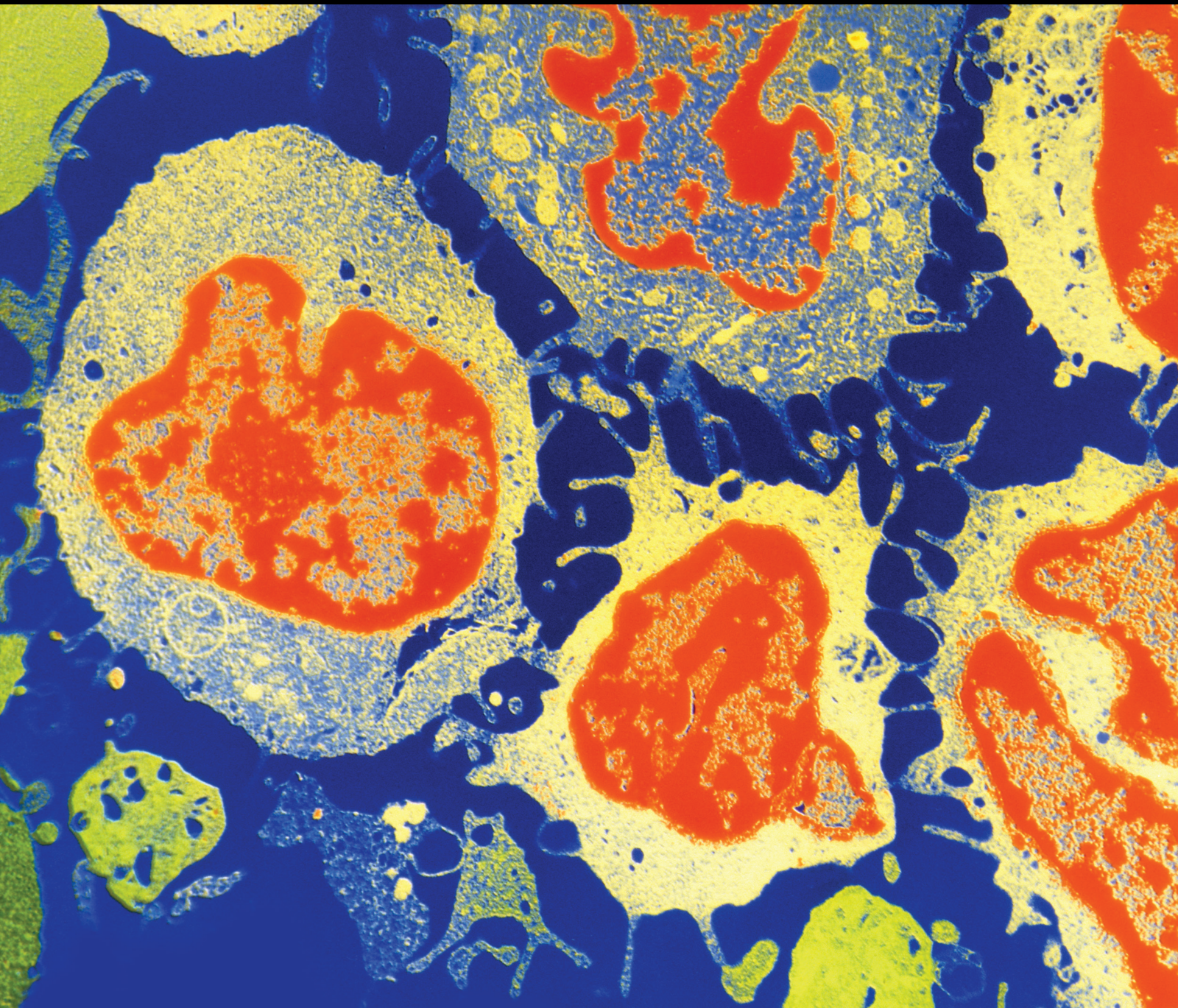# The Role of Lipid Metabolism in Tumor Progression

Lead Guest Editor: Yingkun Xu
Guest Editors: Gaocai Li, Guangzhen Wu, and Ningke Ruan

The Role of Lipid Metabolism in Tumor Progression

The Role of Lipid Metabolism in Tumor Progression

Lead Guest Editor: Yingkun Xu
Guest Editors: Gaocai Li, Guangzhen Wu, and Ningke Ruan

Contents

The Regulatory Role of Lipid Metabolism in Endometrial Cancer
Shuyang Zhang 🆔 and Xingyu Han
Review Article (6 pages), Article ID 6458877, Volume 2022 (2022)

Research Article

Regulatory Role of Fatty Acid Metabolism-Related Long Noncoding RNA in Prostate Cancer: A Computational Biology Study Analysis

Yutao Wang ⓘ, Hao Su ⓘ, Yi Lu ⓘ, and Hongjun Li ⓘ

Department of Urology, Chinese Academy of Medical Sciences, Peking Union Medical College,
Peking Union Medical College Hospital, Beijing, China

Correspondence should be addressed to Hongjun Li; lihongjun@pumch.cn

In elderly men, prostate cancer is a leading cause of death. Tumor cells require more energy to progress than normal cells, and this energy is mainly dependent on the large amount of ATP support generated by lipid metabolism. Therefore, in this study, we focused on long noncoding RNAs related to lipid metabolism in prostate cancer to discover the biological mechanisms of lipid metabolism regulation. The TCGA-PRAD cohort was used in this study for computational biology analysis. In lipid metabolism biological pathways, 1959 long noncoding RNAs were identified by Pearson correlation coefficient analysis of protein-coding genes, then univariate regression with P values fewer than 0.05. We further identified 784 lncRNAs that were lipid metabolism-related lncRNAs considered to have prognostic value for disease-free survival. Subsequently, we constructed two lncRNA expression patterns of lipid metabolism based on these lncRNAs by nonnegative matrix dimensionality reduction. These two expression patterns showed significant differences in disease-free survival curves for those diagnosed with prostate cancer. We found significant differences in mRNA surveillance pathway and mRNA processing between C1 and C2 groups based on the WGCNA method to explore the biological characteristics of these two expression patterns. Finally, we constructed a disease-free survival (PFS) model based on these lncRNAs. The results identified lncRNAs involved in lipid metabolism and revealed differences in their expression patterns. Additionally, the results offer candidate ideas and approaches concerning the precision treatment of prostate cancer by studying lipid metabolism by candidate long noncoding RNAs.

1. Introduction

1.1. Relationship between Lipid Metabolism and Prostate Cancer. The American Cancer Society estimates that American men are most likely to suffer from prostate cancer [1] (PCa) in 2022, making up 27% of cancer diagnoses among men. Moreover, the available data indicate that the highest prostate cancer incidence rates are in Europe and the United States, whereas they are lower in Asia. With the development of PSA detection technology, the incidence rate of prostate cancer is declining or stable in nature [2]. In lipid metabolism, lipids are synthesized and degraded inside cells. It has been shown in many studies that lipid metabolism is closely related to the progression of prostate cancer. The management of prostate cancer based on lipid metabolism

has become a research hotspot [3, 4]. Abnormal metabolism is a sign of cancer, and tumorigenesis depends on the reprogramming of cell metabolism. Because cancer cells require nutrients from malnourished environments to meet their energy needs and other carcinogenic abilities5, like most other tumors, PCa also undergoes metabolic reprogramming. Prostate cancer cells can increase de novo lipogenesis and fatty acid oxidation by up-regulating androgen receptor (AR)-regulated lipogenic enzymes [5]. Several transcription factors regulate lipogenesis, including sterol regulatory element-binding proteins (SREBPs). AR-mediated interaction between androgens and SREBPs can improve the activation and expression of SREBPs [6]. At the same time, SREBPs can also trigger the AR pathway by activating AR gene expression. It appears that there is

a correlation between the two pathways. Moreover, some genetic abnormalities related to PCa also strengthen lipid metabolism. Some studies have shown that the loss or inhibition of p53 activity can reduce androgen receptor-mediated signal transduction in PCa cell lines and inhibit the progression of prostate cancer [7]. As a consequence of the loss of the tumor suppressor gene PTEN, prostate cancer cells undergo metabolic reprogramming, resulting in fatty acid synthase (FAS) overexpression, the production of fatty acids and cholesterol, and the proliferation of prostate cancer cells that are malignant. [8]. Some studies have shown that the overexpression of oncogene MYC can lead to the imbalance of lipid metabolism, induce the expression of fatty acid synthase, and then promote the progression of prostate cancer [9, 10]. Therefore, lipid metabolism plays a vital function in the formation and spread of prostate cancer.

A long noncoding RNA (lncRNA) is a transcript longer than 200 nucleotides with little or no protein-coding potential. There are many processes occurring within cells controlled by lncRNAs, including cell proliferation, metastasis, differentiation, and apoptosis [11]. Localization determines whether lncRNAs are nuclear or cytoplasmic. Nuclear lncRNAs could modulate gene transcription. As a result of chromatin structure regulation, cytoplasmic lncRNAs could regulate mRNA through the interaction between RNAs [12]. SREBPs are crucial in regulating lipid homeostasis by modulating cholesterol and fatty acid metabolism. The SREBP family consists of three subtypes: SREBP1a, SREBP1c, and SREBP2. In many studies, lncRNAs have been shown to contribute to lipid metabolism affecting the biosynthesis of cholesterol and triglycerides, lipid uptake and efflux, cholesterol transport, and other pathways [13]. Some studies have shown that the overexpression of LncARSR, a recently discovered lncRNA, promotes liver cholesterol biosynthesis by increasing the expression of 3-hydroxy-3-methyl-glutaryl coenzyme A reductase (HMGCR), the rate-limiting enzyme for cholesterol synthesis. A possible mechanism by which LncARSR increases HMGCR15 expression is through SREBP-2, the primary transcription factor of HMGCR [14]. Another study identified that a new lncRNA, lncHR1, was negatively related to the expression of SREBP-1c. LncHR1 overexpression inhibits SREBP-1c and fatty acid synthase expression in hepatocytes, inhibiting triglyceride and lipid droplet accumulation caused by oleic acid [15]. In cancer research, nuclear paraspeckle assembly transcript 1 (NEAT1), a nuclear-enriched lncRNA, appears to be overexpressed in various cancerous tissues, and the dysregulation of NEAT1 contributed to cancer progression and metastasis [16]. It has been shown that NEAT1 regulates lipid metabolism via adipose triglyceride lipase (the main enzyme involved in lipolysis), thereby promoting hepatocellular carcinoma [17]. LncRNA MALAT1 (metastasis associated with lung adenocarcinoma transcript 1) has been related to many diseases. It has been found that MALAT1 can induce liver lipid accumulation and insulin resistance via increasing SREBP-1c and target gene expression [18]. Besides regulating key transcription factors for lipid metabolism, lncRNAs can also do so in multiple ways. HULC is a lncRNA that is upregulated in hepatocellular carcinoma. Studies have shown that in hepatoma cells, HULC activates the promoter of Acyl-CoA synthetase long-chain family member1 (ACSL1) by upregulating the transcription factor PPARA, thus regulating lipid metabolism and promoting the proliferation of hepatoma cells [19]. LNMICC (a kind of lncRNA) has been found to reprogramme fatty acid metabolism, recruit nuclear factor NPM1 to FABP5 promoter, and promote cervical cancer lymph node metastasis [20]. Therefore, it appears that lncRNAs regulate lipid metabolism in a major way.

With the development of computational biology, it is necessary to use bioinformatics technology to study the progress of cancer. At present, there are a variety of methods and means for the research of computational biology [21, 22]. Many scholars construct prognostic models of multiple genes for prognostic analysis and screening of prognostic biomarkers. Bioinformatics studies demonstrated that lncRNAs contribute to the progression of many cancers. Cell processes can be influenced by the imbalance of lncRNAs, including proliferation, apoptosis, angiogenesis, and tumor cell metastasis. LncRNAs can also affect the biological progress of cancer through chromatin remodeling and chromatin interaction [23, 24]. Bioinformatics software has been used to investigate prostate cancer through the regulatory networks of lncRNA, miRNA, and mRNA, as well as to examine the genes and pathways involved in PCa pathogenesis [25]. Some studies have established a model that relies on lipid metabolism-related lncRNAs to predict breast cancer patients' survival rates and prognoses, a crucial tool in assessing survival for breast cancer patients [26]. Some studies have developed a contrasting endogenous RNA network (ceRNA) concerning fatty acid metabolism in colorectal cancer (CRC) using bioinformatics methods, identified the lncRNA related to fatty acid metabolism in the ceRNA network pertaining to survival, and constructed a nomogram of the outlook for patients with colorectal cancer [27]. The study was conducted using bioinformatics methods to identify lncRNAs related to lipid metabolism in prostate cancer and constructed a prognostic model of prostate cancer, which is of great significance in guiding prostate cancer management.

2. Materials and Method

2.1. Data Collection. Transcriptome expression data and clinical information following data for prostate adenocarcinoma in The Cancer Genome Atlas (TCGA) were obtained from the GDC Data Portal (https://portal.gdc.cancer.gov/). TPM data from TCGA-PRAD were used in this analysis. Due to the smaller number of overall survival adverse events samples, we used disease-free survival status as the follow-up endpoint of the investigation. The prostate samples totaled 552 in total, including 500 tumor samples and 52 adjacent carcinoma samples.

2.2. Fatty Acid Metabolism Dataset. We downloaded the fatty acid metabolism dataset from the GSEA database (GSEA (https://gsea-msigdb.org)). 42 protein-encoding

genes were identified as part of the fatty acid metabolism pathway. The long noncoding RNAs related to the fatty acid metabolism pathway were determined by a Pearson coefficient of more than 0.4.

2.3. Univariate Cox Regression.

Cox models can be used to examine the effect of several elements on survival time when survival outcome and survival time are the indicators of dependency simultaneously. Data with censored survival times can also be examined without needing the estimation of survival distributions. As a result of these excellent properties, long noncoding RNA survival assessment was conducted using multivariate COX regression.

2.4. Fatty Acid Metabolism-Related lncRNAs Expression Patterns.

We performed nonnegative matrix dimensionality reduction (NMF) on the relevant human coding genes for the long noncoding RNAs identified previously. Before NMF analysis, we preprocessed the data. First, candidate genes with an absolute median (MAD) of less than 0.5 were excluded. Genetic association of all candidates relating to overall survival was then assessed using Cox regression. The "survival" package was applied for analysis. Finally, the absolute median was more significant than 0.5; genes of 0.05 were used for nonnegative matrix factorization. This was performed through the "NMF" [5] R package.

2.5. WGCNA Analysis.

An analysis of coexpression was conducted using WGCNA to develop a model related to C1 and C2 models. In general, gene sets with the same expression pattern tend to have similar expression profiles, and these functionally equivalent genes constitute intricately linked coexpression networks. Therefore, we determined the coexpression network between the expression patterns of long noncoding RNAs related to different fatty acid metabolism using coexpression identification on TCGA-PRAD. We first performed a sample cluster analysis on the TCGA-PRAD cohort. The weighted coexpression network was created with the R language WGCNA package [28]. To calculate the soft threshold for the upcoming network construction, the most appropriate weighted parameters of the adjacent functions were calculated using pickSoft-Threshold. Based on the hierarchical clustering of the dissimilarity measure of the topological overlap matrix, we constructed the weighted adjacency matrix as well as the associated gene modules (TOM) (1-TOM) [29]. Finally, the Pearson correlation coefficient was calculated between different coexpression modules and cluster categories.

2.6. Functional Enrichment Analysis.

To explain biological differences between different fatty acid metabolism-related long noncoding RNA expression patterns, we performed functional analysis on protein-coding genes in the coexpression module. Functional enrichment analysis, including gene ontology (GO) analysis and KEGG pathway enrichment of the coexpression genes, was carried out with the "clusterProfiler" [30] and "pathview" packages [31].

2.7. Immune-Inflammatory Response.

Multiple gene sets able to represent the immune response were tested for their role in the immune microenvironment of prostate cancer involving long noncoding RNA (lncRNA). These gene sets included significant histocompatibility complex class II (MHC-II), lymphocyte-specific kinase (LCK), hematopoietic cell kinase (HCK), immunoglobulin G (IgG), signal transducer and activator of transcription 1 (STAT1), costimulatory molecule (B7-CD28), interferon, and TNF gene sets [32]. An algorithmic tool called ESTIMATE (using expression data to estimate stromal and immune cells in malignant tumor tissue) was used to analyze tumor purity [33].

3. Results

3.1. Research Technical Route.

The research route of this paper is uploaded in Figure 1. There are primarily three aspects to the research. In the first aspect, noncoding RNAs associated with fatty acid metabolism are identified in prostate cancer. The second part constructs the prognosis model of long noncoding RNA related to fatty acid metabolism in prostate cancer. The third aspect looks at different expression patterns of two long noncoding RNAs related to fatty acid metabolism, and the biological differences between them were explored.

3.2. Identification of Fatty Acid Metabolism-Related Long Noncoding RNAs.

According to the $P < 0.01$, Cor < 0.4, we identified 1,959 long noncoding RNAs (Figure 2(a)). We then evaluated the prognostic value of the above 1,959 lncRNAs independently, with disease-free survival status as the end point of follow-up. In univariate Cox regression, we screened 784 lncRNAs associated with fatty acid metabolism. A univariate Cox regression with a P 0.05 was used as the screening criterion. The hazard ratios and confidence intervals for the most significant 42 lncRNAs are shown in Figure 2(b). Subsequently, we performed a cluster analysis based on the above 42 long noncoding RNAs related to fatty acid metabolism. Our clustering results revealed two types of expression patterns for long noncoding RNA (Figure 2(c)). In the survival follow-up curve of the disease-free survival state, patients with two different lncRNA expression patterns displayed significant prognostic disparities, $P < 0.001$ (Figure 2(d)).

3.3. Identification of Biological Differences between Different Fatty Acid Metabolisms Based on Long Noncoding RNA Expression Patterns.

Using lncRNAs involved in fatty acid metabolism, we identified two different expression patterns. To determine the biological differences between the two expression patterns, we constructed coding gene coexpression modules of the two expression patterns using the WGCNA method. Protein-coding genes and clinical samples of prostate cancer were included in the WGCNA entry file, and samples with similar expression patterns were included in the subsequent analysis based on omics cluster analysis. According to the cut-off value of 80000, 492

Part 1:
Determination lipid metabolism related lncRNAs

TCGA-PRAD

Lipid metabolism genes

Pearson coefficient Cor >0.4, p < 0.01

1959 lipid metabolism related lncRNAs

Overall and Disease free survival analysis

Part 2:
Conduction lipid metabolism related lncRNAs prognostic model

784 lncRNAs determined by
Univariate Cox regression analysis by P < 0.05

Lasso regression analysis

Prognostic model

Part 3:
Two lipid metabolism related lncRNAs expression patterns

42 lncRNAs determined by
Univariate Cox regression analysis by P < 0.001

NMF cluster analysis

WGCNA analysis   Function of enrichment

Immune microenvironment analysis

FIGURE 1: Flowchart.

prostate cancer samples with similar expression patterns were obtained. We set the β value to 5, the gene in the minimum module to 30, and finally obtained 14 coexpression modules (Figures 3(a) and 3(b)). We found that the long-chain noncoding trait group of C2 fatty acid metabolism was most strongly associated with the purple module (Figure 3(b); Cor = 0.40). The purple module contained 49 genes. The genes with a correlation greater than 0.4 with the C2 group in the purple module were functionally enriched, and the findings indicated their involvement in RNA splicing, mRNA processing, regulation of RNA splicing, and mRNA surveillance pathway and other biological processes (Figure 4).

3.4. To Construct a Prognostic Model of Prostate Cancer Disease-Free Survival Based on Long Noncoding RNA Related to Fatty Acid Metabolism. A training set was randomly selected from the TCGA-PRAD cohort, followed by a validation set. The samples were sorted according to their IDs,

and random numbers were assigned using SPSS to each to enable categorization. Using Lasso regression, we constructed a prognostic model for long noncoding RNA related to fatty acid metabolism. We took the long noncoding RNA related to fatty acid metabolism as the entry data. Based on the disease-free survival rate as clinical follow-up data, regression analysis was performed. With so many genes, it is difficult to conduct clinical identification. The R package glmnet was used to perform Lasso regression evaluation to limit the scope of long noncoding RNA and maintain high accuracy. Finally, we constructed a 9-gene prognostic risk model. RiskScore = 0.71^{*} expAC106820 + 0.20^{*} expAL359881 + 0.12^{*} expAL645608 − 1.55^{*} expAC026780 + 0.79^{*} expLINC01094 + 0.20^{*} expAC068338 − 0.62^{*} expAC008966 − 0.62^{*} expAL512353 + 0.16^{*} expAL360181. We evaluated the RiskScore according to the TPM value of long noncoding RNA and the corresponding risk coefficient. We obtained the sample distribution by RiskScore, as shown in Figure 5(a). There is a substantial difference between adverse

(a)

(b)

(c)

(d)

Figure 2: Determination of two fatty acid metabolism lncRNAs expression patterns. (a) Fatty acid metabolism-related lncRNAs. (b) 42 fatty acid metabolisms related lncRNAs with $P < 0.001$. (c) Two fatty acid metabolism lncRNAs expression patterns. (d) Disease-free survival analysis between deference lncRNAs expression patterns.

Cluster Dendrogram

(a)

Module−trait relationships

(b)
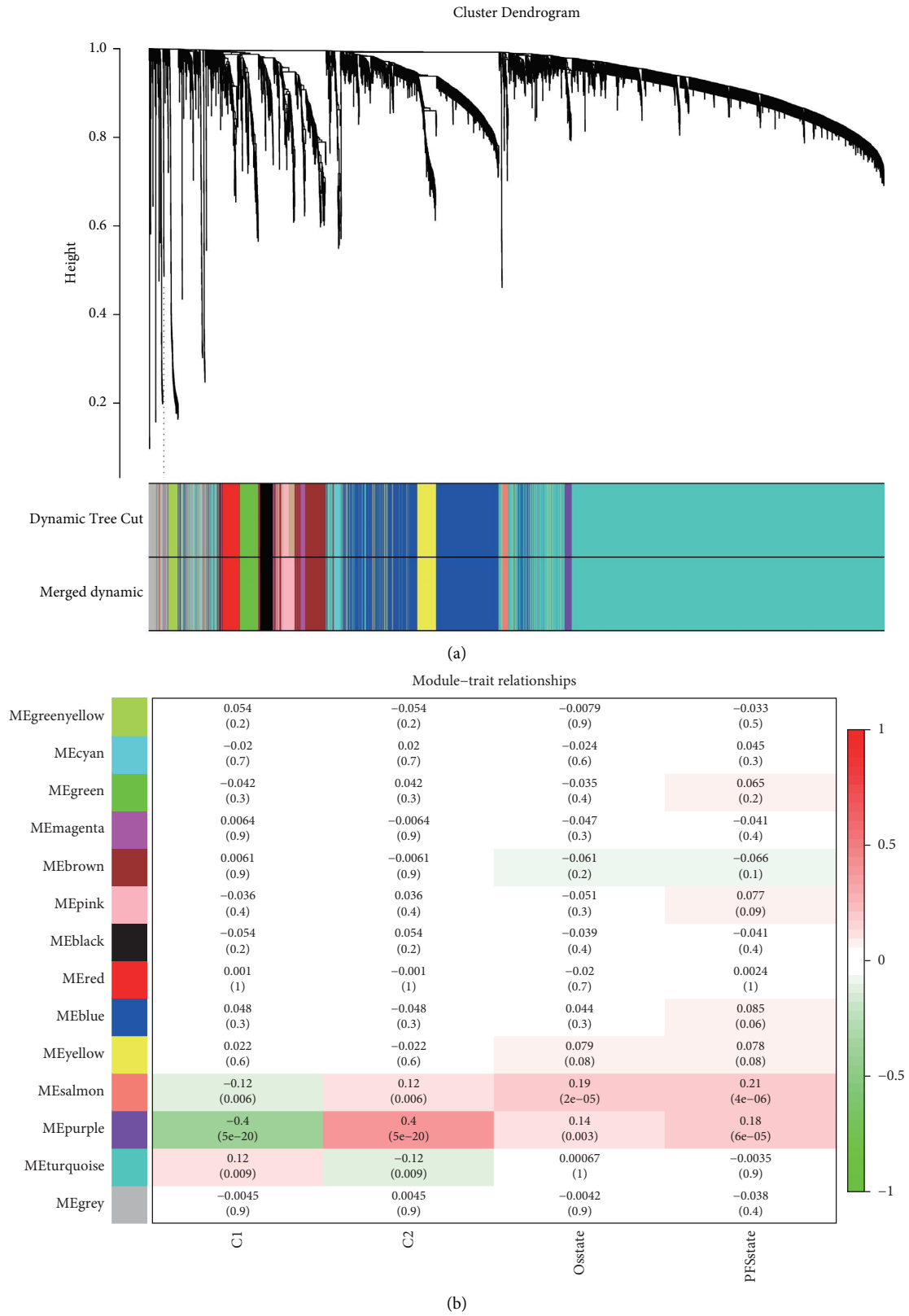
FIGURE 3: WGCNA analysis. (a) Cluster dendrogram. (b) WGCNA coexpression modules related to the C2 cluster, and the correlation coefficient between the purple module and the C2 cluster is 0.40.
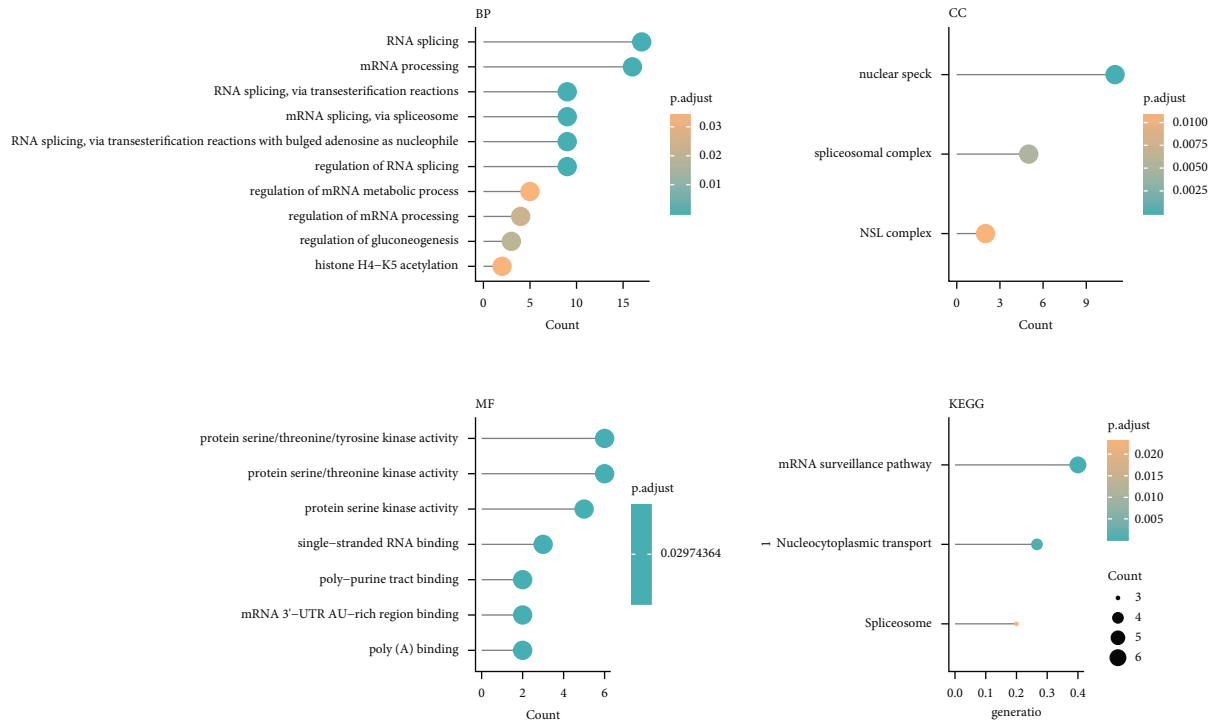
FIGURE 4: The GO and KEGG analysis of the purple coexpression protein-coding genes.

event samples with low and high RiskScores, indicating that adverse event samples with high RiskScores may be at increased risk. The KM curve is shown in Figure 5(b) after we separated RiskScores into low- and high-risk groups. There was a significant survival difference between high- and low-risk scores ($P < 0.001$). Immediately after, we used ROC to evaluate RiskScores. We analyzed the 1.3- and 5-year predictive classification efficiency, and the model is shown in Figure 5(c), with an AUC area of 0.758 of 5 years, 0.792 of 3 years, and 0.776 of 1 year (Figure 5(c)).

3.5. Evaluation of Prognostic Models for Long Noncoding RNAs. In addition, we analyzed the training and test datasets for the association between risk scores and long noncoding RNAs. According to the results of the TCGA-PRAD training set, patients with high-risk scores had a less favorable outcome than those with low-risk scores, $P < 0.001$. The ROC experimental diagnostic efficiency of the risk score model in the training set for disease-free recurrence was 0.797 in the 5-year AUC area. The 3-year AUC area was 0.834, and the 1-year AUC area was 0.820 (Figure 6). At the same time, the prognosis of patients in the high-risk score group was worse than that in the low-risk score group in the validation set, $P < 0.001$. The ROC experimental diagnostic performance of the risk scoring model for disease-free recurrence in the training set was 0.674 in 5 years, 0.707 in 3 years, and 0.658 in 1 year (Figure 7).

3.6. Relationship between LINC01094 and Immune Microenvironment. In our study, we found that LINC01094 was an independent prognostic in prostate cancer disease-free survival. LINC01094 is in conjunction with a poor prognosis, in various cancer types, but its effect on the prostate cancer microenvironment is still unclear. As a result, this analysis examines the significance of LINC01094 in prostate cancer's tumor microenvironment through various immune validation response gene sets. An increase in inflammation and immune responses was positive in association with LINC01094. These reactions were triggered by hematopoietic cell kinases, immunoglobulin G, interferon, lymphocyte-specific kinase, primary histocompatibility complex class I, major histocompatibility complex class II, and activator of transcription 1. This evidence indicated that patients with elevated LINC01094 also displayed more clusters of immune inflammation (Figure 8).

4. Discussion

Among men, prostate cancer is the second most common cancer-related death and the predominant malignancy of the urinary system. Moreover, prostate cancer has evident heterogeneity, and its incidence rate and mortality vary significantly in different regions and ethnic groups, which also brings considerable challenges to treating prostate cancer [34]. For individualized treatment, it is vital to discover prognostic biomarkers and understand the molecular mechanism of prostate cancer. Studies have discovered a strong connection between lipid metabolism disorders and prostate cancer. The change in fatty acid synthesis is a distinct feature of prostate cancer and a treatment target [35]. However, there is still a minimal amount of data on the connection between lipid metabolism and lncRNA in prostate cancer.

(a)

(b)

(c)
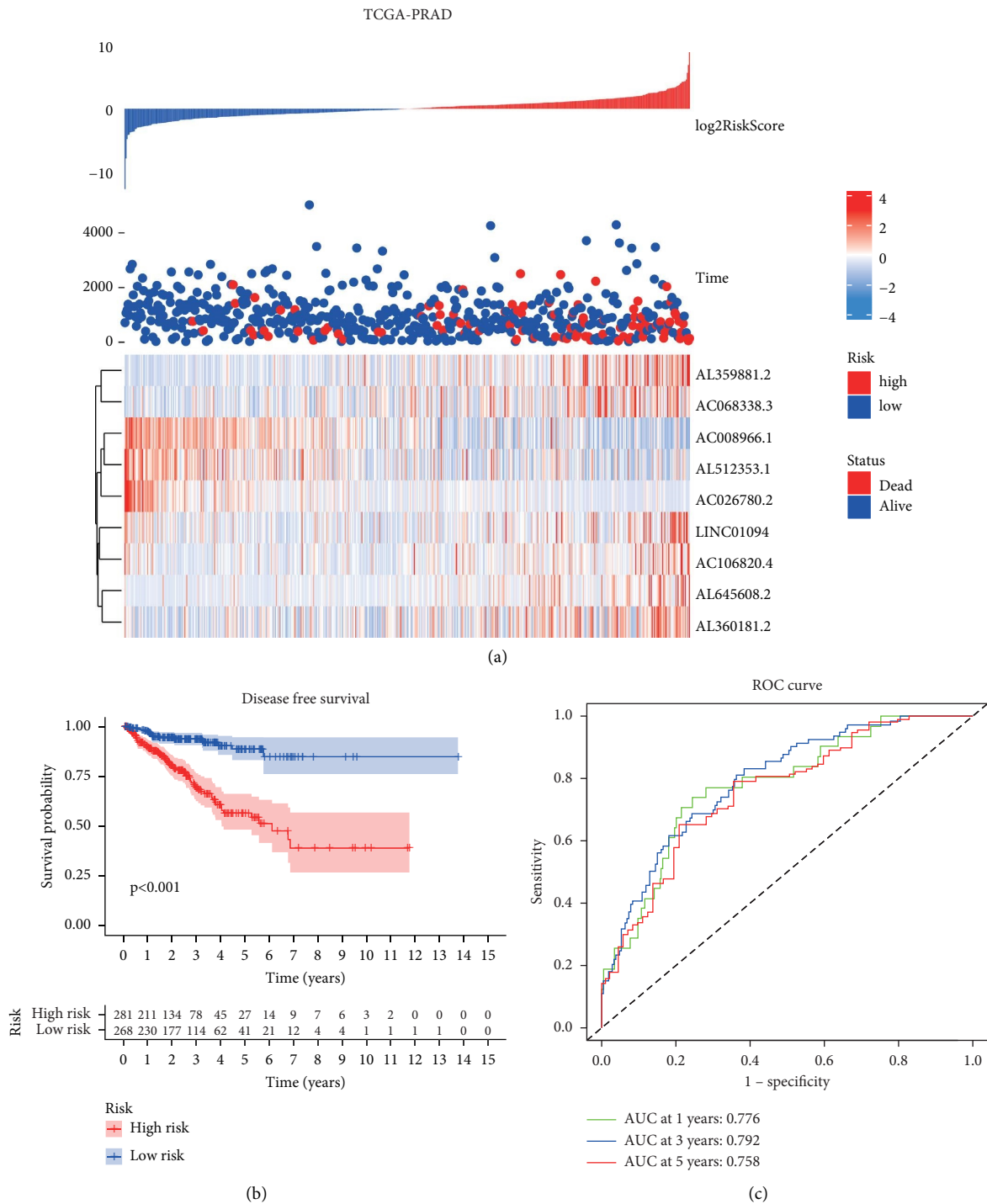
FIGURE 5: The clinical presentation of the prognostic risk signature in the TCGA-PRAD set. (a) The distribution of the risk score and disease-free survival (DFS) status in high- and low-risk groups. (b) Results of the Kaplan–Meier analysis showed that the high-risk group had worse DFS rates in the TCGA-PRAD. (c) ROC diagnostic test.

Based on fatty acid metabolism pathway genes, we identified long-chain noncoding RNA genes affecting fatty acid metabolism pathway genes. Patients with prostate cancer are further clustered using RNA. In patients with different expression patterns of long noncoding RNAs related to fatty acid metabolism pathway genes, survival and disease-free survival showed significant differences. Then, the fatty acid metabolism pathway genes related to long-chain noncoding RNA are used to build the disease-free survival of the prostate cancer prognosis model. The model includes multiple variables, such as AC106820 AL645608, AC026780, LINC01094, AC068338, AC008966, AL51235, and AL360181.

(a)

(b)

(c)
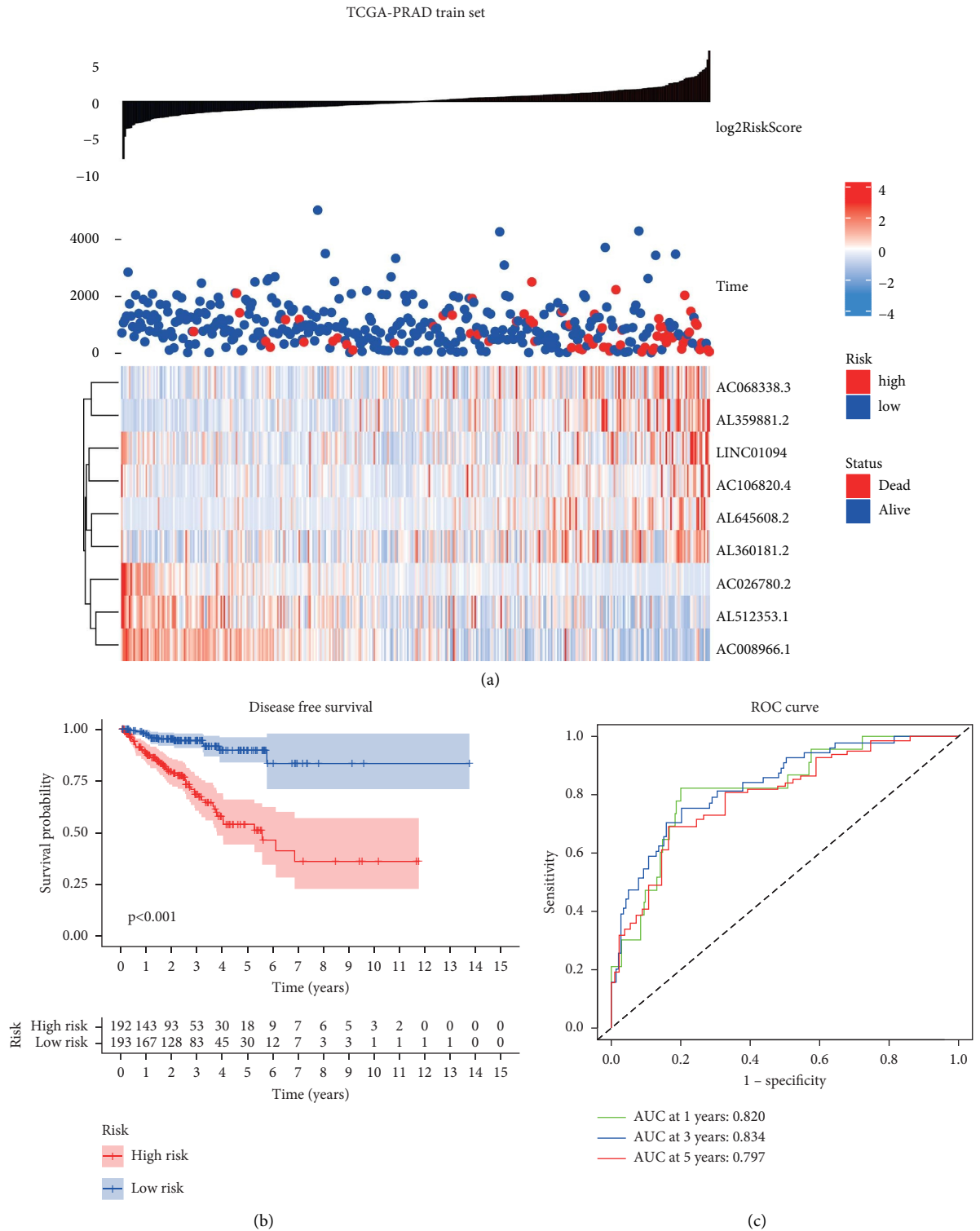
FIGURE 6: The clinical presentation of the prognostic risk signature in the train set. (a) The distribution of the risk score and disease-free survival (DFS) status in high- and low-risk groups. (b) Results of the Kaplan–Meier analysis showed that the high-risk group had worse DFS rates in the train set. (c) ROC diagnostic test.

LINC01094 is a novel lncRNA. According to studies, LINC01094 has an essential function in the advancement and invasion of several cancer types. There is a high expression of LINC01094 in clear cell renal cell carcinoma (ccRCC). LINC01094 acts as a competitive endogenous RNA in ccRCC and plays a tumor-promoting contribution to the progress of ccRCC through the microRNA 224-5p/chondroitin synthase 1 (CHSY1) regulatory axis [36]. Other

(a)

(b)

(c)
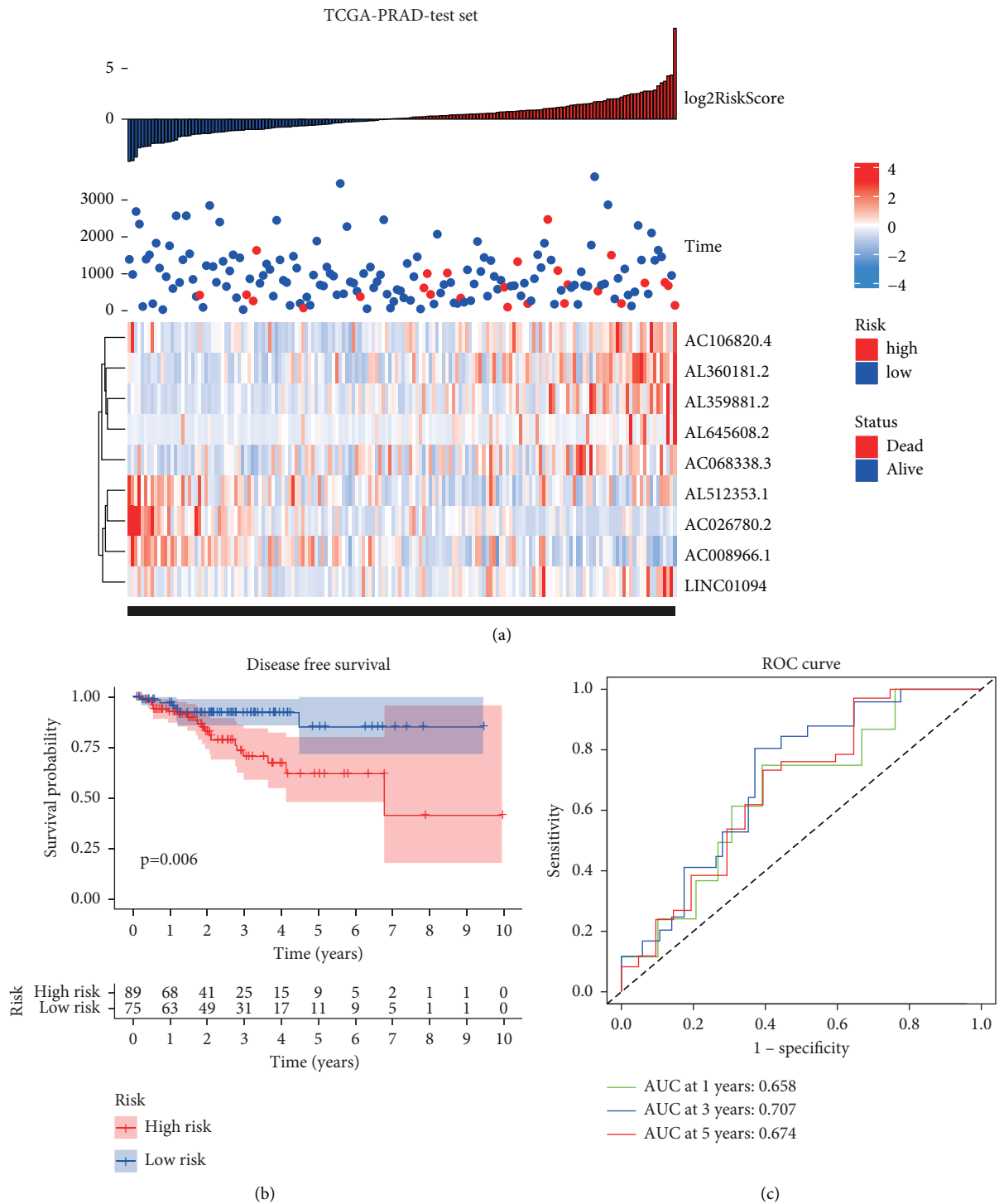
FIGURE 7: The clinical presentation of the prognostic risk signature in the test set. (a) The distribution of the risk score and disease-free survival (DFS) status in high- and low-risk groups. (b) Results of the Kaplan–Meier analysis showed that the high-risk group had worse DFS rates in the test set. (c) ROC diagnostic test.

studies have found that LINC01094 is significantly upregulated in ovarian cancer (OC) tissues and cells. LINC01094 can promote the proliferation, migration, and invasion of OC cells by downregulating miR-532-3p [37]. In addition, further studies have found that LINC01094 is overexpressed in pancreatic cancer. LINC01094 regulates lin-28 homolog B

(LIN28B) expression and PI3K/AKT pathway serving as a ceRNA of miR-577, which promotes the proliferation and metastasis of pancreatic cancer [38]. The expression of LINC01094 in glioma tissues and cell lines is highly correlated with high-grade gliomas, according to some studies. A miR-330-3p/MSI1 axis is regulated by LINC01094 to
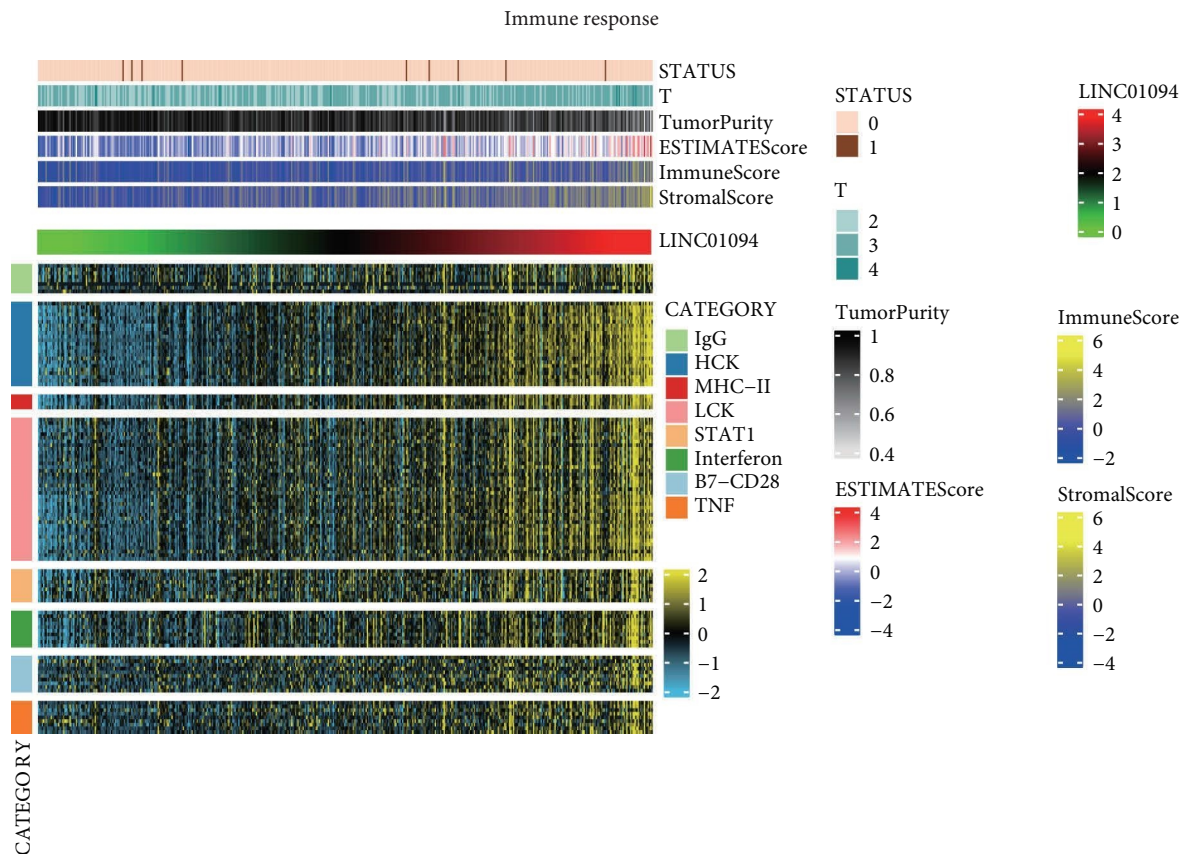
Immune response

FIGURE 8: The correlation between immune-inflammation response and LINC01094.

promote glioma cell proliferation, migration, and invasion [39]. Other studies have found that LINC01094 is more abundant in breast cancer tissues than in normal tissues. There is a correlation between high LINC01094 expression and shorter overall survival for breast cancer patients. LINC01094 induces cell cycle progression by regulating the microRNA-340-5p (miR-340-5p)/E2F transcription factor 3 (E2F3) molecular axis, as a result, facilitating the spread and progression of breast cancer cells [40]. Some studies have found that LINC01094 is highly expressed in gastric cancer tissues and is an independent index to estimate adverse survival rate. LINC01094 could participate in epithelial-mesenchymal transition (EMT) and tumor-associated macrophages (TAMs) infiltration of gastric cancer to promote the progression and metastasis of gastric cancer [41]. In addition, studies have found that LINC01094 is highly expressed in colorectal cancer cells. LINC01094 can promote the progression of colorectal cancer by regulating the miR-1266-5p/ secretory leukocyte protease inhibitor (SLPI) axis [41]. Therefore, LINC01094 can function as an oncogenic factor that may accelerate cancer progression across numerous cancer types.

Our research is of great significance. It reveals the regulatory role of lncRNAs in the lipid metabolism of prostate cancer and introduces a novel direction for the prognosis and treatment of prostate cancer. But there are still many limitations to this study. First, all prostate cancer information comes from the TCGA database, in which the patients are primarily American. There are no prostate cancer patients from other regions and countries. Second, the lncRNAs-related mechanism of lipid metabolism in prostate cancer needs further in vivo and in vitro experiments to clarify as well as further experimental research.

Abbreviations

NMF: Nonnegative matrix factorization
WGCNA: Weighted correlation network analysis
Lasso: Least absolute shrinkage and selection
              operator
GSEA: Gene set enrichment analysis
ESTIMATE: Estimation of stromal and immune cells in
              malignant tumor tissues using
              expression data.

Data Availability

The original data of the samples in this study can be obtained from the open-source database TCGA.

Conflicts of Interest

All authors declare that they have no conflicts of interest.

Authors' Contributions

All authors listed have contributed significantly, directly, and intellectually to this work and have consented to its

publication. Yutao Wang and Hongjun Li conceptualized the study, designed the methodology, performed the software analysis, wrote, reviewed, and edited the manuscript. Yutao Wang and Hao Su revised the manuscript.

References

[1] R. L. Siegel, K. D. Miller, H. E. Fuchs, and A. Jemal, "Cancer statistics, 2022," *CA: A Cancer Journal for Clinicians*, vol. 72, no. 1, pp. 7–33, 2022.

[2] M. B. Culp, I. Soerjomataram, J. A. Efstathiou, F. Bray, and A. Jemal, "Recent global patterns in prostate cancer incidence and mortality rates," *European Urology*, vol. 77, no. 1, pp. 38–52, 2020.

[3] G. E. Stoykova and I. R. Schlaepfer, "Lipid metabolism and endocrine resistance in prostate cancer, and new opportunities for therapy," *International Journal of Molecular Sciences*, vol. 20, no. 11, p. 2626, 2019.

[4] J. C. Pardo, V. Ruiz de Porras, J. Gil, A. Font, M. Puig-Domingo, and M. Jorda, "Lipid metabolism and epigenetics crosstalk in prostate cancer," *Nutrients*, vol. 14, no. 4, p. 851, 2022.

[5] D. D. Browning, I. K. Kwon, and R. Wang, "CGMP-dependent protein kinases as potential targets for colon cancer prevention and treatment," *Future Medicinal Chemistry*, vol. 2, no. 1, pp. 65–80, 2010.

[6] X. Li, J. B. Wu, L. W. Chung, and W. C. Huang, "Anti-cancer efficacy of SREBP inhibitor, alone or in combination with docetaxel, in prostate cancer harboring p53 mutations," *Oncotarget*, vol. 6, no. 38, pp. 41018–41032, 2015.

[7] M. V. Cronauer, W. A. Schulz, T. Burchardt, R. Ackermann, and M. Burchardt, "Inhibition of p53 function diminishes androgen receptor-mediated signaling in prostate cancer cell lines," *Oncogene*, vol. 23, no. 20, pp. 3541–3549, 2004.

[8] X. Zhou, X. Yang, X. Sun et al., "Effect of PTEN loss on metabolic reprogramming in prostate cancer cells," *Oncology Letters*, vol. 17, no. 3, pp. 2856–2866, 2019.

[9] C. Priolo, S. Pyne, J. Rose et al., "AKT1 and MYC induce distinctive metabolic fingerprints in human prostate cancer," *Cancer Research*, vol. 74, no. 24, pp. 7198–7204, 2014.

[10] C. Priolo and M. Loda, "Untargeted metabolomics for profiling oncogene-specific metabolic signatures of prostate cancer," *Molecular & Cellular Oncology*, vol. 2, no. 4, Article ID e1001197, 2015.

[11] H. Sun, Z. Huang, W. Sheng, and M. D. Xu, "Emerging roles of long non-coding RNAs in tumor metabolism," *Journal of Hematology & Oncology*, vol. 11, no. 1, p. 106, 2018.

[12] Y. Zeng, K. Ren, X. Zhu, Z. Zheng, and G. Yi, "Long non-coding RNAs: advances in lipid metabolism," *Advances in Clinical Chemistry*, vol. 87, pp. 1–36, 2018.

[13] Z. Chen, "Progress and prospects of long noncoding RNAs in lipid homeostasis," *Molecular Metabolism*, vol. 5, no. 3, pp. 164–170, 2016.

[14] J. Huang, S. Chen, D. Cai, D. Bian, and F. Wang, "Long noncoding RNA lncARSR promotes hepatic cholesterol biosynthesis via modulating Akt/SREBP-2/HMGCR pathway," *Life Sciences*, vol. 203, pp. 48–53, 2018.

[15] D. Li, M. Cheng, Y. Niu et al., "Identification of a novel human long non-coding RNA that regulates hepatic lipid metabolism by inhibiting SREBP-1c," *International Journal of Biological Sciences*, vol. 13, no. 3, pp. 349–357, 2017.

[16] C. Yang, Z. Li, Y. Li et al., "Long non-coding RNA NEAT1 overexpression is associated with poor prognosis in cancer patients: a systematic review and meta-analysis," *Oncotarget*, vol. 8, no. 2, pp. 2672–2680, 2017.

[17] X. Liu, Y. Liang, R. Song et al., "Long non-coding RNA NEAT1-modulated abnormal lipolysis via ATGL drives hepatocellular carcinoma proliferation," *Molecular Cancer*, vol. 17, no. 1, p. 90, 2018.

[18] C. Yan, J. Chen, and N. Chen, "Long noncoding RNA MALAT1 promotes hepatic steatosis and insulin resistance by increasing nuclear SREBP-1c protein stability," *Scientific Reports*, vol. 6, no. 1, Article ID 22640, 2016.

[19] M. Cui, Z. Xiao, Y. Wang et al., "Long noncoding RNA HULC modulates abnormal lipid metabolism in hepatoma cells through an miR-9–mediated RXRA signaling pathway," *Cancer Research*, vol. 75, no. 5, pp. 846–857, 2015.

[20] C. Shang, W. Wang, Y. Liao et al., "LNMICC promotes nodal metastasis of cervical cancer by reprogramming fatty acid metabolism," *Cancer Research*, vol. 78, no. 4, pp. 877–890, 2018.

[21] H. Zhang, N. Zhang, W. Wu et al., "Machine learning-based tumor-infiltrating immune cell-associated lncRNAs for predicting prognosis and immunotherapy response in patients with glioblastoma," *Briefings in Bioinformatics*, vol. 23, no. 6, Article ID bbac386, 2022.

[22] N. Zhang, H. Zhang, W. Wu et al., "Machine learning-based identification of tumor-infiltrating immune cell-associated lncRNAs for improving outcomes and immunotherapy responses in patients with low-grade glioma," *Theranostics*, vol. 12, no. 13, pp. 5931–5948, 2022.

[23] Y. Fang and M. J. Fullwood, "Roles, functions, and mechanisms of long non-coding RNAs in cancer," *Genomics, Proteomics & Bioinformatics*, vol. 14, no. 1, pp. 42–54, 2016.

[24] L. Chen, Y. H. Zhang, G. Lu, T. Huang, and Y. D. Cai, "Analysis of cancer-related lncRNAs using gene ontology and KEGG pathways," *Artificial Intelligence in Medicine*, vol. 76, pp. 27–36, 2017.

[25] J. H. He, Z. P. Han, M. X. Zou et al., "Analyzing the LncRNA, miRNA, and mRNA regulatory network in prostate cancer with bioinformatics software," *Journal of Computational Biology*, vol. 25, no. 2, pp. 146–157, 2018.

[26] G. J. Shi, Q. Zhou, Q. Zhu, L. Wang, and G. Q. Jiang, "A novel prognostic model associated with the overall survival in patients with breast cancer based on lipid metabolism-related long noncoding RNAs," *Journal of Clinical Laboratory Analysis*, vol. 36, no. 6, Article ID e24384, 2022.

[27] Y. Peng, C. Xu, J. Wen et al., "Fatty acid metabolism-related lncRNAs are potential biomarkers for predicting the overall survival of patients with colorectal cancer," *Frontiers in Oncology*, vol. 11, Article ID 704038, 2021.

[28] P. Langfelder and S. Horvath, "WGCNA: an R package for weighted correlation network analysis," *BMC Bioinformatics*, vol. 9, no. 1, p. 559, 2008.

[29] E. Ravasz, A. L. Somera, D. A. Mongru, Z. N. Oltvai, and A. L. Barabási, "Hierarchical organization of modularity in metabolic networks," *Science*, vol. 297, no. 5586, pp. 1551–1555, 2002.

[30] T. Wu, E. Hu, S. Xu et al., "clusterProfiler 4.0: a universal enrichment tool for interpreting omics data," *Innovation; New York*, vol. 2, no. 3, Article ID 100141, 2021.

[31] W. Luo and C. Brouwer, "Pathview: an R/Bioconductor package for pathway-based data integration and visualization," *Bioinformatics*, vol. 29, no. 14, pp. 1830-1831, 2013.

[32] A. Rody, U. Holtrich, L. Pusztai et al., "T-cell metagene predicts a favorable prognosis in estrogen receptor-negative and HER2-positive breast cancers," *Breast Cancer Research*, vol. 11, no. 2, p. R15, 2009.

[33] K. Yoshihara, M. Shahmoradgoli, E. Martínez et al., "Inferring tumour purity and stromal and immune cell admixture from

expression data," *Nature Communications*, vol. 4, no. 1, p. 2612, 2013.

[34] S. Badal, W. Aiken, B. Morrison et al., "Disparities in prostate cancer incidence and mortality rates: solvable or not?" *The Prostate*, vol. 80, no. 1, pp. 3–16, 2020.

[35] J. Dłubek, J. Rysz, Z. Jabłonowski, A. Gluba-Brzozka, and B. Franczyk, "The correlation between lipid metabolism disorders and prostate cancer," *Current Medicinal Chemistry*, vol. 28, no. 10, pp. 2048–2061, 2021.

[36] Y. Jiang, H. Zhang, W. Li, Y. Yan, X. Yao, and W. Gu, "FOXM1-Activated LINC01094 promotes clear cell renal cell carcinoma development via MicroRNA 224-5p/CHSY1," *Molecular and Cellular Biology*, vol. 40, no. 3, Article ID e00357-19, 2020.

[37] H. Chen, Y. Liu, P. Liu, Q. Dai, and P. Wang, "LINC01094 promotes the invasion of ovarian cancer cells and regulates the Wnt/β-catenin signaling pathway by targeting miR-532-3p," *Experimental and Therapeutic Medicine*, vol. 22, no. 5, p. 1228, 2021.

[38] C. Luo, K. Lin, C. Hu, X. Zhu, J. Zhu, and Z. Zhu, "LINC01094 promotes pancreatic cancer progression by sponging miR-577 to regulate LIN28B expression and the PI3K/AKT pathway," *Molecular Therapy - Nucleic Acids*, vol. 26, pp. 523–535, 2021.

[39] B. Zhu, W. Liu, H. Liu, Q. Xu, and W. Xu, "LINC01094 down-regulates miR-330-3p and enhances the expression of MSI1 to promote the progression of glioma," *Cancer Management and Research*, vol. 12, pp. 6511–6521, 2020.

[40] X. Wu, C. Kong, and Y. Wu, "Long intergenic non-protein coding RNA 1094 (LINC01094) promotes the progression of breast cancer (BC) by regulating the microRNA-340-5p (miR-340-5p)/E2F transcription factor 3 (E2F3) axis," *Bio-engineered*, vol. 12, no. 1, pp. 9046–9057, 2021.

[41] Y. Ye, O. Ge, C. Zang, L. Yu, J. Eucker, and Y. Chen, "LINC01094 predicts poor prognosis in patients with gastric cancer and is correlated with EMT and macrophage in-filtration," *Technology in Cancer Research and Treatment*, vol. 21, Article ID 15330338221080977, 2022.

Research Article

MSC Senescence-Related Genes Are Associated with Myeloma Prognosis and Lipid Metabolism-Mediated Resistance to Proteasome Inhibitors

Yang-Jia Cao [iD],[1,2] **Yan-Hua Zheng** [iD],[3] **Qing Li,**[1] **Jin Zheng** [iD],[4] **Li-Tian Ma** [iD],[4,5] **Can-Jun Zhao** [iD],[4] **and Tian Li** [iD][6]

[1]*State Key Laboratory of Experimental Hematology, National Clinical Research Center for Blood Diseases, Haihe Laboratory of Cell Ecosystem, Institute of Hematology & Blood Diseases Hospital, Chinese Academy of Medical Sciences & Peking Union Medical College, Tianjin 300020, China*

[2]*Department of Hematology, The First Affiliated Hospital of Xi'an Jiaotong University, Xi'an, Shaanxi, China*

[3]*Department of Hematology, Tangdu Hospital, Fourth Military Medical University (Air Force Medical University), Xi'an, Shaanxi, China*

[4]*Department of Traditional Chinese Medicine, Tangdu Hospital, Fourth Military Medical University (Air Force Medical University), Xi'an, China*

[5]*Department of Gastroenterology, Tangdu Hospital, Fourth Military Medical University (Air Force Medical University), Xi'an, China*

[6]*School of Basic Medicine, Fourth Military Medical University (Air Force Medical University), 169 Changle West Road, Xi'an, China*

Correspondence should be addressed to Li-Tian Ma; malitian1234@fmmu.edu.cn, Can-Jun Zhao; zhaocanjun163@163.com, and Tian Li; tian@fmmu.edu.cn

Background. Complex carcinogenic mechanisms and the existence of tumour heterogeneity in multiple myeloma (MM) prevent the most commonly used staging system from effectively interpreting the prognosis of patients. Since the microenvironment plays an important role in driving tumour development and MM occurs most often in middle-aged and elderly patients, we hypothesize that ageing of bone marrow mesenchymal stem cells (BM-MSCs) may be associated with the progression of MM. *Methods.* In this study, we collected the transcriptome data on MM from The Cancer Genome Atlas (TCGA) and the Gene Expression Omnibus (GEO) databases. Differentially expressed genes in both senescent MSCs and MM tumour cells were considered relevant damaged genes. GO and KEGG analyses were applied for functional evaluation. A PPI network was constructed to identify hub genes. Subsequently, we studied the damaged genes that affected the prognosis of MM. Least absolute shrinkage and selection operator (lasso) regression was used to identify the most important features, and a risk model was created. The reliability of the risk model was evaluated with the other 3 GEO validation cohorts. In addition, ROC analysis was used to evaluate the novel risk model. An analysis of immune checkpoint-related genes, tumour immune dysfunction and exclusion (TIDE), and immunophenotypic scoring (IPS) were performed to assess the immune status of risk groups. pRRophetic was utilized to predict the sensitivity to administration of chemotherapeutic agents. *Results.* We identified that MAPK, PI3K, and p53 signalling pathways were activated in both senescent MSCs and tumour cells, and we also located hub genes. In addition, we constructed a 14-gene prognostic risk model, which was analysed with the ROC and validated in different datasets. Further analysis revealed significant differences in predicted risk values across the International Staging System (ISS) stage, sex, and 1q21 copy number. A high-risk group with higher immunogenicity was predicted to have low proteasome inhibitor sensitivity and respond poorly to immunotherapy. Lipid

metabolism pathways were found to be significantly different between high-risk and low-risk groups. A nomogram was created by combining clinical data, and the optimization model was further improved. Finally, real-time qPCR was used to validate two bortezomib-resistant myeloma cell lines, and the test confirmed that 10 genes were detected to be expressed in resistant cell lines with the same trend as in the high-risk cohort compared to nonresistant cells. *Conclusion.* Fourteen genes related to ageing in BM-MSCs were associated with the prognosis of MM, and by combining this genotypic information with clinical factors, a promising clinical prognostic model was established.

1. Introduction

Multiple myeloma (MM) is a cancer entailing heterogeneous clonal proliferation of plasma cells and accounts for more than 10% of all haematologic malignancies [1]. The main clinical presentation of MM is the development of osteolytic bone lesions, hypercalcaemia, renal insufficiency, and manifestations associated with bone marrow failure [2]. Although the continuous emergence of new treatments has led to higher survival rates for patients with MM, it remains incurable for several reasons, including relapse or refractory disease, drug resistance, and disease-related organ dysfunction. Due to the high heterogeneity of tumour cells, the staging and classification of multiple myeloma have been keys to individualized and precise treatment. Currently, prognostic assessment of patients with multiple myeloma relies on tumour load markers and cytogenetics. However, in clinical practice, we often find that neither the International Staging System (ISS) nor the Durie–Salmon (DS) staging accurately interpret the prognoses of patients. Especially for elderly patients, cytogenetics contributes progressively less to risk, and tumour cell load is not a good measure of prognosis [3].

Smouldering multiple myeloma (SMM) is very likely to progress to active multiple myeloma (with a probability of approximately 73%) [4]. Mice with a smouldering phenotype have been found to produce higher levels of serum immunoglobulin and exhibit decreased bone density only later in life [5], suggesting that ageing may accelerate disease development. A recent study found that undetermined significance (MGUS) and SMM development into MM are not only dependent on intrinsic PC characteristics but also influenced by biology of the surrounding microenvironment [6, 7]. Further research on the tumour microenvironment will be necessary to unravel mechanisms underlying myeloma initiation and development.

Mesenchymal stem cells (MSCs) play an important role in the bone marrow microenvironment. Bone marrow mesenchymal stem cells (BM-MSCs) are adult stromal cells of mesodermal origin with the ability to modulate immune system responses, self-renewal, injury repair, and multipotent differentiation [8]. However, low cell proliferation capacity and a decline in differentiation potential appear in MSCs with donor ageing [9]. The weakening of MSCs leads to poor osteogenic differentiation and disordered immunoregulation [7]. Malignant MM cells cooperate with stromal cells to secrete cytokines and growth factors that are responsible for the biological and clinical manifestations of the disease. Even after successful antitumour therapy, the inflammatory state of the bone marrow persists [10]. Tumour treatment remains limited to killing tumour cells, but this may also cause damage to microenvironmental cells. Therefore, it is important to consider the interaction between tumour cells and other cells in the microenvironment. Effective therapeutic interventions must target both myeloma cells and the BM niche.

BM-MSCs could be more than victims; they may constitute the cause of microenvironmental inflammation in the development of myeloma [11]. The inflammatory microenvironment promotes multiple myeloma cell growth and resistance to conventional therapies [12]. To date, few studies have demonstrated a link between MSC ageing and MM progression. In addition, the significance of microenvironment ageing-related genes in MM prognosis has not been determined. Here, we explored the significance of MSC-based ageing characteristics in MM patients by examining the expression of MSC ageing-related genes in MM from a comprehensive gene expression database (GEO) and related clinical information using bioinformatics analysis. The predictive value of the model was further validated using external GEO sequences.

2. Materials and Methods

2.1. Source and Description of the Gene Expression Dataset.
Transcript levels and matched clinical information were collected from the GEO (https://www.ncbi.nlm.nih.gov/geo/) database and The Cancer Genome Atlas (TCGA) database (https://portal.gdc.cancer.gov/). GEO accession number GSE7888 contains cultivated BM-MSCs samples from 6 healthy humans and 6 matched senescent stage samples obtained from an in vitro culture. Multiple myeloma expression profiles were obtained from accession number GSE6447, with 125 MM (excluding MUGS) and 15 healthy donor plasma cell samples. The MSC senescence-related gene prognostic signature was reconstructed based on the training dataset (MMRF-CoMMpass downloaded from TCGA) ($n = 858$). The other MM data were obtained from GEO accession numbers GSE57317 ($n = 55$), GSE83503 ($n = 586$, 16 patients with missed visits were excluded), and GSE4581 ($n = 414$) to validate the outcome. A flowchart of the investigation is depicted in Figure 1.

2.2. Acquisition of Mesenchymal Stem Cell Senescence-Related Genes and Differentially Expressed Genes (DEGs) in Normal Plasma Cells and Multiple Myeloma.
The relative gene expression of MSC senescence-related genes was normalized and identified using the "limma" package with adj. p value <0.05 as the screening condition. Genes differentially expressed between MM samples and normal samples were identified by using the "limma" *R* package. Differentially
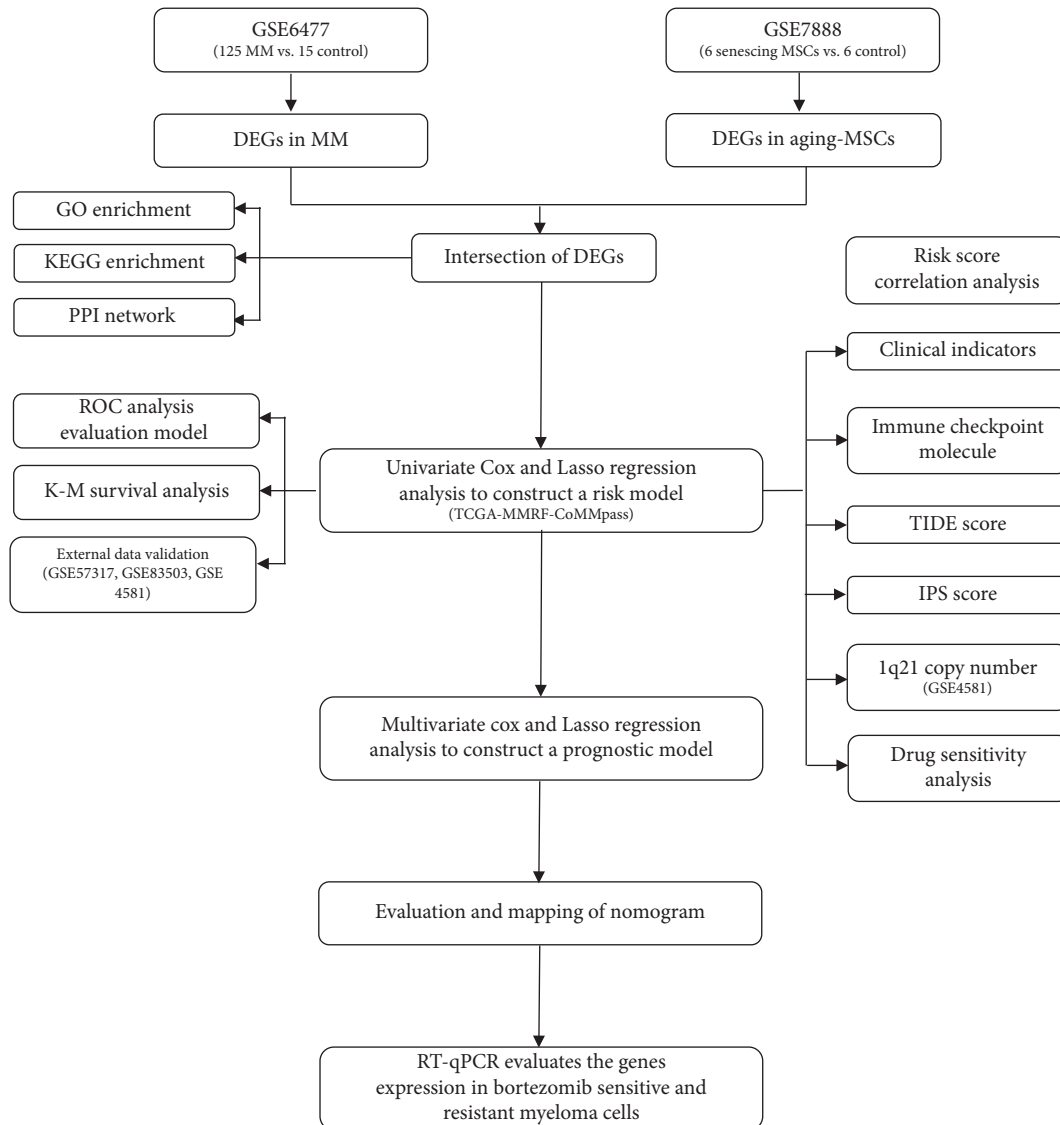
FIGURE 1: The flowchart of this study.

expressed genes (DEGs) were identified using adj. p value <0.05 as the screening condition.

2.3. Enrichment Analysis and Protein Interaction Network Construction.

The intersection of genes differentially expressed between MM and normal plasma cells with MSC senescence-related genes was examined. The roles of intersecting genes in biological pathways were explored using the "clusterProfiler" package. Intersected DEGs were entered into the STRING database to obtain a protein-protein interaction (PPI) network, which was visualized using Cytoscape software. Differential gene enrichment analysis for high and low-risk groups was obtained from the Metascape database.

2.4. Construction of the Risk Model.

The samples in TCGA-MMRF-COMMPASS were used as the training set, and genes significantly associated with survival were identified using univariate Cox proportional hazards analysis. The candidate

genes obtained from one-way Cox regression analysis were subjected to lasso regression analysis using the R package "glmnet." The risk model was constructed based on the expression of genes obtained from lasso regression. Risk scores were calculated, and patients were classified into high-risk and low-risk groups according to the median risk score. Differences in survival between patients in high-risk and low-risk groups were analysed using Kaplan–Meier (KM) curves. ROC curve analysis was used to evaluate the performance of risk scores for predicting patient survival status.

2.5. Evaluation of Risk Model Prediction Performance.

The constructed model was validated using the validation set (GEO accession numbers GSE57317, GSE83503, and GSE4581), and based on the model, the risk score was calculated for each patient. According to the median risk score, patients were divided into a high-risk group and a low-risk group, and survival differences between patients

in the high-risk and low-risk groups were analysed using Kaplan–Meier (KM) curves. ROC curve analysis was also used to evaluate the performance of risk scores in the prediction of patient survival status.

2.6. Evaluation of the Sensitivity of Chemotherapeutic Agents. The 50% inhibition concentration (IC50) values of 138 drugs were inferred using the "pRRophetic" algorithm, comparing the IC50 of chemotherapeutic agents in the high-risk and low-risk groups.

2.7. Immune-Related Characteristics in the Low-Risk and High-Risk Score Groups. A total of 282 immune checkpoint-related genes (ICRGs) were collected based on a previous study. The differences in ICRGs between the high-risk and low-risk groups were analysed. Tumour immune dysfunction and exclusion (TIDE) was used to evaluate the prognostic effect of immune checkpoint inhibition therapy. Analytical data were based on TPM data of all tumour samples ($n = 858$) from the TCGA dataset after $\log_2$ (TPM+1) transformation. The data were normalized using the mean of all samples as a control, as required by official documents. Processed data were uploaded to the TIDE website (https://tide.dfci.harvard.edu). TIDE analysis results were obtained. An analysis of correlations between TIDE and risk scores was conducted, and the differences in TIDE scores between the high-risk and low-risk groups were examined. Moreover, immunophenotypic scoring (IPS) of all 858 tumour samples was performed using the "IOBR" package.

2.8. Correlations with Clinical Indicators and Independent Prognostic Analysis. For the GSE4581 dataset, we compared risk scores between patients with a 1q21 copy number greater than 2 and patients with a normal copy number, and we used the TCGA dataset to compare risk scores by sex, race, age, and ISS stage.

2.9. Establishment of a Nomogram and Statistical Analysis. Using the "rms" package in R, we built clinical prognostic models based on the TCGA dataset using the risk scores generated in the previous phase and clinical data from patients, including sex, ethnicity, and stage. Prognostic models were constructed using univariate Cox analysis and multivariate Cox regression, respectively. The accuracy of the nomogram was predicted by plotting calibration curves over time. Multivariate Cox regression analysis was also performed to determine whether the prognostic risk score model could be employed as an independent predictor of OS in MM. The nomogram's prognostic value was then computed using AUC values from online ROC curves. All data analyses employed R software (version 4.1.3 for Windows, https://www.R-project.org). Differences between the two groups were evaluated using the Wilcoxon test. Kaplan–Meier analysis was applied to evaluate survival differences between the low-risk and high-risk score groups. A value of $p < 0.05$ was considered statistically significant.

2.10. Cell Lines and Cultures. In this experimental study, we used the RPMI-8226 and OMP-2 cell lines from Fourth Military Medical University, and RPMI-8266 bortezomib-resistant cells and OMP-2bortezomib-resistant cells were previously developed and cultured in the presence of bortezomib (Selleckchem PS-341) (Houston, TX, USA).

2.11. Quantitative Real-Time Polymerase Chain Reaction Assessment and Statistical Analysis. Total RNA was isolated from the bortezomib-resistant and nonresistant RPMI-8226 and OMP-2 according to the TRIzol manufacturer's protocol (Invitrogen; Thermo Fisher Scientific, Inc.). RNA was reverse transcribed to cDNA using Transcriptor First Strand cDNA Synthesis Kit (Roche Diagnostics) according to the manufacturer's protocols. Quantitative real-time polymerase chain reaction (qRT-PCR) was performed with SYBR Green PCR Master Mix (Roche Diagnostics). Table1 shows the primer sequences used in this experiment. The qPCR program cycling parameters were: qPCR was performed as follows: initial denaturation for 30 sec at 95°C, followed by 40 cycles of 95°C for 15 sec and 60°C for 30 sec. GADPH was used as an internal control, and data analysis was performed by $2^{-\Delta\Delta CT}$ to calculate the fold change for relative expression. Data were presented as a mean ± standard deviation. Statistical analysis was performed with the GraphPad Prism 8.0.3 software. The mean values of two groups were compared by Student's *t*-tests. $P < 0.05$ was considered statistically significant.

3. Results

3.1. Identification of the Intersection of Genes Differentially Expressed in Aged BM-MSCs and Multiple Myeloma. Differentially expressed genes were identified in CD138+ plasma cells from multiple myeloma patients ($n = 125$) and plasma cells from healthy individuals ($n = 15$) in data from GEO accession number GSE6477. A total of 3568 differentially expressed genes (MM vs. control) were identified, of which 1842 were upregulated and 1726 were downregulated. The volcano map and the gene heatmap of MM DEGs are plotted in Figures 2(a) and 2(b).

There were 217 differentially expressed genes identified (MSCs in the senescing stage vs. MSCs in the early stage), with 128 genes upregulated and 89 genes downregulated. A volcano map and a heatmap of genes differentially expressed in ageing MSCs are shown in Figures 2(c) and 2(d).

The intersection of differentially expressed MM and MSC genes included a total of 48 genes. Venn diagram mapping is shown in Figure 2(e). Since senescence is defined by the buildup of damage [13], to simplify terminology, we label these damage-related genes.

3.2. Enrichment Analysis of Damage-Related Genes and Construction of the PPI Network. A total of 48 damage-related genes obtained were subjected to GO enrichment. These genes were found to be enriched in biological processes (BPs), such as activation of MAPK activity, oestrogen response, positive regulation of epithelial cell proliferation, response to magnesium ions, and positive regulation of actin

TABLE 1: Primer sequences.

Genes	Primer
GAPDH	F: GGAAGCTTGTCATCAATGGAAATC R: TGATGACCCTTTTGGCTCCC
COBLL1	F: CAGATAAGAGTCCCTGTGAAGCA R: TGGCTGTAAGGCAGTCACACG
CCND1	F: AGCTGTGCATCTACACCGAC R: GAAATCGTGCGGGGTCATTG
MANSC1	F: CCTGTCCATTGAAACCAGCAA R: TCGGTGGGCTTTGAATAATCTG
MAN2A1	F: ACTATTTCGCCCTGAGACAAGC R: AAGTCTGGTACCATAATCCACAACC
EGR1	F: AAGGCCCTCAATACCAGCTAC R: ACTCCACTGGGCAAGCGTAA
HSPB8	F: AAGACCAAAGATGGATACGTGGAG R: AATGTTGAGTAAGGAGGGACCTG
SCN9A	F: ACAGCTTCTGCCAGAGGTGATA R: GAGGTTGGGATCATTCAGCATA
RGS7	F: TAAGATTCTGGCTGGCAGTGG R: CTCCTGAGCATCTTCAAATGTGTAT
NTF3	F: TTGCCACGATCTTACAGGTGAA R: TCCTTAACGTCCACCATCTGCT
OCLN	F: TTCCTATAAATCCACGCCGG R: TGTCTCAAAGTTACCACCGCTG
SLC31A2	F: GTGGTCATCGGCTACTTCATCAT R: CTGAGAAGTGGGTAAGCTAGGTAGTA
ZBED1	F: GAGGAGTGAGAATCAGAACCGC R: TGATGGTCTCCGCCGTGTT
SCN3A [1]	F: ATGTGGGACTGTATGGAGGTCG R: GGAAACACTCCCGCATCTTATT
SCN3A [2]	F: AAGAAATGCGGCAAGCTCAA R: CGTCGTCCTCATCCAGAAACA
SOX11 [1]	F: TTCAGTTTCAGAGGTCGGGC R: TTCTGTGGTGGTGCCGTTAC
SOX11 [2]	F: AAGCCCAAAATGGACCCCT R: ATTTCTTGCTGGAGCCCTTG

cytoskeleton reorganization. Furthermore, lattice protein vesicles, inhibitory synapses, voltage-gated sodium channel complexes, sodium channel complexes, lattice protein vesicle membranes, and other cellular components (CCs) were enriched. The main molecular functions (MFs) included voltage-gated sodium channel activation, sodium channel activity, catalytic-specific chromosome binding, and activation of RNA polymerase II-specificDNA-binding transcriptional activators (Figure 3(a)).

According to KEGG enrichment analyses, differentially expressed genes were mainly involved in the MAPK signalling pathway, PI3K-Akt signalling pathway, acute myeloid leukaemia, p53 signalling pathway, chronic myeloid leukaemia, and other signalling pathways (Figure 3(b)).

Damage-related genes were entered into the STRING database to obtain the protein-protein interaction (PPI) network (Figure 3(c)). Genes with a degree greater than 2 were used as hub genes. These hub genes were TEK, HSPB8, HIST1H2AC, HIST1H1C, GADD45A, GAD1, FLNC, EGR1, and CCND1 (Figure 3(d)).

3.3. Prognostic Risk Modelling of Multiple Myeloma. A total of 858 samples with clinical information from TCGA-MMPF-COMMPASS were used as the training set, and a one-way Cox analysis was performed on 48 damage-related genes to screen out 16 genes associated with prognosis. The forest diagram is shown in Figure 4(a).

Lasso regression is a statistical method for obtaining a more refined model by constructing a penalty function, compressing some regression coefficients, reducing data dimensionality, and avoiding multicollinearity and overfitting in multiple regression models (Figures 4(b) and 4(c)). Sixteen candidate genes identified by one-way Cox regression analysis were subjected to lasso regression analysis. Fourteen genes whose regression coefficients were not penalized to 0 were finally obtained using lambda.min = 0.008623835 and 10-fold cross-validation: COBLL1, CCND1, MANSC1, MAN2A1, EGR1, SLC31A2, HSPB8, SCN3A, SCN9A, SOX11, RGS7, NTF3, OCLN, and ZBED1.

The risk model was constructed based on the expression of 14 genes obtained by lasso regression. The coefficient from the linear term of the lasso regression model was used to calculate the risk score Risk score $= \sum_{i=1}^{n} \beta i * xi$, where β_i is the coefficient and x_i is the sample expression corresponding gene i. The coefficients for all 14 genes are calculated and shown in Table 2.

The formula was used to calculate risk scores for 858 patients, and patients were divided into the high-risk group ($n = 429$) and the low-risk group ($n = 429$) based on the median risk score. The distribution of patients' risk scores and survival status is shown in Figures 4(d) and 4(e).

3.4. Performance Evaluation of Risk Model Prediction. The difference in survival between the high-risk and low-risk groups in the training set was analysed using the Kaplan–Meier (KM) curve. As shown in Figure 5(a), log-rank analysis revealed a significant difference in survival between the two groups ($p < 0.05$). Additional validation with two datasets. There was no median follow-up time in this dataset GSE83503, we removed the 16 samples of the missing visit data and used the chi-square test to calculate the survival rate in the high-risk and low-risk groups, and the results showed that the mortality rate was significantly higher in the high-risk group than in the low-risk group ($p < 0.05$). GSE4581 ($n = 414$) showed significant differences in survival between the high-risk and low-risk groups distinguished by the model constructed in this study (Figures S1A and S1B).

ROC curve analysis was also used to evaluate the performance of risk scores in the prediction of patient survival status, and ROC curves were plotted for 1, 3, and 5 years. The results are shown in Figure 5(b). The results showed that the AUC exceeded 0.66, indicating that the risk score could accurately predict the survival status of patients.

The constructed model was validated using the validation set ($n = 55$). Combined with the model, risk scores were calculated for each patient. Patients were divided into the high-risk group ($n = 27$) and the low-risk group ($n = 28$)

(a)

(b)

(c)

(d)

(e)
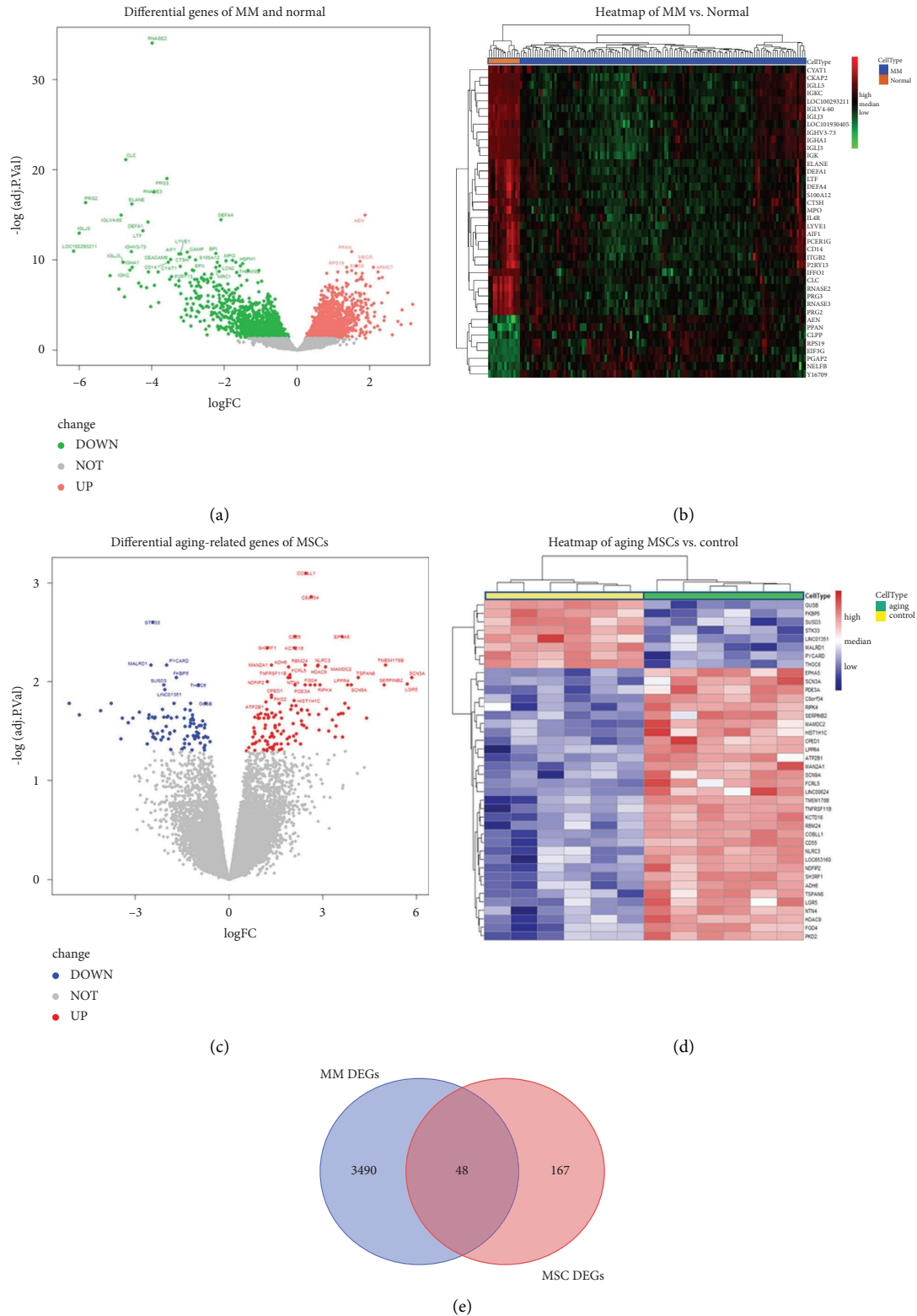
FIGURE 2: Identification of damage-associated genes. (a) A volcano map of genes differentially expressed in MM. Red dots indicate upregulated genes. Green dots indicate downregulated genes. Grey indicates nonsignificant differentially expressed genes. (b) A heatmap of differential gene expression between MM and normal control. Red indicates high expression, and green indicates low expression. (c) A volcano map of genes differentially expressed in MSC senescence. Red dots indicate upregulated genes. Blue dots indicate downregulated genes. Grey indicates nonsignificant differentially expressed genes. (d) A heatmap of differential gene expression in MSC senescence. Red indicates high expression, and blue indicates low expression. (e) A Venn diagram of MSC ageing genes and genes differentially expressed in MM.
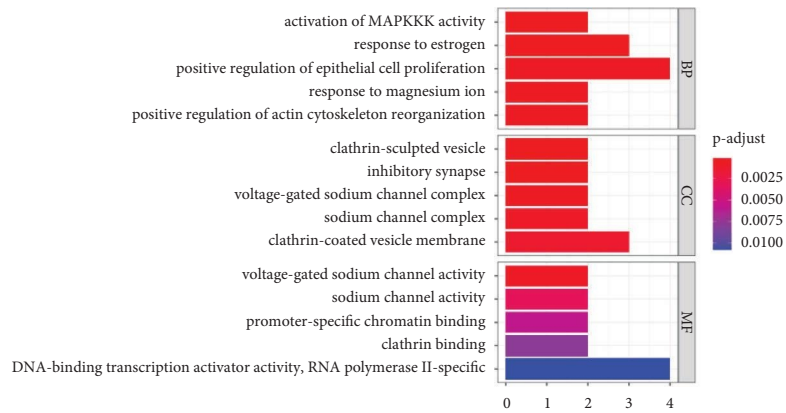
(a)
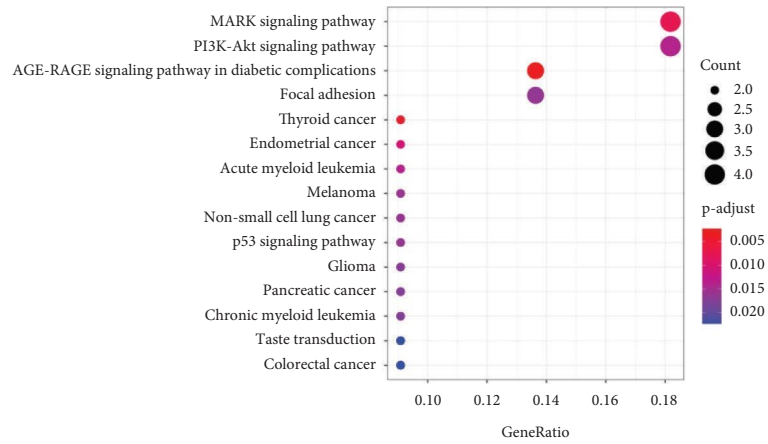
(b)
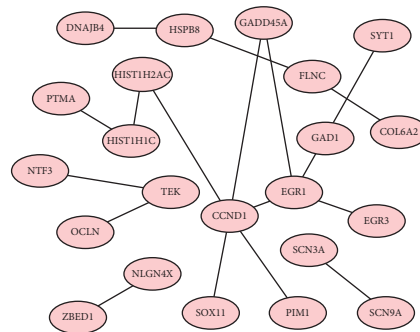
(c)
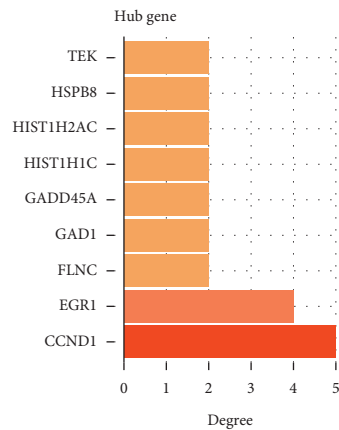
(d)

FIGURE 3: Functional enrichment of damage-associated genes and screening for hub genes. (a) GO enrichment of damage-associated genes. (b) KEGG enrichment of damage-associated genes. (c) PPI network diagram. (d) Hub genes displayed according to a degree.

(a)

(b)

(c)

(d)

(e)
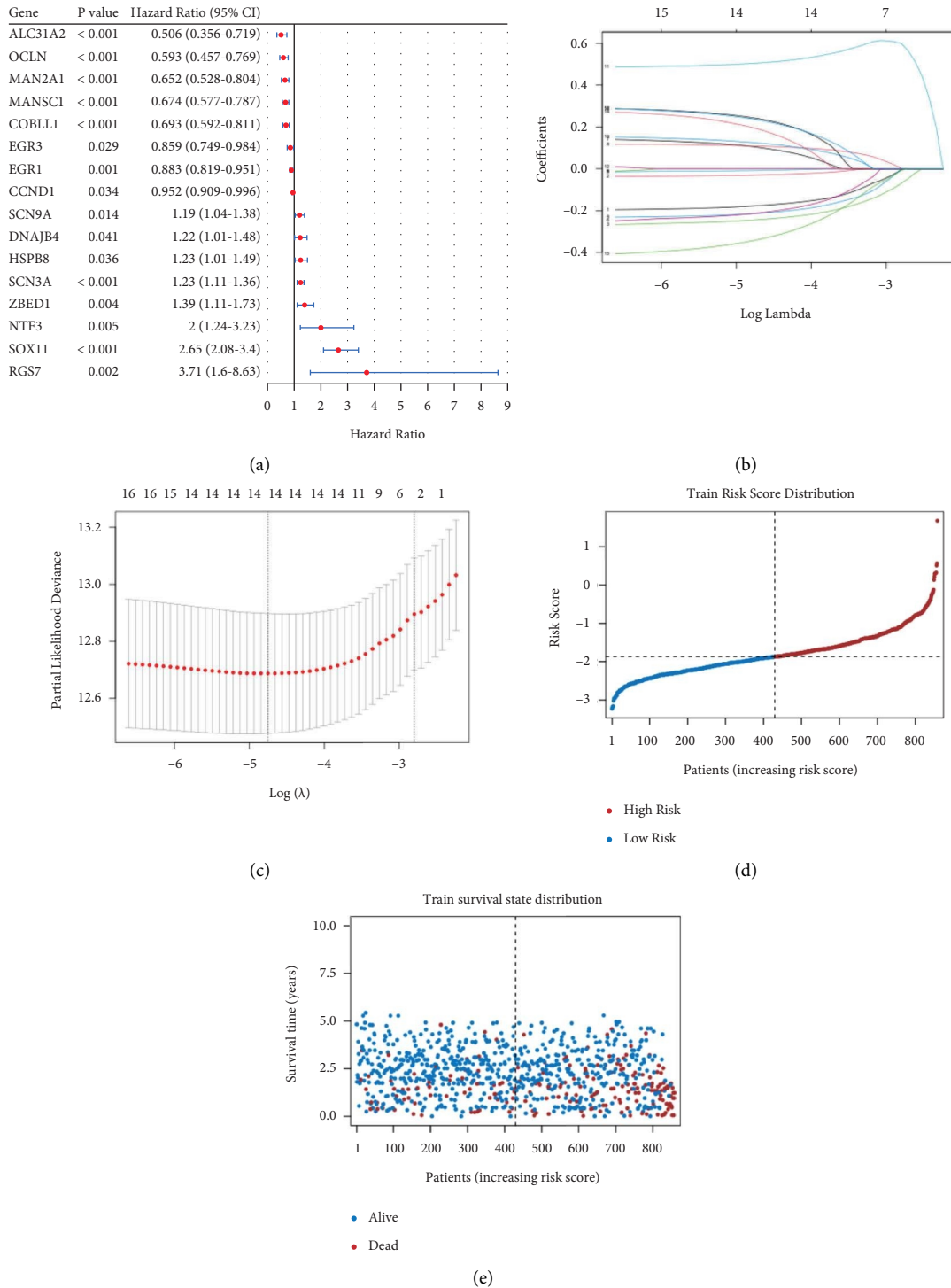
FIGURE 4: Construction of the risk model. (a) Univariate Cox regression analysis to screen for prognosis-related genes. (b) A curve of changes in the λ-value from lasso analysis. (c) The confidence interval for the value of λ. (d) Risk score distribution of the training set. (e) Survival state distribution of the training set.

based on the median risk score. The distribution of risk scores and survival status of patients are shown in Figures 5(c) and 5(d).

The Kaplan–Meier (KM) curve was used to analyse the difference in survival between the high-risk and low-risk groups of patients in the validation group. Log-rank analysis showed a significant difference in survival between the two groups ($p < 0.05$), as shown in Figure 5(e).

The performance of risk scores for predicting patient survival status was also evaluated using ROC curve analysis,

TABLE 2: The list of lasso regression coefficients.

Lasso genes	Coefficients
COBLL1	−0.177149459
CCND1	−0.029966789
MANSC1	−0.244343196
MAN2A1	−0.213850062
EGR1	−0.008368273
SLC31A2	−0.212850188
HSPB8	0.104505406
SCN3A	0.108917827
SCN9A	0.124850287
SOX11	0.504817715
RGS7	0.242200199
NTF3	0.194016607
OCLN	−0.341804389
ZBED1	0.236016978

and the 1-year, 3-year, and 5-year ROC curves were plotted, with the results shown in Figure 5(f). The AUC exceeded 0.67, indicating that the model was capable of accurate prediction.

3.5. Immune-Related Characteristics in the Low-Risk and High-Risk Score Groups.

The differences in immune checkpoint molecules between the high-risk and low-risk groups were then examined. The TCGA-MMRF-COMMPASS dataset corresponded to 46 genes related to immune checkpoint molecules. Using the Wilcoxon test ($p < 0.05$), 20 immune checkpoint molecules were found to differ significantly between the high-risk and low-risk groups: ADORA2L, BTLA, BTNL2, C10orf54, CD200, CD274, CD28, CD40, CD70, CTLA4, IDO2, KIR3DL1, LAG3, LAIR1, TIGIT, TMIGD2, TNFRSF14, TNFRSF4, TNFRSF8, and TNFRSF9 (Figure 6(a)). Markers representing T cell exhaustion, such as CD274 (PD1), LAG3, CTLA4, and TIGIT, were highly expressed in the low-risk group, which predicts that immunotherapy will not be effective for patients in the high-risk group.

A correlation analysis was conducted between the TIDE scores and risk scores of the TCGA-MMRF-COMMPASS dataset, and the differences in TIDE scores between the high-risk and low-risk groups were examined. Figure 6(b) shows the distributions of TIDE and risk scores, both of which conform to a normal distribution. Therefore, Pearson's coefficient was used for correlation analysis. The correlation coefficient was 0.28 with a highly significant p value, which indicated that the risk score and TIDE obtained from the previous analysis were strongly correlated, and as the risk score increased, the TIDE score also increased, which implied poor efficacy of immune checkpoint blockade therapy (ICB) in the high-risk group and short survival after receiving ICB treatment. Furthermore, TIDE scores were significantly different between the high-risk and low-risk groups, as shown in Figure 6(c), with a higher TIDE score in the high-risk group. This is consistent with previous findings.

Immunophenotypic scoring (IPS) was performed on all 858 tumour samples. The results were plotted on a mountain plot (Figure 6(d)); overall, the IPS in the high-risk group was higher than that in the low-risk group, indicating high immunogenicity.

3.6. High-Risk Group Is Resistant to Proteasome Inhibitors and Associated with the Lipid Metabolism Pathway.

The half-maximal inhibitory concentration (IC50) was calculated to predict the treatment response to chemotherapy drugs in the cohort from TCGA. 137 chemotherapeutic agents were evaluated in the high-risk and low-risk groups of patients in the TCGA dataset, and MG.132 (a proteasome inhibitor) was found to be least sensitive to tumour cells in the high-risk group, while some CDK inhibitors and multitarget kinase inhibitors had lower drug sensitivity in the high-risk group (Figure 6(e)). Additionally, in the GSE4581 dataset, the low-risk group was more sensitive to bortezomib than the high-risk group (Figure 7(a)). We further analysed differential genes between the high-risk and low-risk groups and found that genes upregulated in the high-risk group were mainly enriched in cell cycle-related pathways compared to the low-risk group (Figure 7(b)) and that genes downregulated in the high-risk group were mainly enriched in membrane trafficking pathways and metabolism of lipids compared to the low-risk group (Figure 7(c)). This result suggests that the high-risk group, which was divided by our model, is resistant to proteasome inhibitors and associated with lipid metabolism pathways.

3.7. Risk Prediction Models Are Independent of Patient Clinical Characteristics.

The risk score for the TCGA-MMRF-COMMPASS dataset was calculated, and the variation in risk scores with clinical indicators was analysed. The results showed that risk scores differed significantly among ISS stages and sexes (Figure 8(a)), which is consistent with clinical observations. In the GSE4581 dataset, the risk scores of patients with a 1q21 copy number greater than 2 were significantly higher than those of patients with a normal copy number (Figure 8(b)).

Univariate Cox analysis screened for clinical factors associated with prognosis, and the effect of race was not significant (Figure 8(c)). Among factors associated with OS in univariate analysis, including ISS stage, sex, race, and risk score, only the ISS stage, sex, and risk clinical score were independent predictors of OS in multivariate analysis (Figure 8(d)). Finally, the nomogram plot is shown in Figure 8(e). To evaluate the clinical prognostic model, ROC curve analysis (Figure 8(f)) and calibration curves (Figure 8(g)) suggested that the model was capable of accurate prediction.

3.8. Genes Expressed in Bortezomib-Resistant Cell Lines with the Same Trend as in the High-Risk Cohort Compared to Nonresistant Cells.

We evaluated mRNA levels of 14 genes
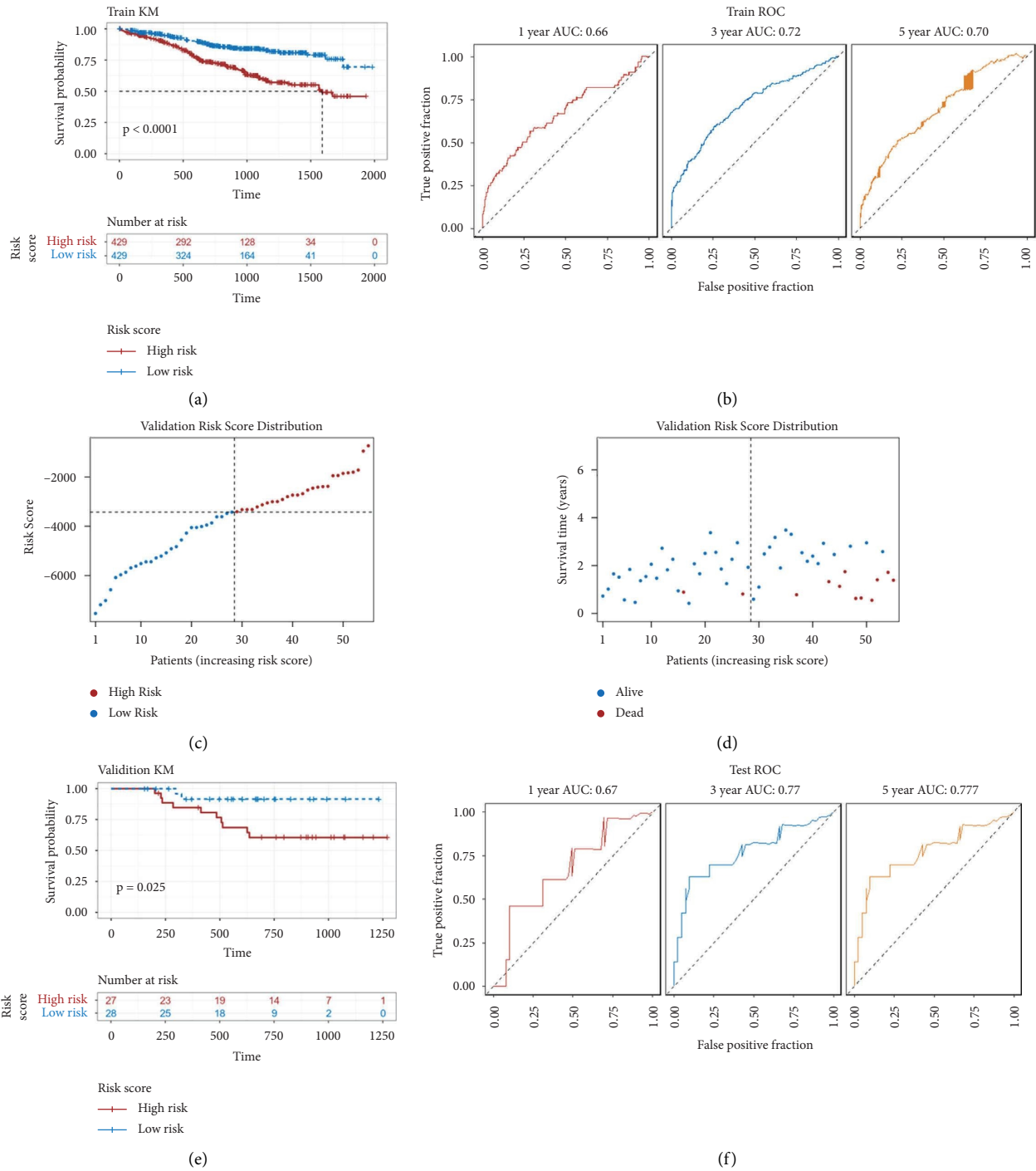
FIGURE 5: Evaluation of risk model prediction performance. (a) The training set Kaplan–Meier curve. (b) An ROC curve of the training set. (c) Risk score distribution of the validation set. (d) Survival state distribution of the validation set. (e) The validation set Kaplan–Meier curve. (f) An ROC curve of the training set.

in myeloma cell lines. In agreement with the gene model, compared with bortezomib-sensitive myeloma cell lines (negative control), there was an increase in mRNA expression of SCN9A, RGS7, NTF3, HSPB8, and ZBED1 and a decrease in CCND1, COBLL1, EGR1, OCLN, and ZBED1

mRNA expression of bortezomib-resistant cell lines (Figure 9). The expression trend of these genes was consistent with the high-risk group gene expression trend predicted by the model. SOX11 and SCN3A were not detected in these cell lines because their expression was too low.
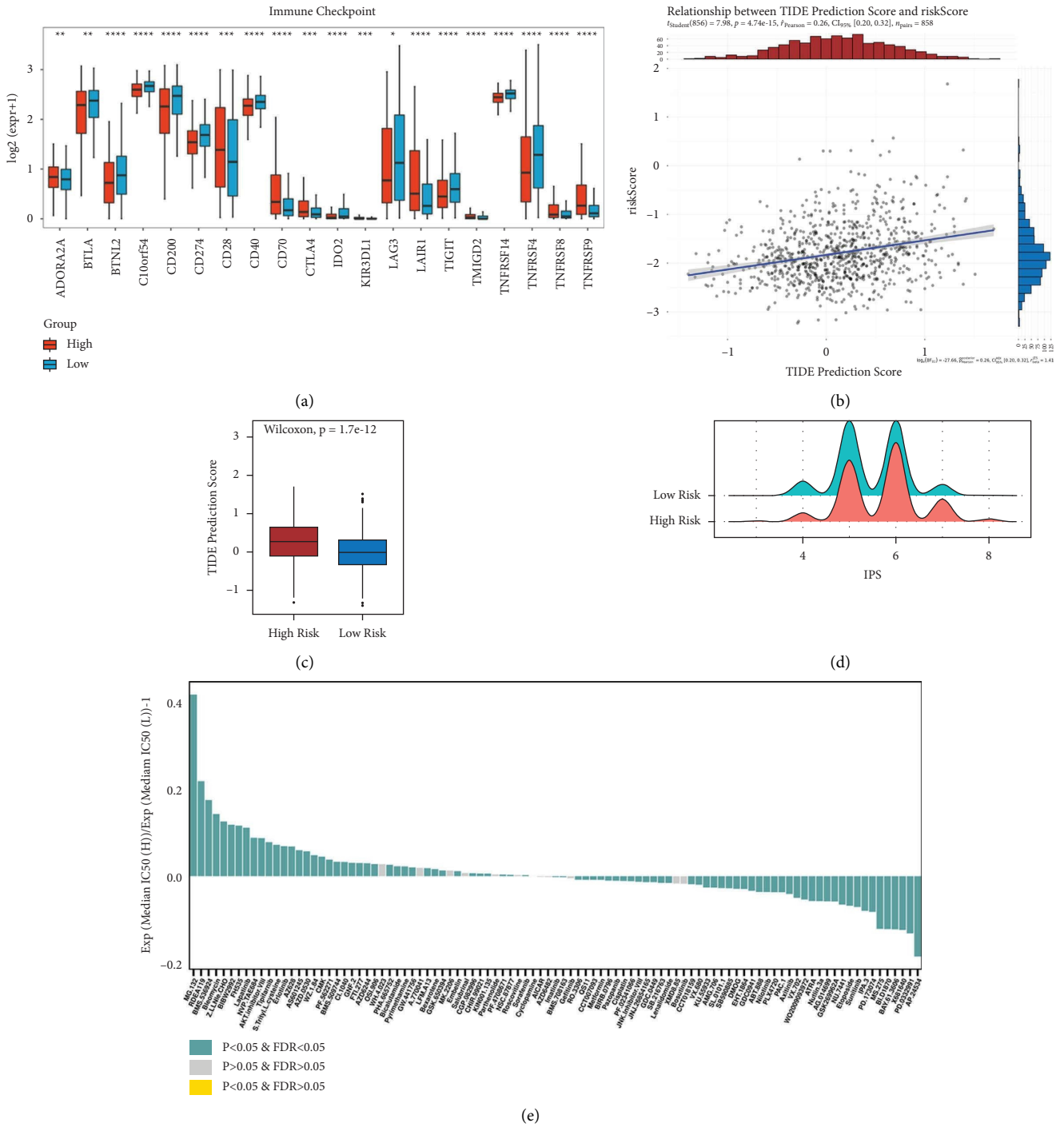
Figure 6: Immune-related characteristics and chemotherapy drug sensitivity in the TCGA dataset. (a) Differential immunoassay point molecules. (b) Correlation analysis of TIDE scores and risk scores. (c) A boxplot of differences in TIDE scores between the high-risk and low-risk groups. (d) A mountain plot of the difference in IPS scores between the high-risk and low-risk groups. (e) A histogram of the IC50 ratio for the high-risk and low-risk groups. The green column indicates a statistically significant difference.

4. Discussion

Multiple myeloma has a complicated pathogenesis, and mechanisms underlying its occurrence and progression remain largely unknown. For decades, resistance to drugs (particularly bortezomib), relapse, refractory disease, and inconsistency in the treatment of older individuals have been bottlenecks that hinder myeloma treatment. Furthermore, most of the genetic complexity of MM might be present at asymptomatic stages, but how initiating plasma cell clones acquire the potential for oncogenic transformation to MM is a crucial factor that has eluded researchers [14]. There is mounting evidence that multiple myeloma is linked to abnormal mRNA expression, which is

(a)

(b)

(c)
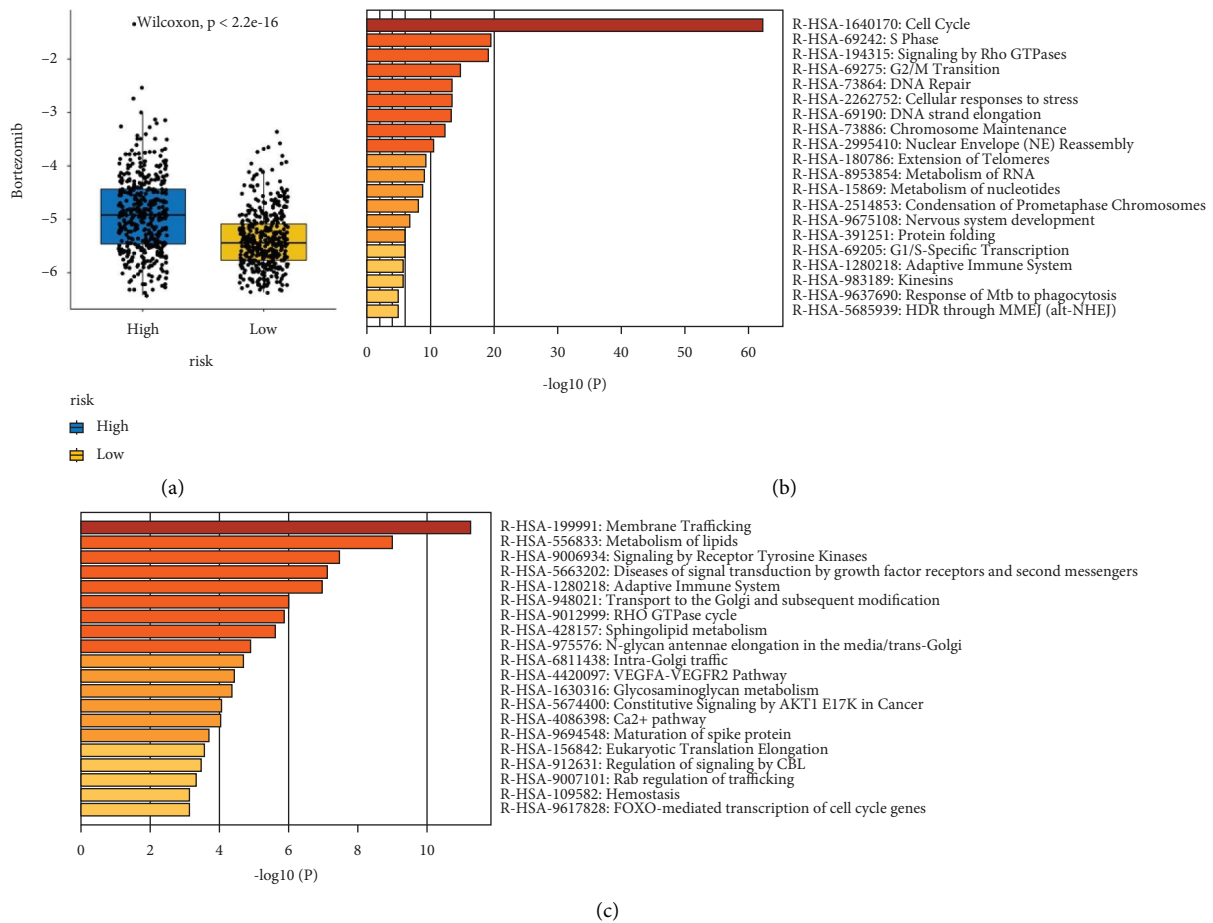
FIGURE 7: Differential bortezomib resistance and differential gene enrichment in the high and low-risk groups of GSE4581. (a) A boxplot of differences in predicted bortezomib IC50 between the high-risk and low-risk groups. (b) Enrichment pathways of genes upregulated in myeloma in the high-risk group than in the low-risk group. (c) Enrichment pathways of genes downregulated by myeloma in the high-risk group than in the low-risk group.

connected to the occurrence, progression, and prognosis of the disease. Individual patient survival remains variable and cannot be accurately predicted using current prognostic models [15–18]. Current mRNA-based prognostic models are primarily concerned with identifying special tumour subtypes and exploring differential gene expression or activation pathways in tumour cells. Currently, the influence of the tumour microenvironment on tumour progression and drug resistance has become the focus of research. Treatment modalities that take the microenvironment into account may be more helpful for patient survival.

A growing number of studies confirm that the bone marrow microenvironment is not always passive in the development of tumours [19]. The inflammatory environment provides conditions for tumour induction and promotion, especially in myeloma, and MSCs play a crucial role as the niche of the microenvironment. According to Schinke et al., markers of MSCs are independent prognostic factors for MM and SMM, and microenvironmental immune dysfunction caused by MSCs plays a key role in disease progression [6]. Single-cell sequencing also confirmed that

antitumour induction therapy fails to restore bone marrow inflammation, predicting a role for mesenchymal stromal cells in disease persistence [10]. Furthermore, impaired osteogenic differentiation of BM-MSCs is an important cause of myeloma bone disease [20]. Bone disease is one of the most prominent clinical symptoms of MM patients, affecting 80% of MM patients, and seriously affects the quality of life and survival time of patients [21]. However, a few drugs are currently available to target bone regeneration and treat adult bone weakness; pathway-based tumour treatment options may not be sufficient to improve bone disease. For example, inhibition of the Wnt signalling pathway blocks tumour progression while obstructing osteogenesis [22]. To better improve patient survival, therapy should not be limited to targeting tumour cells only. Bidirectional interferences between microenvironmental cells and the immune system may be potential targets for anticancer drugs. Microenvironmentalcell-targeted therapy as a possible systemic anticancer effect is receiving increasing attention [23]. MSCs play a very important immunomodulatory role in the tumour microenvironment, but the immunomodulatory capacity of MSCs depends on

(a)

(b)

(c)

(d)

(e)

(f)
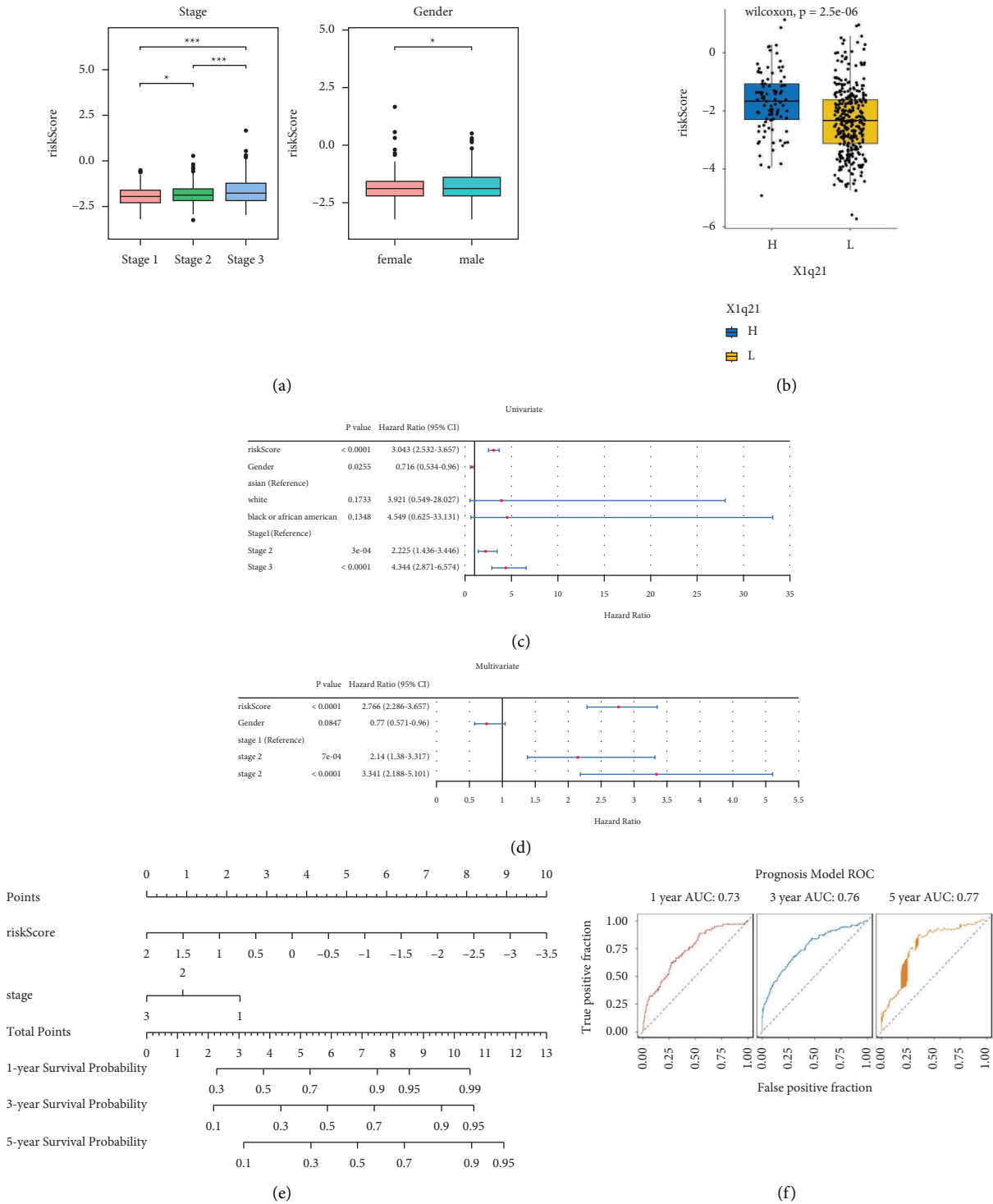
FIGURE 8: Continued.

(g)
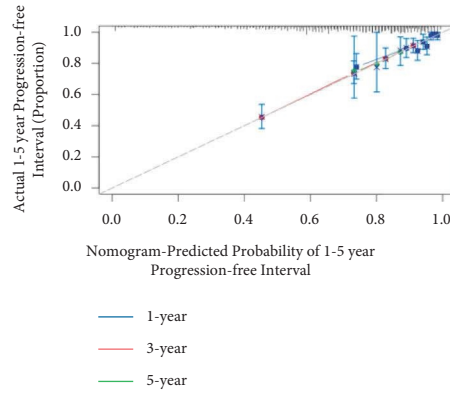
Figure 8: Clinical features and nomogram construction. (a) A boxplot of differences in risk scores across clinical indicators in the TCGA cohort. (b) A boxplot of differences in risk scores across the 1q21 copy number. Group H represents a 1q21 copy number greater than 2, and Group L represents a 1q21 copy number less than 2. (c) Univariate Cox analysis of prognostic clinical indicators. (d) Multivariate Cox analysis of prognostic clinical indicators. (e) Nomogram to predict survival in MM patients. (f) An ROC curve of the prognostic model. (g) The prognostic model evaluated using 1-year, 3-year, and 5-year calibration curves. The x-axis shows survival anticipated from the column plots, while the y-axis shows actual survival.
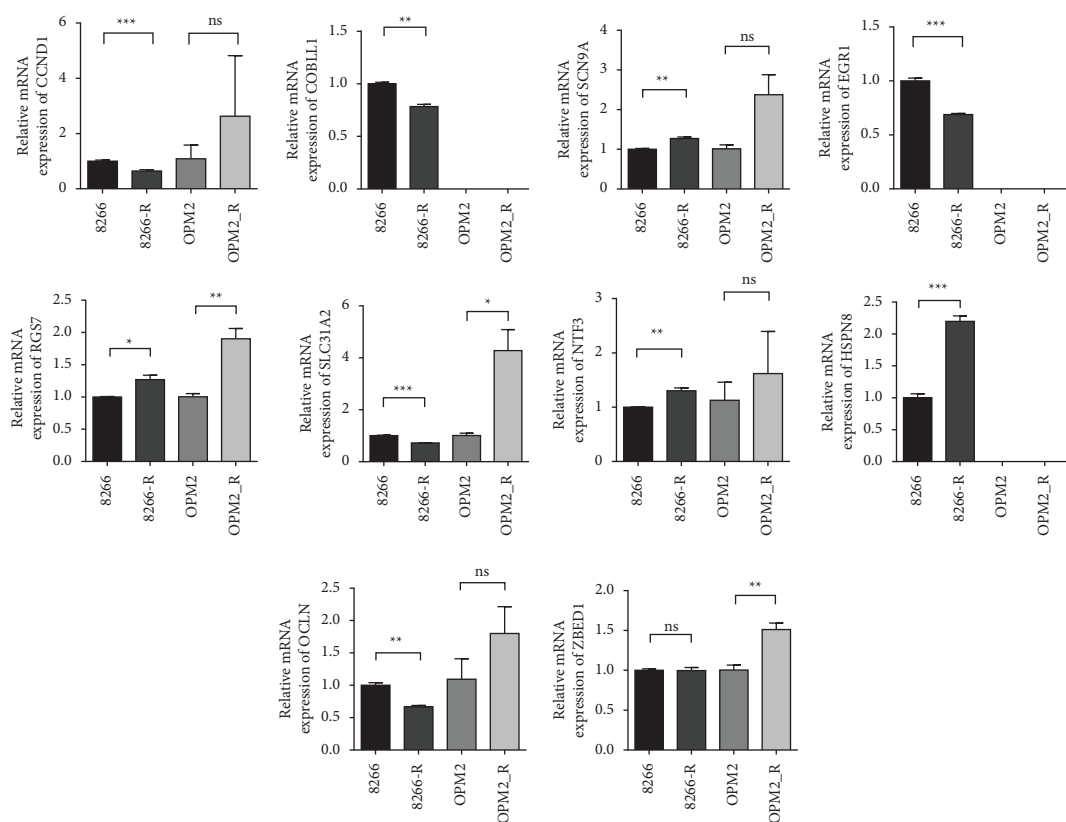
Figure 9: The RT-qPCR results. CCND1, COBLL1, EGR1, OCLN, and ZBED1 expression were low in bortezomib-resistant cell lines, and SCN9A, RGS7, NTF3, HSPB8 and ZBED1 expression were high in bortezomib-resistant cell lines (*$p < 0.05$, **$p < 0.01$, ***$p < 0.001$, ****$p < 0.0001$, ns: no statistical significance, 8266-R: bortezomib-resistant RIPM-8266, OPM2_R: bortezomib-resistant OPM-2).

the type and intensity of inflammatory signals they receive. A high inflammatory state causes MSCs to produce T cell suppression, while a low inflammatory state causes MSCs to produce T cell activation [24]. Ageing MSCs secrete more

inflammation-associated cytokines, and inflammatory cues may scramble the delicate balance of regulatory networks necessary to govern tissue-specific regeneration and remodelling [25]. Since multiple myeloma primarily affects

elderly individuals, we speculate that ageing MSCs play an important role in the tumour microenvironment. We designed this study to identify genes coexpressed by tumour cells and senescent BM-MSCs in an attempt to provide evidence for a link between MSC senescence and MM progression. This research may shed light on future research for the treatment of MM. Perhaps by targeting these genes, it is possible to eliminate tumour cells while also improving the function of BM-MSCs.

In this study, we discovered a set of gene signatures that are essential in predicting MM progression and linked to MSC senescence, suggesting that early prevention of ageing in MSCs could help slow disease progression. The MAPK pathway and DNA repair pathway-related genes have been shown to be independent prognostic factors for high-risk SMM [26], and these pathways have been previously shown to be involved in the progression of myeloma [27–29]. The genes that we screened were also mainly the enriched MAPK pathway, PI3K pathway, and p53 signalling pathway, which further illustrates the relevance of our results to the progression and prognosis of myeloma. Further analysis revealed poor efficacy of immune checkpoint blockade therapy (ICB) in high-risk patients with strong immunogenicity, which suggests that in high-risk patients, the bone marrow microenvironment is extremely inflammatory and resistant to immune checkpoint drugs. We also found that patients with a copy number of 1q21 larger than 2 had a higher risk score, which confirms that grouping based on our model is reasonable. Chemotherapy drug sensitivity analysis shows that high-risk patients are less responsive to proteasome inhibitors. Numerous studies have confirmed the close relationship between MM drug resistance and MSCs. Tumour drug resistance is affected by MSCs through adhesion and paracrine effects [30]. Interestingly, in this study, myeloma cells from patients in the high-risk group were found to express fewer lipid metabolism-related genes than those in the low-risk group. Recent reports confirmed that abnormal lipid accumulation in multiple myeloma cells was enhanced by proteasome inhibitors; lipid-lowering drugs and MG-132 exerted a synergistic effect to kill multiple myeloma cells [31, 32]. These findings suggest that the combination of a lipid metabolism target with a broad-spectrum proteasome inhibitor may be effective in the presence of proteasome inhibitor resistance in high-risk patients as predicted in our model. Finally, we verified 14 genes in the model by RT-qPCR and found that the expression trend of 10 genes in bortezomib-resistant myeloma cell lines was consistent with our prediction. This suggests that these high-risk tumours are associated with drug resistance and that there is an urgent need to develop new drugs or new drug combinations to treat these high-risk patients. In the analysis of gene function, SCN9A, NTF3, and RGS7 tended to promote cell proliferation and migration. More experiments are needed in the future to further explore the role of these genes in MM. Perhaps therapies that target these genes will help improve tumour resistance and patient survival. What is noteworthy is that although SOX11 was not detected, it has been shown to be an important prognostic marker for mantle cell lymphoma and is associated with tumour aggressiveness [33].

Unfortunately, we did not validate this gene in drug-resistant cell lines, probably because of the influence of the in vitro culture environment on the transcriptome of cells or because the cell lines differ significantly from tumour primary cells in terms of genetic background.

The following are some of the study's limitations: First, all of the patient records included in the study were obtained from the GEO database; second, the lack of some crucial clinical data hindered further investigation. BM-MSCs from healthy individuals, cultured in vitro and proven to be senescent, were chosen as targets for differential gene selection in this work because their transcriptomes were influenced by tumour cells in vivo. Only one study's selection of the MSC gene for ageing may have resulted in biased gene selection, while several studies may have introduced batch-to-batch variation.

This is the first study to use the intersection of genes in ageing MSCs with differential genes in myeloma to find biomarkers that represent prognosis. We found genes in tumour cells with the same expression trend observed in MSC senescence that may provide targets for developing therapies capable of treating tumours while improving the ageing status of MSCs. Our research may help advance the development of drugs that not only kill MM cells but also improve the microenvironment. We offer new insights into the clinical diagnosis and treatment of MM, as well as suggestions for further research into the pathogenic mechanisms of drug resistance in myeloma. Overall, this research marks a step towards the ideal of data-driven clinical decision-making, in which better MM treatment options are determined using statistical models.

5. Conclusion

This research uncovered a collection of genes associated with ageing in MSCs that were linked to MM prognosis. The prognostic model was also constructed by incorporating clinical characteristics, which will facilitate individualized treatment. Moreover, the combination of drugs targeting lipid metabolism is expected to be a better treatment option for our predicted high-risk patients.

Data Availability

Raw data used to support the findings of this study are available at https://www.jianguoyun.com/p/DSmHWXMQzd_XChi70McEIAA.

Conflicts of Interest

The authors declare that there are no conflicts of interest.

Authors' Contributions

LTM, CJZ, and QL provided financial support, designed the research, and revised the manuscript. JZ and YHZ helped collect data and gave advice. TL provided the project administration, and YJC designed the research, summarized and analysed the sequencing data, and drafted the manuscript. All authors read and approved the final manuscript.

Acknowledgments

Supplementary Materials

The additional supplemental figure showed survival analysis of records from GEO accession numbers GSE83503 and GSE4581 grouped by the risk model. The validation set (GSE2658) Kaplan–Meier curve (A) and the validation set (GSE4581) Kaplan–Meier curve (B). (*Supplementary Materials*)

References

[1] S. V. Rajkumar, "Multiple myeloma: 2020 update on diagnosis, risk-stratification and management," *American Journal of Hematology*, vol. 95, no. 5, pp. 548–567, 2020.

[2] J. Laubach, P. Richardson, and K. Anderson, "Multiple myeloma," *Annual Review of Medicine*, vol. 62, no. 1, pp. 249–264, 2011.

[3] J. Croft, S. Ellis, A. L. Sherborne et al., "Copy number evolution and its relationship with patient outcome-an analysis of 178 matched presentation-relapse tumor pairs from the Myeloma XI trial," *Leukemia*, vol. 35, no. 7, pp. 2043–2053, 2021.

[4] R. A. Kyle, E. D. Remstein, T. M. Therneau et al., "Clinical course and prognosis of smoldering (asymptomatic) multiple myeloma," *New England Journal of Medicine*, vol. 356, no. 25, pp. 2582–2590, 2007.

[5] M. Chesi, D. F. Robbiani, M. Sebag et al., "AID-dependent activation of a MYC transgene induces multiple myeloma in a conditional mouse model of post-germinal center malignancies," *Cancer Cell*, vol. 13, no. 2, pp. 167–180, 2008.

[6] C. Schinke, P. Qu, S. J. Mehdi et al., "The pattern of mesenchymal stem cell expression is an independent marker of outcome in multiple myeloma," *Clinical Cancer Research*, vol. 24, no. 12, pp. 2913–2919, 2018.

[7] N. F. Andersen, I. B. Kristensen, B. S. Preiss, J. H. Christensen, and N. Abildgaard, "Upregulation of Syndecan-1 in the bone marrow microenvironment in multiple myeloma is associated with angiogenesis," *European Journal of Haematology*, vol. 95, no. 3, pp. 211–217, 2015.

[8] A. Uccelli, L. Moretta, and V. Pistoia, "Mesenchymal stem cells in health and disease," *Nature Reviews Immunology*, vol. 8, no. 9, pp. 726–736, 2008.

[9] H. Lin, J. Sohn, H. Shen, M. T. Langhans, and R. S. Tuan, "Bone marrow mesenchymal stem cells: Aging and tissue engineering applications to enhance bone healing," *Biomaterials*, vol. 203, 2019.

[10] M. M. E. de Jong, Z. Kellermayer, N. Papazian et al., "The multiple myeloma microenvironment is defined by an inflammatory stromal cell landscape," *Nature Immunology*, vol. 22, no. 6, pp. 769–780, 2021.

[11] R. Das, T. Strowig, R. Verma et al., "Microenvironment-dependent growth of preneoplastic and malignant plasma cells in humanized mice," *Nat Med*, vol. 22, no. 11, pp. 1351–1357, 2016.

[12] T. Hideshima, C. Mitsiades, G. Tonon, P. G. Richardson, and K. C. Anderson, "Understanding multiple myeloma pathogenesis in the bone marrow to identify new therapeutic targets," *Nature Reviews Cancer*, vol. 7, no. 8, pp. 585–598, 2007.

[13] C. D. Wiley and J. Campisi, "The metabolic roots of senescence: mechanisms and opportunities for intervention," *Nat Metab*, vol. 3, no. 10, pp. 1290–1301, 2021.

[14] A. K. Dutta, J.-B. Alberge, R. Sklavenitis-Pistofidis, E. D. Lightbody, G. Getz, and I. M. Ghobrial, "Single-cell profiling of tumour evolution in multiple myeloma - opportunities for precision medicine," *Nature Reviews Clinical Oncology*, vol. 19, no. 4, pp. 223–236, 2022.

[15] F. Zhan, Y. Huang, S. Colla et al., "The molecular classification of multiple myeloma," *Blood*, vol. 108, no. 6, pp. 2020–2028, 2006.

[16] A. Broyl, D. Hose, H. Lokhorst et al., "Gene expression profiling for molecular classification of multiple myeloma in newly diagnosed patients," *Blood*, vol. 116, no. 14, pp. 2543–2553, 2010.

[17] N. Weinhold, C. J. Heuck, A. Rosenthal et al., "Clinical value of molecular subtyping multiple myeloma using gene expression profiling," *Leukemia*, vol. 30, no. 2, pp. 423–430, 2016.

[18] J.-B. Alberge, F. Kraeber-Bodere, B. Jamet et al., "Molecular signature of ^{18}F-fdg pet biomarkers in newly diagnosed multiple myeloma patients: a genome-wide transcriptome analysis from the cassiopet study," *Journal of Nuclear Medicine*, vol. 63, no. 7, pp. 1008–1013, 2022.

[19] Y. Kawano, M. Moschetta, S. Manier et al., "Targeting the bone marrow microenvironment in multiple myeloma," *Immunological Reviews*, vol. 263, no. 1, pp. 160–172, 2015.

[20] A. Garcia-Gomez, T. Li, C. de la Calle-Fabregat et al., "Targeting aberrant DNA methylation in mesenchymal stromal cells as a treatment for myeloma bone disease," *Nature Communications*, vol. 12, no. 1, p. 421, 2021.

[21] E. Terpos, I. Ntanasis-Stathopoulos, and M. A. Dimopoulos, "Myeloma bone disease: from biology findings to treatment approaches," *Blood*, vol. 133, no. 14, pp. 1534–1539, 2019.

[22] H. van Andel, K. A. Kocemba, M. Spaargaren, and S. T. Pals, "Aberrant Wnt signaling in multiple myeloma: molecular mechanisms and targeting options," *Leukemia*, vol. 33, no. 5, pp. 1063–1075, 2019.

[23] S. Rizzo, A. Galvano, F. Pantano et al., "The effects of enzalutamide and abiraterone on skeletal related events and bone radiological progression free survival in castration resistant prostate cancer patients: an indirect comparison of randomized controlled trials," *Critical Reviews in Oncology*, vol. 120, pp. 227–233, 2017.

[24] W. Li, G. Ren, Y. Huang et al., "Mesenchymal stem cells: a double-edged sword in regulating immune responses," *Cell Death Differ*, vol. 19, no. 9, pp. 1505–1513, 2012.

[25] G. Lepperdinger, "Inflammation and mesenchymal stem cell aging," *Current Opinion in Immunology*, vol. 23, no. 4, pp. 518–524, 2011.

[26] M. Bustoros, R. Sklavenitis-Pistofidis, J. Park et al., "Genomic profiling of smoldering multiple myeloma identifies patients at a high risk of disease progression," *Journal of Clinical Oncology*, vol. 38, no. 21, pp. 2380–2389, 2020.

[27] J. L. Kaufman, C. Gasparetto, F. H. Schjesvold et al., "Targeting BCL-2 with venetoclax and dexamethasone in patients with relapsed/refractory t(11;14) multiple myeloma," *American Journal of Hematology*, vol. 96, no. 4, pp. 418–427, 2021.

[28] C. Hofmann, T. Stühmer, N. Schmiedl et al., "PI3K-dependent multiple myeloma cell survival is mediated by the PIK3CA isoform," *British Journal of Haematology*, vol. 166, no. 4, pp. 529–539, 2014.

[29] J. Abdi, N. Rastgoo, L. Li, W. Chen, and H. Chang, "Role of tumor suppressor p53 and micro-RNA interplay in multiple myeloma pathogenesis," *Journal of Hematology & Oncology*, vol. 10, no. 1, p. 169, 2017.

[30] P. Robak, I. Drozdz, J. Szemraj, and T. Robak, "Drug resistance in multiple myeloma," *Cancer Treatment Reviews*, vol. 70, pp. 199–208, 2018.

[31] G. Xu, S. Huang, J. Peng et al., "Targeting lipid metabolism in multiple myeloma cells: rational development of a synergistic strategy with proteasome inhibitors," *British Journal of Pharmacology*, vol. 178, no. 23, pp. 4741–4757, 2021.

[32] M. K. Bennett, M. Li, M. N. Tea et al., "Resensitising proteasome inhibitor-resistant myeloma with sphingosine kinase 2 inhibition," *Neoplasia*, vol. 24, no. 1, pp. 1–11, 2022.

[33] A. Mozos, C. Royo, E. Hartmann et al., "SOX11 expression is highly specific for mantle cell lymphoma and identifies the cyclin D1-negative subtype," *Haematologica*, vol. 94, no. 11, pp. 1555–1562, 2009.

Research Article

Integrin α6 Indicates a Poor Prognosis of Craniopharyngioma through Bioinformatic Analysis and Experimental Validation

Yanfei Jia [iD],[1] **Wentao Wu** [iD],[1] **Youchao Xiao** [iD],[1] **Kefan Cai** [iD],[1] **Songbai Gui** [iD],[1] **Qiang Li** [iD],[2] **and Tian Li** [iD][3]

[1]*Department of Neurosurgery, Beijing Tiantan Hospital, Capital Medical University, Beijing 100070, China*
[2]*Department of Neurosurgery, The Second Affiliated Hospital of Lanzhou University, Lanzhou 730000, China*
[3]*School of Basic Medicine, Fourth Military Medical University, Xi'an 710032, China*

Correspondence should be addressed to Songbai Gui; guisongbai@yeah.net, Qiang Li; strong908@163.com, and Tian Li; tian@fmmu.edu.cn

Background. Craniopharyngioma (CP) is a benign slow-growing tumor. It tends to affect children, and the number of patients is on rise. Considering the high morbidity and mortality of CP, it is urgent and pivotal to identify new biomarkers to uncover the etiology and pathogenesis of CP. *Methods*. The "limma" package was utilized to calculate the data from the Gene Expression Omnibus (GEO) database. Based on differentially expressed genes (DEGs), gene ontology and pathway analysis were deduced from the DAVID web tool. Further, we constructed a protein-protein interaction (PPI) network. Weighted correlation network analysis (WGCNA) was utilized to build a coexpression network. Finally, Western blotting and survival analysis were performed to examine the expression level of important metabolism-related genes. *Results*. Three hundred and eighty-four DEGs were identified between normal tissues and CPs from the GSE94349 and GSE26966 datasets. The Venn diagram for DEGs and hub genes in the 'turquoise' module revealed four key genes. Finally, the outcome of the survival analysis suggested that Integrin α6 (ITGA6) significantly affected the overall survival time of the patients with CP. *Conclusion*. IGTA6, as a metabolism-related molecule, was found to be substantially related to the overall survival of patients with CP.

1. Introduction

Craniopharyngioma (CP) is a locally aggressive tumor with a low histological grade (WHO I grade) [1], mostly occurs in the sellar and suprasellar regions [2]. Globally, the incidence rate of CP in children's ranged the third of intracranial tumors and it is also the most common nonneuroepithelial neoplasm in the hypothalamus and pituitary regions [3]. Despite the benign histologic appearance [4], due to invasion to important structures around the tumor, such as the optic chiasma, Willis ring, pituitary, and hypothalamus [5], hence, symptoms and signs of hypothalamic and pituitary dysfunctions are evident in patients with CP. Currently, surgery is the most effective treatment; however, the complexity of CP creates challenges for surgery treatment and leads to a high mortality rate. Difficulties still exist in the removal of the tumor owing to the anatomical structure adjacent to the suprasellar region and adhesion around tumor with the surrounding tissues. Some controversies regarding the etiology, histology, and pathology of CP, as also the optimal treatment strategy persist [3]. In short, it is urgent and important to identify new biomarkers to uncover the etiology and pathogenesis of CP.

Microarray-based high-throughput platform is a promising and efficient technique, which is widely used to screen epigenetic or genetic alternations and identify cancer biomarkers [6, 7]. Comprehensive calculation of data provides

(a)
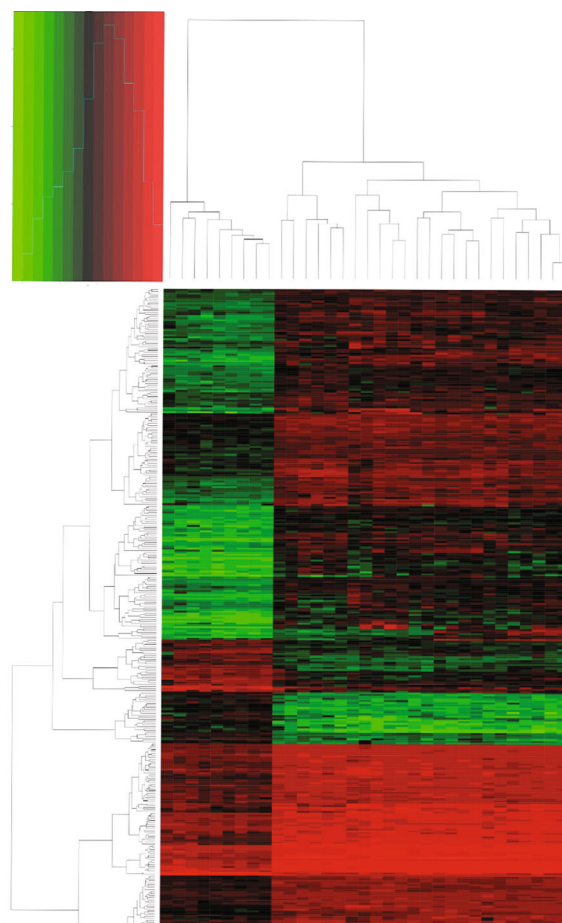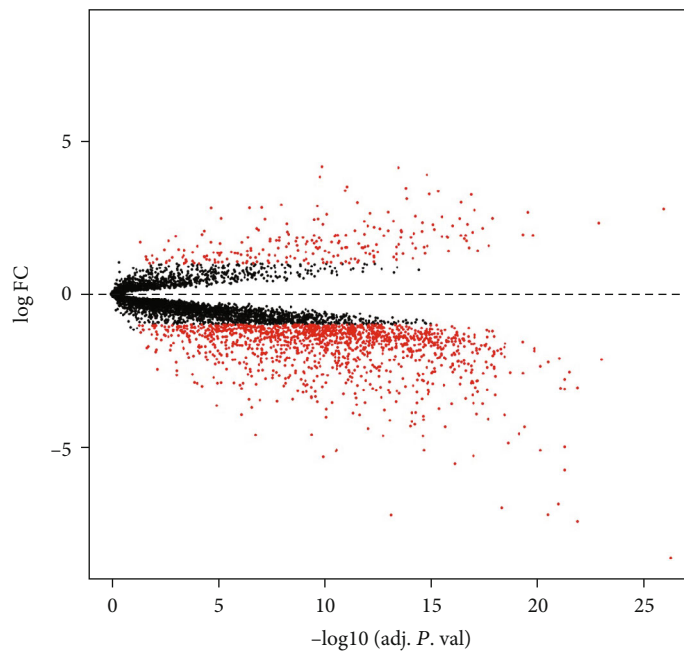
(b)

FIGURE 1: Heatmap and volcano plot of DEGs. (a) Heatmap of the differently expressed genes according to the values of |logFC| > 2. (b) Volcano map of differently expressed genes between CP tissues and normal pituitary tissues.

TABLE 1: Gene ontology analysis for aberrant differentially expressed genes in craniopharyngioma.

Category	Term	Count	%	p value
Low expression				
GOTERM_BP_DIRECT	GO:1902018 ~ negative regulation of cilium assembly	2	3.64	0.01697
GOTERM_BP_DIRECT	GO:0072577 ~ endothelial cell apoptotic process	2	3.64	0.01697
GOTERM_BP_DIRECT	GO:0006355 ~ regulation of transcription, DNA-templated	9	16.36	0.02695
GOTERM_BP_DIRECT	GO:0070588 ~ calcium ion transmembrane transport	3	5.45	0.034121
GOTERM_BP_DIRECT	GO:0042462 ~ eye photoreceptor cell development	2	3.64	0.043071
High expression				
GOTERM_CC_DIRECT	GO:0005925 ~ focal adhesion	30	9.35	$5.60E-12$
GOTERM_CC_DIRECT	GO:0070062 ~ extracellular exosome	90	28.12	$2.77E-11$
GOTERM_CC_DIRECT	GO:0009986 ~ cell surface	28	8.75	$1.64E-07$
GOTERM_CC_DIRECT	GO:0005615 ~ extracellular space	46	14.35	$1.51E-06$
GOTERM_CC_DIRECT	GO:0031012 ~ extracellular matrix	18	5.63	$5.44E-06$
GOTERM_BP_DIRECT	GO:0007155 ~ cell adhesion	28	8.75	$1.07E-08$
GOTERM_BP_DIRECT	GO:0030198 ~ extracellular matrix organization	17	5.31	$1.58E-07$
GOTERM_BP_DIRECT	GO:0016337 ~ single organismal cell-cell adhesion	9	2.81	$2.60E-04$
GOTERM_BP_DIRECT	GO:0071404 ~ cellular response to low-density lipoprotein particle stimulus	4	1.25	$3.43E-04$
GOTERM_BP_DIRECT	GO:0042060 ~ wound healing	8	2.50	$3.43E-04$
GOTERM_MF_DIRECT	GO:0050839 ~ cell adhesion molecule binding	8	2.50	$5.23E-05$
GOTERM_MF_DIRECT	GO:0001948 ~ glycoprotein binding	8	2.50	$7.12E-05$
GOTERM_MF_DIRECT	GO:0004871 ~ signal transducer activity	13	4.06	$9.79E-05$
GOTERM_MF_DIRECT	GO:0098641 ~ cadherin binding involved in cell-cell adhesion	15	4.69	$2.15E-04$
GOTERM_MF_DIRECT	GO:0005515 ~ protein binding	166	51.88	$5.92E-04$

key avenues to explore the mechanisms of tumors [8]. Several gene expression profiling microarrays have been employed to identify the differentially expressed genes (DEGs) in CP, and some bioinformatic methods have been used to analyze the data. In this study, we processed raw data of CP samples in the GSE94349 and GSE26966 datasets downloaded from GEO. DEGs were analyzed, and WGCNA was performed to elucidate the possible mechanisms underlying CP more clearly.

2. Methods

2.1. Microarray Data. Two gene expression profiling datasets (GSE94349 and GSE26966 from GPL55999 platform), acquired from the GEO, comprise 9 normal pituitary tissues and 9 CP tissues. The two datasets were chosen for integrated analysis owing to their same platform.

2.2. Data Processing. We used the 'limma' package (V3.29.0) with standard data processing conditions to identify DEGs. The cut-off criteria were $p < 0.05$ and $|\text{logFC}| \geq 2$. Subsequently, the DEGs were analyzed by Gene Ontology (GO) term enrichment analysis and Kyoto Encyclopedia of Genes and Genomes (KEGG) pathway analysis using the 'clusterprofiler' package (V4.4.3) in R V3.5.5. The protein-protein interaction (PPI) network was constructed using STRING Database (http://string-db.org/) and the Cytoscape software. Subsequently, the WGCNA package (V1.61) was employed

to search the correlations among genes and identify the significantly correlated gene modules. The soft thresholding power was set at 6.

2.3. GO Term Annotation and KEGG Pathway Enrichment Analyses. We utilized clusterProfiler to perform GO and KEGG analyses, for a detailed comprehension of the DEGs. $p < 0.05$ was considered a significant enrichment.

2.4. Protein-Protein Interaction (PPI) Network Construction. The DEGs used for constructing PPI network were obtained through the 'limma' package. The Cytoscape software (V3.8.1) was thereafter employed to analyze the interactive relationships among the candidate proteins [9]. The "Molecular Complex Detection" (MCODE) module (V2.0.2) was used to detect densely connected regions in large PPI networks that may represent molecular complexes [10].

2.5. Weighted Correlation Network Analysis (WGCNA). Weighted correlation network analysis (WGCNA) was used for identifying modules of highly correlated genes, summarizing clusters using the module eigengenes or an intramodular hub gene, and correlating modules to one another and to the external sample traits (using eigengene network methodology) [11]. We used the WGCNA package to construct the gene coexpression network, identify modules, and finally obtain the genes in the modules of interest.

Table 2: Results of KEGG enrichment for the differentially expressed genes.

Category	Term	Count	%	p value	Genes
Low expression					
KEGG_PATHWAY	hsa04972: pancreatic secretion	3	5.454545	0.009187	CEL, ATP2B3, GNAS
KEGG_PATHWAY	hsa04261: adrenergic signaling in cardiomyocytes	3	5.454545	0.019518	ATP2B3, CACNB2, GNAS
High expression					
KEGG_PATHWAY	hsa05200: pathways in cancer	18	5.625	$1.66E-04$	PTGER3, PTGS2, ERBB2, CDH1, GLI3, MMP2, CTNNB1, JUP, MAPK1, CBLC, ITGA6, RAC2, JUN, SLC2A1, RAC1, LAMC1, HHIP, FGF1
KEGG_PATHWAY	hsa04510: focal adhesion	14	4.375	$2.41E-05$	ERBB2, TNC, ITGB5, FLNA, MYL9, CTNNB1, MAPK1, ITGA6, RAC2, JUN, RAC1, LAMC1, SPP1, PARVA
KEGG_PATHWAY	hsa05205: proteoglycans in cancer	13	4.0625	$8.27E-05$	LUM, ERBB2, ITGB5, TLR4, MMP2, FLNA, CTNNB1, CBLC, MAPK1, SDC1, CD44, RAC1, MSN
KEGG_PATHWAY	hsa04151: PI3K-Akt signaling pathway	12	3.75	0.022876	MAPK1, SGK1, YWHAZ, ITGA6, TNC, RAC1, YWHAB, ITGB5, TLR4, LAMC1, FGF1, SPP1
KEGG_PATHWAY	hsa04810: regulation of actin cytoskeleton	11	3.4375	0.001989	MAPK1, ENAH, ITGA6, RAC2, CHRM3, RAC1, ITGB5, ITGB2, MSN, FGF1, MYL9
KEGG_PATHWAY	hsa05412: arrhythmogenic right ventricular cardiomyopathy (ARVC)	8	2.5	9.23E-05	JUP, ITGA6, DSG2, ITGB5, GJA1, DSP, CACNA2D3, CTNNB1

Table 3: The six clusters obtained from module analysis using MCODE.

Cluster	Score (density*#nodes)	Nodes	Edges	Node IDs
1	6	9	24	CCL5, PPBP, APLNR, ANXA1, GPR65, F2RL1, PTGER3, CHRM3, APP
2	5	5	10	GBP6, HLA-DPA1, HLA-DPB1, CD44, IRF6
3	4.5	5	9	TOP2A, ENTPD3, RRM1, TYMS, RRM2
4	4	4	6	XYLT1, BGN, SDC1, CSPG4
5	3	3	3	LRRFIP1, FGF1, ERLIN2
6	3	3	3	ITGA6, YWHAB, YWHAZ

2.6. *Identification of Key Genes.* The final key genes were identified as the intersecting genes between those in the 'turquoise' module from WGCNA and DEGs.

2.7. *Tissue Collection.* A total of 21 human CP tissues were acquired from the patients, and 10 normal pituitary tissues from other patients with common pediatric brain tumor types. No local or systematic neoadjuvant radiotherapy, or/ and chemotherapy, and targeted therapy were managed. The study design was approved by the Research Ethics Committee of Lanzhou University (Lanzhou, Gansu, PR China) and all patients enrolled in this study provided signed informed consent.

2.8. *Western Blotting.* Initially, we selected four of the 21 human CP tissues and four normal pituitary tissues, as previously described. Total proteins of each sample were extracted with Cell lysis buffer for Western and IP (Beyotime Biotechnology, China), followed by quantification using

bicinchoninic acid (BCA) kit (Beyotime Biotechnology, China). After being separated by 10% sodium dodecyl sulfate polyacrylamide gel electrophoresis (SDS-PAGE), the total protein was transferred onto the polyvinylidene fluoride (PVDF) membranes (Beyotime Biotechnology, China) which were then blocked for 1 h. Thereafter, the membranes were incubated first with primary antibodies against at 4°C overnight and then with a horseradish peroxidase-conjugated secondary antibody for 2 h. Later, protein-antibody complexes were visualized and analyzed using ECL chemiluminescent solution (Beyotime Biotechnology, China). Finally, the ImageJ software (Rawak Software, Germany) and GraphPad Prism (version 7, GraphPad Software, San Diego, USA) were used to analyze the grayscale values of the bands.

2.9. *Survival Analysis.* The survival analysis was performed of all 21 CP samples using the SPSS version 22.0 software (IBM Corp. Chicago, IL, USA). Kaplan-Meier curve and
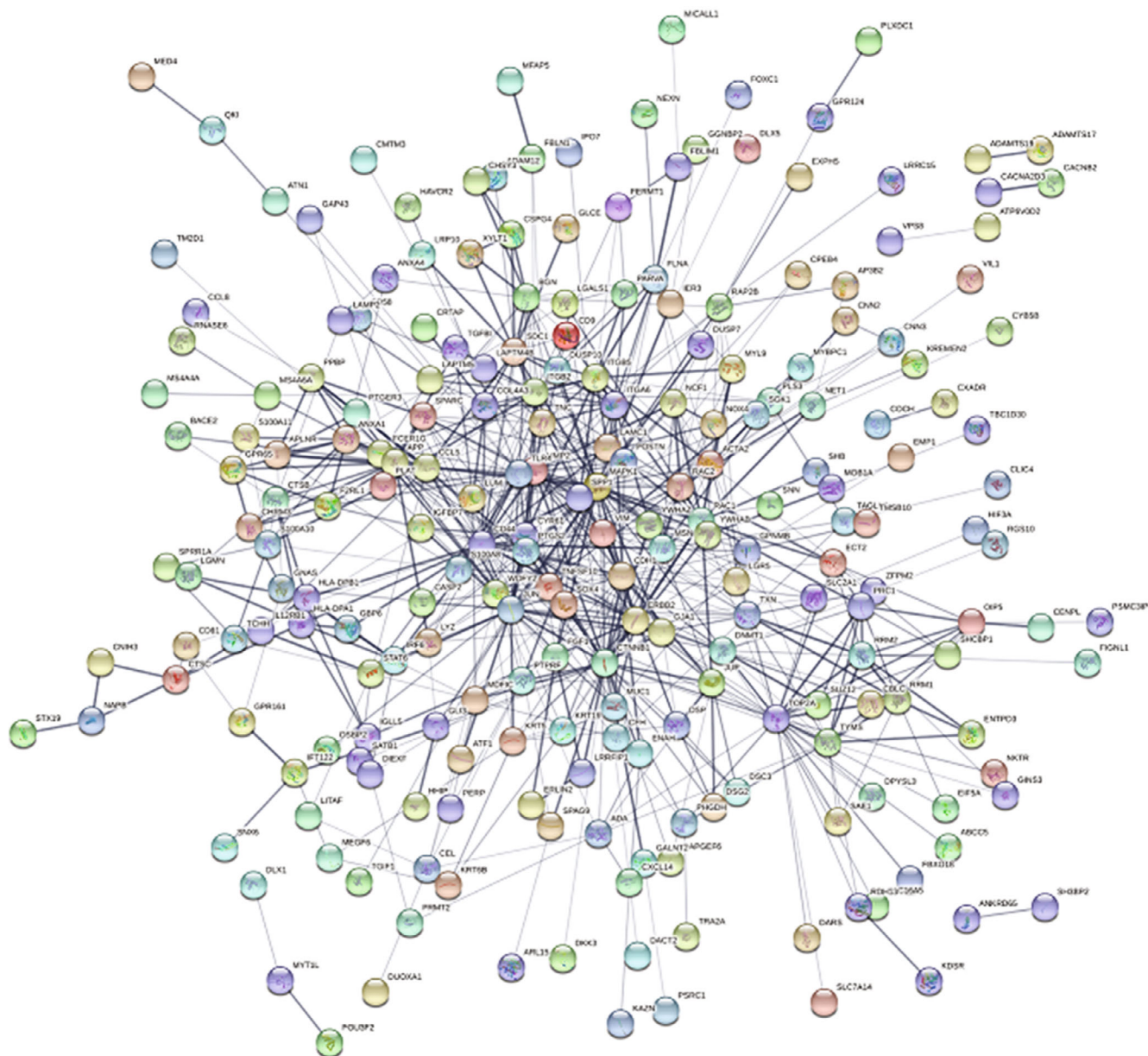
FIGURE 2: Cluster analysis of the PPI network. Three-hundred and differently eighty-four expressed genes were filtered into the DEGs' PPI network complex.

Cox's proportional hazards regression model were performed to analyze the overall survival, and the differences were analyzed for significance using the log-rank test. The statistically significant modules were defined as those with $p < 0.05$.

3. Results

3.1. Identification of Aberrant DEGs in CP.
We used the 'limma' package with the preprocessing parameters to analyze and obtain the DEGs among the GSE94349 and GSE26966 datasets. Using $p < 0.05$ and $|logFC| \geq 2$ as the threshold criteria, a total of 384 DEGs were identified, including 56 downregulated and 328 upregulated genes in CP tissues as compared to the normal pituitary tissues

(Figure 1(a)). These DEGs are shown in the volcano map (Figure 1(b)).

3.2. GO Functional Enrichment Analysis.
Significant terms from GO enrichment analysis using DAVID are listed in Table 1. All the significant genes with a low expression are listed in the table. These genes were enriched in the biological processes (BP) involved in negative regulation of cilium assembly, endothelial cell apoptosis, regulation of transcription, DNA template, calcium ion transmembrane transport, and eye photoreceptor cell development. The results from DAVID analyses showed that there were no genes with a low expression enriched in molecular functions (MF) and cell components (CC). For the genes with a high expression, Table 1 shows the corresponding top five significant GO

(a)

(b)

Figure 3: Continued.

Network heatmap plot, selected genes

(c)

Module membership vs. gene significance
cor = 0.99, $p < 1e-200$
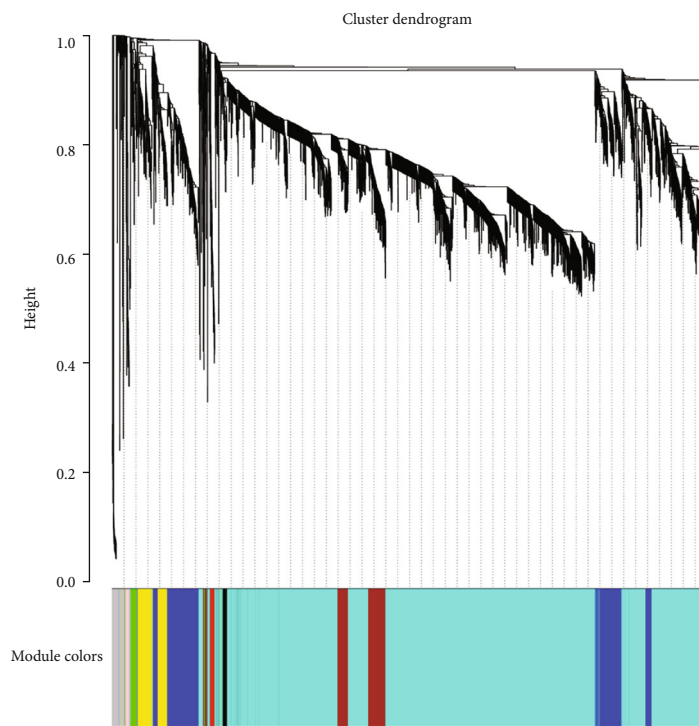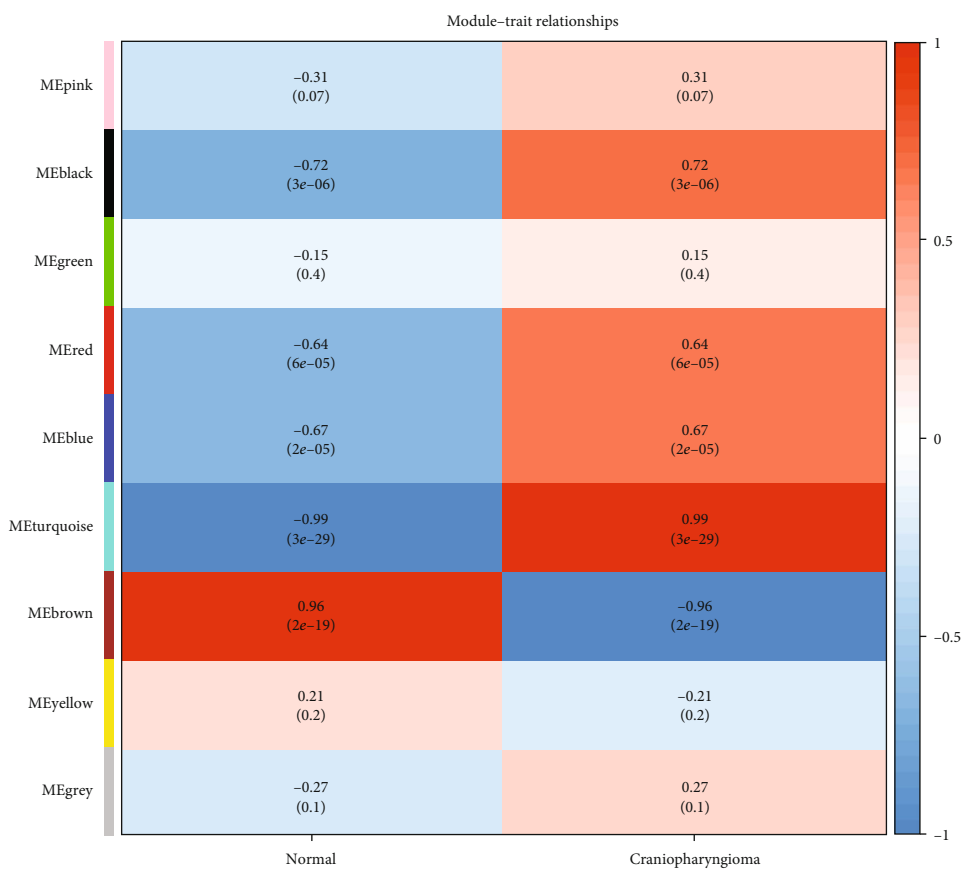
(d)
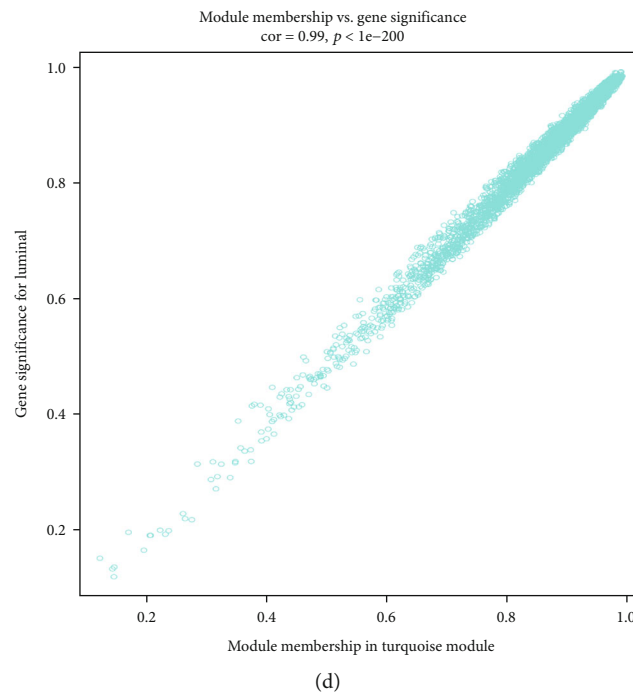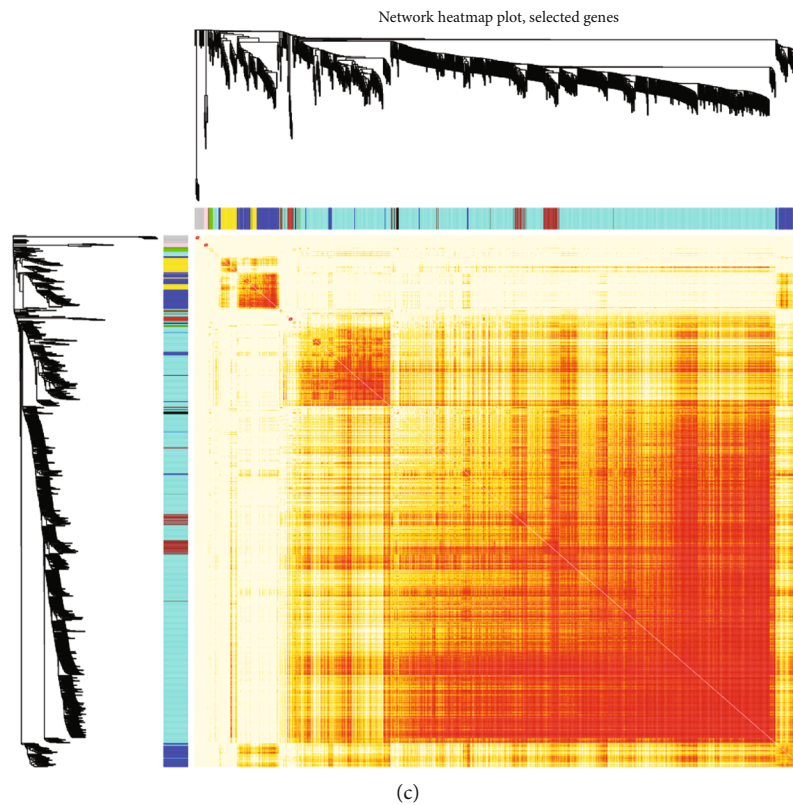
FIGURE 3: WGCNA for the GSE94349 and GSE26966 datasets. (a) The top image shows a gene dendrogram, and the bottom image shows the gene modules with different colors. (b) Correlation between modules and traits. The upper number in each cell refers to the correlation coefficient of each module in the trait, and the lower number is the corresponding p value. Among them, the turquoise modules were the most relevant modules with cancer traits. (c) A heatmap of 1,000 genes was selected at random. The intensity of the red color indicates the strength of the correlation between pairs of modules on a linear scale. (d) A scatter plot of CP tissues and normal pituitary tissues in the turquoise module. Intramodular analysis of the genes found in the turquoise module, which contains genes that have a high correlation with cervical cancer, with $p < 1e - 200$ and correlation = 0.99.

enrichment terms analyzed in DAVID. Molecular functions were enriched in cell adhesion molecule binding,

	C1	C2	C3	C4	T1	T2	T3	T4
IGTA6 (CD49f)	+++	+++	++	+++	+++	–	–	+
SDC1	+++	+	+++	++	++	+	+	+
PPBP (CLCX7)	++	++	+	++	+	+	+	+
CD44	+++	+++	+	+	++	++	+	–

(a)   (b)
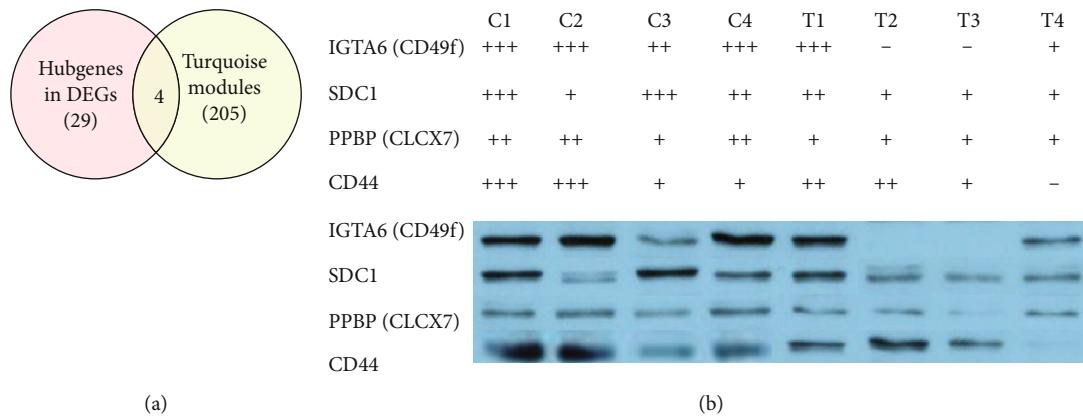
FIGURE 4: The key intersecting genes obtained from Venn diagram of DEGs and verified by Western blot. (a) A Venn diagram of DEGs and hub genes in the turquoise module shows 4 key intersecting genes. (b) Results verified by Western blot and obtained from the selected 8 samples. Abbreviations: C1-C4: craniopharyngioma tissues No.1-No.4; P1-P4: pituitary tissues No.1-No.4.
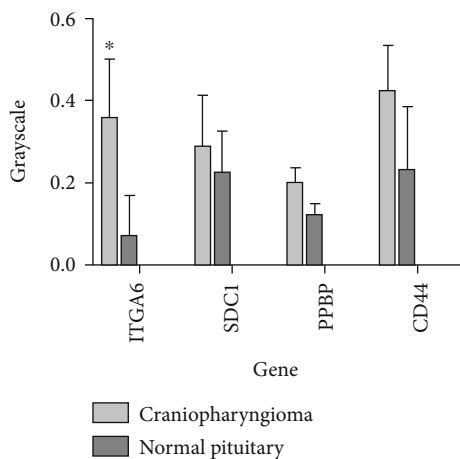
FIGURE 5: Grayscale value analysis for Western blotting. PPBP (CXCL7), CD44, SDC1, and ITGA6 (CD49f) protein levels are shown for the craniopharyngioma tissues and pituitary tissues. $*p$ value < 0.05.

glycoprotein binding, signal transducer activity, cadherin binding involved in cell-cell adhesion, and protein binding. Additionally, cellular component enrichment was found in focal adhesion, extracellular exosome, cell surface, extracellular space, and extracellular matrix while biological processes enrichment was found in cell adhesion, extracellular matrix organization, single organismal cell-cell adhesion, cellular response to low-density lipoprotein particle stimulus, and wound healing.

3.3. KEGG Pathway Analysis. As shown in Table 2, the results of KEGG suggested genes with a low expression were significantly enriched in pathways including adrenergic signaling and pancreatic secretion in cardiomyocytes. Genes with a high expression demonstrated enrichment in pathways of cancer, focal adhesion, proteoglycans in cancer, leishmaniasis, lysosome, PI3K-Akt signaling, and arrhythmogenic right ventricular cardiomyopathy (ARVC).

3.4. PPI Network and Cluster Analysis. The PPI network was constructed using the STRING database. The Cytoscape software was used to analyze the interactive relationships among the candidate proteins. Module analysis was conducted using MCODE (Table 3). In the clusters, the following 29 genes: CCL5/PPBP/APLNR/ANXA1/GPR65/F2RL1/PTGER3/CHRM3/APP/GBP6/HLA-DPA1/HLA-DPB1/CD44/IRF6/TOP2A/ENTPD3/RRM1/TYMS/RRM2/XYLT1/BGN/SDC1/CSPG4/LRRFIP1/FGF1/ERLIN2/ITGA6/YWHAB/YWHAZ, were found to form the hub according to the MCODE findings (Figure 2).

3.5. WGCNA. Among the modules, the 'turquoise' one was found to be the most relevant for the cancer traits (Figures 3(a) and 3(b)). A total of 1,000 genes were selected at random for plotting the heatmap (Figure 3(c)). As shown in Figure 3(d), the 'turquoise' module showed a high correlation. The genes in this module were then selected as the hub genes with a cut-off of correlation ≥ 0.5. Finally, 205 hub genes were identified from the chosen 'turquoise' module.

3.6. Key Genes Identified among Hub Genes in Turquoise Module and DEGs. To obtain valuable clues from these data, key genes were identified from among the hub genes in the turquoise module and DEGs. In total, four key genes were obtained, namely PPBP, CD44, SDC1, and ITGA6 (Figure 4(a)).

3.7. Western Blotting and the Survival Curve Analyses. From the selected 8 tissues, only ITGA6 showed a low expression in all normal pituitary tissues (Figure 4(b)). Besides, in the tissues C1, C2, and C4, ITGA6 was overexpressed. As shown in Figure 5, the expression of ITGA6 was significantly different between the CP and pituitary tissues.

Further, survival analysis for these four genes was employed to evaluate their effects on the overall survival of patients with CP. No significant differences were obtained in patients with CP showing differential levels of CD44, SDC1, and PPBP expressions (Figures 6(a)–6(c)). The results of the survival analysis indicated that the overall
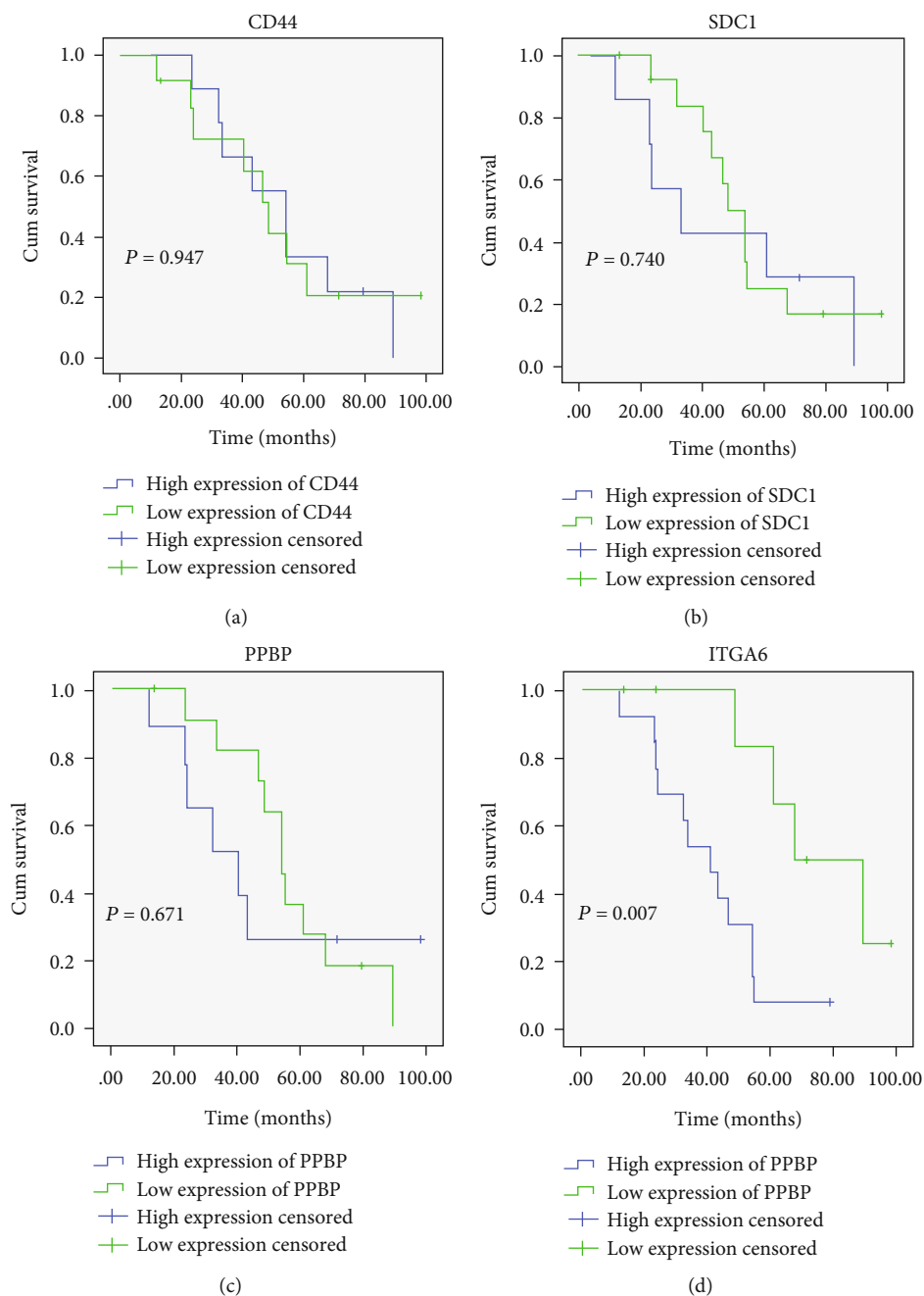
FIGURE 6: Survival analysis according to the levels of CD44, SDC1, PPBP, and ITGA6 expressions. (a) Effects of CD44 expression on craniopharyngioma patient survival. (b) Effects of SDC1 expression on craniopharyngioma patient survival. (c) Effects of PPBP expression on craniopharyngioma patient survival. (d) Effects of ITGA6 expression on craniopharyngioma patient survival.

survival time of CP pantients could have significant differences between the high ITGA6 expression group and low ITGA6 expression group (Figure 6(d)).

4. Discussion

4.1. Main Finding. Neoplasm remains the main leading cause of death worldwide. Although CP is a benign slow-growing tumor [12], it appears partially aggressive and has an arachnoid interface with surrounding structures, thus rendering it incurable [12–15]. Hence, studies on invasion and the migration of CP are becoming increasingly popular. Previous studies show that the tumor microenvironment of craniopharyngioma has some particular characteristics, such as infiltration of leukocytes, a local abundance of adenosine triphosphate (ATP) and elevated levels of proinflammatory cytokines that are thought to be responsible for the local invasion. Yin et al. show that CXCL12/CXCR4 promotes proliferation, migration, and invasion of adamantinomatous CP via the PI3K/AKT signaling pathway [16]. In this study, using the GEO datasets and clinical samples, we aimed to identify new prognosis predictors for this disease.

4.2. Interpretation. Herein, we collected two GEO datasets and performed an integrated analysis using both DEGs and WGCNA to obtain valuable clues. A total of 384 DEGs were identified, including 56 downregulated genes and 328 upregulated genes in CP tissues compared to normal tissues. Enrichment analyses using GO annotation and KEGG pathways were subsequently performed to further analyze the functions of these genes. As suggested by the results of the DAVID analysis, genes with a high expression in CP tissues were enriched in biological processes of pathways in cell adhesion, extracellular matrix organization, and wound healing. Molecular functions from GO analysis showed enrichment in cell adhesion molecule binding, glycoprotein binding, and protein binding. This was reasonable as frequent cellular proliferation and loss of cell adhesion are hallmarks of malignant diseases including CP [17]. The results of the KEGG pathway enrichment analysis suggested significant enrichment in pathways including PI3K-Akt signaling and regulation of actin cytoskeleton. This was consistent with the fact that PI3K-Akt signaling is known to be frequently dysregulated in CP [16].

Four key genes identified from among the hub genes, PPBP (CXCL7), CD44, SDC1, and ITGA6 (CD49f), were selected for further experimental analyses. A total of four CP and four normal pituitary samples were processed for Western blotting, and we found the differential expressions of the four tested genes. After analyzing the results of Western blotting, ITGA6 was selected as the target gene to perform survival analysis.

Many studies show that ITGA6 is overexpressed in several carcinomas, including breast cancer, colorectal cancer, kidney cancer, and gallbladder carcinoma [18–20]. Moreover, the overexpression of ITGA6 suggests a poor prognosis in breast, colorectal, kidney, and gallbladder cancers. For instance, Zhang et al. report that ITGA6 overexpression is associated with invasion, metastases, and poor prognoses in human gallbladder carcinoma [19]. Several studies suggest that ITGA6 expression is associated with the progression and invasion of malignant lesions [21, 22].

Several researchers have invented new ways to inhibit the growth of cancers by targeting ITGA6 [23–25]. Wang et al. have successfully shown that miR-127-3p inhibits cellular growth and invasiveness by targeting ITGA6 in human osteosarcoma [24]. Laudato et al. report that P53-induced miR-30e-5p inhibits colorectal cancer invasion and metastases by targeting ITGA6 and ITGB1 [25]. However, the importance of ITGA6 in the CP remains unknown. Our findings demonstrated that the overexpression of ITGA6 was associated with the overall survival of patients with CP. The present study is, to the best of our knowledge, the first to investigate the association among the important biomarkers and characteristics of CP. Herein, the survival analysis indicated that ITGA6 was a poor prognostic factor for CP, which means patients with a high expression of ITGA6 had a significantly shorter overall survival relative to those with a low expression ($p = 0.007$).

4.3. Limitations. Although we found that IGTA6 affected the overall survival of patients with CP, some limitations to this investigation should be acknowledged. Further molecular experiments are needed to confirm the findings on the importance of ITGA6 for cellular invasion and proliferation in CP. Moreover, the regulatory factors for the expression of ITGA6 and the underlying pathways need further elucidation. For instance, Zhang et al. show that Twist2 promotes proliferation and invasion of kidney cancer cells by regulating ITGA6 and CD44 expressions in the ECM-receptor-interaction pathway [26]. We plan to address these in the future.

4.4. Conclusion. Several studies have been conducted over the past few years to investigate the pathogenesis of CP, yet little is known about the formation and progression of this disease [27–32]. In summary, our findings indicated that ITGA6 was significantly correlated with the survival of the patients. Moreover, it can serve as a clinical prognostic marker for CP. Further experiments shall be performed in the future to confirm our findings.

Data Availability

The datasets used and/or analyzed during the current study are available from corresponding author.

Ethical Approval

The study was approved by the Ethics Committee of Lanzhou University.

Consent

Written informed consent was obtained from all participants and their guardians.

Conflicts of Interest

The authors declare that they have no conflicts of interest.

Authors' Contributions

Writing was done by Yanfei Jia and Wentao Wu. Experiments were performed by Youchao Xiao, Lei Cao, and Ning Qiao. Manuscript revision was done by Shijia Zhai. Figure design and statistics were done by Kefan Cai and Songbai Gui. Idea and supervision were provided by Qiang Li and Tian Li. Yanfei Jia and Wentao Wu contributed equally to this work.

Acknowledgments

References

[1] A. M. M. Daubenbüchel and H. L. Müller, "Neuroendocrine disorders in pediatric craniopharyngioma patients," *Journal of Clinical Medicine*, vol. 4, no. 3, pp. 389–413, 2015.

[2] M. E. Sughrue, I. Yang, A. J. Kane et al., "Endocrinologic, neurologic, and visual morbidity after treatment for craniopharyngioma," *Journal of Neuro-Oncology*, vol. 101, no. 3, pp. 463–476, 2011.

[3] J. Zhu and C. You, "Craniopharyngioma: Survivin expression and ultrastructure," *Oncology Letters*, vol. 9, no. 1, pp. 75–80, 2015.

[4] P. K. Brastianos and S. Santagata, "BRAF V600E mutations in papillary craniopharyngioma," *European Journal of Endocrinology*, vol. 174, no. 4, pp. R139–R144, 2016.

[5] L. Iughetti and P. Bruzzi, "Obesity and craniopharyngioma," *Italian Journal of Pediatrics*, vol. 37, no. 1, pp. 1–6, 2011.

[6] R. Edgar and T. Barrett, "NCBI GEO standards and services for microarray data," *Nature Biotechnology*, vol. 24, no. 12, pp. 1471-1472, 2006.

[7] S. E. Wilhite and T. Barrett, "Strategies to explore functional genomics data sets in NCBI's GEO database," *Methods in Molecular Biology (Clifton, Nj)*, vol. 802, pp. 41–53, 2012.

[8] L. Xia, X. Su, J. Shen et al., "ANLN functions as a key candidate gene in cervical cancer as determined by integrated bioinformatic analysis," *Cancer Management and Research*, vol. 10, pp. 663–670, 2018.

[9] G. Su, J. H. Morris, B. Demchak, and G. D. Bader, "Biological network exploration with Cytoscape 3," *Current Protocols in Bioinformatics*, vol. 47, pp. 8–13, 2014.

[10] G. D. Bader and C. W. Hogue, "An automated method for finding molecular complexes in large protein interaction networks," *BMC Bioinformatics*, vol. 4, no. 1, pp. 1–27, 2003.

[11] P. Langfelder and S. Horvath, "WGCNA: an R package for weighted correlation network analysis," *BMC Bioinformatics*, vol. 9, no. 1, pp. 1–13, 2008.

[12] M. R. Garnett, S. Puget, J. Grill, and C. Sainte-Rose, "Craniopharyngioma," *Orphanet Journal of Rare Diseases*, vol. 2, p. 18, 2007.

[13] Y. Liu, S. T. Qi, C. H. Wang et al., "Pathological relationship between adamantinomatous craniopharyngioma and adjacent structures based on QST classification," *Journal of Neuropathology and Experimental Neurology*, vol. 77, no. 11, pp. 1017–1023, 2018.

[14] M. B. S. Lopes, "The 2017 World Health Organization classification of tumors of the pituitary gland: a summary," *Acta Neuropathologica*, vol. 134, no. 4, pp. 521–535, 2017.

[15] J. Nie, G. L. Huang, S. Z. Deng et al., "The purine receptor P2X7R regulates the release of pro-inflammatory cytokines in human craniopharyngioma," *Endocrine-Related Cancer*, vol. 24, no. 6, pp. 287–296, 2017.

[16] X. Yin, Z. Liu, P. Zhu, Y. Wang, Q. Ren, H. Chen et al., "CXCL12/CXCR4 promotes proliferation, migration, and invasion of adamantinomatous craniopharyngiomas via PI3K/AKT signal pathway," *Journal of Cellular Biochemistry*, vol. 120, no. 6, pp. 9724–9736, 2019.

[17] J. Liu, H. Li, L. Sun, Z. Wang, C. Xing, and Y. Yuan, "Aberrantly methylated-differentially expressed genes and pathways in colorectal cancer," *Cancer Cell International*, vol. 17, no. 1, pp. 1–10, 2017.

[18] H. J. Zhang, J. Tao, L. Sheng et al., "Twist2 promotes kidney cancer cell proliferation and invasion by regulating ITGA6 and CD44 expression in the ECM-receptor interaction pathway," *OncoTargets and Therapy*, vol. 9, p. 1801, 2016.

[19] D. H. Zhang, Z. L. Yang, E. X. Zhou et al., "Overexpression of Thy1 and ITGA6 is associated with invasion, metastasis and poor prognosis in human gallbladder carcinoma," *Oncology Letters*, vol. 12, no. 6, pp. 5136–5144, 2016.

[20] E. Herring, S. Kanaoka, É. Tremblay, and J. F. Beaulieu, "Droplet digital PCR for quantification of ITGA6 in a stool mRNA assay for the detection of colorectal cancers," *World Journal of Gastroenterology*, vol. 23, no. 16, pp. 2891–2898, 2017.

[21] V. Carloni, A. Mazzocca, P. Pantaleo, C. Cordella, G. Laffi, and P. Gentilini, "The integrin, alpha6beta1, is necessary for the matrix-dependent activation of FAK and MAP kinase and the migration of human hepatocarcinoma cells," *Hepatology*, vol. 34, no. 1, pp. 42–49, 2001.

[22] S. O. Yoon, S. Shin, and E. A. Lipscomb, "A novel mechanism for integrin-mediated ras activation in breast carcinoma cells: the alpha6beta4 integrin regulates ErbB2 translation and transactivates epidermal growth factor receptor/ErbB2 signaling," *Cancer Research*, vol. 66, no. 5, pp. 2732–2739, 2006.

[23] J. Yuan, P. Li, H. Pan, Y. Li, Q. Xu, T. Xu et al., "miR-542-5p attenuates fibroblast activation by targeting integrin alpha6 in silica-induced pulmonary fibrosis," *International Journal of Molecular Sciences*, vol. 19, no. 12, p. 3717, 2018.

[24] D. Wang, L. Tang, H. Wu, K. Wang, and D. Gu, "MiR-127-3p inhibits cell growth and invasiveness by targeting ITGA6 in human osteosarcoma," *IUBMB Life*, vol. 70, no. 5, pp. 411–419, 2018.

[25] S. Laudato, N. Patil, M. L. Abba et al., "P53-induced miR-30e-5p inhibits colorectal cancer invasion and metastasis by targeting ITGA6 and ITGB1," *International Journal of Cancer*, vol. 141, no. 9, pp. 1879–1890, 2017.

[26] H. J. Zhang, J. Tao, L. Sheng et al., "Retracted: Twist2 promotes kidney cancer cell proliferation and invasion via regulating ITGA6 and CD44 expression in the ECM-Receptor-Interaction pathway," *Biomedicine & Pharmacotherapy = Biomedecine & Pharmacotherapie*, vol. 81, pp. 453–459, 2016.

[27] G. Barkhoudarian and E. R. Laws, "Craniopharyngioma: history," *Pituitary*, vol. 16, no. 1, pp. 1–8, 2013.

[28] L. Chunhui, L. Chuzhong, L. Zhenye, S. Yilin, and Z. Yazhuo, "Malignant transformation of radiotherapy-naive craniopharyngioma," *World Neurosurgery*, vol. 88, pp. 690.e1–690.e5, 2016.

[29] J. C. Fernandez-Miranda, P. A. Gardner, C. H. Snyderman et al., "Craniopharyngioma: a pathologic, clinical, and surgical review," *Head & Neck*, vol. 34, no. 7, pp. 1036–1044, 2012.

[30] J. C. Martinez-Gutierrez, M. R. D'Andrea, D. P. Cahill, S. Santagata, F. G. Barker 2nd, and P. K. Brastianos, "Diagnosis and management of craniopharyngiomas in the era of genomics and targeted therapy," *Neurosurgical Focus*, vol. 41, no. 6, p. E2, 2016.

[31] P. Mortini, "Craniopharyngiomas: a life-changing tumor," *Endocrine*, vol. 57, no. 2, pp. 191-192, 2017.

[32] A. N. Savateev, Y. Y. Trunin, and N. A. Mazerkina, "Radiotherapy and radiosurgery in treatment of craniopharyngiomas," *Zhurnal Voprosy Neirokhirurgii Imeni N N Burdenko*, vol. 81, no. 3, pp. 94–106, 2017.

Research Article

Correlation Study on the Expression of INSR, IRS-1, and PD-L1 in Nonsmall Cell Lung Cancer

Ma Ting [iD],[1,2] **Yu-e Miao,**[3] **Feng-xiu Yu,**[4] **Guang-cai Luo,**[5] **Xin Xu,**[5] **Li-xia Xiao,**[2] **Guo-qing Zhang** [iD],[5] **and Jin Chang** [iD][5]

[1]*Shandong First Medical University & Shandong Academy of Medical Sciences, Tai'an, 271000 Shandong Province, China*
[2]*The Second Affiliated Hospital of Shandong First Medical University, Tai'an, 271000 Shandong Province, China*
[3]*Department of Chemotherapy, The Second Affiliated Hospital of Shandong First Medical University, Tai'an 271000, Shandong Province, China*
[4]*Basic Medical College, Shandong First Medical University and Shandong Academy of Medical Sciences, Tai'an, 271000 Shandong Province, China*
[5]*Department of Radiation Oncology, The Second Affiliated Hospital of Shandong First Medical University, Tai'an 271000, Shandong Province, China*

Correspondence should be addressed to Guo-qing Zhang; viki-1868@163.com and Jin Chang; jchang@sdfmu.edu.cn

Objective. To study the expression and correlation of insulin receptor (INSR), insulin receptor substrate-1 (IRS-1), and programmed cell death ligand-1 (PD-L1) in nonsmall cell lung cancer (NSCLC). *Methods.* 45 lung cancer tissues and 30 adjacent normal tissues of NSCLC patients diagnosed in the Second Affiliated Hospital of Shandong First Medical University from June 2019 to August 2020 were selected. The expressions of INSR, IRS-1, and PD-L1 proteins in tumor tissues and adjacent tissues of NSCLC were detected by immunohistochemical staining. *Results.* The expression of INSR and IRS-1 in NSCLC was significantly higher than that in adjacent normal lung tissue ($P < 0.05$). INSR expression had statistical significance with the degree of pathological differentiation of nonsmall cell carcinoma ($P = 0.031$), but had no significant association with age, gender, pathological type, TNM stage, and lymph node metastasis status ($P > 0.05$). There was no significant correlation between IRS-1 positive expression and NSCLC patients' age, gender, pathological typing, degree of differentiation, TNM stage, and lymph node metastasis ($P > 0.05$). PD-L1 positive expression was correlated with lymph node metastasis of NSCLC ($P = 0.028$), while there was no significant correlation with gender, age, pathological type, TNM stage, and pathological differentiation degree of NSCLC patients ($P > 0.05$). Spearman correlation analysis showed that PD-L1 protein expression had a significant positive correlation with IRS-1 protein expression ($r = 0.373$), but was not correlated with the expression of INSR protein. *Conclusion.* IRS-1 may be involved in the regulation of PD-L1 expression and mediate the occurrence of tumor immune escape, which is expected to become a new target for NSCLC immunotherapy and provide new clinical evidence for immunosuppressive therapy.

1. Introduction

Lung cancer is a common malignant tumor in the world. According to the latest data released by the international agency for research on cancer in *CA:A Cancer Journal for Clinicians* [1], there were 2.207 million new lung cancer cases and 1.796 million reported deaths worldwide, accounting for 11.7% and 18.0% of the global cancer incidence rate

and mortality, respectively. Nonsmall cell lung cancer (NSCLC) has decreased in incidence overall in the past decade in the United States but the incidence of stage I NSCLC has increased along with its prevalence [2], highlighting the need for research in this area. Surgical resection can be the first choice for the treatment of NSCLC. However, more than 70% of patients with NSCLC were often accompanied by tumor proliferation and metastasis and lost the

best opportunity for surgery due to the limitations of early diagnosis [3]. According to a global cancer detection report, lung cancer patients in most countries had a 5-year survival rate of only 10-20% [4]. With the continuous development of cancer treatment methods and technologies, the situation has improved [5]. But the problems of drug resistance and immunotoxicity cannot be ignored. Therefore, seeking new treatment targets and exploring their related mechanisms in the occurrence and development of lung cancer are the current research focus and urgent problem to be solved. Therefore, seeking new treatment targets and exploring their related mechanisms in the occurrence and development of lung cancer are the current research focus and urgent problem to be solved.

INSR and IRS-1 can mediate tumorigenesis and development as key mediators in the insulin signal transduction pathway, but their specific biological roles have not been fully clarified. Zhang et al. [6] found that downregulation of INSR can inhibit tumor cell proliferation, angiogenesis, lymphangiogenesis, and metastasis. Kim et al. [7] studied the effect of INSR expression on the survival of patients with NSCLC for the first time and found that INSR expression could be used as an independent prognostic factor for OS and RFS in patients with surgically resected early NSCLC. INSR has been proved to be abnormally expressed in a variety of tumor tissues, such as breast cancer, lung cancer, and gastric cancer [7–9]. Li et al. [10] first found that overexpression of IRS-1 can promote the malignant transformation of mouse embryonic fibroblasts. Subsequently, Tanaka et al. [11] further confirmed that IRS-1 overexpression can induce malignant transformation and proliferation of NIH3T3 fibroblasts by activating ERK1/2 pathway under low serum conditions. In addition, fibroblasts transfected with IRS can form colonies in soft agar, which is also highly tumorigenic when injected into nude mice. As a transmembrane protein, PD-L1 is considered to be an inhibitor of immune responses. It can combine with PD-1 to mediate the occurrence of tumor immune evasion [12]. With the approval of immune checkpoint inhibitors (ICIS), the treatment of immune checkpoints based on regulating PD-1/PD-L1 signaling pathway provides more options for the treatment of patients with advanced NSCLC [13, 14]. Gene expression studies indicate that PD-L1 expression is a biomarker of improved survival and response to immune checkpoint blockade therapy [15, 16]. IRS-1 expression is also associated with prognosis [17].

However, there are few reports on the correlation between INSR, IRS-1, and PD-L1 in NSCLC patients. Therefore, it is of great significance to explore the correlation between the expression levels of INSR, IRS-1, and PD-L1 and reveal the potential mechanism of insulin pathway-related receptors in the occurrence and development of lung cancer.

2. Materials and Methods

2.1. Tissue Samples. 45 patients with NSCLC diagnosed in the Second Affiliated Hospital of Shandong First Medical University from June 2019 to August 2021 were selected.

The 45 patients with nonsmall cell lung cancer, including 26 males and 19 females, did not receive radiotherapy, chemotherapy, and other antitumor treatments before surgery. The clinical data of all patients included in the experiment were complete, and the postoperative pathology had confirmed NSCLC. The TNM stage was determined according to the 2018 AJCC staging guidelines. This experiment has been approved by the medical ethics committee of our hospital before it is started.

2.2. Immunohistochemistry. The expression of INSR, IRS-1, and PD-L1 in 45 NSCLC tissues and 30 adjacent normal tissues were detected by immunohistochemistry (IHC). The results of immunohistochemical staining were determined by two pathologists using semiquantitative analysis method. The positive staining of INSR was localized in the cell membrane and cytoplasm, while the positive staining of IRS-1 was localized in the cytoplasm and nucleus. Observed the staining intensity and count the proportion of positive cells under a high power microscope. The intensity of the immunostaining was scored as follows: (a) no staining, 0; (b) pale yellow, 1; (c) brown-yellow, 2; and (d) brown, 3. The percentage of positive tumor cells was scored as (a) <5%, 0; (b) 5-25%, 1; (c) 26-50%, 2; (d) 51-75%, 3; and (e) >75%, 4. The two scores were multiplied to produce a weighted score for each case. Cases with weighted scores of more than 3 were defined as positive; otherwise; they were defined as negative. The positive staining of PD-L1 was mainly localized in the cell membrane, which was scored according to the proportion of tumor pigmented cells (TPS Score). When $TPS \geq 1\%$, it was defined as positive, otherwise, it was defined as negative.

2.3. Statistical Analysis. SPSS26.0 statistical software was used for data processing, and the comparison between positive expression rate, expression of each indicator, and clinicopathological data among groups was performed by chi-square test; the correlation between INSR, IRS-1, and PD-L1 expression was tested by Spearman rank correlation analysis. When the default $P < 0.05$, the difference was considered statistically significant.

3. Results

3.1. Expression of INSR and IRS-1 in NSCLC and Adjacent Normal Tissues. The expression of INSR and IRS-1 in 45 cases of nonsmall cell lung cancer and 30 cases of adjacent normal lung tissues was detected by immunohistochemical staining (Figure 1). The results showed that INSR and IRS-1 are expressed in both lung cancer and adjacent normal tissues. The expression of INSR was dramatically higher in 29 (64.4%) cases compared with 11 (36.7%) cases in adjacent normal tissues ($X^2 = 5.580$, $P = 0.018$). IRS-1 expression was positive in 26 (57.8%) lung cancer tissues, which was significantly higher than 10 (33.3%) cases in adjacent tissues ($X^2 = 4.309$, $P < 0.05$) (Table 1).

3.2. The Relationship between INSR, IRS-1 Expression, and Clinicopathological Features in NSCLC. The results of statistical analysis showed that the positive expression of INSR
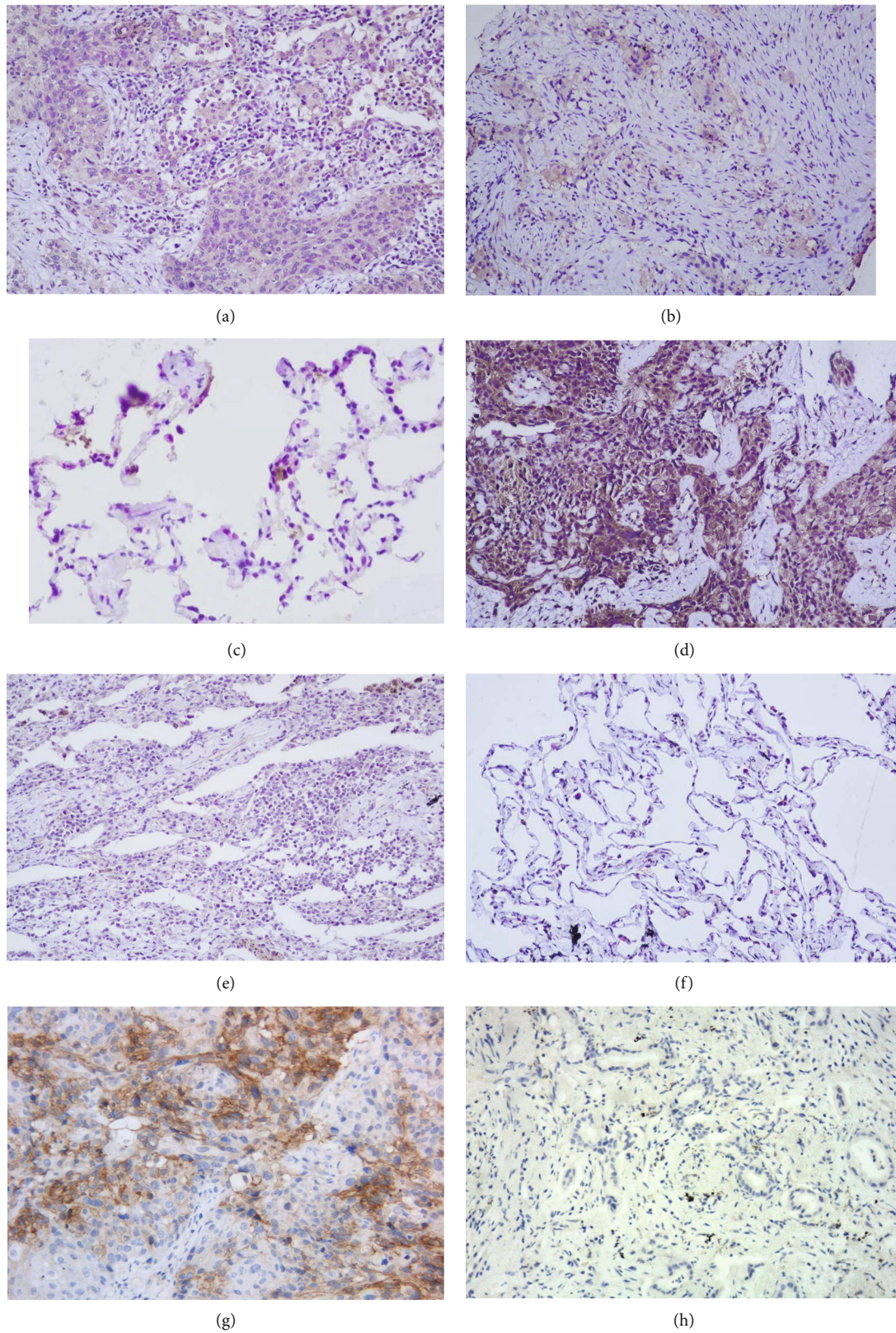
Figure 1: Representative immunohistochemical staining images of INSR, IRS-1, and PD-L1 in NSCLC tissues and adjacent normal tissues. (Original magnification: ×200). (a) Positive expression of INSR in NSCLC tissues. (b) Negative expression of INSR in NSCLC tissues. (c) Negative expression of INSR in adjacent normal tissues. (d) Positive expression of IRS-1 in NSCLC tissues. (e) Negative expression of IRS-1 in NSCLC tissues. (f) Negative expression of IRS-1 in adjacent normal tissues. (g) Positive expression of PD-L1 in NSCLC tissues. (h) Negative onpression of PD-L1 in NSCLC tissues.

TABLE 1: Difference of expression of INSR and IRS-1 in lung cancer and normal lung tissue.

Variable	Total	INSR (%)		X^2	P	IRS-1 (%)		X^2	P
		+	-			+	-		
Tumor tissues	45	29 (64.4)	16 (35.6)	5.580	0.018	26 (57.8)	19 (42.2)	4.309	0.038
Adjacent tissues	30	11 (36.7)	19 (63.3)			10 (33.3)	20 (66.7)		

was correlated with the degree of pathological differentiation of NSCLC patients, and the difference was statistically significant ($P = 0.031$). There was no correlation with age, gender, pathological type, TNM stage, and lymph node metastasis status ($P > 0.05$). There was no significant correlation between the positive expression of IRS-1 and NSCLC patients' age, gender, pathological typing, degree of differentiation, TNM stage, and lymph node metastasis ($P > 0.05$) (Table 2).

3.3. The Relationship between PD-L1 Expression and Clinicopathological Features in NSCLC.

There were 24 patients with positive expression, including 6 patients with high expression of PD-L1 (TPS ≥ 50%) and 18 patients with low expression of PD-L1 (1% ≤ TPS < 50%) (Figure 1). The results of statistical analysis showed that the positive expression of PD-L1 protein was correlated with lymph node metastasis ($P = 0.028$), while there was no significant correlation with gender, age, pathological type, TNM stage, and pathological differentiation degree of NSCLC patients ($P > 0.05$) (Table 3).

3.4. Correlation between INSR and PD-L1 Expressions in NSCLC.

Spearman rank correlation was used to analyze the correlation between INSR, IRS-1, and PD-L1 expressions in nonsmall cell lung cancer. The results showed that there was no correlation between the expression of INSR and PD-L1 in nonsmall cell lung cancer ($r = 0.143$, $P > 0.05$) (Table 4). There was a positive correlation between the expression of IRS-1 and PD-L1 in nonsmall cell lung cancer ($r = 0.373$, $P < 0.005$) (Table 5).

4. Discussion

The reprogramming of tumor energy metabolism is considered to be one of the typical features of cancer, which endows tumor cells with the potential to continue to grow and proliferate in the tumor microenvironment (TME) with nutrient deficiency [18, 19]. As early as 1924, Ott Warburg first observed this abnormality of energy metabolism of tumor cells. Even in the case of sufficient oxygen supply, tumor cells still prefer to change their metabolic dependence from mitochondrial oxidative phosphorylation (OXPHOS) to glycolysis to generate energy [20]. After that, Zhou et al. [21] also found that drug-resistant cell lines have higher levels of aerobic glycolysis capacity, suggesting that there is a biochemical link between drug resistance and glycolysis. Oronsky et al. [22] further proposed that ATP produced by intracellular metabolism is the key determinant of chemoradiotherapy resistance. Controlling the metabolic process in vivo to limit ATP level can improve

chemoradiotherapy sensitivity. In conclusion, energy metabolism reprogramming plays an important role in tumorigenesis and development. Therefore, targeted intervention on glycolysis has brought a new idea for tumor treatment, and the relevant studies have also confirmed the effectiveness of this treatment method [23]. Glucose transmembrane transport is considered as the rate limiting step of glycolysis [24]. In order to make up for the low efficiency of glycolysis energy production, tumor cells tend to ingest glucose at a higher rate, which is mediated by glucose transporters (GLUTs). As a transmembrane protein, gluts are widely distributed in human tissues. Up to now, 14 glut subtypes (Glut 1-14) have been found. Gluts, especially Glut1/3, have been observed to be highly expressed in a variety of different types of tumors, such as lung cancer and pancreatic cancer. Its overexpression not only significantly enhanced glucose uptake but also showed a close relationship with the poor tumor prognosis [24–26]. Small molecule inhibitors targeting gluts, including phloretin, WZB117, and STF-31, had also shown good effects in antitumor therapy [27, 28]. Studies have shown that phosphoinositide-3 kinase (PI3K/AKT) and other pathways are central regulators of glycolysis, tumor metabolism, and cancer cell proliferation [29]. In tumor cells, PI3K/AKT pathway can induce the expression of gluts and enhance the glycolysis process [30–33]. In addition, PI3K-Akt pathway is also a classical insulin downstream signaling pathway. In the insulin signaling pathway, when insulin binds to the INSRs on the cell membrane, it enhances the binding affinity between the receptor and IRS protein, causing the phosphorylation of IRSs to be activated. Then, IRSs can activate this pathway by recruiting and activating PI3K. Therefore, we have reason to believe that INSR and IRS-1 are involved in the process of glycolysis metabolism and play an important role in maintaining the survival and proliferation of tumor cells. They are expected to become potential targets for antitumor therapy. Our studies also showed that the positive rate of INSR and IRS-1 protein expression in NSCLC tissues was significantly higher than that in adjacent normal tissues ($P < 0.05$), suggesting that the expression of they may be involved in the occurrence and development of nonsmall cell lung cancer, which further verified our hypothesis. Heckl et al. have shown that PI3K-Akt pathway activation by insulin serves as an oncogenic driver for the development of NSCLC [34], which supports the investigation of insulin signaling pathways. Furthermore, insulin also acts to induce PD-L1 in pancreatic cancer, and while its role in NSCLC is not directly experimentally verified, it suggests a need to investigate insulin signaling and PD-L1 in NSCLC [35]. In the present study, tissue differentiation was significantly associated with INSR, while lymph node metastasis was linked to PD-L1.

TABLE 2: The relationship between INSR, IRS-1 expression, and clinicopathological features in NSCLC.

Clinicopathological features		Total	INSR (%)		P	IRS-1 (%)		P
			+	-		+	-	
Gender	Man	26	17 (65.4)	9 (34.6)	0.878	14 (33.3)	12 (33.3)	0.532
	Female	19	12 (63.2)	7 (36.8)		12 (63.2)	7 (36.8)	
Age	<60	20	13 (65.0)	7 (35.0)	0.944	12 (60.0)	8 (40.0)	0.787
	≥60	25	16 (64.0)	9 (36.0)		14 (56.0)	11 (44.0)	
Pathological type	Squamous carcinoma	12	7 (58.3)	5 (41.7)	0.606	5 (41.7)	7 (58.3)	0.187
	Adenocarcinoma	33	22 (66.7)	11 (33.3)		21 (63.6)	12 (36.4)	
TNM stage	I + II	19	10 (52.6)	9 (47.4)	0.157	12 (63.2)	7 (36.8)	0.532
	III + IV	26	19 (73.1)	7 (26.9)		14 (53.8)	12 (46.2)	
Tissue differentiation	Moderately-well	27	14 (51.9)	13 (48.1)	0.031	16 (59.3)	11 (40.7)	0.805
	Poorly	18	15 (83.3)	3 (16.7)		10 (55.6)	8 (44.4)	
Lymph node metastasis	No	18	11 (61.1)	7 (38.9)	0.712	10 (55.6)	8 (44.4)	0.309
	Yes	27	15 (55.6)	12 (44.4)		19 (70.4)	8 (29.6)	

TABLE 3: The relationship between PD-L1 expression and clinicopathological features in NSCLC.

Clinicopathological features		Total	PD-L1 (%)		P
			+	-	
Gender	Man	26	14 (53.8)	12 (46.2)	0.936
	Female	19	10 (52.6)	9 (47.4)	
Age	<60	20	12 (60.0)	8 (40.0)	0.423
	≥60	25	12 (48.0)	13 (52.0)	
Pathological type	Squamous carcinoma	12	8 (66.7)	4 (33.3)	0.280
	Adenocarcinoma	33	16 (48.5)	17 (51.5)	
TNM stage	I + II	19	7 (36.8)	12 (63.2)	0.058
	III + IV	26	17 (65.4)	9 (34.6)	
Tissue differentiation	Moderately-well	27	14 (51.9)	13 (48.1)	0.807
	Poorly	18	10 (55.6)	8 (44.4)	
Lymph node metastasis	No	18	6 (33.3)	12 (66.7)	0.028
	Yes	27	18 (66.7)	9 (33.3)	

TABLE 4: Correlation between INSR and PD-L1 expression in NSCLC.

INSR	PD-L1		n	r	P
	+	-			
+	17	12	29		
-	7	9	16	0.143	0.350
n	24	21	45		

PD-L1 is a recognized immunosuppressive molecule. Tumor cells can negatively regulate the activity of T cells by increasing the expression of PD-L1 on the cell surface, so as to achieve the occurrence of immune escape. With the approval of immune checkpoint inhibitor, immunotherapy against PD-L1 has shown good therapeutic effect in nonsmall cell lung cancer, but its immune-related adverse toxicity cannot be ignored. Therefore, looking for new targets to specifically regulate PD-L1 expression will help to more accurately block tumor-related PD-1/PD-L1 pathway and reduce adverse immune reactions. Previous studies have shown that PI3K/AKT pathway activation can promote PD-L1 expression by increasing exogenous signals or reducing the expression of negative regulatory factors such as PTEN [36]. Zhao et al. [37] confirmed that PD-1/PD-L1 blockade may inhibit the apoptosis of CD8+ T cells in gastrointestinal stromal tumors (GIST) by regulating PI3K/Akt/mTOR pathway. Stutvoet et al. [38] showed that inhibition of MAPK pathway can regulate EGF- and IFN-induced PD-L1 expression in lung adenocarcinoma. These results all suggest that the expression of PD-L1 can be regulated by PI3K/AKT and MAPK signaling pathway. These two pathways happen to be the most important downstream pathways of INSR and IRS-1. Whether they can regulate the abnormal

Table 5: Correlation between IRS-1 and PD-L1 expression in NSCLC.

| IRS-1 | PD-L1 | | n | r | P |
	+	-			
+	18	8	26		
-	6	13	19	0.373	0.012
n	24	21	45		

expression of PD-L1 through these pathways has not been clarified yet. IRS proteins play a key role in tumor metabolism by regulating signaling of INSR. However, IRS-1 is also ubiquitously expressed in cancer cells. The differential expressions of IRS-1 versus IRS-2 may regulate drug responses. Further studies are essential to clarify complex signaling mechanisms [39]. Therefore, we used spearman correlation analysis to explore the relationships between them. The result showed that there is a positive correlation between the expression of IRS-1 and PD-L in NSCLC tissues ($r = 0.373$). Therefore, we speculate that IRS-1 may participate in the expression regulation of PD-L1 and mediate the immune escape process of NSCLC. However, the specific regulatory mechanism between IRS-1 and PD-L1 needs to be further explored in the follow-up study. At the same time, clinical studies with larger sample sizes are essential to understand the specific disease characteristics and prognosis concerning this regulatory axis. The present study utilized IHC alone, and studies at gene, mRNA, and protein expression levels are essential.

5. Conclusion

INSR and IRS-1 are both overexpression in lung cancer tissues, and IRS-1 expression had a significant positive correlation with PD-L1 expression. The expression of IRS-1 may further mediate the occurrence of tumor immune escape. Therefore, a better understanding of the regulatory mechanism of IRS-1 on PD-L1 expression will help to find new targets for NSCLC immunotherapy and provide new clinical ideas for immunosuppressive therapy.

Data Availability

The study data presented may be made available from the corresponding author upon reasonable request.

Conflicts of Interest

The authors report no conflicts of interest.

Authors' Contributions

Ting Ma (email: dcarol@une.edu) and Yu-e Miao (email: miaoyue0626@126.com) contributed equally as the co-first authors. Guo-qing Zhang (email: viki-1868@163.com) and Jin Chang (email: jchang@sdfmu.edu.cn) contributed equally as the corresponding author.

References

[1] Z. C. Liu, Z. X. Li, and Y. Zhang, "Interpretation of 2020 global cancer statistical report," *Journal of Multidisciplinary Cancer Management*, vol. 7, no. 2, pp. 1–14, 2021.

[2] A. K. Ganti, A. B. Klein, I. Cotarla, B. Seal, and E. Chou, "Update of incidence, prevalence, survival, and initial treatment in patients with non–small cell lung cancer in the US," *JAMA Oncology*, vol. 7, no. 12, pp. 1824–1832, 2021.

[3] W. D. Travis, E. Brambilla, and G. J. Riely, "New pathologic classification of lung cancer: relevance for clinical practice and clinical trials," *Journal of Clinical Oncology*, vol. 31, no. 8, pp. 992–1001, 2013.

[4] C. Allemani, T. Matsuda, V. Di Carlo et al., "Global surveillance of trends in cancer survival 2000-14 (CONCORD-3): analysis of individual records for 37 513 025 patients diagnosed with one of 18 cancers from 322 population-based registries in 71 countries," *The Lancet*, vol. 391, no. 10125, pp. 1023–1075, 2018.

[5] R. L. Siegel, K. D. Miller, H. E. Fuchs, and A. Jemal, "Cancer statistics, 2022," *CA: a Cancer Journal for Clinicians*, vol. 72, no. 1, pp. 7–33, 2022.

[6] H. Zhang, D. H. Fagan, X. Zeng, K. T. Freeman, D. Sachdev, and D. Yee, "Inhibition of cancer cell proliferation and metastasis by insulin receptor downregulation," *Oncogene*, vol. 29, no. 17, pp. 2517–2527, 2010.

[7] J. S. Kim, E. S. Kim, D. Liu et al., "Prognostic impact of insulin receptor expression on survival of patients with nonsmall cell lung cancer," *Cancer*, vol. 118, no. 9, pp. 2454–2465, 2012.

[8] J. H. Law, G. Habibi, K. Hu et al., "Phosphorylated insulin-like growth factor-i/insulin receptor is present in all breast cancer subtypes and is related to poor survival," *Cancer Research*, vol. 68, no. 24, pp. 10238–10246, 2008.

[9] M. Saisana, S. M. Griffin, and F. E. B. May, "Insulin and the insulin receptor collaborate to promote human gastric cancer," *Gastric Cancer*, vol. 25, no. 1, pp. 107–123, 2022.

[10] L. Li, Y. Liang, L. Kang et al., "Transcriptional regulation of the Warburg effect in cancer by SIX1," *Cancer Cell*, vol. 33, no. 3, pp. 368–385.e7, 2018.

[11] S. Tanaka, T. Ito, and J. R. Wands, "Neoplastic transformation induced by insulin receptor substrate-1 overexpression requires an interaction with both Grb2 and Syp signaling molecules*," *Journal of Biological Chemistry*, vol. 271, no. 24, pp. 14610–14616, 1996.

[12] L. Ai, A. Xu, and J. Xu, "Roles of PD-1/PD-L1 pathway: signaling, cancer, and beyond," *Regulation of Cancer Immune Checkpoints*, vol. 1248, pp. 33–59, 2020.

[13] K. C. Ohaegbulam, A. Assal, E. Lazar-Molnar, Y. Yao, and X. Zang, "Human cancer immunotherapy with antibodies to the PD-1 and PD-L1 pathway," *Trends in Molecular Medicine*, vol. 21, no. 1, pp. 24–33, 2015.

[14] J. Qu, Q. Mei, L. Liu et al., "The progress and challenge of anti-PD-1/PD-L1 immunotherapy in treating non-small cell lung cancer," *Therapeutic Advances in Medical Oncology*, vol. 13, p. 175883592199296, 2021.

[15] P. N. Aguiar Jr., R. A. De Mello, P. Hall, H. Tadokoro, and G. D. Lima Lopes, "PD-L1 expression as a predictive bio-marker in advanced non-small-cell lung cancer: updated survival data," *Immunotherapy*, vol. 9, no. 6, pp. 499–506, 2017.

[16] C. Wang, T. Lu, R. Xu et al., "A bioinformatics-based immune-related prognostic index for lung adenocarcinoma that predicts patient response to immunotherapy and common treatments," *Journal of Thoracic Disease.*, vol. 14, no. 6, pp. 2131–2146, 2022.

[17] A. J. Piper, J. L. Clark, J. Mercado-Matos et al., "Insulin receptor substrate-1 (IRS-1) and IRS-2 expression levels are associated with prognosis in non-small cell lung cancer (NSCLC)," *PLoS One*, vol. 14, no. 8, article e0220567, 2019.

[18] D. Hanahan and R. A. Weinberg, "Hallmarks of cancer: the next generation," *Cell*, vol. 144, no. 5, pp. 646–674, 2011.

[19] R. J. DeBerardinis and N. S. Chandel, "Fundamentals of cancer metabolism," *Science Advances*, vol. 2, no. 5, article e1600200, 2016.

[20] P. Vaupel, H. Schmidberger, and A. Mayer, "The Warburg effect: essential part of metabolic reprogramming and central contributor to cancer progression," *International Journal of Radiation Biology*, vol. 95, no. 7, pp. 912–919, 2019.

[21] Y. Zhou, F. Tozzi, J. Chen et al., "Intracellular ATP levels are a pivotal determinant of chemoresistance in colon cancer cells," *Cancer Research*, vol. 72, no. 1, pp. 304–314, 2012.

[22] T. Oronsky, N. Oronsky, G. Fanger et al., "Follow the ATP: tumor energy production: a perspective," *Anti-Cancer Agents in Medicinal Chemistry*, vol. 14, no. 9, pp. 1187–1198, 2014.

[23] Y. Zhao, E. B. Butler, and M. Tan, "Targeting cellular metabolism to improve cancer therapeutics," *Cell Death & Disease*, vol. 4, no. 3, pp. e532–e532, 2013.

[24] C. C. Barron, P. J. Bilan, T. Tsakiridis, and E. Tsiani, "Facilitative glucose transporters: implications for cancer detection, prognosis and treatment," *Metabolism*, vol. 65, no. 2, pp. 124–139, 2016.

[25] J. Y. Sung, G. Y. Kim, S. J. Lim, Y. K. Park, and Y. W. Kim, "Expression of the GLUT1 glucose transporter and p53 in carcinomas of the pancreatobiliary tract," *Pathology-Research and Practice*, vol. 206, no. 1, pp. 24–29, 2010.

[26] C. Yin, B. Gao, J. Yang, and J. Wu, "Glucose transporter-1 (GLUT-1) expression is associated with tumor size and poor prognosis in locally advanced gastric cancer," *Medical Science Monitor Basic Research*, vol. 26, article e920778, 2020.

[27] D. Kraus, J. Reckenbeil, N. Veit et al., "Targeting glucose transport and the NAD pathway in tumor cells with STF-31: a re-evaluation," *Cellular Oncology*, vol. 41, no. 5, pp. 485–494, 2018.

[28] E. B. Butler, Y. Zhao, C. Muñoz-Pinedo, J. Lu, and M. Tan, "Stalling the engine of resistance: targeting cancer metabolism to overcome therapeutic resistance," *Cancer Research*, vol. 73, no. 9, pp. 2709–2717, 2013.

[29] R. Courtnay, D. C. Ngo, N. Malik, K. Ververis, S. M. Tortorella, and T. C. Karagiannis, "Cancer metabolism and the Warburg effect: the role of HIF-1 and PI3K," *Molecular Biology Reports*, vol. 42, no. 4, pp. 841–851, 2015.

[30] A. Barthel, S. T. Okino, J. Liao et al., "Regulation of *GLUT1* gene transcription by the serine/threonine kinase Akt1∗," *Journal of Biological Chemistry*, vol. 274, no. 29, pp. 20281–20286, 1999.

[31] H. M. Wang, Y. J. Lu, L. He et al., "HPV16 E6/E7 promote the translocation and glucose uptake of GLUT1 by PI3K/AKT pathwayviarelieving miR-451 inhibitory effect on CAB39 in lung cancer cells," *Therapeutic Advances in Chronic Disease*, vol. 11, p. 204062232095714, 2020.

[32] J. Yu, J. Li, S. Zhang et al., "IGF-1 induces hypoxia-inducible factor 1α-mediated GLUT3 expression through PI3K/Akt/mTOR dependent pathways in PC12 cells," *Brain Research*, vol. 1430, pp. 18–24, 2012.

[33] J. Jiang, H. Y. Ren, G. J. Geng et al., "Oncogenic activity of insulin in the development of non-small cell lung carcinoma," *Oncology Letters*, vol. 15, no. 1, pp. 447–452, 2018.

[34] S. M. Heckl, F. Mau, A. Senftleben et al., "Programmed death-ligand 1 (PD-L1) expression is induced by insulin in pancreatic ductal adenocarcinoma cells pointing to its role in immune checkpoint control," *Medical Science*, vol. 9, no. 3, 2021.

[35] X. Liu, K. Yamaguchi, K. Takane et al., "Cancer-associated IDH mutations induce Glut1 expression and glucose metabolic disorders through a PI3K/Akt/mTORC1-Hif1α axis," *PLoS One*, vol. 16, no. 9, article e0257090, 2021.

[36] J. Chen, C. C. Jiang, L. Jin, and X. D. Zhang, "Regulation of PD-L1: a novel role of pro-survival signalling in cancer," *Annals of Oncology*, vol. 27, no. 3, pp. 409–416, 2016.

[37] R. Zhao, Y. Song, Y. Wang et al., "PD-1/PD-L1 blockade rescue exhausted CD8+ T cells in gastrointestinal stromal tumours via the PI3K/Akt/mTOR signalling pathway," *Cell Proliferation*, vol. 52, no. 3, article e12571, 2019.

[38] T. S. Stutvoet, A. Kol, E. G. E. de Vries et al., "MAPK pathway activity plays a key role in PD-L1 expression of lung adenocarcinoma cells," *The Journal of Pathology*, vol. 249, no. 1, pp. 52–64, 2019.

[39] L. M. Shaw, "The insulin receptor substrate (IRS) proteins: at the intersection of metabolism and cancer," *Cell Cycle*, vol. 10, no. 11, pp. 1750–1756, 2011.

Research Article

Identification of Downregulated Exosome-Associated Gene ENPP1 as a Novel Lipid Metabolism and Immune-Associated Biomarker for Hepatocellular Carcinoma

Zhilan. Li [ID],[1] **Qingchun. He** [ID],[2,3,4] **Jinwu. Peng** [ID],[5] **Yuanliang. Yan** [ID],[6] **and Chencheng. Fu** [ID][1]

[1]*Department of Pathology, Xiangya Changde Hospital, Changde, China*
[2]*Department of Emergency, Xiangya Hospital, Central South University, Changsha, China*
[3]*Department of Emergency, Xiangya Changde Hospital, Changde, China*
[4]*National Clinical Research Center for Geriatric Disorders, Xiangya Hospital, Central South University, Changsha, China*
[5]*Department of Pathology, Xiangya Hospital, Central South University, Changsha, China*
[6]*Department of Pharmacy, Xiangya Hospital, Central South University, Changsha, China*

Correspondence should be addressed to Jinwu. Peng; jinwupeng@csu.edu.cn and Chencheng. Fu; cc15973753970@163.com

Exosome plays an important role in the occurrence and development of tumors, such as hepatocellular carcinoma (LIHC). However, the functions and mechanisms of exosome-associated molecules in LIHC are still underexplored. Here, we investigated the role of the exosome-related gene ENPP1 in LIHC. Comprehensive bioinformatics from multiple databases revealed that ENPP1 was significantly downregulated in LIHC tissues. The patients with downregulated ENPP1 displayed a poor prognosis. Immunohistochemistry (IHC) was used to further confirm the downregulated ENPP1 in LIHC tissues. In addition, the coexpression network of ENPP1 was also explored to understand its roles in the underlying signaling pathways, including fatty acid degradation and the PPAR signaling pathway. Simultaneously, GSEA analysis indicated the potential roles of ENPP1 in the lipid metabolism-associated signaling pathways in the pathogenesis of LIHC, including fatty acid metabolism, fatty acid synthesis, and so on. Finally, immunological analysis indicated that ENPP1 might also be involved in multiple immune-related features, including immunoinhibitors, immunostimulators, and chemokines. Taken together, these findings could enhance our understanding of ENPP1 in LIHC pathogenesis and immune response and provide a new target for ENPP1-related immunotherapy in clinical treatment.

1. Introduction

The 5-year survival rate of hepatocellular carcinoma (LIHC) ranks second among all cancers [1, 2]. In terms of diagnosis, as the only serum biomarker widely used in daily practice, alpha-fetoprotein (AFP) has low sensitivity and specificity in the early diagnosis of LIHC [3]. In terms of treatment, immunotherapy has been applied to LIHC; however, the response of patients to immunotherapy is still limited [4, 5, 6]. Therefore, it is crucial to improve our understanding of the complex pathogenesis of LIHC.

Exosomes are a subset of extracellular vesicles (EVs) with a diameter of 40–160 nm [7, 8]. Exosomes contain a variety of substances, such as proteins, amino acids, nucleic acids, lipids, and metabolites, and can mediate cell-to-cell communication [9, 10]. Furthermore, exosomes have been shown to play an important role in the regulation of the immune system [11, 12]. Recent reports have demonstrated the potential roles of exosomes in the tumorigenesis and progression of cancers [13], including LIHC [14]. However, the detailed molecular mechanisms of exosome-associated genes in LIHC have not been fully elucidated.

Ectonucleotide pyrophosphatase/phosphodiesterase 1 (ENPP1), also known as plasma cell glycoprotein 1 (PC-1), is a type II transmembrane glycoprotein with nucleotide pyrophosphatase and phosphodiesterase activities [15].

Nikonorova et al. demonstrated the biological function of exosome-loaded ENPP1 in mediating intercellular communication, involving various physiological and pathological states [16]. In recent years, ENPP1 has been found to play an important role in immune responses to various stimuli [17]. Studies have shown that aberrantly expressed ENPP1 participates in the pathogenesis and therapeutic response of human cancers, including ovarian cancer, glioma, and breast cancer [18, 19, 20]. However, the diagnostic value and functional mechanism of ENPP1 in LIHC have not been explored.

Here, we comprehensively evaluated the expression profiles and potential prognostic values of ENPP1 in LIHC. We demonstrated that the exosome-related gene ENPP1 was significantly downregulated in LIHC. Moreover, the patients with downregulated expression of ENPP1 showed a poor prognosis. Immunological analysis revealed the association between ENPP1 levels and immune infiltrating cells in LIHC. Taken together, these data collectively suggested that ENPP1 could be a promising biomarker for LIHC prognosis and immune response and may serve as a new immunotherapy-associated target.

2. Materials and Methods

2.1. Data Acquisition and Bioinformatics Analysis.

Three public LIHC datasets, GSE6764 [21], GSE14323 [22], and GSE14520 [23], were downloaded from the Gene Expression Omnibus (GEO) database. Then, the differently expressed genes (DEGs) between the normal liver tissues and LIHC were screened with the following criteria: P value <0.01 and |logFC| > 1 (Table 1). Next, Venn plots were employed to identify the co-DEGs among the exosome-associated gene dataset (Supplementary Table 1) [24] and the above-mentioned GEO datasets. After then, Xiantao Xueshu [25], TNMplot [26], and UALCAN [27] were used to confirm the downregulated expression levels of ENPP1 in LIHC tissues.

The prognostic values of co-DEGs in LIHC patients were explored by the Kaplan–Meier plotter [28]. The prognostic indexes mainly included disease-specific survival (DSS) and overall survival (OS). Subsequently, the LinkedOmics platform [29] was used to analyze the coexpressed molecules associated with ENPP1. At the same time, using LinkedOmics, we performed the enrichment analysis of ENPP1 coexpressed molecules, including gene ontology (GO) and Kyoto encyclopedia of genes and genomes (KEGG). Using single-sample GSEA (ssGSEA) in Xiantao Xueshu and TISIDB [30], we explored the roles of ENPP1 in the immune-associated features in LIHC patients.

2.2. Immunohistochemistry (IHC).

The paraffin-embedded LIHC samples and corresponding peritumoral samples were obtained from Xiangya Hospital, Central South University. The ethics was approved by Xiangya Hospital, Central South University (No. 202205113). Immunohistochemistry (IHC) was performed using a universal two-step IHC staining kit (PV-9000, ZSGB-BIO, Beijing, China) according to the instructions. The primary antibody used in this study was anti-ENPP1 (1 : 500, ab223268, Abcam). The IHC results were identified according to the staining percentage and staining intensity.

2.3. Statistical Analysis.

On the Kaplan–Meier platform, the comparison of OS and DSS between tumor and normal groups was performed using the log-rank test. A Cox risk proportional regression model was used to analyze and calculate hazard ratios (HRs). The Mann–Whitney U test was used for comparison of normal and tumor specimens, and the Wilcoxon test was used for comparison of tissues with its matched adjacent specimens. All the critical values of statistical significance were $P < 0.05$.

3. Results

3.1. Identification of the DEGs between the LIHC Group and the Normal Group.

The DEGs between LIHC and normal liver tissue were analyzed from three GEO datasets, GSE6764, GSE14323, and GSE14520. We identified 830 upregulated and 866 downregulated molecules in GSE6764, 505 upregulated and 590 downregulated molecules in GSE14520, and 343 upregulated and 258 downregulated molecules in GSE14323 (Supplementary Table 2).

In order to explore the role of exosome-associated genes in LIHC, we used Venn analysis to screen the co-DEGs between the three GEO datasets and the exosome-associated gene dataset. As shown in Figure 1, we identified two codownregulated molecules, interleukin 1 receptor accessory protein (IL1RAP) and ENPP1 in LIHC tissues. However, no coupregulated molecules were found in Supplementary Figure 1.

3.2. The Prognosis Values of IL1RAP and ENPP1 in LIHC Patients.

To explore whether aberrant expression of IL1RAP and ENPP1 affected the patients' prognosis in LIHC, we used the Kaplan–Meier plotter database and found that patients with a high ENPP1 level displayed a good OS rate (hazard ratio (HR) = 0.69, 95% CI = 0.49–0.98, $P = 0.039$) and DSS (HR = 0.63, 95% CI = 0.41–0.99, $P = 0.041$), whereas, there was no clear connection between the level of IL1RAP and LIHC patients' prognosis (Figures 2(a)-2(b)). Therefore, these data collectively revealed the important prognostic roles of ENPP1 expression in LIHC.

3.3. ENPP1 Was Confirmed to Be Downregulated in LIHC.

To investigate the role of ENPP1 in LIHC progression, the TCGA-LIHC dataset in Xiantao Xueshu was used to predict ENPP1 mRNA expression patterns in 374 liver cancer samples and 50 normal tissue samples. As shown in Figure 3(a), the results showed that the expression level of ENPP1 mRNA in liver cancer tissues was lower than that in normal liver tissues. In addition, the expression of ENPP1 was confirmed to be significantly downregulated in 50 LIHC specimens compared with matched adjacent samples (Figure 3(b)). Next, the RNA-seq data and gene chip data in

TABLE 1: The features of three GEO datasets on gene expression.

GEO datasets	Platform	Sample size		DEGs	References
		Cancer	Normal		
GSE6764	GPL570	35	10	854 upregulated genes and 893 downregulated genes	[21]
GSE14323	GPL571	38	19	343 upregulated genes and 258 downregulated genes	[22]
GSE14520	GPL571	22	21	632 upregulated genes and 650 downregulated genes	[23]
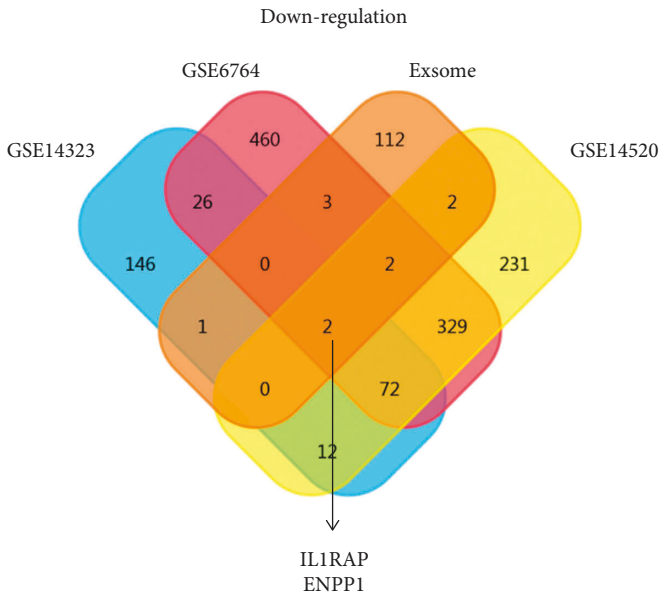
FIGURE 1: Identification of co-DEGs between the exosome-associated gene dataset and three GEO-LIHC datasets. In this Venn plot, we found two co-downregulated molecules, IL1RAP, and ENPP1, in LIHC tissues.

TNMplot showed that the expression of ENPP1 mRNA in cancer tissues was lower than that in normal liver tissues (Figures 3(c)-3(d)). We also confirmed that the expression of ENPP1 was significantly downregulated in tumor groups from the three abovementioned GEO datasets, GSE6764, GSE14323, and GSE14520 (Figures 3(e)–3(g)). In addition, the UALCAN database was used to demonstrate the downregulated protein expression level of ENPP1 in LIHC (Figure 3(h)), indicating that the protein expression and mRNA expression of ENPP1 in different databases were consistent. Accordingly, our IHC data also showed that ENPP1 expression was significantly downregulated in tumor tissues compared with paracancerous tissues (Figures 3(i)-3(j)). These results collectively suggested that ENPP1 may play an inhibitory role in the occurrence and development of LIHC.

3.4. The Enrichment of ENPP1 Coexpression Network in LIHC. To explore the underlying biological significance of ENPP1 in LIHC, we analyzed the coexpression pattern of ENPP1 in TCGA-LIHC through LinkedOmics. The volcano plots showed that the coexpressed molecules were positively (red dots) and negatively (blue dots) correlated with ENPP1 (Figure 4(a)). The heatmap displayed the top 30 molecules that were positively and negatively correlated with ENPP1 in

LIHC (Figures 4(b)-4(c), Supplementary Table 3, Supplementary Table 4). Interestingly, the top 30 positively-associated molecules might be the low-risk biomarkers for LIHC patients, with 13/30 molecules possessing the protective HR (Figure 4(d)). Conversely, the top 30 negatively-associated molecules might be the high-risk biomarkers for LIHC patients, with 14/30 negative molecules possessing an unfavorable HR (Figure 4(e)).

Moreover, GO enrichment analysis conveyed that ENPP1 coexpressed molecules mainly participated in the regulation of several biological processes (BP), such as organic hydroxy compound transmembrane transporter activity, anion transmembrane transporter activity, and lipid transporter activity. As for the cellular components (CC), ENPP1 coexpressed molecules mainly took part in the regulation of the microbody and peroxisome. As for the molecular function (MF), the coexpressed genes of ENPP1 were significantly involved in the regulation of organic hydroxy compound transport (Figure 5(a)). Moreover, the KEGG enrichment analysis conveyed that the enriched signaling pathways of ENPP1 coexpressed molecules were fatty acid degradation, PPAR signaling pathway, and others (Figure 5(b)). At the same time, GSEA analysis was performed to identify several fatty metabolic pathways that could be significantly regulated by ENPP1-associated molecules, such as fatty acid metabolism and nonalcoholic fatty liver disease (Figures 6(a)-6(b)). We also found that ENPP1 might participate in the regulation of other fatty metabolic pathways, such as fatty acid omega oxidation and fatty acid biosynthesis (Figures 6(c)–6(f)).

3.5. The Regulatory Roles of ENPP1 in Immune Regulation. To assess whether ENPP1 expression levels were related to the tumor-infiltrating immune cells in LIHC, the ssGSEA algorithm in Xiantao Xueshu was used to show the association between ENPP1 expression and several immune infiltrating cells, such as dendritic cells (DCs), CD56 (bright) natural killer cell (NK CD56bright), and Th1 cells (Figure 7(a)). Similarly, the immune infiltrating cells, such as Th1 cells, DC, and NK CD56bright, were significantly downregulated in the ENPP1-highly expressed group (Figure 7(b)). Furthermore, the negative associations between ENPP1 expression and infiltration of Th1 cells, DC, and NK CD56bright were confirmed by the TISIDB platform (Figure 7(c)).

Next, we explored whether ENPP1 levels were associated with the immune checkpoints in LIHC. The heatmap (Figure 7(d)) and scatterplot (Figure 7(e)) showed a negative correlation between ENPP1 expression and three immune checkpoints, which include programmed cell death protein 1

(a)

(b)
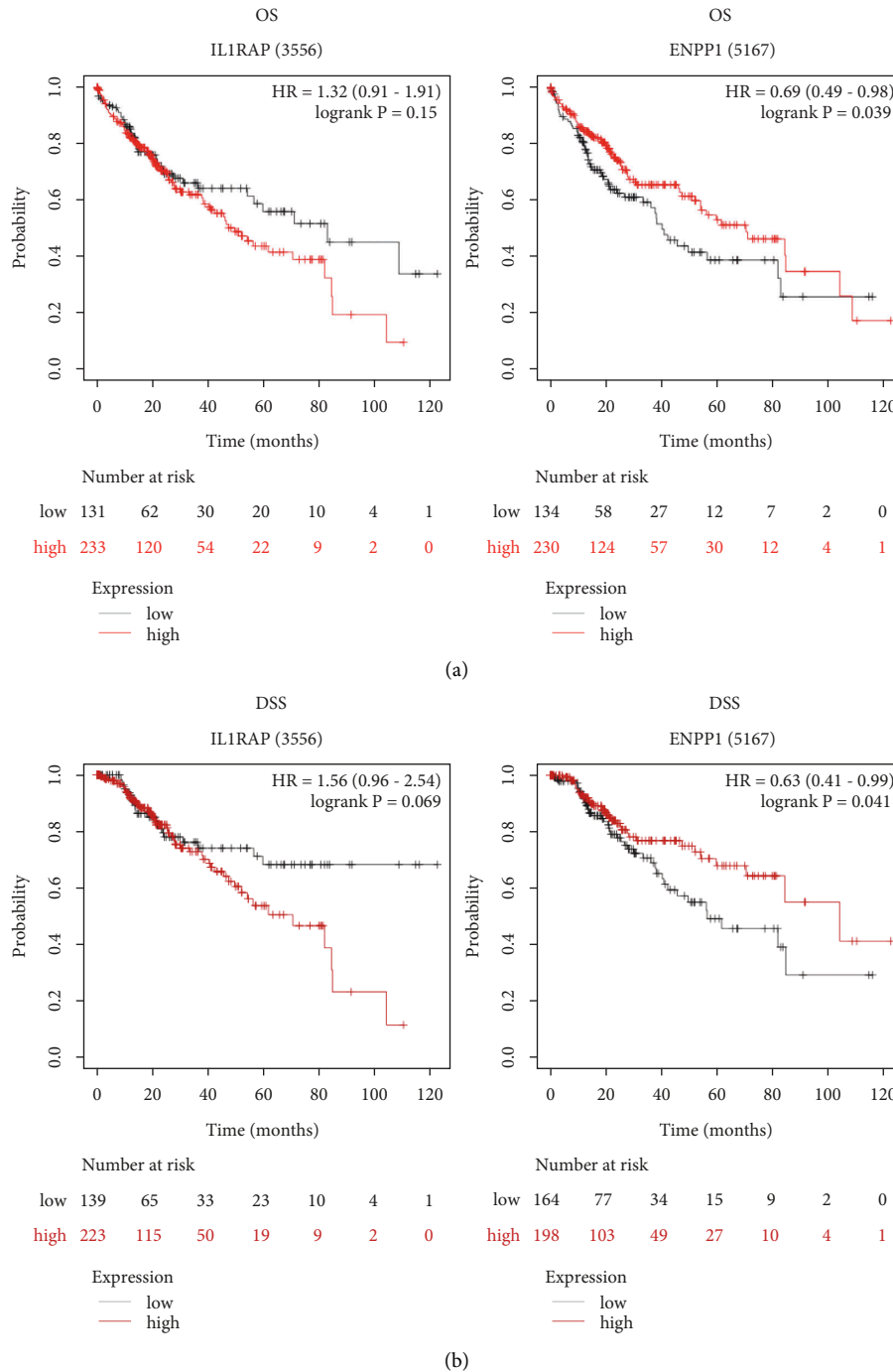
Figure 2: The effect of IL1RAP and ENPP1 on the patients' prognosis in LIHC. (a-b) The Kaplan–Meier plotter database indicated the prognostic values of aberrantly expressed IL1RAP and ENPP1 in LIHC patients, including overall survival and disease-specific survival.

(PDCD1), hepatitis A virus cellular receptor 2 (HAVCR2), and cytotoxic T-lymphocyte associated protein 4 (CTLA4).

We used the TISIDB platform to explore the underlying roles of ENPP1 in several immune-associated signatures, including immunoinhibitors and immunostimulators. Figure 8(a) demonstrates the association between ENPP1 expression and several immunoinhibitors in TCGA-LIHC patients. The results showed that ENPP1 was significantly negatively correlated with the following immunoinhibitors,

TGFB1 (Spearman $r = -0.362$, $P = 7.05e - 13$, $P = 7.05e - 13$), HAVCR2 (Spearman $r = -0.274$, $P = 8.34e - 08$), LGALS9 (Spearman $r = -0.34e-08$), -0.393, $P = 2.46e - 15$), and CSF1R (Spearman $r = -0.219$, $P = 2.1e - 05$) (Figure 8(b)). Figure 9(a) demonstrates the association between ENPP1 expression and several immunostimulators in TCHA-LIHC patients. The results showed that ENPP1 was significantly negatively correlated with the following immunostimulators, TNFSF15 (Spearman

(a)

(b)

(c)

(d)

(e)

(f)

(g)

(h)

FIGURE 3: Continued.

Case 1

(i)

Case 2

(j)
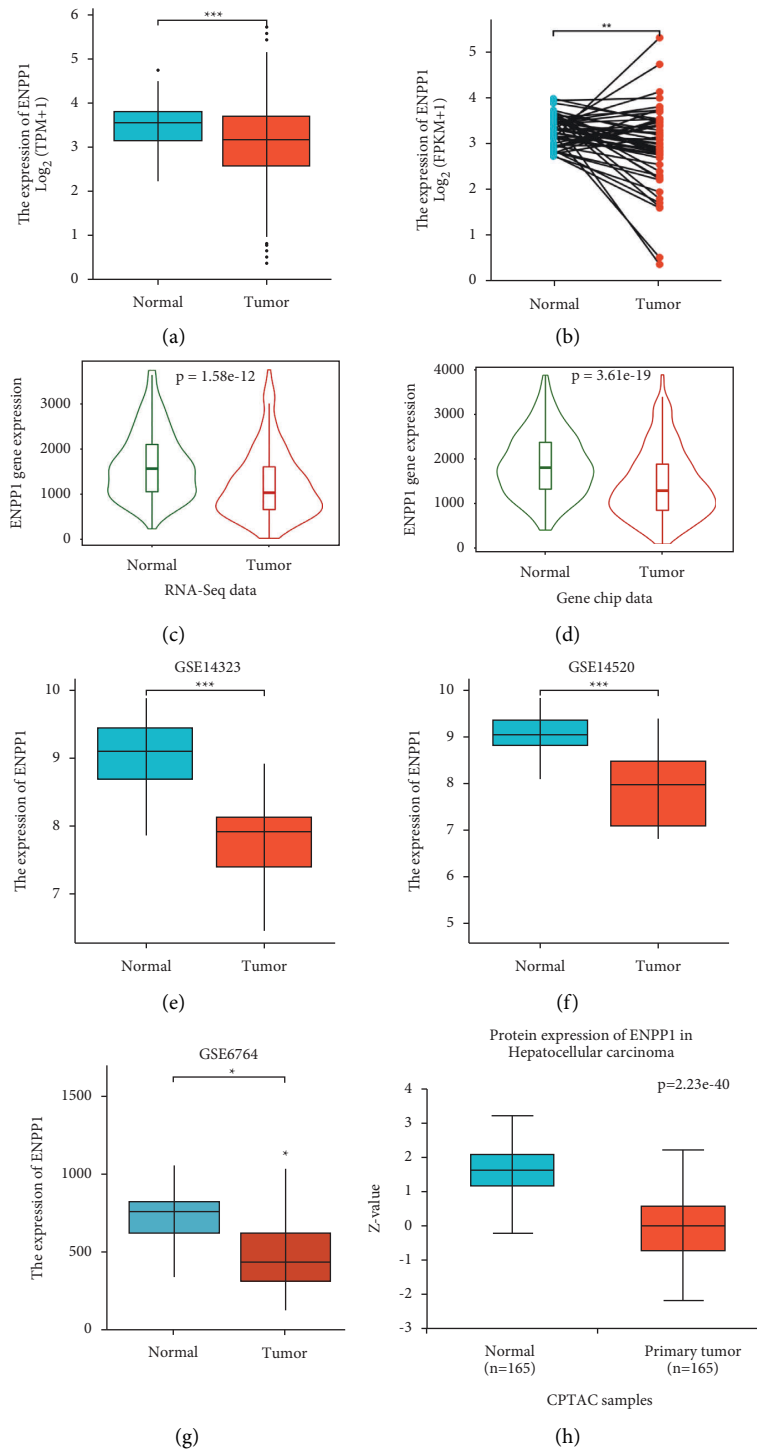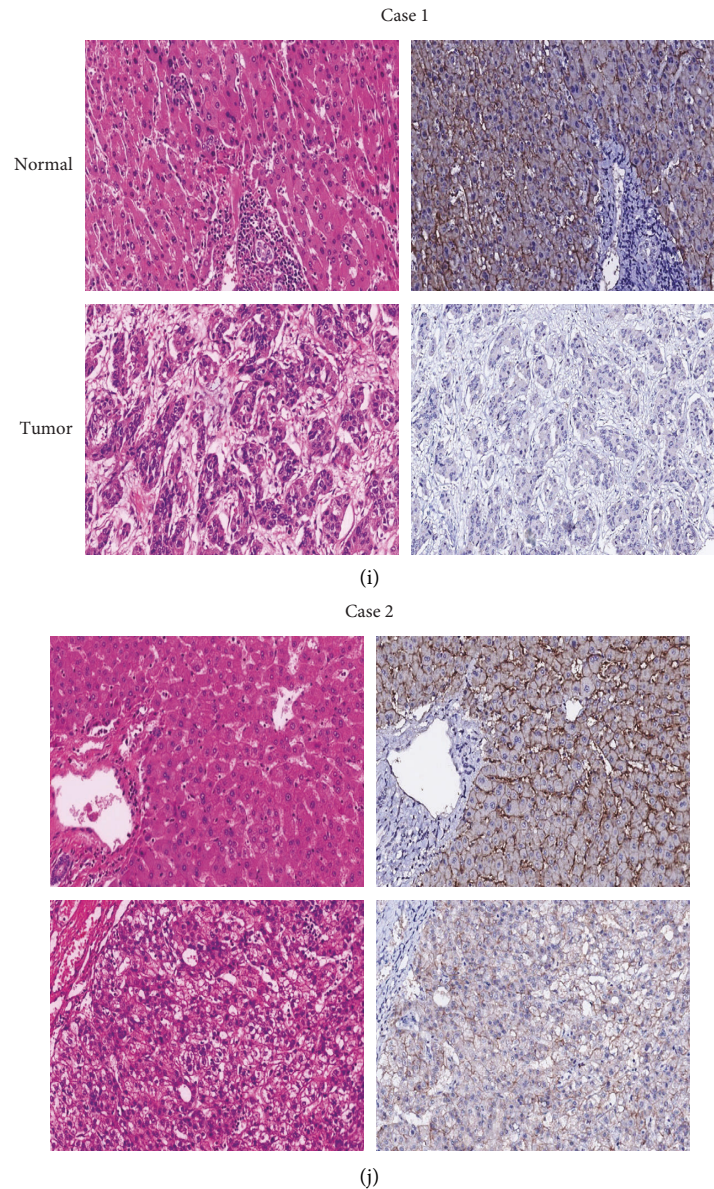
FIGURE 3: Downregulation of ENPP1 in LIHC patients. (a-b) Xiantao Xueshu indicated the downregulated expression level of ENPP1 in TCGA-LIHC, (c-d) TNMplot database depicted the downregulated ENPP1 mRNA in LIHC tissues. (e-g) ENPP1 expression was significantly diminished in the three GEO-LIHC datasets. (h) UALCAN indicated the downregulated protein expression of ENPP1 in LIHC tissues, and (i-j) IHC results confirmed that ENPP1 was significantly downregulated in tumor tissues compared with adjacent tissues ($^{*}P < 0.05$, $^{**}P < 0.01$, and $^{***}P < 0.001$).

$r = -0.272$, $P = 1.09e - 07$), TNFRSF18 (Spearman $r = -0.315$, $P = 6.26e - 10$), CD86 (Spearman $r = -0.264$, $P = 2.47e - 07$), and CXCR4 (Spearman $r = -0.267$, $P = 1.92e - 07$) (Figure 9(b)). We further explored the relationship between ENPP1 and chemokines and chemokine receptors. Supplementary Figure 2A shows the relationship between ENPP1 expression and chemokines in TCGA-LIHC patients. The chemokines were negatively-correlated with ENPP1 and mainly included CXCL1 (Spearman $r = -0.334$, $P = 4.82e - 11$), CCL26 (Spearman $r = -0.342$, $P = 1.48e - 11$), CXCL8 (Spearman $r = -0.336$,

$P = 3.43e - 11$), and CXCL3 (Spearman $r = -0.289$, $P = 1.45e - 08$) (Supplementary Figure 2B). Supplementary Figure 3A shows the association between ENPP1 expression and chemokine receptors. The chemokine receptors were negatively-correlated with ENPP1 and mainly included CCR5 (Spearman $r = -0.195$, $P = 0.00016$), CCR10 (Spearman $r = -0.135$, $P = 0.00916$), CXCR3 (Spearman $r = -0.207$, $P = 5.64e - 05$), and CXCR4 (Spearman $r = -0.267$, $P = 1.92e - 07$) (Supplementary Figure 3B). Taken together, these data suggested the promising roles of aberrant ENPP1 in the regulation of multiple immune-related signals in LIHC.
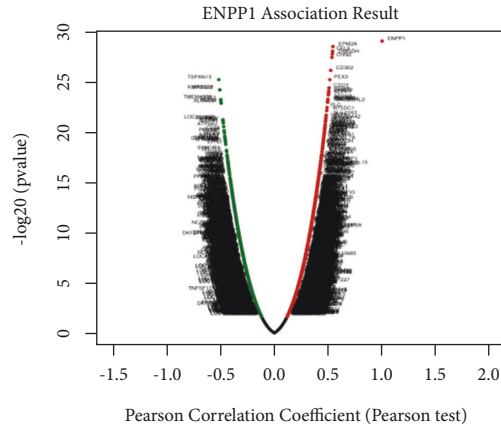
(a)
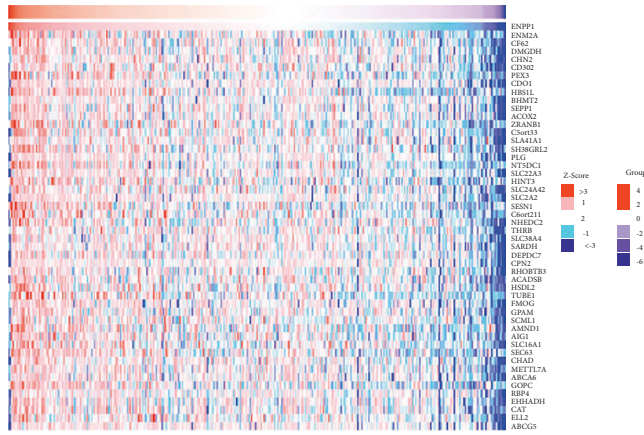
(b)
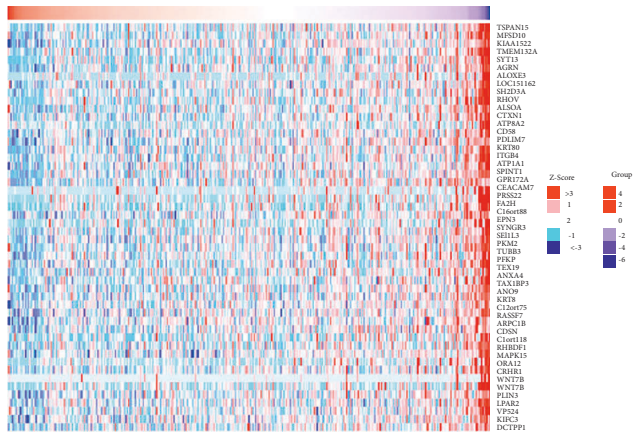
(c)
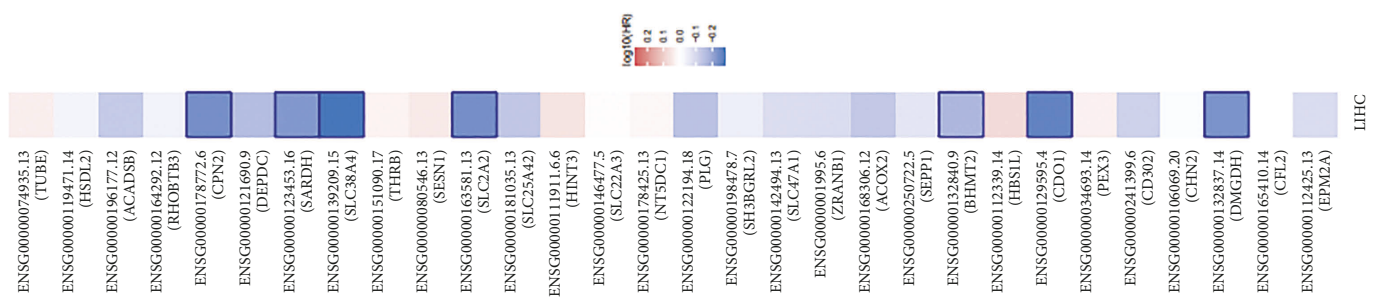
(d)

Figure 4: Continued.

(e)
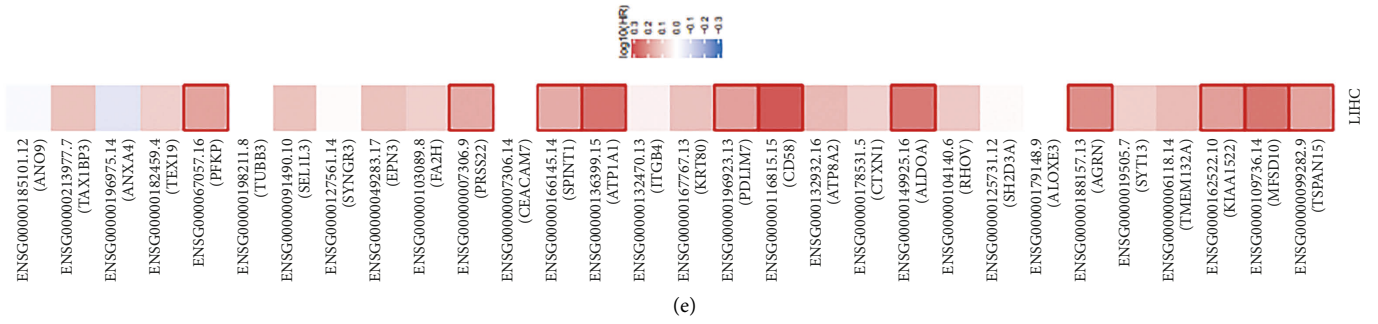
Figure 4: The ENPP1 coexpression molecules in LIHC from LinkedOmics. (a) The volcano plots showed the coexpressed molecules correlated with ENPP1, (b-c) the heatmap showed the top 30 coexpressed molecules correlated with ENPP1 in LIHC, and (d-e) the prognostic values of the coexpressed molecules were correlated with ENPP1 in LIHC.

(a)
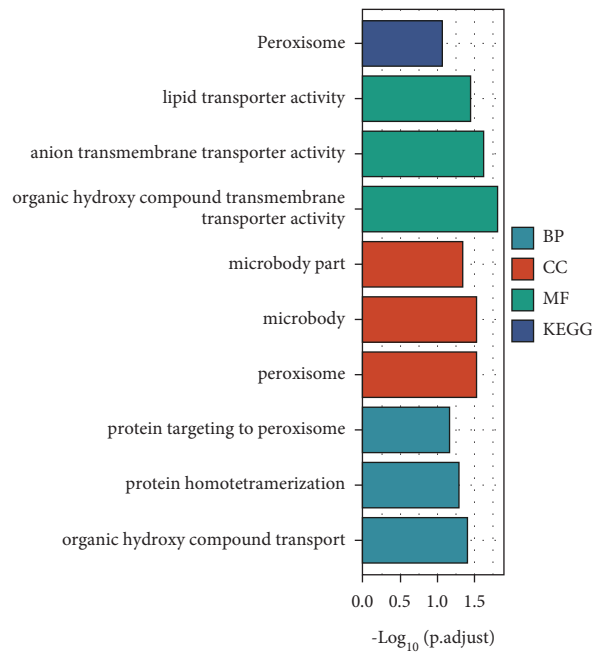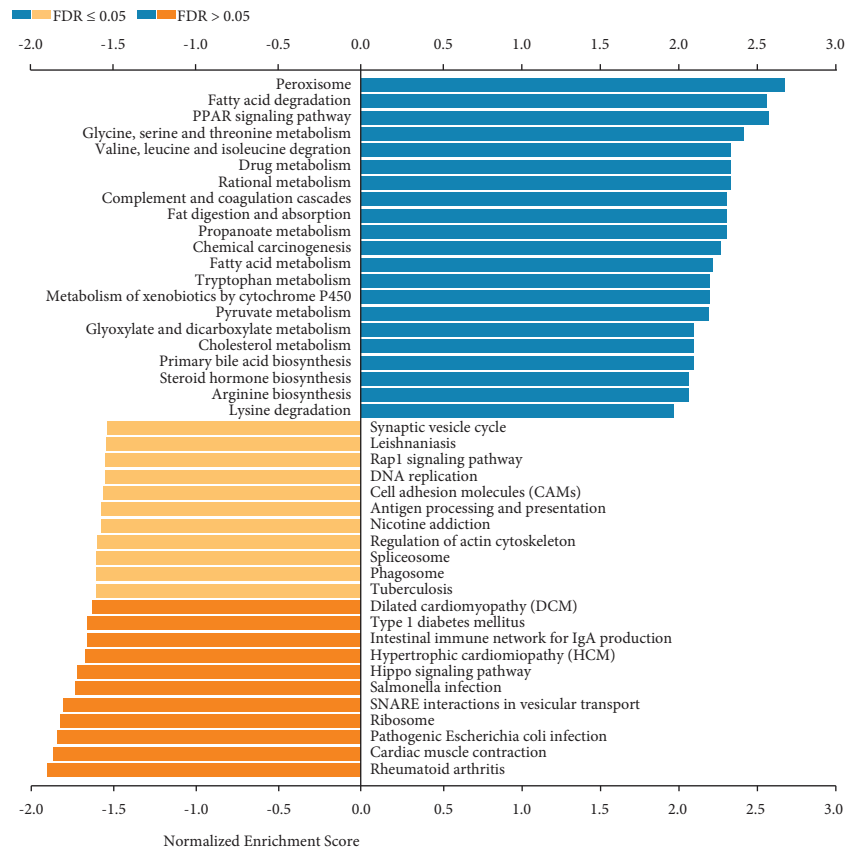
Figure 5: Continued.

(b)

FIGURE 5: The functional enrichment of ENPP1 coexpressed molecules in LIHC. (a) GO enrichment of ENPP1 coexpressed molecules in LIHC and (b) the KEGG signaling pathway of ENPP1 coexpressed molecules in LIHC.

(a)

(b)
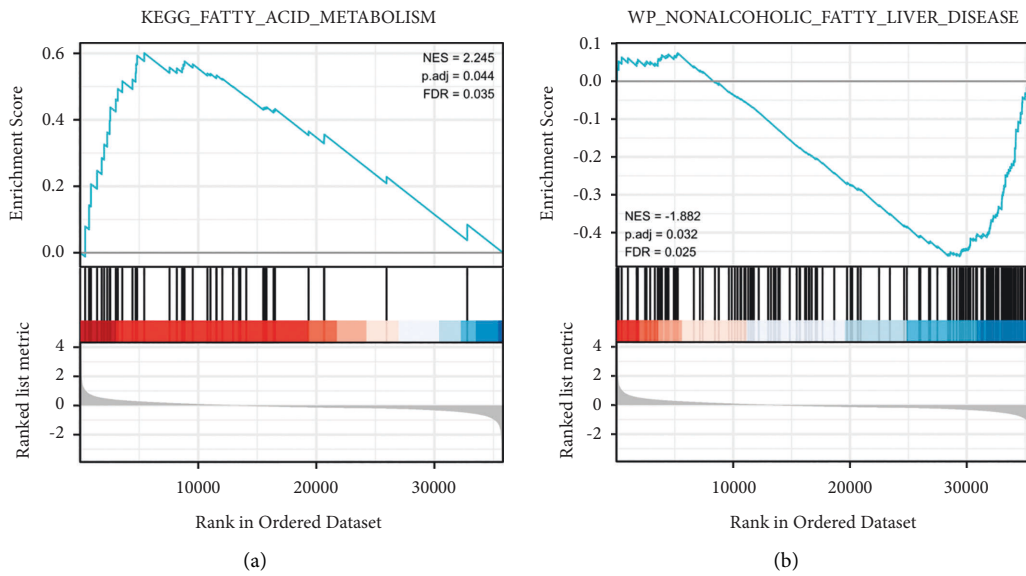
FIGURE 6: Continued.
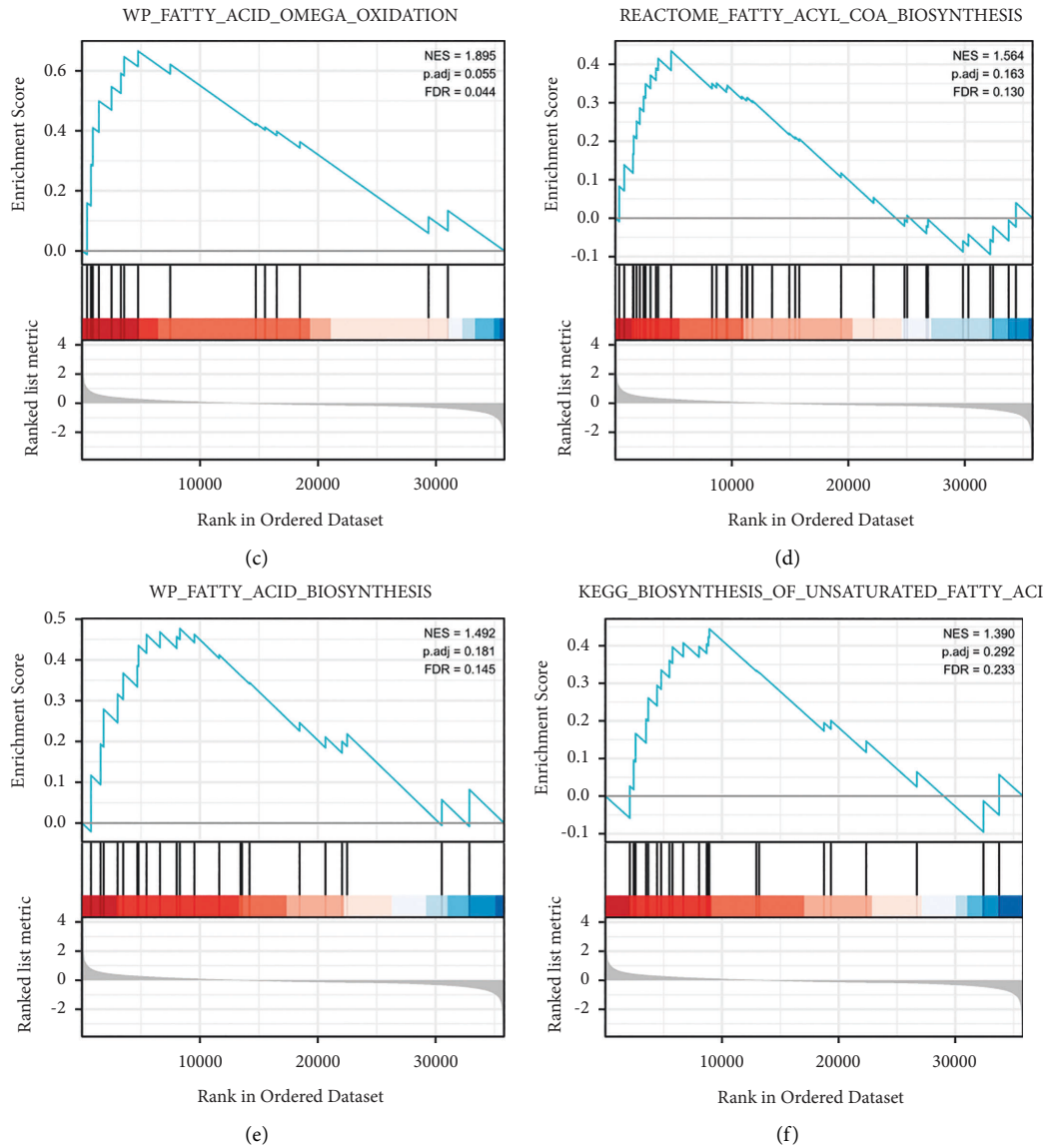
Figure 6: The GSEA enrichment analysis of ENPP1 differentially expressed genes in LIHC. (a-f) The fatty acid metabolism, nonalcoholic fatty liver disease, fatty acids omega oxidation, fatty acyl COA biosynthesis, fatty acid biosynthesis, and the biosynthesis of unsaturated fatty acid pathways were enriched in ENPP1 differentially expressed genes in LIHC.

4. Discussion

The tumor microenvironment (TME) is an important intrinsic link in the occurrence, development, invasion, and metastasis of LIHC. Exosomes are increasingly recognized as professional information carriers in TME regulation [31, 32], which play important roles in tumor therapeutic response [33]. A growing number of studies have shown that exosomes can affect LIHC progression from multiple aspects, such as angiogenesis, chemoresistance, and immune response. Dai et al. found that downregulation of exosomal CLEC3B in LIHC promotes cell metastasis and angiogenesis through AMPK and VEGF signaling [34]. Cho et al. found that exosomal microRNA-4661-5p could be used as a potential diagnostic biomarker for early LIHC [35]. Circulating exo-miR-1307-5p has been shown to promote cell metastasis

in LIHC [36]. The above results suggest that exosomes play a crucial role in LIHC development, and an in-depth exploration of their mechanisms may help to discover new therapeutic strategies. However, the detailed roles of exosome-related gene ENPP1 in LIHC have not been reported. Using comprehensive bioinformatics platforms, we would like to investigate the underlying roles of exosome-related molecules in LIHC in this report. By exploring the co-DEGs between the exosome-associated dataset and three GEO-LIHC datasets, we found that the exosome-associated molecule ENPP1 was significantly downregulated in LIHC patients and was correlated with unfavorable patient prognosis. LinkedOmics also indicated the roles of ENPP1 coexpressed genes in the prognosis of LIHC patients.

Emerging studies have shown aberrant ENPP1 in cancer pathology. Hu et al. demonstrated that dysregulated ENPP1
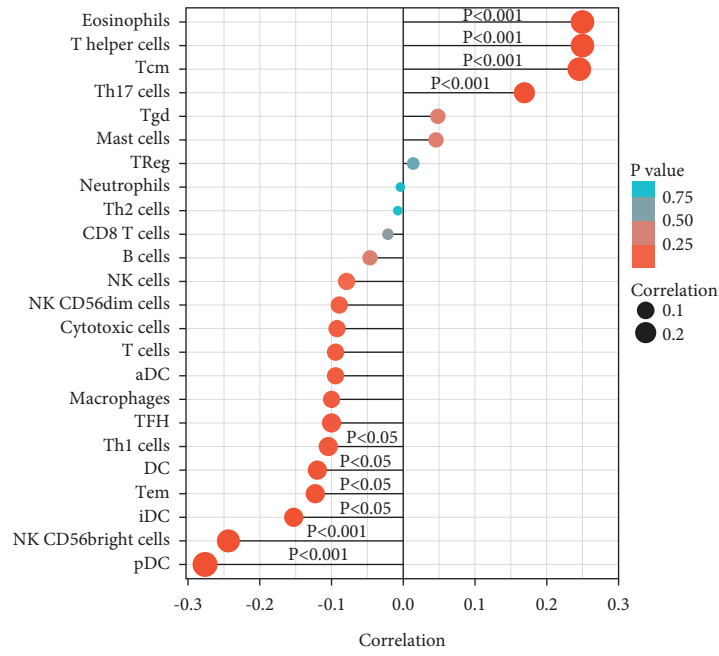
(a)
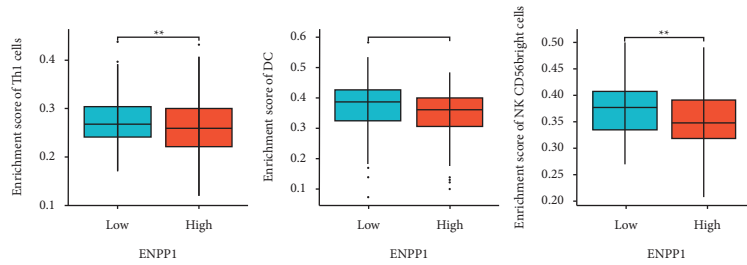
(b)
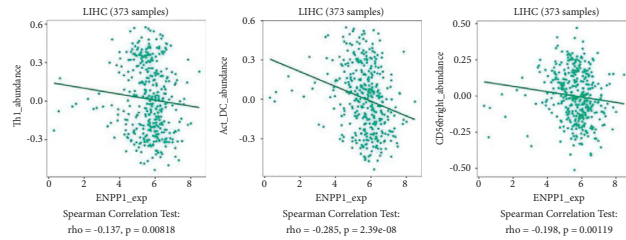
(c)
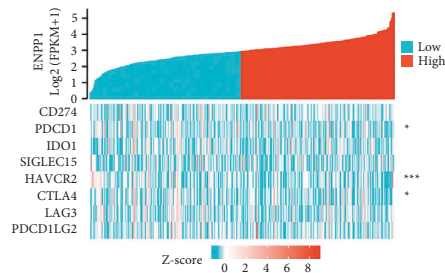
(d)

FIGURE 7: Continued.

(e)
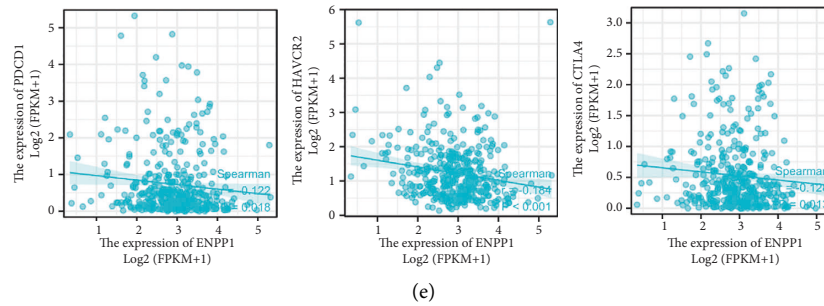
Figure 7: Relationship between ENPP1 expression and tumor-infiltrating immune cells in LIHC. (a) The Xiantao Xueshu indicated the correlation between ENPP1 level and the infiltrating immune cells, (b) the histogram showed the downregulated Th1 cells, DC, and NK CD56bright in ENPP1-highly expressed group, and (c) the histogram shows the negative relationship between ENPP1 and infiltration of Th1 cells, DC, and NK CD56bright. (d) Heat map and (e) scatter plot showed the negative correlation between ENPP9 and three immune checkpoints, PDCD1, HAVCR2, and CTLA4.

(a)

(b)
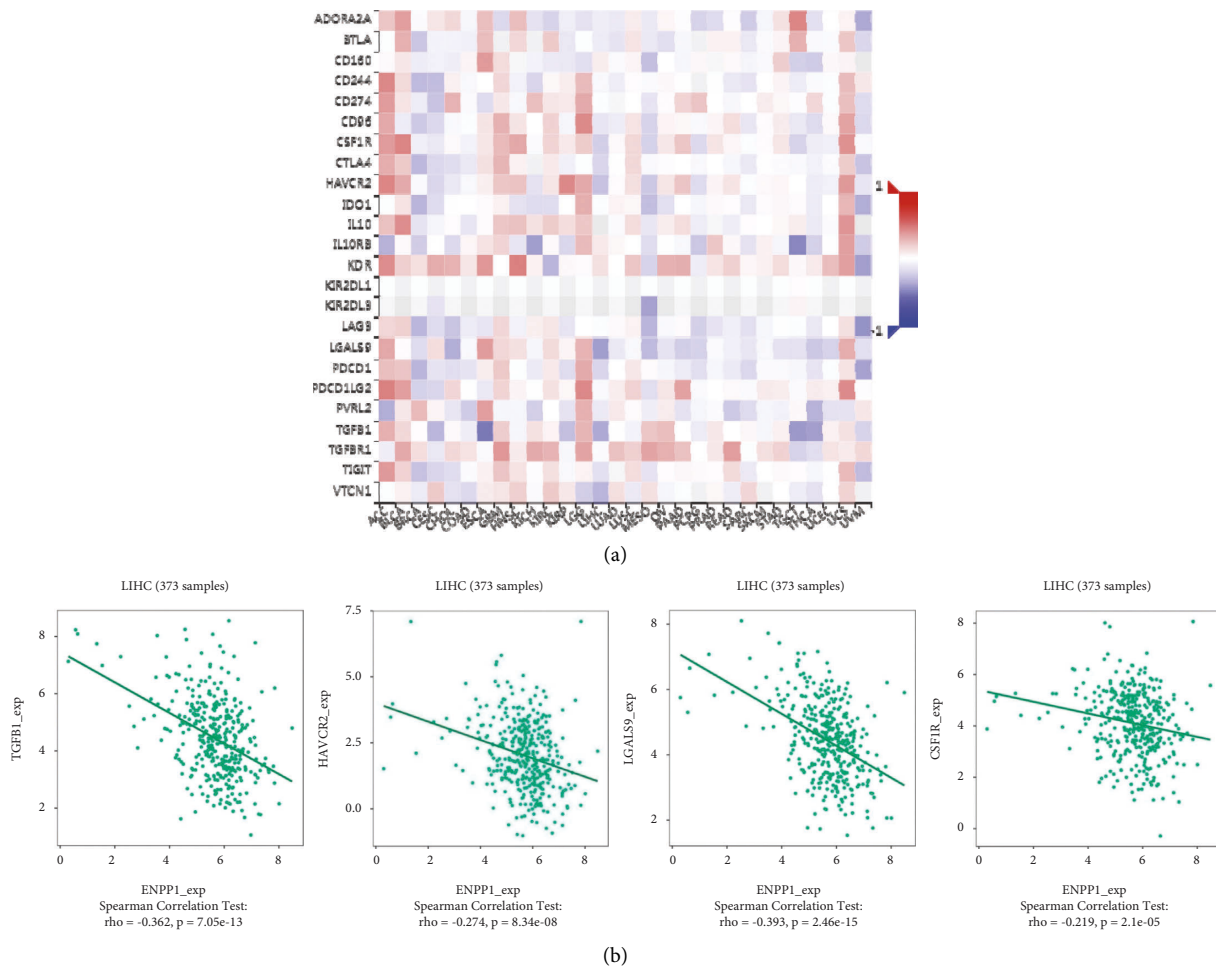
Figure 8: The relationship between ENPP1 and immunoinhibitors in TCGA-LIHC patients. (a) The heatmap indicated the association between ENPP1 and several immunoinhibitors. (b) The correlation analysis between several immunoinhibitors, TGFB1, HAVCR2, LGALS9, and CSF1R, and ENPP1 expression.

increases the malignancy of human lung cancer by inducing epithelial-mesenchymal transition and stem cell characteristics [37]. Wang et al. demonstrated that high expression of ENPP1 in high-grade serous ovarian cancer predicts a poor prognosis and therapeutic response [18]. These studies have demonstrated that ENPP1 plays an important role in the development and treatment of tumors. In our study, ENPP1 was downregulated in LICH tissues compared with normal liver tissues. The LIHC patients with high ENPP1 expression had a good prognosis.

(a)

(b)
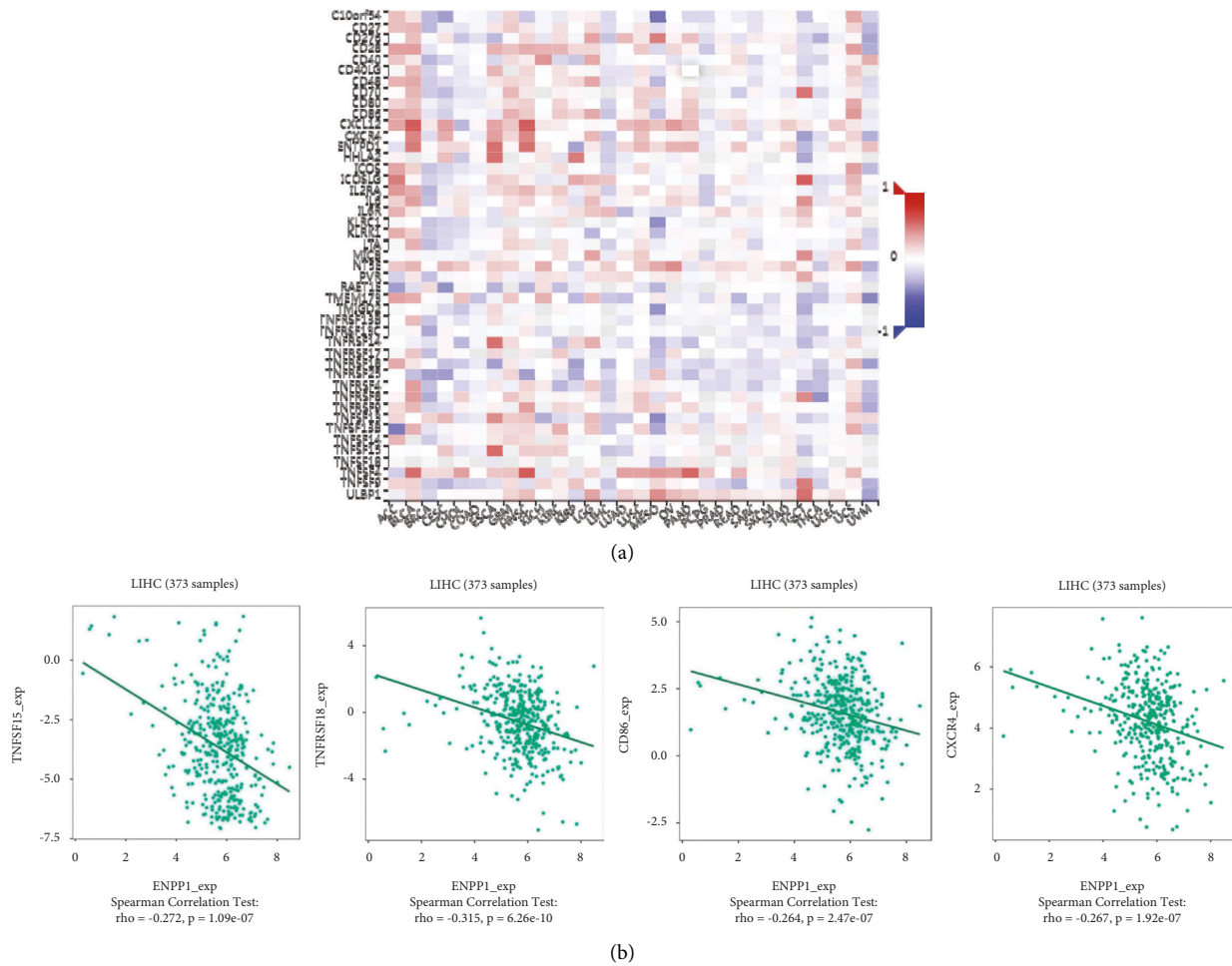
FIGURE 9: The relationship between ENPP1 and immunostimulators in TCGA-LIHC patients. (a) The heatmap indicated the association between ENPP1 and several immunostimulators. (b) The correlation analysis between several immunostimulators, TNFSF15, TNFRSF18, CD86, and CXCR4, and ENPP1 expression.

The immune microenvironment is formed by complex interactions between tumor cells and the host immune response [38]. LIHC shows a high degree of malignant biological properties, which is closely related to the suppression of host immune response [31]. NK cells play a very important role in the prevention of LIHC and have been considered a potential cell therapy resource. NK cell dysfunction is involved in multiple mechanisms leading to the occurrence of LIHC [4]. Additionally, in LIHC, regulatory DCs produce indoleamine-2,3-dioxygenase (IDO) to promote tumor immune escape [39]. Studies have shown that infiltration of Th17 cells correlate with poor prognosis in LIHC [40]. These results indicate that NK cells, DCs, and Th17 are closely related to LIHC. In this paper, the roles of ENPP1 in the regulation of the immune environment were studied. The results showed that ENPP1 was significantly negatively correlated with NK CD56bright cells, DC cells, and Th1 cells. These results suggested that ENPP1 might be a promising biomarker for immunotherapy in LIHC patients.

5. Conclusions

In conclusion, we demonstrated that exosome-associated ENPP1 was downregulated in LIHC and correlated with patient prognosis. In addition, ENPP1 might be involved in the occurrence and development of hepatocellular carcinoma by affecting the immune cell infiltration. Therefore, our study revealed that ENPP1 might be a promising biomarker for LIHC.

Data Availability

The data used to support the findings of this study are included within the supplementary information files.

Conflicts of Interest

The authors declare that they have no conflicts of interest.

Authors' Contributions

Li Z was involved in the acquisition, analysis, and interpretation of data. He Q, Peng J, and Yan Y were involved in conception and design. Li Z and Fu C wrote and revised the manuscript. All authors contributed to the article and approved the submitted version. Zhilan Li 1 and Qingchun He contributed equally to this work.

Acknowledgments

Supplementary Materials

Supplementary Figure 1. Identification of coupregulated molecules between the exosome-associated gene dataset and three GEO-LIHC datasets. Supplementary Figure 2. The relationship between ENPP1 and chemokines in TCGA--LIHC patients. (a) The heatmap indicated the association between ENPP1 and several chemokines and (b) the correlation analysis between several chemokines, CXCL1, CCL26, CXCL8, and CXCL3, and ENPP1 expression. Supplementary Figure 3. The relationship between ENPP1 and chemokine receptors in TCGA-LIHC patients. (a) The heatmap indicated the association between ENPP1 and several chemokine receptors and (b) the correlation analysis between several chemokine receptors, CCR5, CCR10, CXCR3, and CXCR4, and ENPP1 expression. Supplementary Table 1. The exosome-associated gene dataset. Supplementary Table 2. The DEGs between LIHC and normal liver tissue were analyzed from three GEO datasets, GSE6764, GSE14323, and GSE14520. Supplementary Table 3. The top 30 genes were positively linked with ENPP1 in LIHC. Supplementary Table 4. The top 30 genes were negatively linked with ENPP1 in LIHC. (*Supplementary Materials*)

References

[1] D. Cui, W. Li, D. Jiang, J. Wu, J. Xie, and Y. Wu, "Advances in Multi-Omics Applications in HBV-Associated Hepatocellular Carcinoma," *Frontiers in medicine*, vol. 8, Article ID 754709, 2021.

[2] R. I. R. Macias, M. J. Monte, M. A. Serrano et al., "Impact of aging on primary liver cancer: epidemiology, pathogenesis and therapeutics," *Aging*, vol. 13, no. 19, pp. 23416–34, 2021.

[3] D. He, X. Zhang, and J. Tu, "Diagnostic significance and carcinogenic mechanism of pan-cancer gene POU5F1 in liver hepatocellular carcinoma," *Cancer Med*, vol. 9, no. 23, pp. 8782–800, 2020.

[4] S. L. Huang, Y. M. Wang, Q. Y. Wang et al., "Mechanisms and Clinical Trials of Hepatocellular Carcinoma Immunotherapy," *Front Genet*, vol. 12, Article ID 691391, 2021.

[5] X. Yang, W. Lam, Z. Jiang et al., "YIV-906 potentiated anti-PD1 action against hepatocellular carcinoma by enhancing adaptive and innate immunity in the tumor microenvironment," *Scientific reports*, vol. 11, no. 1, Article ID 13482, 2021.

[6] M. Akasu, S. Shimada, A. Kabashima et al., "Intrinsic activation of beta-catenin signaling by CRISPR/Cas9-mediated exon skipping contributes to immune evasion in hepatocellular carcinoma," *Scientific reports*, vol. 11, no. 1, Article ID 16732, 2021.

[7] J. M. Carnino, Z. Hao Kwok, and Y. Jin, "Extracellular Vesicles: A Novel Opportunity for Precision Medicine in Respiratory Diseases," *Frontiers in medicine*, vol. 8, Article ID 661679, 2021.

[8] Y. Lai, L. Dong, H. Jin, H. Li, M. Sun, and J. Li, "Exosome long non-coding RNA SOX2-OT contributes to ovarian cancer malignant progression by miR-181b-5p/SCD1 signaling," *Aging*, vol. 13, no. 20, pp. 23726–38, 2021.

[9] N. Wang, Q. Wang, T. Du et al., "The Potential Roles of Exosomes in Chronic Obstructive Pulmonary Disease," *Frontiers in medicine*, vol. 7, Article ID 618506, 2020.

[10] S. Zhou, J. Fang, M. Hu et al., "Determining the influence of high glucose on exosomal lncRNAs, mRNAs, circRNAs and miRNAs derived from human renal tubular epithelial cells," *Aging*, vol. 13, no. 6, pp. 8467–80, 2021.

[11] R. Rezaei, K. Baghaei, S. M. Hashemi, M. R. Zali, H. Ghanbarian, and D. Amani, "Tumor-Derived Exosomes Enriched by miRNA-124 Promote Anti-tumor Immune Response in CT-26 Tumor-Bearing Mice," *Frontiers in medicine*, vol. 8, Article ID 619939, 2021.

[12] Y. Shimada, J. Matsubayashi, Y. Kudo et al., "Serum-derived exosomal PD-L1 expression to predict anti-PD-1 response and in patients with non-small cell lung cancer," *Scientific reports*, vol. 11, no. 1, p. 7830, 2021.

[13] W. J. Gu, Y. W. Shen, L. J. Zhang et al., "The multifaceted involvement of exosomes in tumor progression: Induction and inhibition," *MedComm*, vol. 2, no. 3, pp. 297–314, 2021.

[14] H. Zhou, Z. H. Yan, Y. Yuan, C. Xing, and N. Jiang, "The Role of Exosomes in Viral Hepatitis and Its Associated Liver Diseases," *Front Med (Lausanne)*, vol. 8, Article ID 782485, 2021.

[15] F. Roberts, D. Zhu, C. Farquharson, and V. E. Macrae, "ENPP1 in the Regulation of Mineralization and Beyond," *Trends in Biochemical Sciences*, vol. 44, no. 7, pp. 616–28, 2019.

[16] I. A. Nikonorova, J. Wang, A. L. Cope et al., "Isolation, profiling, and tracking of extracellular vesicle cargo in *Caenorhabditis elegans*," *Current Biology*, vol. 32, no. 9, pp. 1924–36.e6, 2022.

[17] K. I. Onyedibe, M. Wang, and H. O. Sintim, "ENPP1, an Old Enzyme with New Functions, and Small Molecule Inhibitors-A STING in the Tale of ENPP1," *Molecules*, vol. 24, no. 22, p. 4192, 2019.

[18] H. Wang, F. Ye, C. Zhou, Q. Cheng, and H. Chen, "High expression of ENPP1 in high-grade serous ovarian carcinoma predicts poor prognosis and as a molecular therapy target," *PLoS One*, vol. 16, no. 2, Article ID e0245733, 2021.

[19] J. Bageritz, L. Puccio, R. M. Piro et al., "Stem cell characteristics in glioblastoma are maintained by the ectonucleotidase E-NPP1," *Cell Death Differ*, vol. 21, no. 6, pp. 929–40, 2014.

[20] R. U. Takahashi, H. Miyazaki, F. Takeshita et al., "Loss of microRNA-27b contributes to breast cancer stem cell generation by activating ENPP1," *Nat Commun*, vol. 6, no. 1, p. 7318, 2015.

[21] E. Wurmbach, Y. B. Chen, G. Khitrov et al., "Genome-wide molecular profiles of HCV-induced dysplasia and hepatocellular carcinoma," *Hepatology*, vol. 45, no. 4, pp. 938–47, 2007.

[22] V. R. Mas, D. G. Maluf, K. J. Archer et al., "Genes involved in viral carcinogenesis and tumor initiation in hepatitis C virus-induced hepatocellular carcinoma," *Mol Med*, vol. 15, no. 3-4, pp. 85–94, 2009.

[23] C. Wang, Y. Liao, W. He et al., "Elafin promotes tumour metastasis and attenuates the anti-metastatic effects of erlotinib via binding to EGFR in hepatocellular carcinoma," *J Exp Clin Cancer Res*, vol. 40, no. 1, p. 113, 2021.

[24] Z. Xu, Y. Cai, W. Liu et al., "Downregulated exosome-associated gene FGF9 as a novel diagnostic and prognostic target for ovarian cancer and its underlying roles in immune regulation," *Aging (Albany NY)*, vol. 14, no. 4, pp. 1822–35, 2022.

[25] X. Ren, X. Wang, B. Peng et al., "Significance of TEAD Family in Diagnosis, Prognosis and Immune Response for Ovarian Serous Carcinoma," *International journal of general medicine*, vol. 14, pp. 7133–43, 2021.

[26] A. Bartha and B. Gyorffy, "TNMplot.com: A Web Tool for the Comparison of Gene Expression in Normal, Tumor and Metastatic Tissues," *International Journal of Molecular Sciences*, vol. 22, no. 5, p. 2622, 2021.

[27] D. S. Chandrashekar, S. K. Karthikeyan, P. K. Korla et al., "UALCAN: An update to the integrated cancer data analysis platform," *Neoplasia*, vol. 25, pp. 18–27, 2022.

[28] O. Menyhart, A. Nagy, and B. Gyorffy, "Determining consistent prognostic biomarkers of overall survival and vascular invasion in hepatocellular carcinoma," *R Soc Open Sci*, vol. 5, no. 12, Article ID 181006, 2018.

[29] S. V. Vasaikar, P. Straub, J. Wang, and B. Zhang, "LinkedOmics: analyzing multi-omics data within and across 32 cancer types," *Nucleic Acids Research*, vol. 46, no. D1, pp. D956–D963, 2018.

[30] B. Ru, C. N. Wong, Y. Tong et al., "TISIDB: an integrated repository portal for tumor-immune system interactions," *Bioinformatics*, vol. 35, no. 20, pp. 4200–2, 2019.

[31] Q. Wu, L. Zhou, D. Lv, X. Zhu, and H. Tang, "Exosome-mediated communication in the tumor microenvironment contributes to hepatocellular carcinoma development and progression," *J Hematol Oncol*, vol. 12, no. 1, p. 53, 2019.

[32] Y. Zhang, M. Zhu, J. Mo, and L. Xian, "Tumor microenvironment characterization in esophageal cancer identifies prognostic relevant immune cell subtypes and gene signatures," *Aging*, vol. 13, no. 24, pp. 26118–36, 2021.

[33] V. F. Rauca, L. Patras, L. Luput et al., "Remodeling tumor microenvironment by liposomal codelivery of DMXAA and simvastatin inhibits malignant melanoma progression," *Scientific reports*, vol. 11, no. 1, Article ID 22102, 2021.

[34] W. Dai, Y. Wang, T. Yang, J. Wang, W. Wu, and J. Gu, "Downregulation of exosomal CLEC3B in hepatocellular carcinoma promotes metastasis and angiogenesis via AMPK and VEGF signals," *Cell Commun Signal*, vol. 17, no. 1, p. 113, 2019.

[35] H. J. Cho, G. O. Baek, C. W. Seo et al., "Exosomal microRNA-4661-5p-based serum panel as a potential diagnostic biomarker for early-stage hepatocellular carcinoma," *Cancer Med*, vol. 9, no. 15, pp. 5459–72, 2020.

[36] J. W. Eun, C. W. Seo, G. O. Baek et al., "Circulating Exosomal MicroRNA-1307-5p as a Predictor for Metastasis in Patients with Hepatocellular Carcinoma," *Cancers (Basel)*, vol. 12, no. 12, p. 3819, 2020.

[37] M. Hu, W. Guo, Y. Liao et al., "Dysregulated ENPP1 increases the malignancy of human lung cancer by inducing epithelial-mesenchymal transition phenotypes and stem cell features," *Am J Cancer Res*, vol. 9, no. 1, pp. 134–44, 2019.

[38] R. Shi, Y. Q. Tang, and H. Miao, "Metabolism in tumor microenvironment: Implications for cancer immunotherapy," *MedComm*, vol. 1, no. 1, pp. 47–68, 2020.

[39] J. T. Cheng, Y. N. Deng, H. M. Yi et al., "Hepatic carcinoma-associated fibroblasts induce IDO-producing regulatory dendritic cells through IL-6-mediated STAT3 activation," *Oncogenesis*, vol. 5, no. 2, p. e198, 2016.

[40] J. P. Zhang, J. Yan, J. Xu et al., "Increased intratumoral IL-17-producing cells correlate with poor survival in hepatocellular carcinoma patients," *Journal of Hepatology*, vol. 50, no. 5, pp. 980–9, 2009.

Research Article

The Underlying Roles of Exosome-Associated PIGR in Fatty Acid Metabolism and Immune Signaling in Colorectal Cancer

Ying Liu [ID],[1] Yongbin Hu [ID],[2,3] and Langmei Deng [ID][4]

[1]*Department of Pathology, Xiangya Changde Hospital, Changde, China*
[2]*Department of Pathology, Basic Medical School, Central South University, Changsha, China*
[3]*Department of Pathology, Xiangya Hospital, Central South University, Changsha, China*
[4]*Department of Emergency, The Third Xiangya Hospital, Central South University, Changsha, China*

Correspondence should be addressed to Langmei Deng; denglm@csu.edu.cn

The polymeric immunoglobulin receptor (PIGR), an exosome-associated glycoprotein, plays an important role in the occurrence and development of different tumors. This study aimed to investigate whether PIGR is essential for colorectal cancer (CRC). Comprehensive bioinformatics analysis and immunohistochemistry (IHC) revealed that expression of PIGR was significantly decreased in CRC patients. Upregulated PIGR displayed favorable prognostic values in CRC patients. Several algorithms, such as TISIDB and TIMER, were used to evaluate the roles of PIGR expression in the regulation of immune response in CRC. Moreover, GSEA enrichment analysis indicated the underlying role of PIGR in the regulation of fatty acid metabolism in CRC. Taken together, our findings might provide a new potential prognostic and immune-associated biomarker for CRC and supply a new destination for PIGR-related immunotherapy in clinical treatment.

1. Introduction

Colorectal cancer (CRC) is one of the most common cancers worldwide, with a high incidence and mortality rate [1, 2]. In recent years, various types of clinical treatments have been applied to CRC patients, including systemic chemotherapy and radiation. However, the average 5-year survival rate of CRC patients with positive regional lymph nodes is only 40%, while less than 5% of patients with distant metastases survive beyond 5 years [3, 4]. Therefore, it is significantly important to explore a novel biomarker to improve the overall survival rate of CRC patients.

The tumor immune microenvironment (TIME) has an important role in mediating cytotoxic drug response and tumor progression [5]. Exploring the underlying mechanisms of TIME displays an important role in the occurrence and development of CRC [6, 7]. Immune cells combined with signaling biomarkers could play a crucial role in the prognostic prediction of CRC patients [8, 9]. Therefore, it is very important to further study the tumor microenvironment to improve the patients' overall survival. Exosomes, the nano-sized vesicles, have the inherent potential to shuttle diverse biomolecules like proteins, lipids, and nucleic acids to the recipient cells [10, 11]. Employing exosomes as vehicles for the delivery of products to initiate antitumor immune responses shows striking therapeutic effects [12, 13]. Thus, exosomes could be considered as potential therapeutic targets and valuable biomarkers for the treatment of malignancies.

The polymeric immunoglobulin receptor (PIGR), an exosome-associated glycoprotein, picks up its cargo on the basolateral surface and carries it by the process of transcytosis to the apical face. The function and regulation of PIGR may be closely related to the immune defense of organisms [14]. Numerous studies have recently demonstrated the important roles of aberrant PIGR in different tumors' tumorigenesis. Qi et al. considered that the PIGR may be a tumor suppressor in nasopharyngeal carcinoma [15]. Increased expression of PIGR was correlated with hepatic metastasis and poor prognosis in colon carcinoma

patients [16]. Whereas, more studies are still required to investigate the relationship between PIGR expression and the prognosis of CRC patients.

In this article, we explored the underlying mechanism of PIGR in CRC. Based on bioinformatics analysis and immunohistochemical technology, it was found that the exosome-related gene PIGR was significantly downregulated in CRC tissues. Survival analysis showed that high expression of PIGR was associated with a good prognosis in CRC patients. Furthermore, we analyzed the relationship between PIGR and tumor-infiltrating immune cells (TIICs) in CRC. These findings indicate that PIGR could be a novel prognostic and immune-related biomarker in CRC patients.

2. Materials and Methods

2.1. Data Acquisition. Three CRC datasets, GSE20842 [17], GSE23878 [18] and GSE25070 [19], were downloaded from gene expression omnibus (GEO) database [20] (Table 1). Then, we explored the codifferently expressed genes (co-DEGs) between CRC tissues and normal colorectal tissues. The screening criteria was shown as follows: $|\log FC| \geq 1.5$ and p value <0.05. Next, we used Venn plots to explore the overlapping molecules between the exosome-associated dataset and three GEO datasets. Moreover, we employed the Cancer Genome Atlas (TCGA) database [21] to evaluate the effects of co-DEGs on the clinical characteristics of CRC patients.

2.2. Bioinformatics Platforms. The profiles of co-DEGs were analyzed by comprehensive bioinformatic technologies (Table 2). The Kaplan–Meier plotter [22] was used to evaluate the prognostic values of the overlapping molecules, including overall survival (OS) and recurrence-free survival (RFS). In addition, several databases, such as TNMplot [23], GEPIA2.0 24 and TCGA-CRC, were used to confirm the downregulated expression level of PIGR. Subsequently, we used the Linked-Omics platform [25] to evaluate the interaction between PIGR and its coexpressed genes. Meanwhile, the Linked-Omics platform was used to analyze the gene enrichment. We employed the TISIDB [26], TIMER [27] and single-sample GSEA (ssGSEA) to evaluate the roles of PIGR expression in the regulation of immune response in CRC. We also evaluated the probable relationships between PIGR expression and several immune checkpoints, such as indoleamine 2,3-dioxygenase 1 (IDO1), CD274, programmed cell death 1 (PDCD1), cytotoxic T-lymphocyte associated protein 4 (CTLA4), and lymphocyte activating 3 (LAG3).

2.3. Immunohistochemistry (IHC). Tissue sections were deparaffinized in xylene and rehydrated with ethanol, and then preincubated with 10% normal goat serum in pharmaceutical benefits scheme (PBS) (pH 7.5). Then, the tissue slides were incubated with the primary antibody overnight at 4°C and then stained with a biotinylated secondary antibody (SAB4600042, Sigma-Aldrich) for 1 h at room temperature. The peroxidase reaction was visualized with a 3, 3-

diaminobenzidine chromogenic kit (ZLI-9019, ORI-GENE). After that, the tissues were photographed under a conventional microscope (DMI3000 B, Leica). The formalin-fixed, paraffin-embedded specimens of CRC and adjacent tissues were obtained from the Department of Pathology, Xiangya Hospital, Central South University. The ethics for this study (202205114) was approved by the Ethical Committee of Xiangya Hospital, Central South University.

2.4. Statistical Analysis. In this report, the statistical difference was investigated by t-test assay. And the data were mainly depicted as the mean ± standard deviation (SD). P values <0.05 was considered to demonstrate statistically significant differences.

3. Results

3.1. Identification of the Co-DEGs in Colorectal Cancer. We explored the co-DEGs between CRC tissues and normal colorectal tissues from three GEO-CRC datasets. And we found 1262 upregulated genes and 883 downregulated genes in GSE20842, 258 upregulated genes and 1011 downregulated genes in GSE23878, and 86 upregulated genes and 222 downregulated genes in GSE25070 (Supplementary Table S1). A Venn analysis (http://bioinformatics.psb.ugent. be/webtools/Venn/) was used to explore the potential differently-expressed exosome-related genes in CRC. Accordingly, one downregulated exosome-related gene, PIGR, was identified in CRC tissues (Figure 1(a)). Then, the Kaplan–Meier plotter database was used to analyze the effects of PIGR expression on the prognosis in CRC patients. As shown in Figures 1(b) and 1(c), high expression level of PIGR was related with good OS (HR = 0.39, 95% CI = 0.17–0.88, $p = 0.018$) and RFS (HR = 0, 95% CI = 0-Inf, $p = 0.013$) in CRC patients. These results collectively suggest that PIGR overexpression could be significantly associated with a favorable prognosis in CRC patients.

3.2. Downregulated Expression of PIGR in Colorectal Cancer. By comprehensively analyzing the expression levels of PIGR in the three GEO-CRC datasets, we found that PIGR was lowly expressed in CRC tissues ($p < 0.0001$) (Figures 2(a)–2(c)). Besides, the data results from TCGA-CRC further verified that the expression level of PIGR was significantly different between the normal group and the CRC group ($p < 0.0001$) (Figure 2(d)). What's more, the TNMplot database indicated that PIGR mRNA expression was both lower in CRC tissues from gene chip data ($p = 3.06e - 17$) and RNA-seq data ($p = 5.68e - 07$) (Figures 2(e) and 2(f)). In addition, the IHC results confirmed that PIGR was downregulated in CRC tissues. Together, these results proved the lower expression of PIGR at mRNA and protein levels in CRC.

3.3. The Coexpression Network of PIGR in Colorectal Cancer. We explored the coexpression network and biological functions of PIGR in the TCGA-Colorectal adenocarcinoma

TABLE 1: The upregulated genes and downregulated genes in the three GEO datasets.

GEO datasets	Platform	Sample size		DEGs	References
		Cancer	Normal		
GSE20842	GPL4133	65	65	1263 upregulated genes and 884 downregulated genes	[17]
GSE23878	GPL570	35	24	258 upregulated genes and1012 downregulated genes	[18]
GSE25070	GPL6883	26	26	87 upregulated genes and 223 downregulated genes	[19]

TABLE 2: Bioinformatics platforms that are employed to analyze the role of PIGR in colorectal cancer.

Database	URL	References
GEO	https://www.ncbi.nlm.nih.gov/gds/?term=	[20]
TCGA	https://portal.gdc.cancer.gov/	[21]
Kaplan–Meier plotter	https://kmplot.com/analysis/	[22]
TNMplot	https://www.tnmplot.com	[23]
GEPIA2.0	https://gepia.cancer-pku.cn/	[24]
Linked-Omics	https://www.linkedomics.org/admin.php	[25]
TISIDB	https://cis.hku.hk/TISIDB/	[26]
TIMER	https://cistrome.shinyapps.io/timer/	[27]
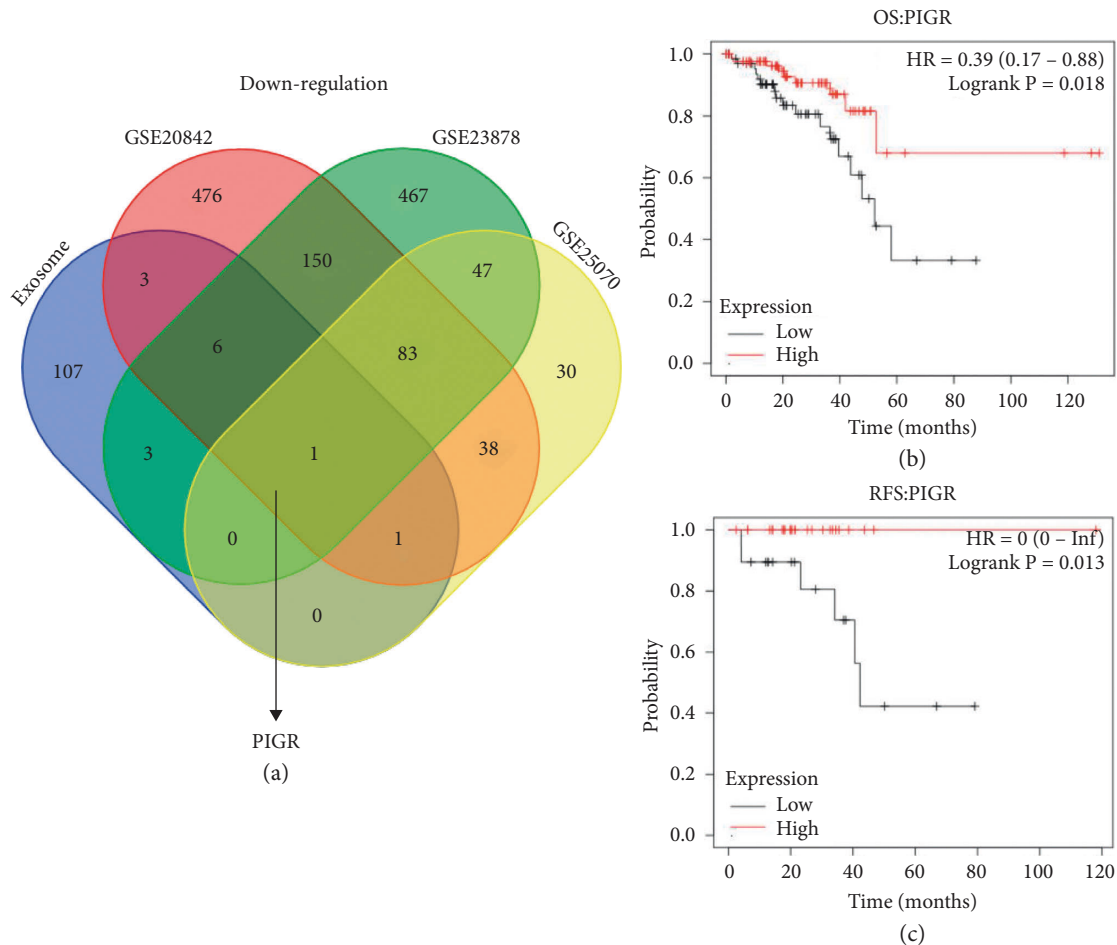
FIGURE 1: Identification of downregulated exosome-related PIGR in CRC. (a) The Venn plot showed one downregulated exosome-correlated gene (PIGR) in CRC progression. (b-c) The prognostic values of PIGR in CRC patients. Abbreviations: OS, overall survival; RFS, recurrence-free survival.

(COADREAD) cohort. In Figure 3(a) and Supplementary Table S2, we presented the PIGR coexpressed genes. Meanwhile, Figures 3(b) and 3(c) and Supplementary Tables S3 and S4 have demonstrated these candidate genes that are positively and negatively correlated with PIGR in CRC patients. Notably, the top 20 positively-related genes
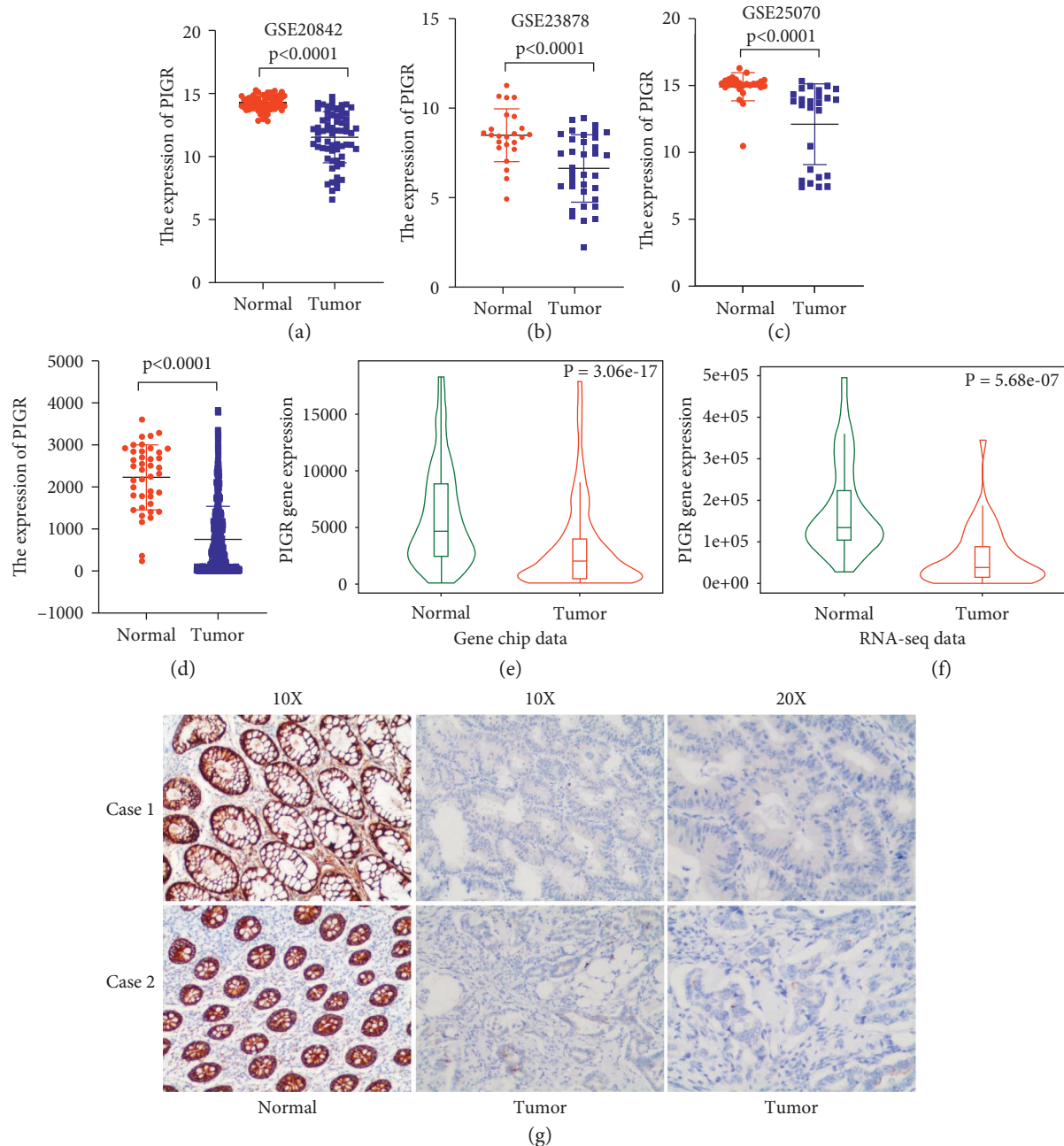
Figure 2: PIGR was downregulated in CRC patients. (a-c) The expression level of PIGR was lower in the three GEO-CRC datasets. (d) The expression level of PIGR was lower in the TCGA-CRC. (e-f) TNMplot database depicting the downregulated PIGR expression in CRC tissues from gene chip data and RNA-seq data. (g) Representative IHC results showing the downregulated PIGR expression in CRC tissues.

were highly likely to be low-risk factors for CRC patients (Figure 3(d)). Furthermore, 1 of top 20 negatively-related genes might be the high-risk factor in CRC (Figure 3(e)). In addition, the Gene Ontology showed that the genes coexpressed with PIGR were mainly involved in multiple biological process categories, such as biological regulation, metabolic processes, and response to stimulus. In the category of cellular component, these genes mainly took part in the membrane, nucleus and membrane-enclosed lumen. Then, in the molecular function categories, these coexpressed genes are involved in the protein binding, ion

binding, and nucleic acid binding (Figure 3(f)). Moreover, the KEGG analysis indicated that the most likely enriched pathways were carbon metabolism, fructose and mannose metabolism, hippo signaling pathway, and Notch signaling pathway (Figure 3(g)).

Next, we performed GSEA enrichment analysis of PIGR-related genes in CRC. As shown in Figures 4(a)–4(g), aberrantly expressed PIGR might involve in the regulation of fatty acid metabolism-related signaling pathways, such as mitochondrial fatty acid beta oxidation, mitochondrial fatty acid beta oxidation, fatty acid metabolism, nonalcoholic

(a)

(b)

(c)

(d)

(e)

(f)

(g)
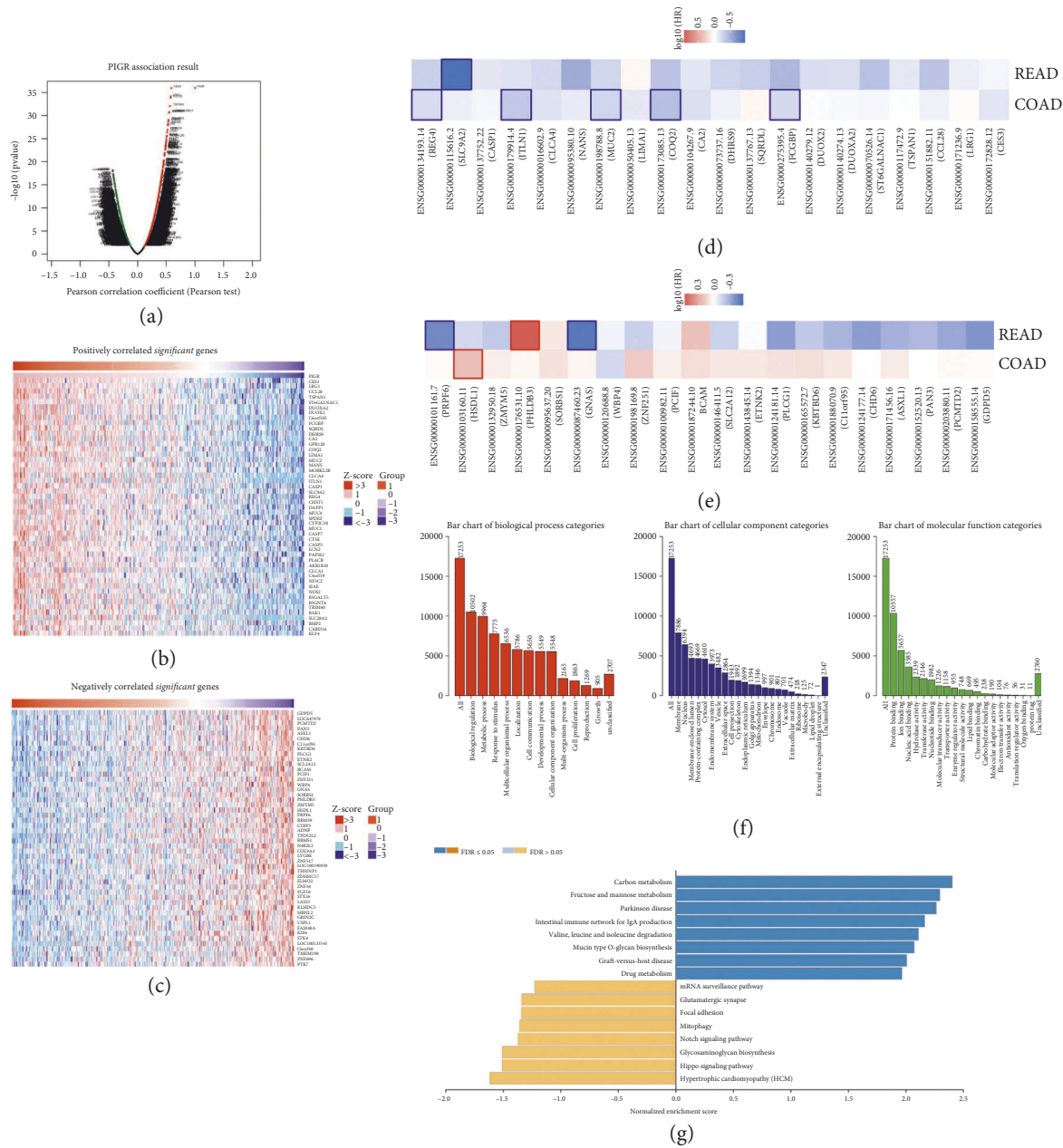
Figure 3: The coexpression network of PIGR in CRC. (a) The Linked-Omics platform portraying the crucially associated genes with PIGR in CRC patients. (b-c) Heatmaps showing the top genes that were positively and negatively correlated with PIGR in CRC. (d-e) Survival heatmaps downloaded from the GEPIA2.0 database displayed that the top genes that were positively and negatively associated with PIGR in CRC. (f-g) GO and KEGG enrichment of PIGR-coexpressed genes in CRC patients.

fatty acids. All the statistical significance was $p < 0.05$. Overall, our results suggest that PIGR may be involved in the cellular metabolism in CRC.

3.4. The Link between PIGR with Immune Regulation.

We used ssGSEA to analyze the effects of PIGR on immune regulation in the TCGA-COADREAD cohort. The expression of PIGR was significantly positively correlated with T helper type 17 (Th17) cells, B cells, and so on (Figure 5(a)). The results obtained from TISIDB database also confirmed the similar findings (Figure 5(b)). The scatter plot from

TIMER database further demonstrated that the expression level of PIGR was strongly positively correlated with B cell in colon adenocarcinoma (COAD) and rectum adenocarcinoma (READ) patients (Figure 5(c)).

Next, we explored the relationship between PIGR expression and several immune checkpoints and found that the expression level of PIGR was positively correlated with IDO1 (Spearman $r = 0.186$, $p < 0.001$), CD274 (Spearman $r = 0.147$, $p < 0.001$), PDCD1 (Spearman $r = 0.186$, $p < 0.001$), CTLA4 (Spearman $r = 0.103$, $p = 0.009$), and LAG3 (Spearman $r = 0.232$, $p < 0.001$) (Figures 6(a)–6(c)). The patients with high level of PIGR displayed overexpressed
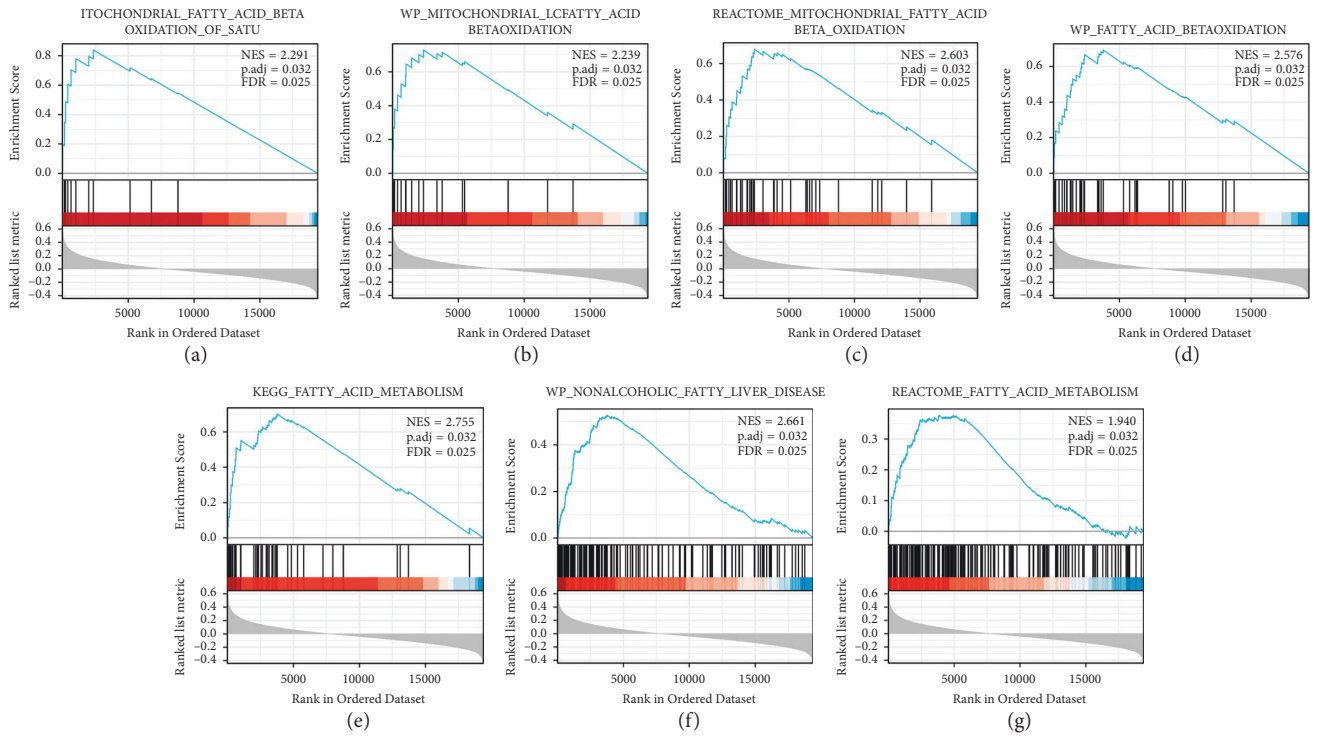
Figure 4: The GSEA enrichment analysis of PIGR-related genes in CRC. (a-g) PIGR-related genes were involved in several fatty acid metabolism pathways in CRC, such as mitochondrial fatty acid beta oxidation.

(a)

Figure 5: Continued.

(b)

(c)
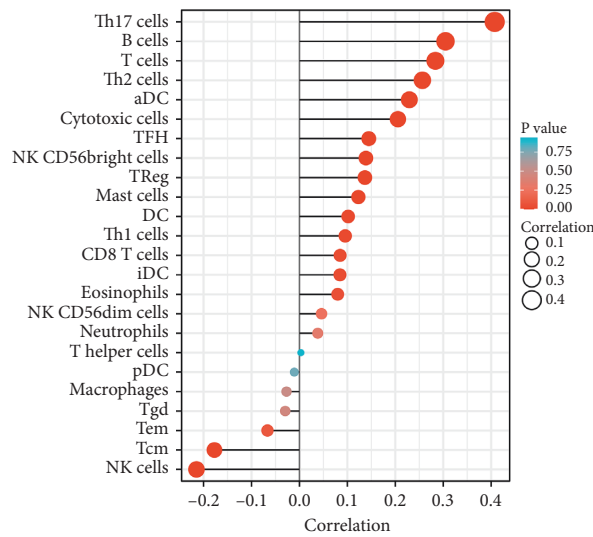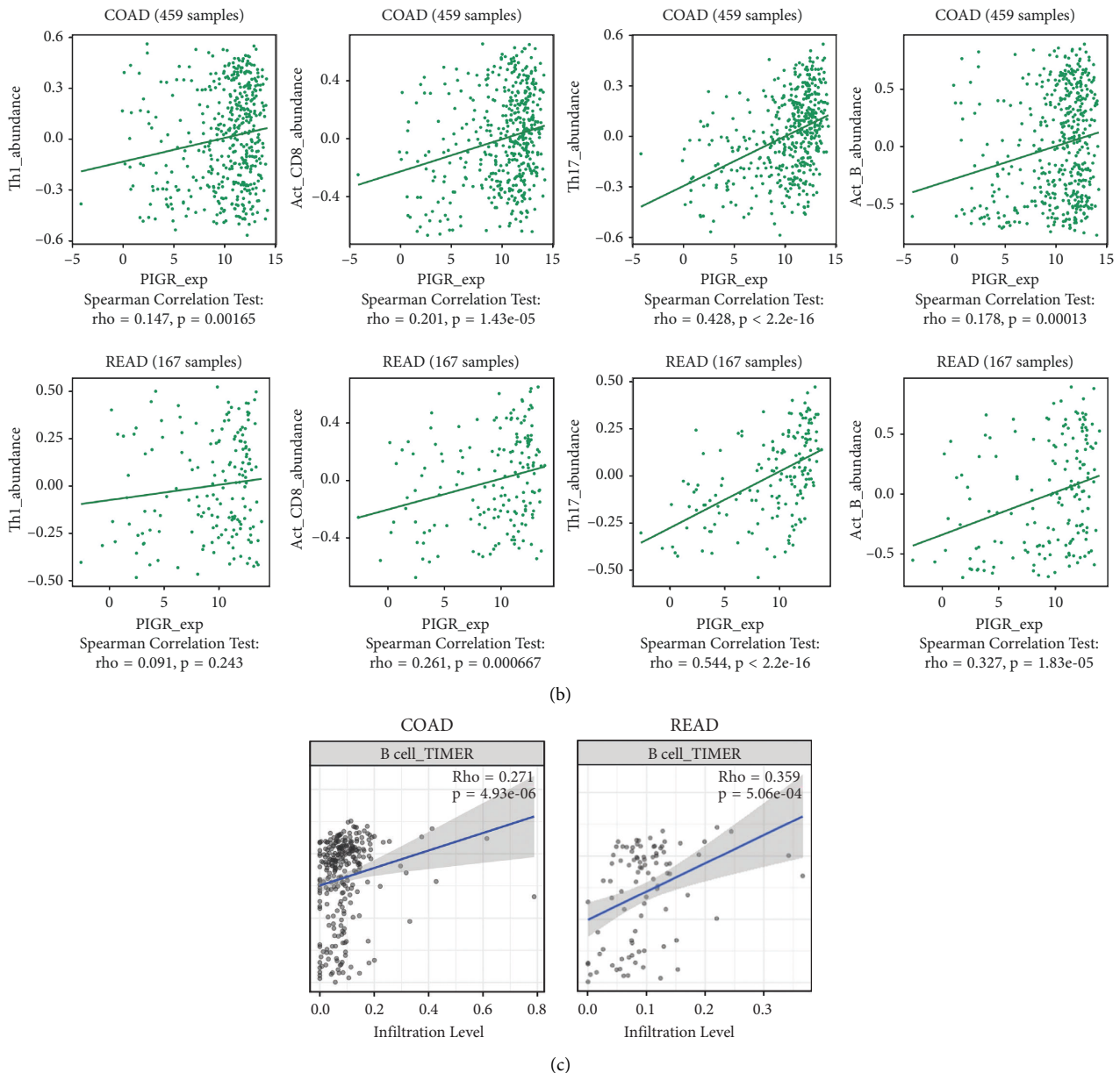
FIGURE 5: The relationship between the expression level of PIGR and immune cells in CRC patients. (a) The diagraph showing the relation between PIGR expression and 24 types of immune cells. (b) TISIDB database showed the relationship between PIGR and immune infiltration cells, such as T helper type 17 (Th17) cells, B cells, and so on. (c) TIMER database showed the relationship between the expression level of PIGR and immune infiltration cells.

IDO1, CD274, PDCD1, CTLA4, and LAG3 (Figure 6(f)). Additionally, the results from the TISIDB platform showed the relationship between PIGR levels and other immune-associated signatures, including immuno inhibitors and cytokine receptors. Figure 7(a) conveyed the correlation between the immuno inhibitors and the expression of PIGR in CRC patients. The top three immuno inhibitors closely related to PIGR were galectin 9 (LGALS9), LAG3, and CD244 (Figure 7(b)). In addition, the correlation between PIGR and cytokine receptors has been displayed in Figure 7(c). And the top three receptors positively associated with PIGR expression were C-X-C motif chemokine ligand 3 (CXCL3), C-X-C motif chemokine ligand 17 (CXCL17), and

C–C motif chemokine ligand 28 (CCL28) (Figure 7(d)). Taken together, these findings suggest that aberrantly expressed PIGR is involved in the immune regulation of CRC patients.

4. Discussion

Numerous studies have indicated the important role of exosomes in the occurrence and development of human cancers [28]. In this article, we elucidated the downregulated exosome-associated gene, PIGR, in the prognosis and immune regulation of CRC patients. Using the Kaplan–Meier plotter database, we found that high expression of PIGR was

(a)

(b)

(c)

(d)

(e)

(f)
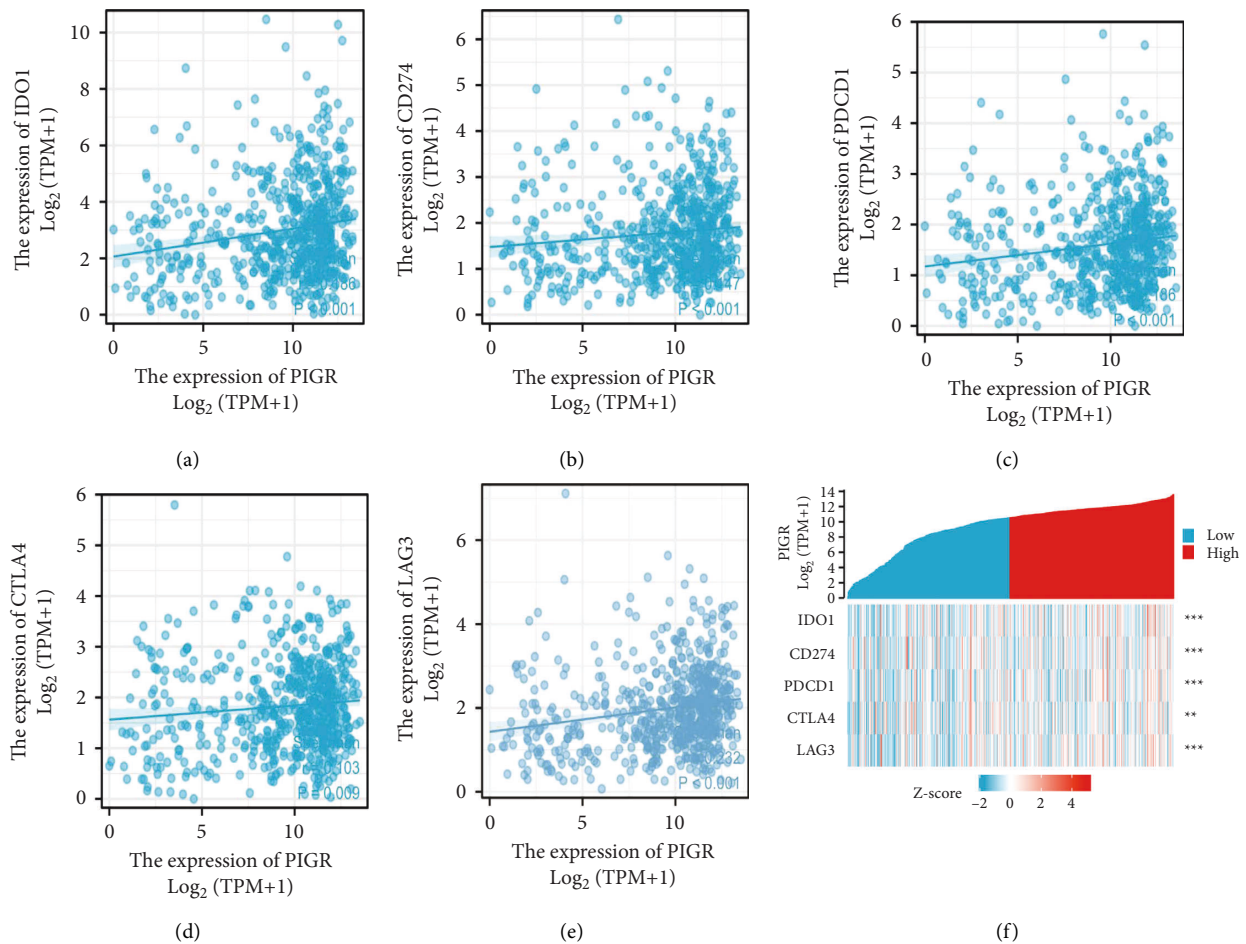
Figure 6: The relationship between PIGR expression and several immune checkpoints. (a-f) The scatterplot and heatmap depicted that PIGR expression was positively correlated to IDO1, CD274, PDCD1, CTLA4, and LAG3.

associated with a better prognosis in CRC patients. Gene enrichment analysis indicated that the coexpressed genes of PIGR were involved in the regulation of the immune microenvironment and fatty acid metabolism in CRC.

Exosomes are small extracellular vesicles secreted by almost all types of cells, including tumor cells. As important mediators of intercellular communication, exosomes provide an alternative cargo-handling mechanism to maintain homeostasis and cell survival [29]. Exosomes enhanced or inhibited certain important mediators and changed the tumor microenvironment, thereby altering the occurrence and development of different types of tumors [30–32]. Some differentially expressed RNAs and proteins in exosomes have been identified as potential biomarkers linked to CRC initiation and progression. Wang et al. considered that CRC cell-derived exosomal miR-146a-5p and miR-155-5p could activate the JAK2-STAT3/NF-κB signaling pathways, thereby enhancing the invasive ability of CRC cells [33]. Studies have found that in human CRC cells, exosomal Nrf2 plays a pivotal role in oxaliplatin resistance [34]. Thus, further studies into the underlying mechanisms of exosomes might be beneficial for the treatment management of CRC patients. Accordingly, our study aimed to explore the prognostic values of PIGR in CRC patients, and we

concluded that a high expression level of PIGR was associated with a good prognosis.

Nowadays, the roles of aberrant PIGR in tumors remain controversial, which might be due to the tumor heterogeneity or the different underlying mechanisms. In hepatocellular carcinoma, PIGR-loaded extracellular vesicles could activate Akt/GSK3β/β-catenin signaling cascades, driving cancer stemness, tumorigenesis, and metastasis [35]. Ohkuma et al. have assessed the prognostic value of PIGR in pancreatic cancer patients after surgical resection and determined that the overexpression of PIGR was correlated with poor prognosis in pancreatic cancer [36]. Through transcriptomic sequencing analysis, Bao et al. demonstrated that PIGR was downregulated in breast cancer. PIGR overexpression could suppress cell proliferation and adhesion in breast cancer cells [37]. In this paper, the bioinformatics and IHC results revealed the downregulated exosome-related PIGR in CRC tissues.

Immunotherapy is a novel anticancer method in the clinic. The combination of traditional treatment methods with immune checkpoint inhibitors could provide promising treatment strategies for cancer patients, including CRC [38]. Numerous studies have shown that immunotherapy can inhibit the growth of colorectal cancer cells and prolong
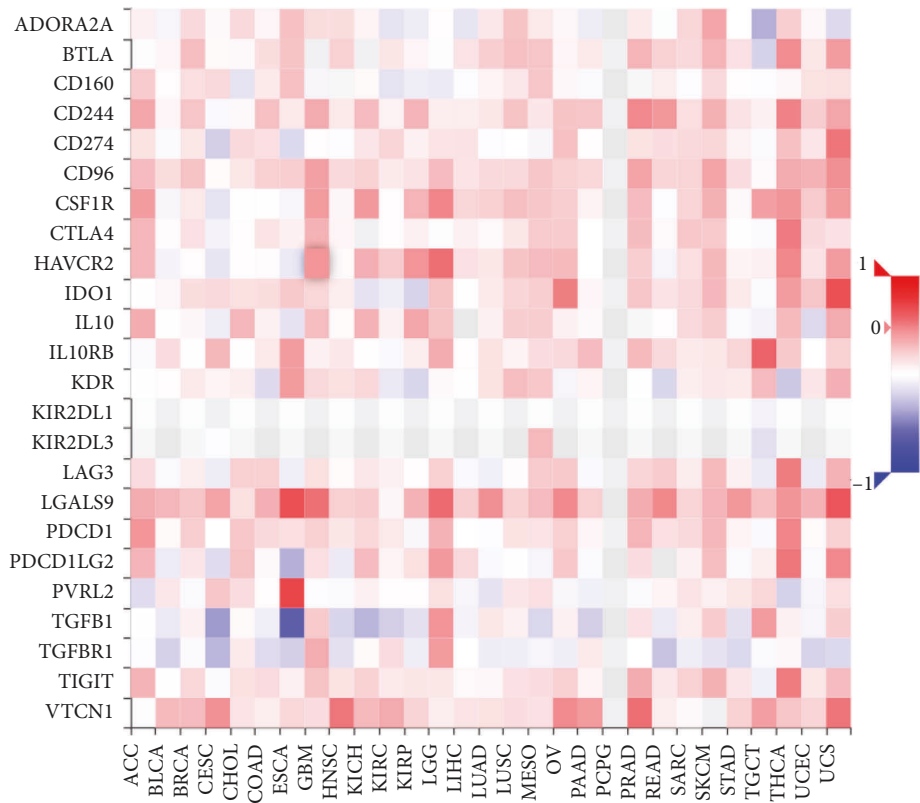
(a)
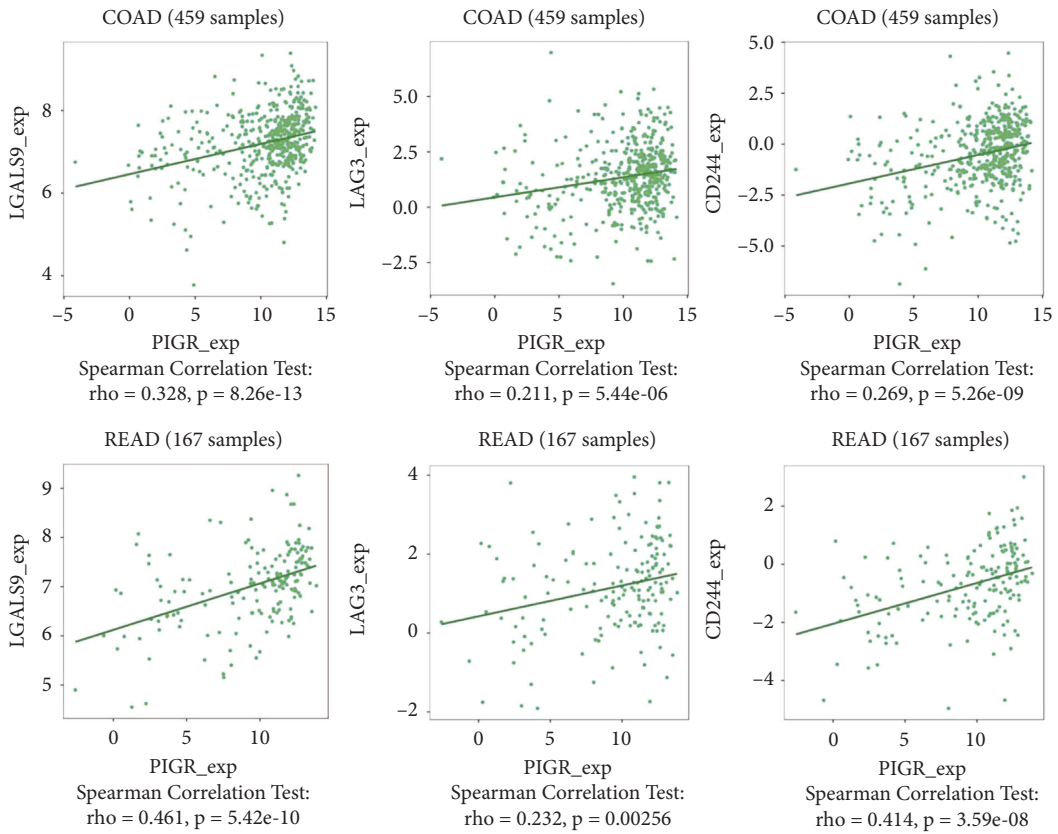
(b)

Figure 7: Continued.

(c)

(d)
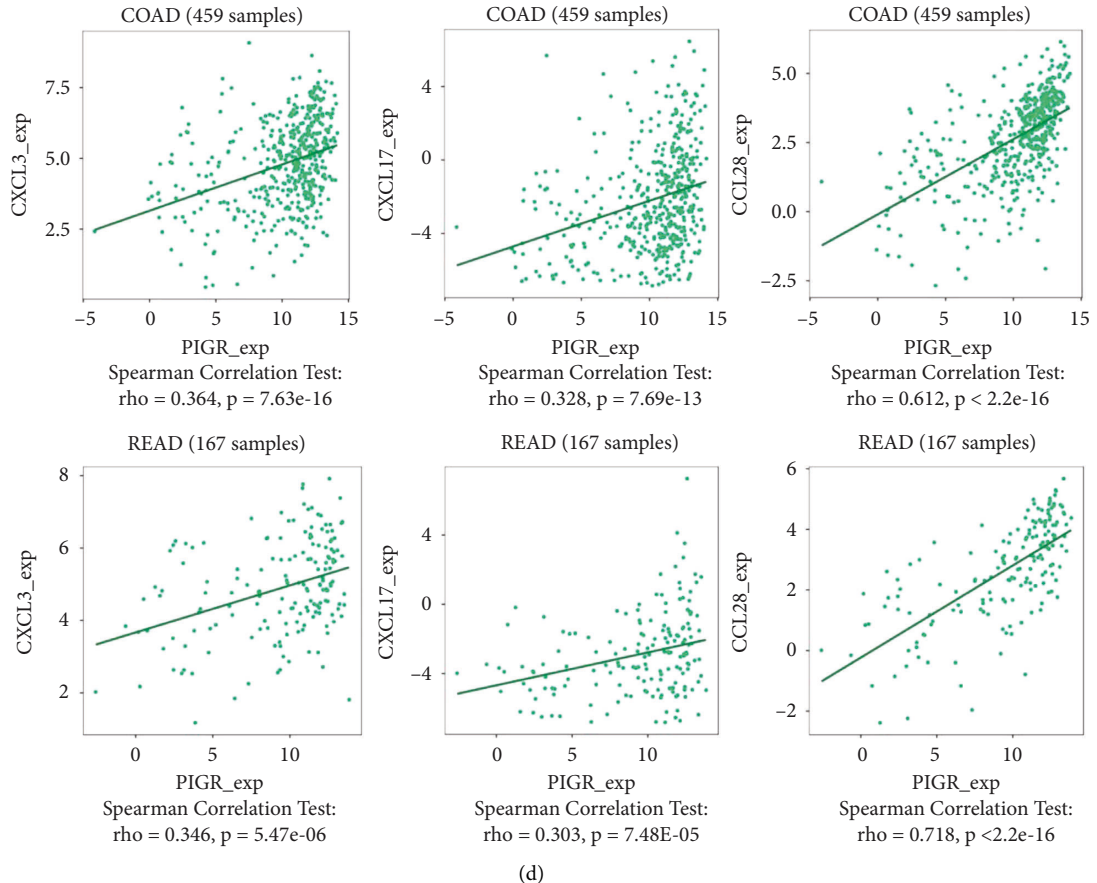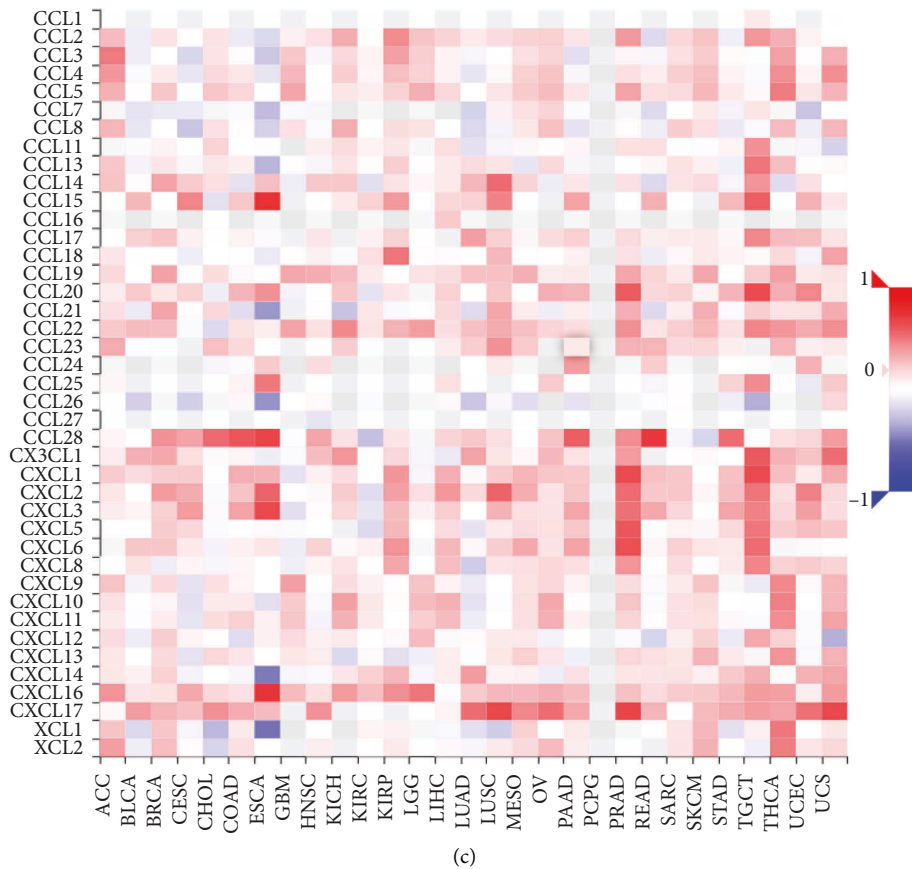
Figure 7: The roles of PIGR in the regulation of immunoinhibitors and cytokine receptors in CRC patients. (a) The diagraph showing the correlation between PIGR expression and immunoinhibitors. (b) The scatter plots depicting the top three immunoinhibitors positively-related with PIGR expression. (c) The picture showing the connection between PIGR expression and cytokine receptors. (d) The scatter plots portraying the top three cytokine receptors positively-related with PIGR expression.

the survival period of patients [39–41]. In this paper, the correlation between PIGR and immune-associated signatures was explored by comprehensive bioinformatic technologies. PIGR was positive with tumor-infiltrating of B cells, Th17 cells, T cells, and Th2 cells. Meanwhile, PIGR had a negative correlation with tumor-infiltrating NK cells and Tcm cells. Studies have demonstrated that immune checkpoint inhibitors have been regarded as potential strategies for enhancing immune responses in patients with CRC [42]. We found that the expression of PIGR had a positive relationship with several immune checkpoints, including IDO1, CD274, PDCD1, CTLA4, and LAG3. These above results implied that PIGR was strongly associated with immune responses and immune regulation, implying that PIGR could be a novel prognostic and immune-related biomarker of CRC patients.

5. Conclusion

Overall, this paper reported that the downregulated exosome-associated gene PIGR was significantly associated with a good prognosis in CRC patients. Aberrant PIGR expression might participate in the regulation of immune response and fatty acid metabolism. Therefore, we identified PIGR as a novel, valuable prognostic and immune-related biomarker for patients with CRC.

Data Availability

The original contributions presented in the study are included in the article/Supplementary Material and are available upon request to the corresponding authors.

Disclosure

Ying Liu and Yongbin Hu are co-first authors.

Conflicts of Interest

The authors declare that there are no conflicts of interest.

Authors' Contributions

YL and YH performed conception and design and also performed writing, reviewing, and/or revision of the manuscript. Administrative, technical, or material support was provided by YL and LD. All authors approved the final version of the manuscript. Ying Liu and Yongbin Hu contributed equallly to this work.

Acknowledgments

Supplementary Materials

Supplementary Table 1. The upregulated genes and down-regulated genes in the three GEO datasets. Supplementary Table 2. The coexpressed genes possess a positive and negative relationships with PIGR. Supplementary Table 3. The top 20 genes positively correlated with PIGR in colorectal cancer. Supplementary Table 4. The top 20 genes negatively correlated with PIGR in colorectal cancer. (*Supplementary Materials*)

References

[1] Z. N. Lei, Q. X. Teng, Z. X. Wu et al., "Overcoming multidrug resistance by knockout of ABCB1 gene using CRISPR/Cas9 system in SW620/Ad300 colorectal cancer cells," *MedComm*, vol. 2, no. 4, pp. 765–777, 2021.

[2] C. Li, K. Zhang, G. Pan et al., "Dehydrodiisoeugenol inhibits colorectal cancer growth by endoplasmic reticulum stress-induced autophagic pathways," *Journal of Experimental & Clinical Cancer Research*, vol. 40, no. 1, p. 125, 2021.

[3] A. Fonseca, S. V. Ramalhete, A. Mestre et al., "Identification of colorectal cancer associated biomarkers: an integrated analysis of miRNA expression," *Aging*, vol. 13, no. 18, 2021.

[4] R. C. Zhou, P. Z. Wang, Y. Y. Li et al., "Quality improvement of sample collection increases the diagnostic accuracy of quantitative fecal immunochemical test in colorectal cancer screening: a pilot study," *Frontiers of Medicine*, vol. 8, Article ID 762560, 2021.

[5] R. Shi, Y. Q. Tang, and H. Miao, "Metabolism in tumor microenvironment: implications for cancer immunotherapy," *MedComm*, vol. 1, no. 1, pp. 47–68, 2020.

[6] Y. F. Chen, Z. L. Yu, M. Y. Lv et al., "Genome-Wide analysis reveals hypoxic microenvironment is associated with immunosuppression in poor survival of stage II/III colorectal cancer patients," *Frontiers of Medicine*, vol. 8, Article ID 686885, 2021.

[7] Y. Liu, L. Cheng, C. Li, C. Zhang, L. Wang, and J. Zhang, "Identification of tumor microenvironment-related prognostic genes in colorectal cancer based on bioinformatic methods," *Scientific Reports*, vol. 11, no. 1, Article ID 15040, 2021.

[8] Y. Yin, S. Yao, Y. Hu et al., "The immune-microenvironment confers chemoresistance of colorectal cancer through macrophage-derived IL6," *Clinical Cancer Research*, vol. 23, no. 23, 2017.

[9] V. Schimek, K. Strasser, A. Beer et al., "Tumour cell apoptosis modulates the colorectal cancer immune microenvironment via interleukin-8-dependent neutrophil recruitment," *Cell Death & Disease*, vol. 13, no. 2, p. 113, 2022.

[10] M. Y. Kim, H. Shin, H. W. Moon, Y. H. Park, J. Park, and J. Y. Lee, "Urinary exosomal microRNA profiling in intermediate-risk prostate cancer," *Scientific Reports*, vol. 11, no. 1, 2021.

[11] R. Koomullil, B. Tehrani, K. Goliwas et al., "Computational simulation of exosome transport in tumor microenvironment," *Frontiers of Medicine*, vol. 8, Article ID 643793, 2021.

[12] Y. Shimada, J. Matsubayashi, Y. Kudo et al., "Serum-derived exosomal PD-L1 expression to predict anti-PD-1 response and in patients with non-small cell lung cancer," *Scientific Reports*, vol. 11, no. 1, Article ID 7830, 2021.

[13] A. Thakur, X. Ke, Y. W. Chen et al., "The mini player with diverse functions: extracellular vesicles in cell biology, disease, and therapeutics," *Protein and cell*, vol. 13, no. 9, pp. 631–654, 2022.

[14] F. E. Johansen and C. S. Kaetzel, "Regulation of the polymeric immunoglobulin receptor and IgA transport: new advances in environmental factors that stimulate pIgR expression and its

role in mucosal immunity," *Mucosal Immunology*, vol. 4, no. 6, pp. 598–602, 2011.

[15] X. Qi, X. Li, and X. Sun, "Reduced expression of polymeric immunoglobulin receptor (pIgR) in nasopharyngeal carcinoma and its correlation with prognosis," *Tumor Biology*, vol. 37, no. 8, 2016.

[16] F. Liu, P. Ye, T. Bi et al., "COLORECTAL polymeric immunoglobulin receptor expression is correlated with hepatic metastasis and poor prognosis in colon carcinoma patients with hepatic metastasis," *Hepato-Gastroenterology*, vol. 61, no. 131, pp. 652–659, 2014.

[17] J. Gaedcke, M. Grade, K. Jung et al., "Mutated KRAS results in overexpression of DUSP4, a MAP-kinase phosphatase, and SMYD3, a histone methyltransferase, in rectal carcinomas," *Genes, Chromosomes and Cancer*, vol. 49, no. 11, 2010.

[18] S. Uddin, M. Ahmed, A. Hussain et al., "Genome-wide expression analysis of Middle Eastern colorectal cancer reveals FOXM1 as a novel target for cancer therapy," *American Journal Of Pathology*, vol. 178, no. 2, pp. 537–547, 2011.

[19] T. Hinoue, D. J. Weisenberger, C. P. Lange et al., "Genome-scale analysis of aberrant DNA methylation in colorectal cancer," *Genome Research*, vol. 22, no. 2, pp. 271–282, 2012.

[20] E. Clough and T. Barrett, "The gene expression omnibus database," *Methods in Molecular Biology*, vol. 1418, pp. 93–110, 2016.

[21] J. McCain, "The cancer genome atlas: new weapon in old war?" *Biotechnology Healthcare*, vol. 3, no. 2, pp. 46–51B, 2006.

[22] A. Lanczky and B. Gyorffy, "Web-Based survival analysis tool tailored for medical research (KMplot): development and implementation," *Journal of Medical Internet Research*, vol. 23, no. 7, Article ID e27633, 2021.

[23] A. Bartha and B. Gyorffy, "TNMplot.com: a web tool for the comparison of gene expression in normal, tumor and metastatic tissues," *International Journal of Molecular Sciences*, vol. 22, no. 5, 2021.

[24] Z. Tang, B. Kang, C. Li, T. Chen, and Z. Zhang, "GEPIA2: an enhanced web server for large-scale expression profiling and interactive analysis," *Nucleic Acids Research*, vol. 47, 2019.

[25] S. V. Vasaikar, P. Straub, J. Wang, and B. Zhang, "LinkedOmics: analyzing multi-omics data within and across 32 cancer types," *Nucleic Acids Research*, vol. 46, 2018.

[26] B. Ru, C. N. Wong, Y. Tong et al., "TISIDB: An integrated repository portal for tumor-immune system interactions," *Bioinformatics*, vol. 35, no. 20, 2019.

[27] T. Li, J. Fan, B. Wang et al., "TIMER: a web server for comprehensive analysis of tumor-infiltrating immune cells," *Cancer Research*, vol. 77, no. 21, pp. e108–e110, 2017.

[28] W. J. Gu, Y. W. Shen, L. J. Zhang et al., "The multifaceted involvement of exosomes in tumor progression: induction and inhibition," *MedComm*, vol. 2, no. 3, pp. 297–314, 2021.

[29] H. Jiang, H. Zhao, M. Zhang et al., "Hypoxia induced changes of exosome cargo and subsequent biological effects," *Frontiers in Immunology*, vol. 13, Article ID 824188, 2022.

[30] A. Thakur, A. Johnson, E. Jacobs et al., "Energy sources for exosome communication in a cancer microenvironment," *Cancers*, vol. 14, no. 7, Article ID 1698, 2022.

[31] W. X. Chen, D. D. Wang, B. Zhu et al., "Exosomal miR-222 from adriamycin-resistant MCF-7 breast cancer cells promote macrophages M2 polarization via PTEN/Akt to induce tumor progression," *Aging*, vol. 13, no. 7, 2021.

[32] W. Tian, H. Yang, and B. Zhou, "Integrative analysis of exosomal microRNA-149-5p in lung adenocarcinoma," *Aging*, vol. 13, no. 5, 2021.

[33] D. Wang, X. Wang, Y. Song et al., "Exosomal miR-146a-5p and miR-155-5p promote CXCL12/CXCR7-induced metastasis of colorectal cancer by crosstalk with cancer-associated fibroblasts," *Cell Death and Disease*, vol. 13, no. 4, p. 380, 2022.

[34] M. Mostafazadeh, H. Kahroba, S. Haiaty et al., "In vitro exosomal transfer of Nrf2 led to the oxaliplatin resistance in human colorectal cancer LS174T cells," *Cell Biochemistry and Function*, vol. 40, no. 4, pp. 391–402, 2022.

[35] S. K. Tey, S. W. K. Wong, J. Y. T. Chan et al., "Patient pIgR-enriched extracellular vesicles drive cancer stemness, tumorigenesis and metastasis in hepatocellular carcinoma," *Journal of Hepatology*, vol. 76, no. 4, pp. 883–895, 2022.

[36] R. Ohkuma, E. Yada, S. Ishikawa et al., "High expression levels of polymeric immunoglobulin receptor are correlated with chemoresistance and poor prognosis in pancreatic cancer," *Oncology Reports*, vol. 44, no. 1, pp. 252–262, 2020.

[37] Y. Bao, L. Wang, L. Shi et al., "Transcriptome profiling revealed multiple genes and ECM-receptor interaction pathways that may be associated with breast cancer," *Cellular and Molecular Biology Letters*, vol. 24, no. 1, p. 38, 2019.

[38] R. Shi, Y. Li, L. Ran et al., "Screening and identification of HLA-A2-restricted neoepitopes for immunotherapy of non-microsatellite instability-high colorectal cancer," *Science China Life Sciences*, vol. 65, no. 3, pp. 572–587, 2022.

[39] Q. Lv, X. Pan, D. Wang et al., "Discovery of (Z)-1-(3-((1H-Pyrrol-2-yl)methylene)-2-oxoindolin-6-yl)-3-(isoxazol-3-yl) urea derivatives as novel and orally highly effective CSF-1R inhibitors for potential colorectal cancer immunotherapy," *Journal of Medicinal Chemistry*, vol. 64, no. 23, 2021.

[40] J. Shi, M. Bao, W. Wang et al., "Integrated profiling identifies PLOD3 as a potential prognostic and immunotherapy relevant biomarker in colorectal cancer," *Frontiers in Immunology*, vol. 12, Article ID 722807, 2021.

[41] J. E. Soh, N. Abu, I. Sagap et al., "Validation of immunogenic PASD1 peptides against HLA-A*24:02 colorectal cancer," *Immunotherapy*, vol. 11, no. 14, 2019.

[42] M. Fathi, I. Pustokhina, S. V. Kuznetsov et al., "T-cell immunoglobulin and ITIM domain, as a potential immune checkpoint target for immunotherapy of colorectal cancer," *IUBMB Life*, vol. 73, no. 5, pp. 726–738, 2021.

Research Article

Characterization of the Lipid Metabolism in Bladder Cancer to Guide Clinical Therapy

Yuan-Yuan Yang (i),[1] **Sen-Yuan Hong** (i),[1] **Yang Xun**,[1] **Chen-Qian Liu** (i),[1] **Jian-Xuan Sun** (i),[1] **Jin-Zhou Xu** (i),[1] **Meng-Yao Xu**,[1] **Ye An**,[1] **Deng He** (i),[2] **Qi-Dong Xia** (i),[1] **and Shao-Gang Wang** (i)[1]

[1]*Department and Institute of Urology, Tongji Hospital, Tongji Medical College, Huazhong University of Science and Technology, No. 1095 Jiefang Avenue, Wuhan 430030, China*
[2]*Department and Institute of Gynecology and Obstetrics, Tongji Hospital, Tongji Medical College, Huazhong University of Science and Technology, No. 1095 Jiefang Avenue, Wuhan 430030, China*

Correspondence should be addressed to Shao-Gang Wang; sgwangtjm@163.com

Background. Bladder cancer is one of the most common malignancies of the urinary system with an unfavorable prognosis. More and more studies have suggested that lipid metabolism could influence the progression and treatment of tumors. However, there are few studies exploring the relationship between lipid metabolism and bladder cancer. This study aimed to explore the roles that lipid metabolism-related genes play in patients with bladder cancer. *Methods.* TCGA_BLCA cohort and GSE13507 cohort were included in this study, and transcriptional and somatic mutation profiles of 309 lipid metabolism-related genes were analyzed to discover the critical lipid metabolism-related genes in the incurrence and progression of bladder cancer. Furthermore, the TCGA_BLCA cohort was randomly divided into training set and validation set, and the GSE13507 cohort was served as an external independent validation set. We performed the LASSO regression and multivariate Cox regression in training set to develop a prognostic signature and further verified this signature in TCGA_BLCA validation set and GSE13507 external validation set. Finally, we systematically investigated the association between this signature and tumor microenvironment, drug response, and potential functions and then verified the differential expression status of signature genes in the protein level by immunohistochemistry. *Results.* A novel 6-lipidmetabolism-related gene signature was identified and validated, and this risk score model could predict the prognosis of patients with bladder cancer. In addition, the prognostic model was tightly related to immune cell infiltration and tumor mutation burden. Gene set variation analysis (GSVA) and gene set enrichment analysis (GSEA) showed that mTOR signaling pathway, G2M checkpoint, fatty acid metabolism, and hypoxia were enriched in patients in the high-risk score groups. Furthermore, 3 therapies specific for bladder cancer patients in different risk scores were identified. *Conclusion*s. In conclusion, we investigated the lipid metabolism-related genes in bladder cancer through comprehensive bioinformatic analysis. A novel 6-gene signature associated with lipid metabolism for predicting the outcomes of patients with bladder cancer was conducted and validated. Furthermore, the risk score model could be utilized to indicate the choice of therapy in bladder cancer.

1. Introduction

Bladder cancer is one of the most common malignancies of the urinary system; it has the 13th highest mortality among all cancers, and the mortality is still rising despite tremendous efforts that have been made for the treatment [1].

The progression of bladder cancer is a multistage process including environmental and genetic factors [2]. Previous studies indicate that tobacco smoking and occupational exposure to carcinogens are major factors [3]. The primary treatment for bladder cancer is transurethral resection of the bladder (TURB) accompanied by intravesical chemotherapy

or immunotherapy [3]. However, the prognosis of patients still remains unfavorable. Therefore, it is essential to identify prognostic biomarkers to guide the selection of treatment for improving the curative effects.

Accumulating evidence demonstrates that clinical outcome, epigenetic status, and treatment resistance are associated with tumor metabolism [4, 5]. Metabolic reprogramming has been considered to be a new hallmark of malignant tumors [6]. Cancer cells usually require more energy to meet their biological needs than normal cells [7], while fatty acid oxidation is an important energy source for cancer cells, so lipid metabolism in cancer cells has been recognized as playing an important role in cancer progression [8].

Recent studies have shown that fatty acid metabolism has a close connection with bladder cancer [9]. Epidemiologic studies have shown that free fatty acid (FFA) level was increased in bladder cancer compared with paracancerous tissues. Cheng et al. demonstrated that inhibition of fatty metabolism is important in sustaining tumor growth through PPAR-γ-mediated pathway [10]. Besides, the molecular mechanism of drug resistance of cancer therapy might include lipid metabolism reprogramming [11]. Rysman E et al. indicated that altered lipid composition of cellular membranes could disrupt the uptake of chemotherapeutic agents and lead to chemotherapeutic resistance [12]. What is more, the tumor microenvironment (TME) plays an important role in the progression of bladder cancer, while metabolic disorders including FA metabolism changes have a crucial impact on cancer [13]. Fatty acid secreted in the microenvironment could affect the function and phenotype of infiltrating immune cells [14].

In this study, we explored the lipid metabolism-related genes in bladder cancer to conduct a model to predict patient prognosis. The prognostic risk score model independently predicted the survival outcome of bladder cancer patients. What is more, the relationship between risk score model and TME cell-infiltrating characteristics was investigated and suitable therapy treatment could be selected through the risk score model. These findings can provide a new sight into exploring the metabolic mechanism and treatment for bladder cancer.

2. Methods

2.1. Data Acquisition.
We included two datasets in this study, and they are TCGA_BLCA cohort and GSE13507 cohort. The transcriptome profiles, somatic mutation profiles, and clinical information about TCGA_BLCA were downloaded from the GDC_Portal (https://portal.gdc.cancer.gov/), and the transcriptome profiles and corresponding clinical information of GSE13507 cohort were downloaded from the GEO database (https://www.ncbi.nlm.nih.gov/gds/?term=GSE13507) and served as independent external validation sets. Notably, the batch effects between TCGA_BLCA and GSE13507 cohorts were normalized by the R package "sva."

2.2. Landscape of Lipid Metabolism-Related Genes in Bladder Cancer.
We firstly investigated the role of lipid metabolism-related genes in TCGA_BLCA cohort, performed

differential expression analysis between tumor and normal samples, and screened differentially expressed lipid metabolism-related genes with a threshold of FC (fold change, FC) > 1.5 and adjusted p value < 0.05. Following this, we performed univariate cox regression of these differentially expressed lipid metabolism-related genes in TCGA_BLCA cohort to further identify the critical differentially expressed lipid metabolism-related genes with significant prognostic value. Subsequently, we explored the somatic mutation of these critical genes and draw the mutation atlas.

2.3. Identification of the Prognostic Signature.
Having systematically summarized the role of lipid metabolism-related genes in TCGA_BLCA cohort, we would like to establish a prognostic signature by these critical genes. Thus, we first randomly split all the patients in TCGA_BLCA cohort with a ratio of 1 : 1 that one for the construction and the other for the verification. Moreover, the GSE13507 cohort was served as an external independent validation cohort. Then, we separately conducted LASSO regression to screen appropriate variables and multivariate cox regression to establish the prognostic signature in the training set, and a formula of risk score based on these lipid metabolism-related genes was established:

$$\text{risk score} = \sum \text{coef}(i) \cdot \exp(i). \tag{1}$$

i represents each gene in the prognostic signature, coef (i) represents the coefficient of this gene, and exp (i) is the expression value of it. Thus, each sample in training set, validation set, and GSE13507 acquired a risk score according to this formula. Moreover, we set the medium value of the risk score in training set as the threshold, and each patient received a risk level that the higher is high risk and the lower is low risk.

2.4. Further Verification of the Prognostic Signature.
We first conducted survival analysis in all three sets to confirm the prognostic value of this signature, then performed univariate Cox regression to calculate the hazard ratio of the risk score, and carried out a meta-analysis to summarize the HR of risk score in three different sets. Besides, the differences in clinical information between high-risk patients and low-risk patients were explored by the chi-square test. Also, the ROC curves of the risk score in three sets were plotted and the area under the curves was calculated. Furthermore, we combined the indicator of tumor mutation burden and our risk score to predict the survival of patients together and explored the difference in TMB between high-/low-risk patients and the correlation between TMB and risk score. Finally, we further investigated the mutation differences between high-risk patients and low-risk patients in all TCGA_BLCA patients.

2.5. Gene Set Enrichment Analysis (GSEA) and Gene Set Variation Analysis (GSVA).
Having constructed and verified the prognostic signature, we wonder about the further potential mechanisms behind the risk score. Thus, we separately conducted the GSEA and GSVA in all

TCGA_BLCA patients by the R package "clusterProfiler" and "GSVA." The gene ontology (GO) gene sets, KEGG gene sets, Hallmarks gene sets, metabolism-related gene sets, and cell death-related gene sets were used to do the corresponding analysis.

2.6. Tumor Microenvironment, Drug Response, and Immunohistochemistry. Notably, we carried out eight different algorithms to quantify the immune cells or immune-related function of each patient according to its transcriptome profile, and they were XCELL, TIMER, QUANTISEQ, MCPCOUNTER, EPIC, CIBERSORT-ABS, CIBERSORT, and ssGSEA. Then, both differential infiltration analysis and correlation tests were conducted. Following this, we separately estimate the drug response of each patient to the commonly used drugs including cisplatin, gemcitabine, and others small molecule drugs by R package "proPhetics." Also, the TIDE score was compared between high-risk patients and low-risk patients to predict the drug response to immunotherapy. Finally, we searched the immunohistochemistry profiles of these signature genes in the Human Protein Atlas database (HPA, https://www.proteinatlas.org/) and compared and verified the differential expression status in the protein expressed level.

2.7. Statistical Analysis. All the data were processed or analyzed by the R program version 4.1.1 and Microsoft Office Excel. $P < 0.05$ was regarded with significant statistical differences.

3. Results

3.1. Identification of 18 Vital Differentially Expressed Lipid Metabolism-Related Genes in Bladder Cancer. Expression data of 309 lipid metabolism-related genes (LMRGs) were collected from the GEO and TCGA cohorts. The flow chart of this research is presented in Figure 1. 89 differently expressed LMRGs were found between normal and bladder cancer tissues, with 57 genes upregulated and 32 genes downregulated in cancer samples when the cutoff was set to FC (fold change, FC) > 1.5 and FDR<0.05 (Figures 2(a) and 2(b)). Univariate Cox regression analysis was conducted on 89 differently expressed LMRGs in TCGA_BLCA cohort. A total of 18 genes with prognostic value were identified with a p value < 0.05 (Figure 2(c)). The somatic mutation profile of 18 LMRGs associated with prognosis was first summarized. A total of 54 of 412 bladder cancer samples experienced mutations of LMRGs, with a frequency of 13.11%. ACOX2, SLC27A2, and ACLY had the highest mutation frequency (Figure 2(d)). Further analyses demonstrated a mutation co-occurrence relationship between ACSF2 and PTGIS, ACOX2 and GPX1, SLC27A2 and CYP1B1, and ACLY and DHCR24 (Figure 2(e)).

3.2. Construction and Verification of the Prognostic Index. To construct a prognostic index of lipid metabolism-related genes, we obtained 404 samples of bladder cancer from

TCGA database and divided them into two groups as training cohort ($N = 204$) and testing cohort ($N = 200$). The basic characteristics of the patients included are shown in Table 1. Then, the least absolute shrinkage and selection operator (LASSO) Cox regression analysis was conducted to narrow the number of genes. Finally, six genes (CYP1B1, ACOT13, NUDT19, SCD, IL4I1, and DECR1) were used for the construction of prognostic risk score model (Figures 3(a) and 3(b)). Then, six genes were shifted from them through multivariate Cox regression (Figure 3(d)). The coefficient of these genes is displayed in Table 2. The chord diagram showed the correlation between the six genes filtered by LASSO Cox regression analysis (Figure 3(c)). To estimate the effectiveness of this model, we also collected 165 samples from GEO database (GSE13507) as validation. We then calculated the risk score of samples and divided the patients into high- and low-risk score groups according to median risk score acquired from training cohort. We also found that patients in the high-risk score group had the worse survival status than those in the low-risk group (Figures 3(f)–3(k)). We found that clinical characteristics such as stage and status were positively related to high-risk group (Figure 3(e)). The Kaplan–Meier survival analyses indicated that patients in the high-risk score group had worse survival outcome (Figures 3(l)–3(n)). The area under curve (AUC) showed the effectiveness of the prognostic index (Figures 3(o)–3(q)). Furthermore, we conducted meta-analysis based on the three cohorts to demonstrate that the risk score was in good validity (HR = 1.49, 95% CI = 1.15–1.94, $p = 0.01$) (Figure 3(r)).

3.3. The Relationship between Tumor Mutation Burden (TMB) and Risk Score. We compared the tumor mutation burden (TMB) in high- and low-risk score patients and found the TMB of patients in the low-risk score group was higher (Figures 4(a) and 4(b)). The mutation spectrum of patients with high-risk score (Figure 4(c)) and low-risk score (Figure 4(d)) was mapped, and 14 significantly mutant genes including (ATAD5, PIK3CA, FGFR3, HUWE1, SPTAN1, GON4L, ALMS1, RELN, STAG2, AHNAK, MED13, UTRN, C2orf16, and ATR) were obtained (Table 3). Survival curves demonstrated that the prognosis of patients with high TMB was better (Figure 4(e)); furthermore, patients with high TMB and low-risk score had the best prognosis (Figure 4(f)).

3.4. The Relationship between Risk Score and Tumor Microenvironment (TME) in Bladder Cancer. We estimated the relationship between risk score and the immune checkpoints (ICBs), and the results indicated that NRP1, CD44, CD276, and TNFSF9 were significantly higher expressed in high-risk score patients (Figure 5(a)). Most ICBs were highly expressed in low-risk score groups (Figure 5(b)). Immune-related function analysis demonstrated that the expression of HLA, inflammation-promoting factors, and cytolytic activity was lower in high-risk score patients compared with low-risk score patients (Figure 5(c)). Then, we explored the composition of immune infiltration cells through seven methods. We found that CD8+T, Treg, and NK-activated cells were
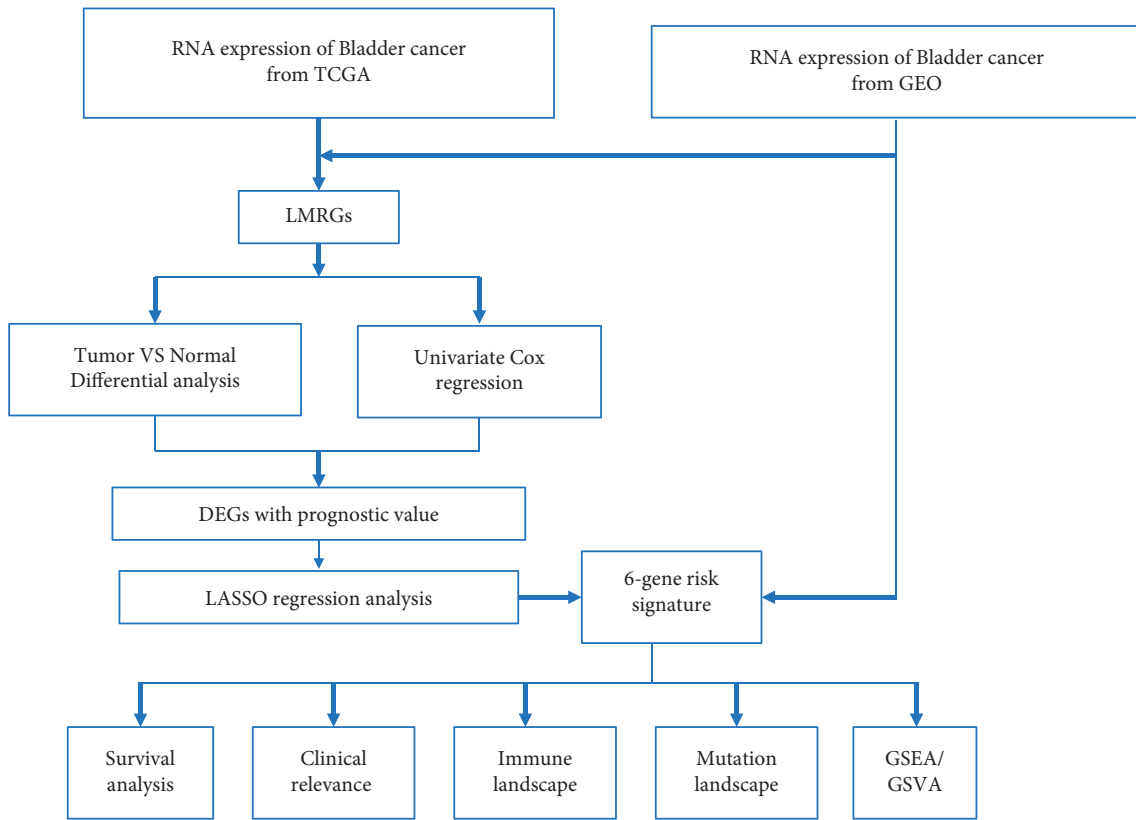
Figure 1: Flowchart of study design.
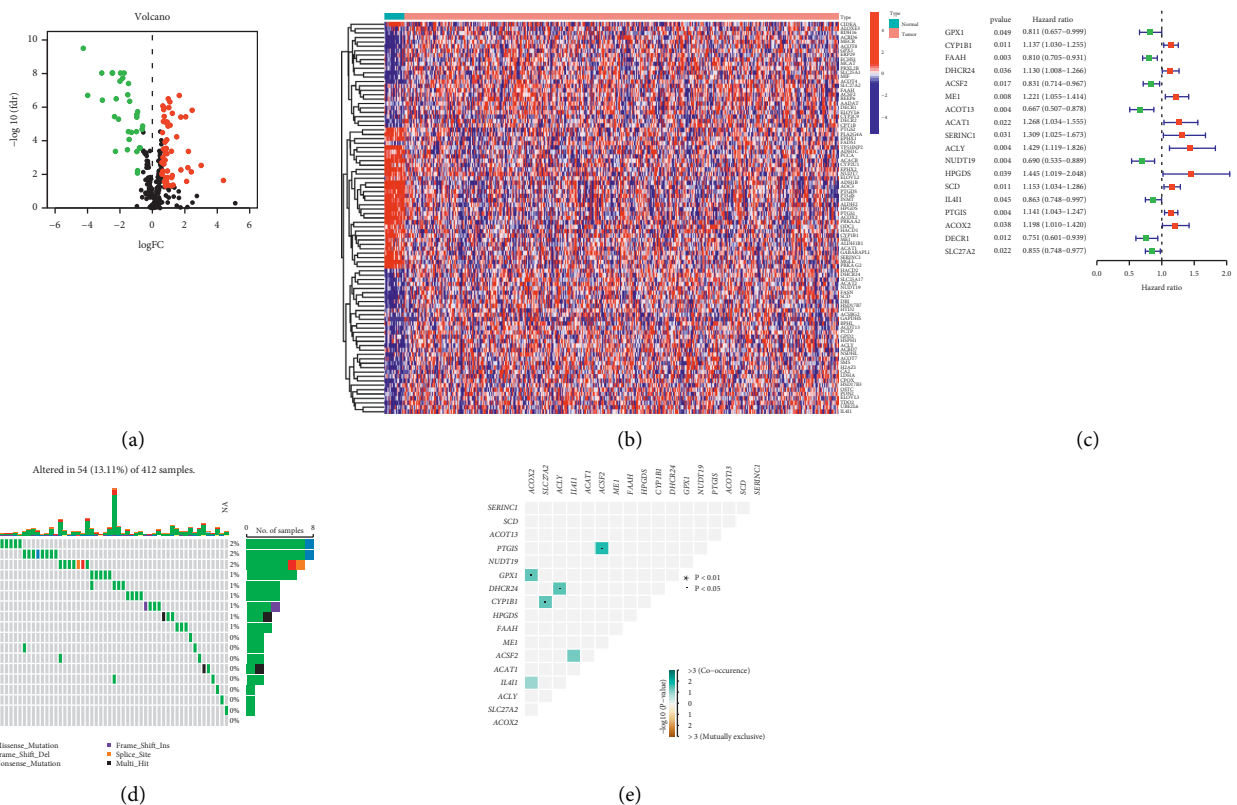
(a)

(b)

(c)

(d)

(e)

Figure 2: Identification of 18 vital differentially expressed lipid metabolism-related genes (LMRGs) in bladder cancer. (a) Volcano map of the expression patterns of 89 LMRGs in bladder cancer, with 57 genes upregulated and 32 genes downregulated. (b) Heat map showing the differently expressed LMRGs between normal and tumor tissues. False discovery rate (FDR) < 0.05. (c) Forrest plot of 18 LMRGs related to prognosis based on univariate analysis. (d) The mutation frequency of 18 LMRGs in 412 patients with bladder cancer from the TCGA cohort. (e) The mutation co-occurrence and exclusion analyses for 18 LMRGs.

TABLE 1: Basic characteristics of included BLCA patients.

	Overall	GSE13507	TCGA_Test	TCGA_Train	p
n	569	165	200	204	
Age (mean (SD))	67.25 (11.10)	65.18 (11.97)	67.77 (11.11)	68.42 (10.12)	0.014
Gender = female/male (%)	135/434 (23.7/76.3)	30/135 (18.2/81.8)	47/153 (23.5/76.5)	58/146 (28.4/71.6)	0.071
Grade (%)					<0.001
High grade	440 (77.3)	60 (36.4)	186 (93.0)	194 (95.1)	
Low grade	126 (22.1)	105 (63.6)	12 (6.0)	9 (4.4)	
Unknown	3 (0.5)	0 (0.0)	2 (1.0)	1 (0.5)	
T (%)					<0.001
T1	83 (14.6)	80 (48.5)	3 (1.5)	0 (0.0)	
T2	150 (26.4)	31 (18.8)	56 (28.0)	63 (30.9)	
T3	210 (36.9)	19 (11.5)	100 (50.0)	91 (44.6)	
T4	69 (12.1)	11 (6.7)	23 (11.5)	35 (17.2)	
Ta	24 (4.2)	24 (14.5)	0 (0.0)	0 (0.0)	
Unknown	33 (5.8)	0 (0.0)	18 (9.0)	15 (7.4)	
M (%)					<0.001
M0	352 (61.9)	158 (95.8)	102 (51.0)	92 (45.1)	
M1	18 (3.2)	7 (4.2)	6 (3.0)	5 (2.5)	
MX	197 (34.6)	0 (0.0)	91 (45.5)	106 (52.0)	
Unknown	2 (0.4)	0 (0.0)	1 (0.5)	1 (0.5)	
N (%)					<0.001
N0	386 (67.8)	151 (91.5)	116 (58.0)	119 (58.3)	
N1	54 (9.5)	8 (4.8)	21 (10.5)	25 (12.3)	
N2	79 (13.9)	4 (2.4)	37 (18.5)	38 (18.6)	
N3	8 (1.4)	1 (0.6)	3 (1.5)	4 (2.0)	
NX	37 (6.5)	1 (0.6)	21 (10.5)	15 (7.4)	
Unknown	5 (0.9)	0 (0.0)	2 (1.0)	3 (1.5)	
Status = alive/dead (%)	324/245 (56.9/43.1)	96/69 (58.2/41.8)	112/88 (56.0/44.0)	116/88 (56.9/43.1)	0.916
Risk score (median (IQR))	0.96 [0.66, 1.46]	0.97 [0.65, 1.47]	0.95 [0.66, 1.45]	0.96 [0.66, 1.45]	0.85
Risk = high/low (%)	286/283 (50.3/49.7)	85/80 (51.5/48.5)	99/101 (49.5/50.5)	102/102 (50.0/50.0)	0.925

(a)

(b)

(c)

(d)

(e)
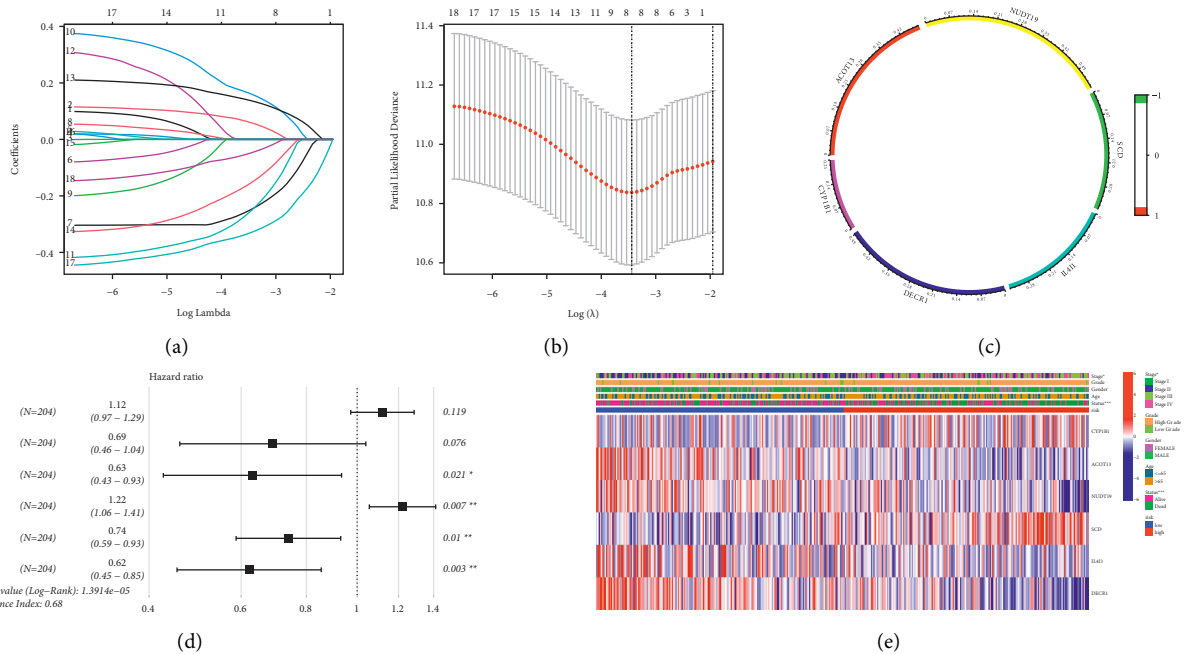
FIGURE 3: Continued.

(f)

(g)

(h)

(i)

(j)

(k)

(l)

(m)

(n)

(o)

(p)

(q)

(r)
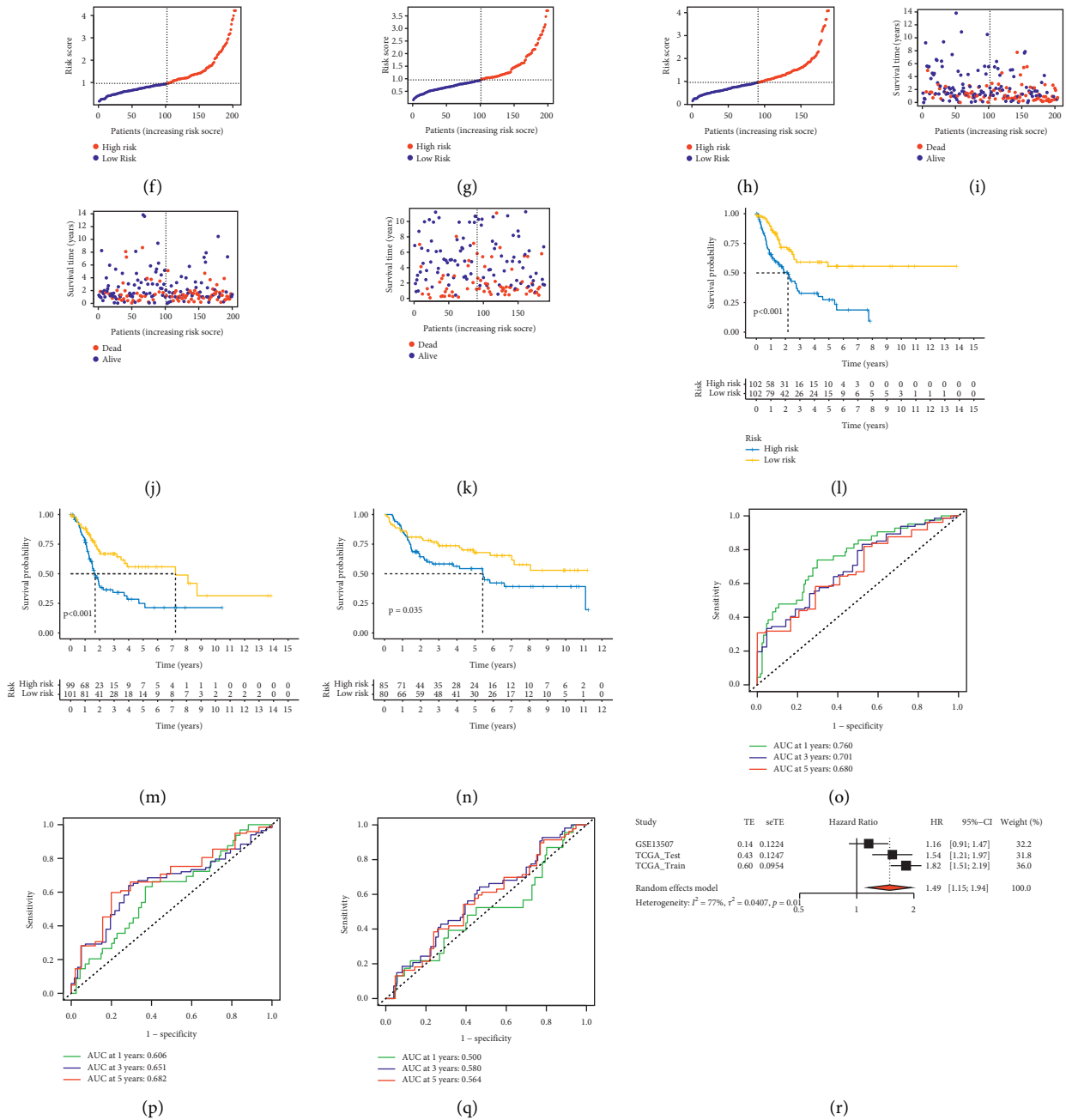
FIGURE 3: Construction and verification of the prognostic index. (a) LASSO coefficients of the 18 lipid metabolism-related genes (LMRGs). (b) Identification of genes for development of prognostic risk score model. (c) Chord diagram showed the correlation between the 6 LMRGs selected through LASSO Cox regression analysis. (d) Hazard ratio of each gene after multivariate Cox regression analysis. (e) The distribution of clinical characteristics of patients in high- and low-risk score groups. (f–k) Risk scores of patients in the training cohort (TCGA), testing cohort (TCGA), and verification cohort (GEO). (l-n) Survival status of each patient in the training cohort, testing cohort, and verification cohort. (k-m) Kaplan–Meier survival analyses of patients in the training cohort ($p < 0.001$, log-rank test), testing cohort ($p < 0.001$, log-rank test), and verification cohort ($P = 0.035$, log-rank test). (o-q) AUC curve of patients in the training cohort, testing cohort, and verification cohort. (r) Meta-analysis of the training cohort, testing cohort, and verification cohort, and the results showed that the risk score was in good validity (HR = 1.49, 95% CI = 1.15–1.94, $p = 0.01$).

TABLE 2: Signature genes and their coefficient.

Symbol	Coef
CYP1B1	0.11119677191537
ACOT13	−0.371344139411004
NUDT19	−0.461089925531869
SCD	0.199677207803535
IL4I1	−0.302776856487651
DECR1	−0.475644491902455

higher in the low-risk score group compared with the high-risk group (Figures 5(d) and 5(e)). In addition, CD8+T cell was negatively associated with the risk score (Figure 5(f)).

3.5. Gene Set Variation Analysis (GSVA) and Gene Set Enrichment Analysis (GSEA).

We performed GSEA and GSVA to verify the correlation between risk score and pathways involved in the formation of bladder cancer. We conducted GSVA using Hallmark gene sets, and the results showed that risk score was positively associated with 31 hallmark pathways including mTOR signaling pathway, G2M checkpoint, fatty acid metabolism, and hypoxia (Figure 6(a)). We performed GSEA in different risk score groups using the Kyoto Encyclopedia of Genes and Genomes (KEGG) signaling pathways (Figures 6(b) and 6(c)). Besides, we confirmed that risk score was associated with pathways in cell death including autophagy and ferroptosis (Figure 6(d)). Also, we performed metabolism analysis and discovered risk score was positively related to fat-soluble vitamins (Figure 6(e)).

3.6. Response to Chemotherapy and Immunotherapy for Bladder Cancer of High- and Low-Risk Score Patients.

We estimated the response to chemotherapy drugs in different risk score groups and found that patients in the low-risk score were more sensitive to methotrexate sensitivity; furthermore, metformin could be used in bladder cancer patients of low-risk score (Figure 7(a) and 7(b)). We also conducted immunotherapy analysis between the high- and low-risk score groups and found that anti-CTLA4 and anti-PD-1 therapy could make a difference in therapeutic effect between two groups no matter whether used alone or in combination, and patients in the high-risk score groups showed better sensitivity compared with those in the low-risk score groups (Figure 7(c)).

3.7. Immunohistochemistry (IHC) Verification of ACOT13, CYP1, DECR1, IL4I1, and SCD.

We obtained the results of immunohistochemical staining of ACOT13, CYP1, DECR1, IL4I1, and SCD in both normal tissues and bladder cancer tissues and found that the expression of CYP1 was higher in normal tissues, while other genes were higher in tumor tissues than in normal tissues (Figure 8).

4. Discussion

Bladder cancer is a common malignant tumor with high rates of recurrence [15]. The treatments of bladder cancer have advanced a lot during the past decade; however, the high morbidity and mortality remain unchanged [16]. Effective therapies and prognostic markers still need to be identified.

Accumulating studies have indicated that lipid metabolism is a crucial step in metabolic reprogramming, while metabolic reprogramming is a new hallmark of malignant tumors [17]. Despite the importance of lipid metabolism in bladder cancer, few studies were conducted to explore the association between lipid metabolism and bladder cancer.

In this study, we identified the potential mechanism and prognostic value of lipid metabolism-related genes in bladder cancer via bioinformatic analysis. A 6-gene prognostic risk model was constructed by LASSO Cox analysis. In addition, these lipid metabolism-relatedgene-based signatures were tightly associated with TNM stage, T stage, N stage, and status. The patients with low-risk scores were found better outcomes than those with high-risk scores. Our findings showed that this risk model was an independent prognostic prediction for survival and was tightly associated with tumor mutation burden (TMB) and tumor microenvironment (TME).

Recently, more and more studies have suggested that the progression and prognosis of bladder cancer were tightly related to immune cell infiltration [18]. Furthermore, the functions of immune cell could be influenced by metabolic reprogramming [19]. Therefore, there must exist a relationship between risk scores and immune cell infiltration. Our results showed that patients in the high-risk score group had higher expression of M0 macrophages, while Tregs and CD8+T cells were upregulated in the low-risk group, demonstrating a differential infiltration pattern between the subgroups. In addition, patients in high-risk groups had higher expression of NRP1, CD44, CD276, and TNFSF9 than those in low-risk groups. These results indicated that the unfavorable prognosis of patients in the high-risk score groups might be due to the immunosuppressive environment and elevated expression of immune checkpoint genes [20]. We also found that tumor mutation burden was negatively associated with the risk score, and the prognosis of patient with high tumor mutation burden and low score was the best. It might be due to that tumor mutations could generate immunogenic neoantigens, thus leading to immune checkpoint blockade [21].

GSEA and GSVA of hallmarks suggested that G2M checkpoint, EMT pathway, and hypoxia were highly expressed in the high-risk score groups. MT Dillon et al. suggested that inhibition of G2M checkpoint could slow down the progression of tumors [22]. Epithelial-mesenchymal transition (EMT) is a process of epithelial cells acquiring mesenchymal features. It is associated with tumor initiation, invasion, metastasis, and resistance to therapy [23]. Hypoxia has emerged as a crucial factor in tumor pathophysiology, and microenvironment promotes altered cellular metabolism including lipid metabolism. Furthermore, reports suggested that hypoxia could trigger EMT in bladder cancer [24]. The pathways of autophagy and ferroptosis were also involved in patients of high-risk score groups, and Enyong Dai et al. suggested that autophagy-

(a)

(b)

(c)

(d)

(e)

(f)
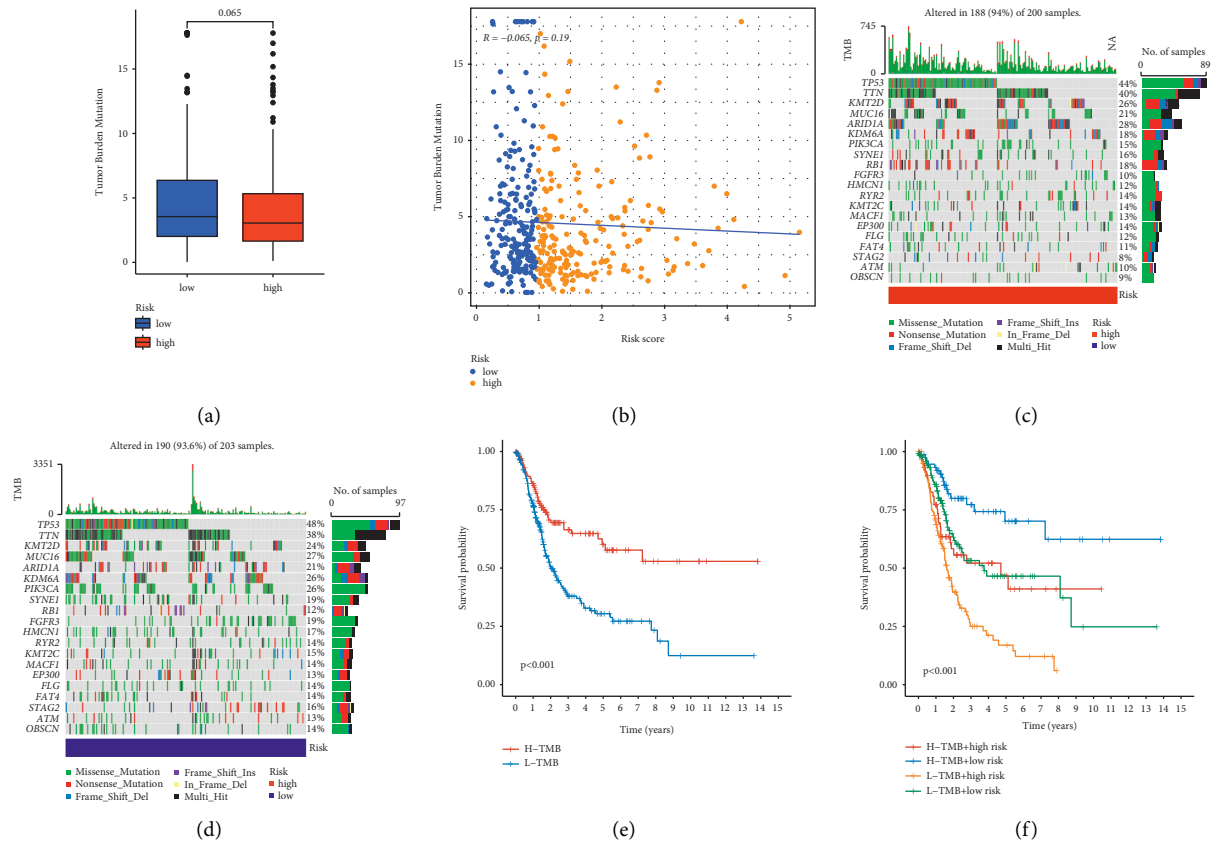
FIGURE 4: Relationship between tumor mutation burden (TMB) and risk score. (a, b) Comparison of TMB between patients in the high- and low-risk score groups, and high tumor mutation burden was associated with low-risk score. (c, d) Mutation spectrum of high-risk and low-risk patients. (e) Survival analyses for low- and high-TMB patient groups using the Kaplan–Meier curves ($P < 0.001$, log-rank test). (f) Survival analyses for four groups of TMB and risk score using the Kaplan–Meier curves. The high-TMB and low-risk score groups indicated better overall survival than the other three groups ($P < 0.001$, log-rank test).

TABLE 3: Mutation atlas differences between high-risk and low-risk patients.

Gene	H-wild	H-mutation	L-wild	L-mutation	p value
ATAD5	195 (97.5%)	5 (2.5%)	183 (90.15%)	20 (9.85%)	0.004334171
PIK3CA	170 (85%)	30 (15%)	151 (74.38%)	52 (25.62%)	0.011636589
FGFR3	181 (90.5%)	19 (9.5%)	165 (81.28%)	38 (18.72%)	0.011988853
HUWE1	19 6 (98%)	4 (2%)	187 (92.12%)	16 (7.88%)	0.012810357
SPTAN1	188 (94%)	12 (6%)	175 (86.21%)	28 (13.79%)	0.014308358
GON4L	195 (97.5%)	5 (2.5%)	187 (92.12%)	16 (7.88%)	0.027357379
ALMS1	192 (96%)	8 (4%)	183 (90.15%)	20 (9.85%)	0.034494781
RELN	192 (96%)	8 (4%)	183 (90.15%)	20 (9.85%)	0.034494781
STAG2	183 (91.5%)	17 (8.5%)	171 (84.24%)	32 (15.76%)	0.037673236
AHNAK	189 (94.5%)	11 (5.5%)	179 (88.18%)	24 (11.82%)	0.037837752
MED13	191 (95.5%)	9 (4.5%)	182 (89.66%)	21 (10.34%)	0.040835835
UTRN	191 (95.5%)	9 (4.5%)	182 (89.66%)	21 (10.34%)	0.040835835
C2orf16	195 (97.5%)	5 (2.5%)	188 (92.61%)	15 (7.39%)	0.042331744
ATR	193 (96.5%)	7 (3.5%)	185 (91.13%)	18 (8.87%)	0.042692803

dependent ferroptosis could drive tumor-associated macrophage polarization [25]. The poorer prognosis of patients in the high-risk score groups might be tightly associated with mechanisms above.

The risk signature was constructed with ACOT13, CYP1, DECR1, IL4I1, NUDT19, and SCD ACOT13, and a member of acy1-CoA thioesterase (ACOT) enzymes can catalyze

hydrolysis of fatty acyl-CoA into free fatty acids. It is usually enriched in oxidative tissues and tightly related to mitochondria [26]. Previous studies found that it was associated with many diseases, including lung cancer, pheochromocytomas, and paragangliomas [27]. CYP1 enzymes could catalyze the metabolic activation of procarcinogens and deactivation of certain anticancer drugs. Inhibition of CYP1

(a)

(b)

(c)

(d)

(e)

(f)
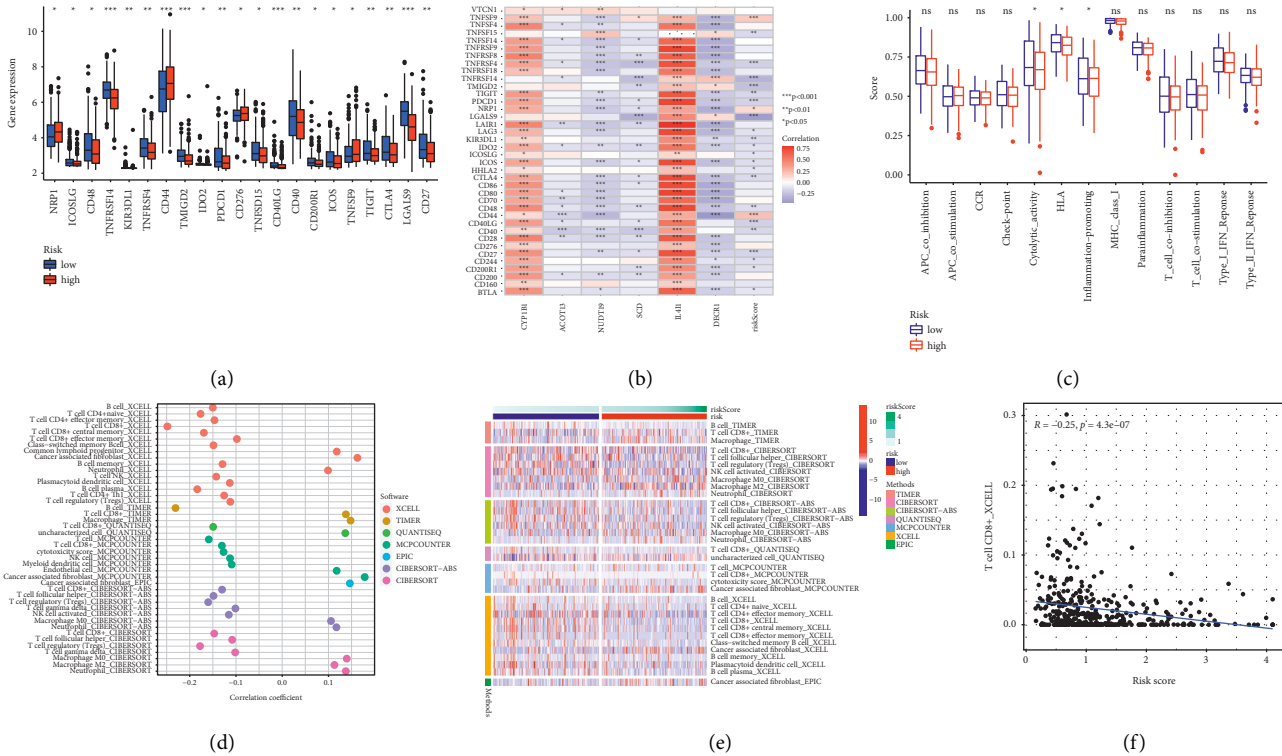
Figure 5: Relationship between risk score and tumor microenvironment (TME) in bladder cancer. (a) Immune checkpoint expression in high- and low-risk score patients ($^*p < 0.05$; $^{**}p < 0.01$; $^{***}p < 0.001$). (b) Correlation between immune checkpoint and six genes ($^*p < 0.05$; $^{**}p < 0.01$; $^{***}p < 0.001$). (c) Immune-related function of high- and low-risk score patients. (d) Correlation of risk score and immune cell infiltration detected by seven different methods. (e) Immune cell infiltration of patients in high- and low-risk score groups; CD8+T, Treg, and NK-activated cells were higher in low-risk score group compared with high-risk group. (f) Correlation between CD8+T-cell infiltration and risk scores.

(a)

(b)

(c)

(d)

(e)
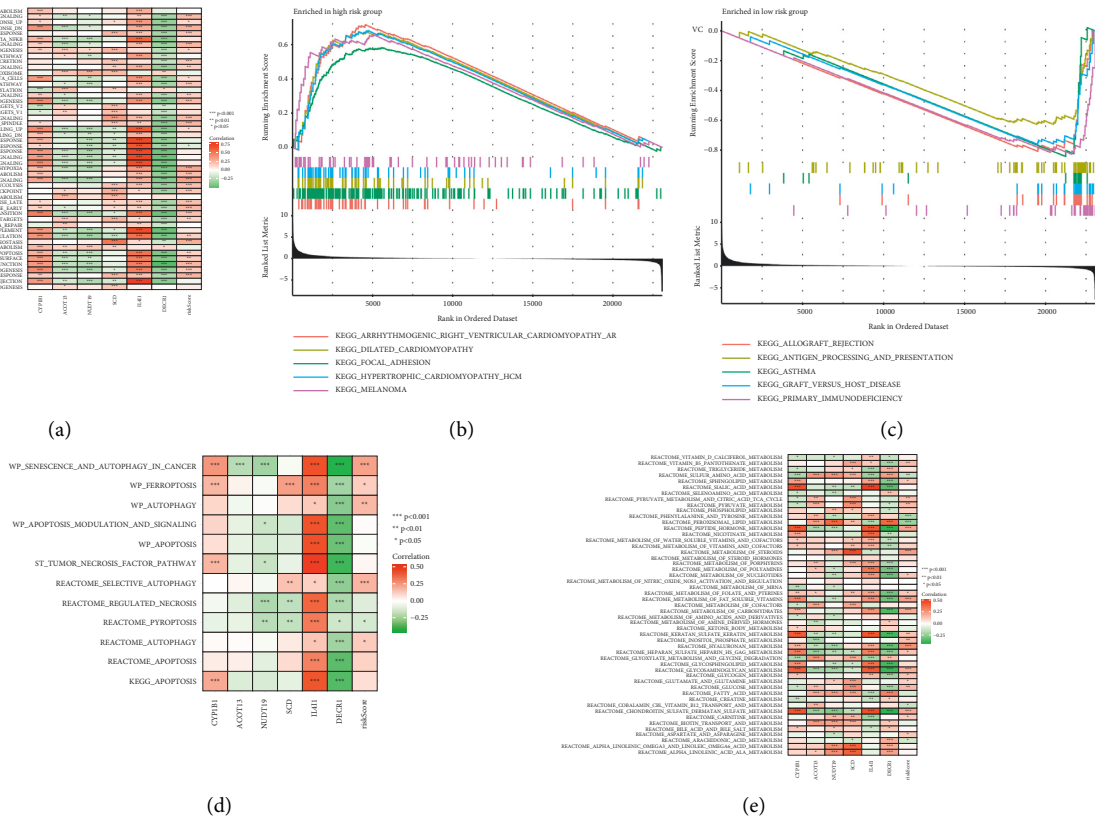
Figure 6: Gene set variation analysis (GSVA) and gene set enrichment analysis (GSEA). (a) GSVA in hallmark gene sets. (b, c) GSEA of patients in high- and low-risk score groups. (d) Correlation between risk score and cell death. (e) Correlation between risk score and metabolism pathways ($^*p < 0.05$; $^{**}p < 0.01$; $^{***}p < 0.001$).

(a)   (b)   (c)
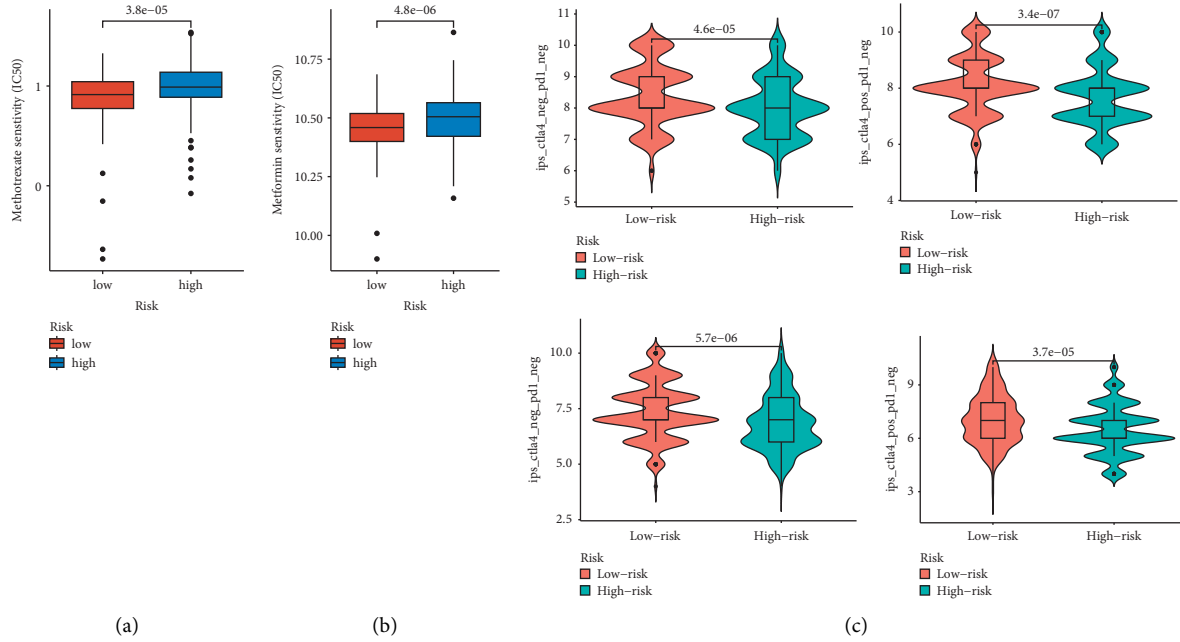
FIGURE 7: Drug response to chemotherapy or immunotherapy for bladder cancer of high- and low-risk score patients. (a) Chemotherapy drug sensitivity in high- and low-risk score patients. (b) Metformin sensitivity in high- and low-risk score patients. (c) Potential response to immunotherapy in high- and low-risk score groups. The *y*-axis means the sensitivity of these drugs, and the unit is IC50 (50% inhibiting concentration).

ACOT13   CYP1   DECR1   IL41I

(a)   (b)   (c)   (d)

SCD

(e)
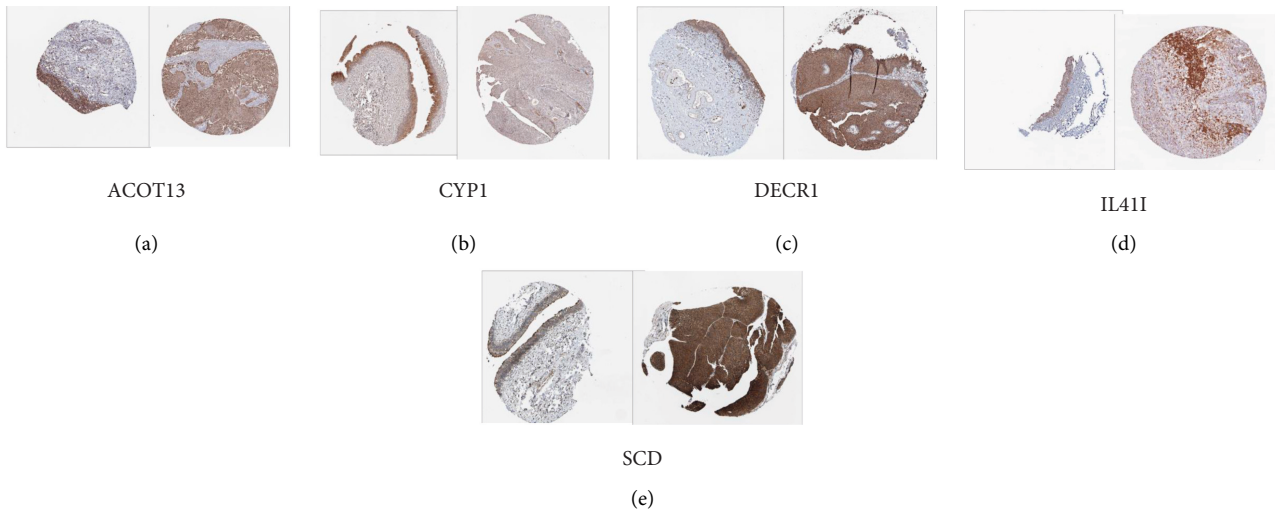
FIGURE 8: IHC staining of genes selected via LASSO Cox regression in normal tissues (left) and bladder cancer tissues (right). (a) ACOT13. (b) CYP1. (c) DECR1. (d) IL4I1. (e) SCD. The expression of CYP1 was higher in normal tissues, while other genes were higher in tumor tissues than in normal tissues.

is an effective approach for chemoprevention, and many studies have suggested that inhibitors and prodrug target CYP1 are promising anticancer strategies [28]. DECR1 is an auxiliary enzyme of beta-oxidation, and it participates in redox homeostasis by controlling the balance between saturated and unsaturated phospholipids. Deletion of DECR1 can impair lipid metabolism and reduce tumor growth; therefore, DECR1 is important in the progression of tumor growth and treatment resistance [29]. NUDT19 has been

identified to promote the proliferation, migration, and EMT process of tumor via mTORC1/P70S6K signaling pathway [30]. IL4I1 frequently associates with AHR (aryl hydrocarbon receptor) activity and activates the AHR through the generation of indole metabolites and kynurenic acid. In summary, it associates with reduced survival in patients with tumor and enhances the progression of tumor [31]. The previous study indicated that upregulation of SCD could proliferate cancer cells in a lipid-depleted environment for it

could synthesize monounsaturated fatty acids. Decreased tumor SCD activity could slow tumor growth [32].

Furthermore, we identified the molecule drugs highly related to lipid metabolism genes for the treatment of bladder cancer. Methotrexate, a well-established antimetabolite, has been used separately or in combination for antitumoral activity for a while [33], and we found it suitable to treat patients with low-risk score. Excepting chemotherapy, immunotherapy is another important treatment for bladder cancer; in our study, we found that anti-CTLA4 and anti-PD1 were sensitive to patients with high-risk score of bladder cancer no matter whether used separately or in combination. These two drugs are immune checkpoint inhibition and have been licensed for the treatment of bladder cancer [34]. Metformin, often used for diabetes, is known to induce apoptosis in many types of cancers and has the feasibility as a drug repositioning used for the treatment of bladder cancer [35]. Our study indicated that patients in the low-risk score groups were suitable for the treatment of metformin compared with patients in the high-risk score groups.

Our study constructed and validated a prognostic signature model based on lipid metabolism genes, which could predict the prognosis of patients with bladder cancer well and guide the treatment for patients with bladder cancer. Our study also has limitations, and the main limitation of the study is that we do not have experimental studies in vivo and in vitro. Further studies would be conducted to validate what roles the lipid metabolism-related genes play in bladder cancer.

5. Conclusions

In conclusion, we investigated the lipid metabolism-related genes in bladder cancer through comprehensive bioinformatic analysis. A novel 6-gene signature associated with lipid metabolism for predicting the outcomes of patients with bladder cancer was conducted and validated. Furthermore, the risk score model could be utilized to indicate the choice of therapy in bladder cancer.

Data Availability

The source data of this study were derived from the public repositories, as indicated in the section of "Methods" of the manuscript. All data that support the findings of this study are available from the corresponding author upon reasonable request.

Conflicts of Interest

The authors declare that they have no conflicts of interest.

Authors' Contributions

YYY, HD, XQD, and WSG designed the study, analyzed and interpreted the data, drafted the manuscript, and critically revised the manuscript; XQD and SJX involved in statistical analysis; YYY, XQD, XY, LCQ, SJX, HD, and WSG designed methodology; HD, XQD, and WSG administered project; all authors wrote the original draft; XQD and WSG wrote, reviewed, and edited the manuscript; and HD, XQD, and WSG are co-correspondence authors and contributed equally to this work.

References

[1] M. G. K. Cumberbatch, I. Jubber, P. C. Black et al., "Epidemiology of bladder cancer: a systematic review and contemporary update of risk factors in 2018," *European Urology*, vol. 74, no. 6, pp. 784–795, 2018.

[2] J. A. Witjes, H. M. Bruins, R. Cathomas et al., "European association of urology guidelines on muscle-invasive and metastatic bladder cancer: summary of the 2020 guidelines," *European Urology*, vol. 79, no. 1, pp. 82–104, 2021.

[3] M. Babjuk, M. Burger, E. M. Compérat et al., "European association of urology guidelines on non-muscle-invasive bladder cancer (tat1 and carcinoma in situ) - 2019 update," *European Urology*, vol. 76, no. 5, pp. 639–657, 2019.

[4] J. M. Karasinska, J. T. Topham, S. E. Kalloger et al., "Altered gene expression along the glycolysis-cholesterol synthesis axis is associated with outcome in pancreatic cancer," *Clinical Cancer Research*, vol. 26, no. 1, pp. 135–146, 2020.

[5] S. Cristea, G. L. Coles, D. Hornburg et al., "The MEK5-ERK5 Kinase axis controls lipid metabolism in small-cell lung cancer," *Cancer Research*, vol. 80, no. 6, pp. 1293–1303, 2020.

[6] C. Thakur and F. Chen, "Connections between metabolism and epigenetics in cancers," *Seminars in Cancer Biology*, vol. 57, pp. 52–58, 2019.

[7] S. Beloribi-Djefaflia, S. Vasseur, and F. Guillaumond, "Lipid metabolic reprogramming in cancer cells," *Oncogenesis*, vol. 5, no. 1, Article ID e189, 2016.

[8] H. Iwamoto, M. Abe, Y. Yang et al., "Cancer lipid metabolism confers antiangiogenic drug resistance," *Cell Metabolism*, vol. 28, no. 1, pp. 104–117, 2018.

[9] F. Massari, C. Ciccarese, M. Santoni et al., "Metabolic phenotype of bladder cancer," *Cancer Treatment Reviews*, vol. 45, pp. 46–57, 2016.

[10] S. Cheng, G. Wang, Y. Wang et al., "Fatty acid oxidation inhibitor etomoxir suppresses tumor progression and induces cell cycle arrest via PPARγ-mediated pathway in bladder cancer," *Clinical Science*, vol. 133, no. 15, pp. 1745–1758, 2019.

[11] Y. Cao, "Adipocyte and lipid metabolism in cancer drug resistance," *Journal of Clinic Investigation*, vol. 129, no. 8, pp. 3006–3017, 2019.

[12] A. J. Hoy, S. R. Nagarajan, and L. M. Butler, "Tumour fatty acid metabolism in the context of therapy resistance and obesity," *Nature Reviews Cancer*, vol. 21, no. 12, pp. 753–766, 2021.

[13] I. Elia and M. C. Haigis, "Metabolites and the tumour microenvironment: from cellular mechanisms to systemic metabolism," *Nature Metabolism*, vol. 3, no. 1, pp. 21–32, 2021.

[14] K. Man, A. Kallies, and A. Vasanthakumar, "Resident and migratory adipose immune cells control systemic metabolism and thermogenesis," *Cellular Molecular Immunol*, vol. 19, no. 3, pp. 421–431, 2022.

[15] V. G. Patel, W. K. Oh, and M. D. Galsky, "Treatment of muscle-invasive and advanced bladder cancer in 2020," *CA: A Cancer Journal for Clinicians*, vol. 70, no. 5, pp. 404–423, 2020.

[16] I. H. Kim and H. J. Lee, "Perioperative systemic treatment for muscle-invasive bladder cancer: current evidence and future perspectives," *International Journal of Molecular Sciences*, vol. 22, no. 13, Article ID 7201, 2021.

[17] J. Liu, Y. Peng, L. Shi et al., "Skp2 dictates cell cycle-dependent metabolic oscillation between glycolysis and TCA cycle," *Cell Research*, vol. 31, no. 1, pp. 80–93, 2021.

[18] S. Shi, T. Ma, and Y. Xi, "Characterization of the immune cell infiltration landscape in bladder cancer to aid immunotherapy," *Archives of Biochemistry and Biophysics*, p. 708, Article ID 108950, 2021.

[19] S. M. Morrissey, F. Zhang, C. Ding et al., "Tumor-derived exosomes drive immunosuppressive macrophages in a pre-metastatic niche through glycolytic dominant metabolic reprogramming," *Cell Metabolism*, vol. 33, no. 10, pp. 2040–2058.e10, 2021.

[20] X. Chen, R. Xu, D. He et al., "CD8$^+$ T effector and immune checkpoint signatures predict prognosis and responsiveness to immunotherapy in bladder cancer," *Oncogene*, vol. 40, no. 43, pp. 6223–6234, 2021.

[21] J. Pei, Y. Li, T. Su et al., "Identification and validation of an immunological expression-based prognostic signature in breast cancer," *Frontiers in Genetics*, vol. 11, p. 912, 2020.

[22] M. T. Dillon, J. S. Good, and K. J. Harrington, "Selective targeting of the G2/M cell cycle checkpoint to improve the therapeutic index of radiotherapy," *Clinical Oncology*, vol. 26, no. 5, pp. 257–65, 2014.

[23] I. Pastushenko and C. Blanpain, "EMT transition states during tumor progression and metastasis," *Trends in Cell Biology*, vol. 29, no. 3, pp. 212–226, 2019.

[24] J. P. Joseph, M. K. Harishankar, A. A. Pillai, and A. Devi, "Hypoxia induced EMT: a review on the mechanism of tumor progression and metastasis in OSCC," *Oral Oncology*, vol. 80, pp. 23–32, 2018.

[25] E. Dai, L. Han, J. Liu et al., "Autophagy-dependent ferroptosis drives tumor-associated macrophage polarization via release and uptake of oncogenic KRAS protein," *Autophagy*, vol. 16, no. 11, pp. 2069–2083, 2020.

[26] N. Du, D. Dong, L. Sun et al., "Identification of ACOT13 and PTGER2 as novel candidate genes of autosomal dominant polycystic kidney disease through whole exome sequencing," *European Journal of Medical Research*, vol. 26, no. 1, p. 142, 2021.

[27] P. L. M. Dahia, "Novel hereditary forms of pheochromocytomas and paragangliomas," *Front Horm Res*, vol. 41, pp. 79–91, 2013.

[28] J. Cui and S. Li, "Inhibitors and prodrugs targeting CYP1: a novel approach in cancer prevention and therapy," *Current Medicinal Chemistry*, vol. 21, no. 5, pp. 519–52, 2014.

[29] A. Blomme, C. A. Ford, E. Mui et al., "2, 4-dienoyl-CoA reductase regulates lipid homeostasis in treatment-resistant prostate cancer," *Nature Communication*, vol. 11, no. 1, p. 2508, 2020.

[30] C. Lan, Y. Wang, X. Su, J. Lu, and S. Ma, "LncRNA LINC00958 Activates mTORC1/P70S6K signalling pathway to promote epithelial-mesenchymal transition process in the hepatocellular carcinoma," *Cancer Investigation*, vol. 39, no. 6-7, pp. 539–549, 2021.

[31] A. Sadik, L. F. Somarribas Patterson, S. Öztürk et al., "IL4I1 is a metabolic immune checkpoint that activates the AHR and promotes tumor progression," *Cell*, vol. 182, no. 5, pp. 1252–1270, 2020.

[32] E. C. Lien, A. M. Westermark, Y. Zhang et al., "Low glycaemic diets alter lipid metabolism to influence tumour growth," *Nature*, vol. 599, no. 7884, pp. 302–307, 2021.

[33] S. Kern, I. Truebenbach, M. Höhn et al., "Combined anti-tumoral effects of pretubulysin and methotrexate," *Pharmacol Res Perspect*, vol. 7, no. 1, Article ID e00460, 2019.

[34] L. Dyck and K. H. G. Mills, "Immune checkpoints and their inhibition in cancer and infectious diseases," *European Journal of Immunology*, vol. 47, no. 5, pp. 765–779, 2017.

[35] J. H. Jang, E. G. Sung, I. H. Song, T. J. Lee, and J. Y. Kim, "Metformin induces caspase-dependent and caspase-independent apoptosis in human bladder cancer T24 cells," *Anticancer Drugs*, vol. 31, no. 7, pp. 655–662, 2020.

Research Article

Chelerythrine Inhibits Stemness of Cancer Stem-Like Cells of Osteosarcoma and PI3K/AKT/mTOR Signal

Zhixing Chen,[1] Hui Yang,[2] Qianlu Zhang,[3] Qiongying Hu ⓘ,[4] and Ziyi Zhao ⓘ[5]

[1]*Department of Burns and Plastic Surgery, West China Hospital, Sichuan University, Chengdu 610041, China*
[2]*Department of Anesthesiology, West China Hospital, Sichuan University, Chengdu 610041, China*
[3]*Department of Anesthesiology, The First Affiliated Hospital of the University of South China, Hengyang, Hunan Province 421205, China*
[4]*Department of Laboratory Medicine, Hospital of Chengdu University of Traditional Chinese Medicine, Chengdu 610072, Sichuan Province, China*
[5]*TCM Regulating Metabolic Diseases Key Laboratory of Sichuan Province, Hospital of Chengdu University of Traditional Chinese Medicine, Chengdu 610072, Sichuan Province, China*

Correspondence should be addressed to Qiongying Hu; qiongyinghu@163.com and Ziyi Zhao; zhaoziyi@cdutcm.edu.cn

Chelerythrine (CHE) is widely found in many herbs and is the main alkaloid constituent of *Toddalia asiatica* (L.) LAM. It has been proved to exert remarkable antitumor, antifungal, anti-inflammatory, and antiparasitic effects. In osteosarcoma, CHE is reported to inhibit proliferation and promote apoptosis. However, the effect of CHE on cancer stem-like cells (CSCs), which contribute to metastasis and recurrence in osteosarcoma, is still largely unknown. In this study, we investigated the effects of CHE on the stemness and malignant behaviors of CSCs derived from osteosarcoma cells. CSCs were enriched by culturing in serum-free medium. The effects of CHE on stemness were measured by detecting stemness factors and sphere formation ability. The effects of CHE on chemosensitivity to doxorubicin and MTX were measured by Annexin V-FITC/PI double staining. The effects of CHE on CSC malignancy were measured by performing CCK-8, colony formation, tumor formation in soft agar, migration, and invasion assays. We first enriched CSCs from osteosarcoma cells, which were characterized by upregulated stemness markers, including Oct4, Nanog, and Nestin. The addition of CHE clearly decreased malignant behaviors, including colony formation, tumor formation in soft agar, migration, and invasion. CHE also inhibited stemness and thus induced the failure of sphere formation. Moreover, CHE promoted apoptosis induced by chemo agents, including doxorubicin (DOX) and methotrexate (MTX). After CHE treatment, the protein expression of MMP-2/9 was significantly decreased, potentially inhibiting invasion. CHE also exhibited an inhibitory effect on the phosphorylation of PI3K, AKT, and mTOR, which is an upstream regulatory signaling pathway of MMP-2/9. In summary, CSCs derived from U2OS and MG-63 cells, CHE could inhibit the stemness and malignant behaviors of CSCs potentially by inhibiting the PI3K/AKT/mTOR signaling pathway.

1. Introduction

Osteosarcoma, as a connective tissue tumor, is the most common primary malignant tumor in bone, originating in mesenchymal tissue. Approximately 80%-90% of osteosarcomas occur in the metaphysis of the long tubular bones of the extremities, with the most common occurring in the distal femur, proximal tibia, and proximal humerus. Osteosar-

comas occurring in nonextremities, such as the spine and pelvis, tend to have a poor prognosis. Generally, patients with osteosarcoma have a 5-year survival rate of less than 20%. Despite the use of surgery, radiotherapy, and neoadjuvant chemotherapy, long-term survival for osteosarcoma has not been significantly ameliorated [1]. To date, scientists have successfully isolated tumor stem cells from osteosarcoma [2]. Tumor stem cells have a close bearing on the

occurrence, metastasis, treatment resistance and recurrence of tumors, and lung metastasis is the primary cause of death in patients with osteosarcoma. Therefore, tumor stem cells in osteosarcoma prevent osteosarcoma from being cured to a large extent. Osteosarcoma is the most common primary malignant tumor of bone in children and adolescents, accounting for nearly 60% of the common histological subtypes of osteosarcoma in children [3]. In view of its high degree of malignancy, poor prognosis, high possibility of lung metastasis in the early stage, and rapid development, timely ,and early treatment of osteosarcoma is extremely necessary.

Despite the poor prognosis, the therapy-resistant cell types in osteosarcoma tumors are poorly understood. The subpopulation of cancer cells with stem/progenitor properties, termed cancer stem-like cells (CSCs), which exhibit stem/progenitor characteristics was explained as the cause of therapy resistance [4]. This subpopulation was characterized by expression of stemness markers, including Nanog, Oct4, and Nestin, formation of spheres in vitro, and tumor-initiating ability in preclinical mouse models [5]. The existence of CSCs derived from osteosarcoma is responsible for the tumor's drug resistance and high metastatic potential, demonstrating that it is critical to have an in-depth investigation of the strategies to be specifically targeted [6]. In our previous findings, CSCs were successfully enriched from colorectal cancer cells by culturing in serum-free medium [7]. After culture with berberine, a compound extracted from the traditional Chinese medicine *Coptis chinensis*, CSCs derived from colorectal cancer cells showed decreased stemness and increased chemosensitivity against regular chemo agents. All of these findings indicate that natural compounds may be promising candidates for the use as specific chemo agents against CSCs.

Chelerythrine (CHE), also known as chelerythrine chloride or celandine quaternary ammonium base, is a benzphenanthridine type of isoquinoline isolated from plants, such as *Toddalia asiatica*, *Chelidonium majus*, *Macleaya cordata*, and *Eomecon chionantha* Hance. CHE can inhibit cell proliferation and induce cell apoptosis against a variety of tumor cells due to its various pharmacological activities, such as antitumor, antibacterial, antifungal, and anti-inflammatory activities. Chmura et al. [8] confirmed via in vitro experiments that CHE showed cytotoxicity to 9 tumor cells, including MCF7, MCF7ADR, HT29, DaOY, SCC35, SCC61, SQ20B, JSQ3, and LnCap, and had a significant inhibitory effect on tumor growth. In particular, in osteosarcoma cells, CHE was reported to exert suppressive effects on malignancies. Wang et al. reported that CHE treatment inhibited migration and invasion capacities by reducing the mass of actin filaments in the cellular actin filament network [9]. It has also been reported that, in osteosarcoma, CHE treatment activates extracellular signal-regulated kinase (ERK) kinase (MEK)/ ERK MAPK signaling and thus promotes apoptosis in a MEK1-dependent manner [10]. All of these data indicate that CHE acts as an efficient tumor suppressor in osteosarcoma. However, its exact role in CSCs derived from osteosarcoma is still largely unknown.

In this study, we sought to evaluate the suppressive effects of CHE on CSCs derived from the osteosarcoma cell lines U2OS and MG-63 and the potential molecular mechanism. We revealed that CHE inhibited CSC malignancies by regulating PI3K/AKT/mTOR signaling and MMP2/9 expression. Moreover, we found that CSCs are significantly more sensitive to CHE than their parental cells, which indicates that CHE may be a promising drug to specifically target CSCs and exert limited side effects.

2. Materials and Methods

2.1. Cell Culture and Treatment. Human osteosarcoma MG-63 and U2OS cell lines were purchased from the American Type Culture Collection (ATCC, Manassas, VA, USA). These cells were cultured in Dulbecco's modified Eagle's medium (DMEM; GIBCO, Grand Island, NY, USA) supplemented with 10% heat-inactivated (56°C, 30 min) fetal bovine serum and 1% antibiotics (penicillin/streptomycin). Cells were maintained in 37°C, 5% CO2, and 95% humidity. Every three days, medium was replaced and cells were passaged.

To enrich CSCs from MG-63 or U2OS, cells were suspended and cell concentration was adjusted to 1×10^7 cells per mL. 1×10^6 cells were seeded in a 6-well plate and cultured in serum-free DMEM/F12 medium supplemented with 20 ng/mL bFGF, 20 ng/mL EGF, and 2% B27. Every three days, medium was half-changed. Briefly, medium was collected and concentrated at 1000 g, 4°C for 5 min. Then supernatant was removed and pelleted spheres were resuspended using fresh medium. After 14 days, formed spheres were imaged using Olympus microscopy X71 (Japan).

2.2. CCK-8 Analysis. MG-63 and U2OS cells were seeded in 96-well plates at a density of 5×10^3 cells per well and maintained in DMEM medium supplemented with 10% heat-inactivated (56°C, 30 min) fetal bovine serum and 1% antibiotics (penicillin/streptomycin). 24-h later, 5, 10, 15, 20, 25, 30, 35, or 40 μmol/L CHE were added, respectively, for 24-hour extra treatment. 10 μL of CCK-8 solution were added to each well, after which the cells were incubated for 2 h at 37°C. After incubation, absorbance was measured at 450 nm.

2.3. Western Blot. MG-63 and U2OS cells (5×10^6 cells, respectively) were treated with 15 or 10 μmol/L CHE for 24 h, and then cells were harvested and lysed using animal tissue/cells/bacteria total protein isolation kit (DocSense, Chengdu, China). Cell lysate protein was fractionated via SDS-PAGE at 100 V for 2 h and transferred to an Immobilon-P transfer membrane (Merck Millipore, Burlington, MA, USA) to a nitrocellulose membrane at 45 V for 2 h. The membranes were blocked with bovine serum albumin (Bovogen, Australia), and incubated with primary antibodies against proteins at 4°C overnight. The used of primary antibodies were listed as follows: anti-Oct4 (cat. No.: ab181557), anti-Nanog (cat. No.: ab109250), anti-Nestin (cat. No.: ab105389), anti-beta Actin (cat. No.: ab8227), anti-MMP2 (cat. No.: ab92536), anti-MMP9 (cat. No.: ab76003), anti-PI3K (cat. No.: ab154598), anti-
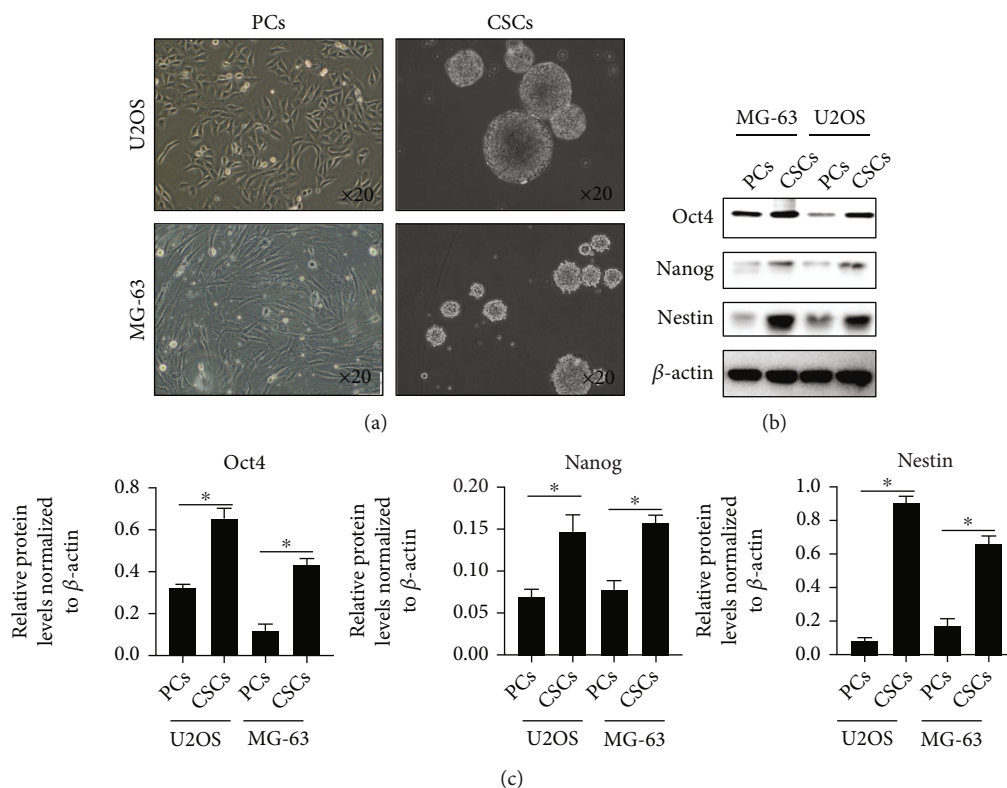
(a)

(b)

(c)

FIGURE 1: Characterization of CSCs enriched from U2OS and MG-63 cells. (a) Cell morphology was observed after being cultured in serum-containing medium or serum-free medium after 14 days. (b and c) Western blot was performed to detect protein levels of Oct4, Nanog, and Nestin in MG-63 and U2OS parental cells (PCs) and CSCs. $*P < 0.05$ vs. PCs group.

phosphate PI3K (cat. No.: ab182651), anti-pan AKT (cat. No.: ab300473), anti-phosphate AKT (cat. No.: ab38449), anti-mTOR (cat. No.: ab), anti-mTOR (cat. No.: ab134903), and anti-phosphate mTOR (cat. No.: 109268). All primary antibodies were bought from Abcam (Cambridge, England) and diluted at 1:1000. The membranes were then washed with TBS-T, and incubated using HRP-conjugated secondary antibody (Jackson Laboratory, Bar Harbor, USA). Chemiluminescence was detected using ECL (Gendepot, Barker, USA) and measured using the ChemiDoc detection system (Bio-Rad, Hercules, CA, USA).

2.4. Tumor Formation in Soft Agar.
Spheres derived from MG-63 or U2OS were separated and obtained single-cell suspension using SoniConvert® single-cell suspension preparation system (DocSense, Chengdu, China) by following manufacturer's instruction. 1×10^4 cells for each CSCs were suspended in 0.35% biotechnology-grade agarose (Bio-Rad, Hercules, CA, USA) in DMEM/F12 supplemented with 10 or 15 μmol/L CHE, 20 ng/mL bFGF, 20 ng/mL EGF, and 2% B27 and plated before solidifying on a solid 0.5% agarose with DMEM/F12. Colonies were maintained for 14 days in a 37°C humidified incubator, after which they were stained with methylene blue (Sigma-Aldrich, St. Louis, MO, USA) and counted.

2.5. Migration and Invasion.
Migration of human breast cancer cells was assessed in a transwell chamber assay. Briefly, spheres derived from MG-63 or U2OS were separated and obtained single -cell suspension using SoniConvert® single-cell suspension preparation system (DocSense, Chengdu, China) by following manufacturer's instruction. 1×10^4 cells were seeded into cell culture inserts containing membranes with 8 μm pores that were placed in wells containing cell culture medium with 2% FBS. 24-hour later, unmigrated cells were removed with cotton swabs, and migrated cells were fixed in cold methanol and stained with Diff-Quik solution. Cells were imaged. Similar results were obtained in three independent experiments.

Invasion assay was performed using BD transwell invasion chamber (BD Biosciences, Bedford, MA, USA). Single-cell suspension was prepared as described as before. Matrigel chambers were rehydrated for two hours using 500 μL of serum-free DMEM/F12 medium. After rehydration, 750 μL normal growth media containing 2% FBS was added to the bottom of the well. 1.0×10^4 cells in DMEM/F12 medium with supplements described as before were added to the Matrigel chamber. Chambers were incubated overnight in a cell culture incubator, at 37°C, 5% CO2 atmosphere. 48-hour later, noninvading cells were removed with a cotton swab. Invaded cells were sequentially transferred through a fixative, then 4% paraformaldehyde solution for 15 min at room temperature. After three washed using PBS, invaded cells were allowed to air dry. Membranes were mounted onto slides using immersion oil and covered with a cover slip. Cells were counted using light microscopy at 40× magnification.
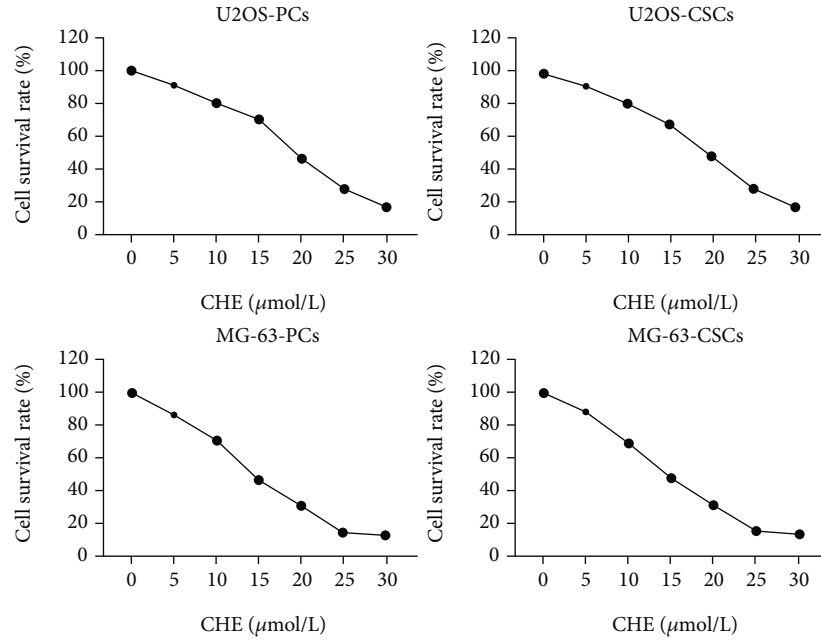
(a)
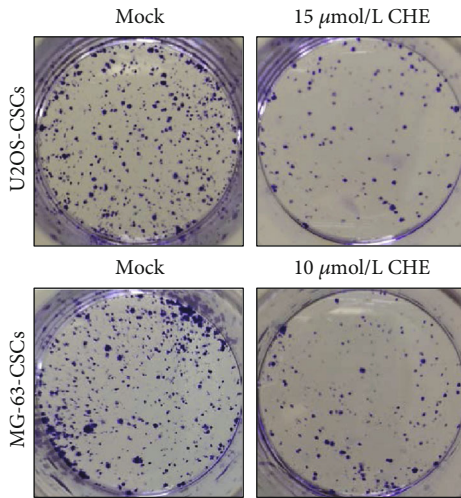
(b)
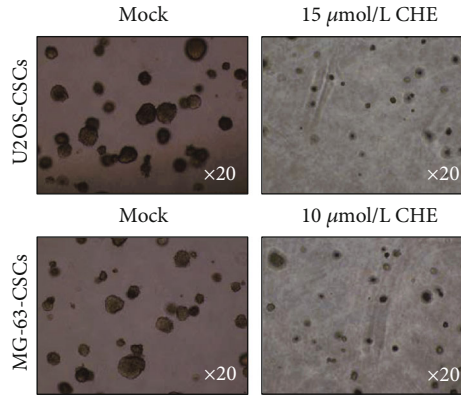
(c)
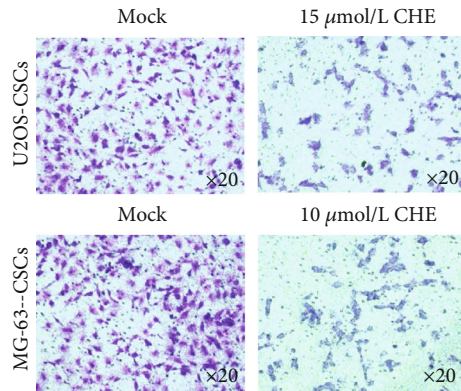
(d)
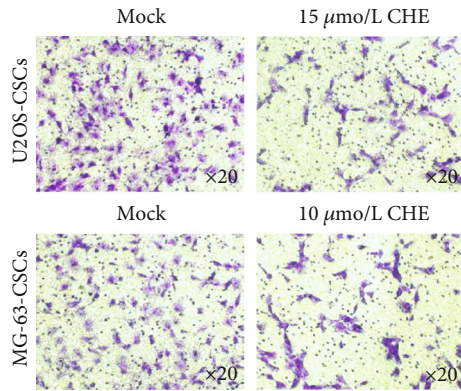
(e)

FIGURE 2: CHE inhibited malignant behaviors in CSCs. (a) After being cultured in 5-30 μmol/L of CHE for 24 h, cell viability was performed by performing CCK-8 assay. After being treated with CHE, colony formation (b), tumor formation in soft agar (c), migration (d), or invasion (e) were analyzed.

(a)

(b)

(c)
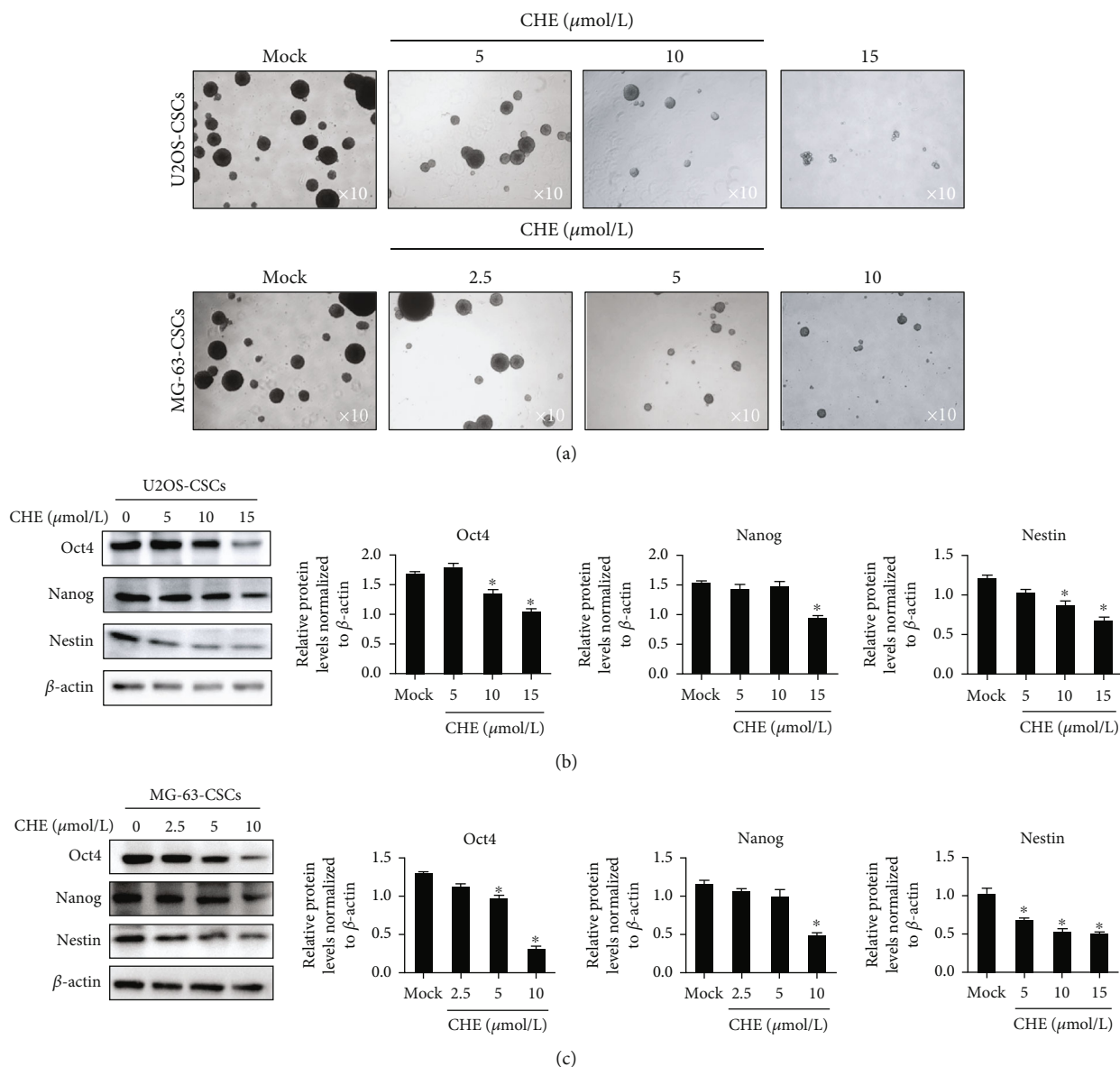
Figure 3: CHE inhibited stemness of CSCs. (a). Single-cell suspension of CSCs was cocultured with CHE for 14 days, and then formed spheres were imaged. After being cultured with CHE for 48 h, total protein was extracted from single-cell suspension of CSCs and analyzed by performing western blot to detect stemness marker proteins, including Oct4, Nanog, and Nestin (b and c).

2.6. Apoptosis Analysis. Annexin-V Apoptosis Detection Kit (Cell Signaling Technology) was used to quantify the levels of apoptosis according to the manufacturer's instructions. Briefly, 1×106 cells were trypsinized and collected by centrifugation at 4°C, 1000 g for 10 min. Then cells were incubated with Annexin V-FITC and propidium iodide. Apoptosis was analyzed by flow cytometry (Beckman, Navios) for the detection of Annexin V-FITC. Data was analyzed using FlowJo (v10). Experiments were performed at least thrice, and statistical analysis was performed with GraphPad Prism.

2.7. Animal experiment. All the animal experiments were conducted according to the ethics committee of the Institutional Animal Care and Use Committee of Institute of

Chengdu University of Traditional Chinese Medicine (No. 2020QKL-001).

Spheres derived from U2OS were separated and obtained single-cell suspension using SoniConvert® single-cell suspension preparation system (DocSense, Chengdu, China) by following manufacturer's instruction. Collected cells were pretreated with 15 μmol/L CHE for 48 h.

Eight female nude mice (SPF) were divided into two groups: Mock group ($n = 4$) and CHE group ($n = 4$). Each mouse was subcutaneously injected with 5×105 cells suspension. The tumor growth was measured every five days from day 10, and the length diameter and short diameter were measured by vernier calipers. Tumor volume was calculated

(a)

(b)
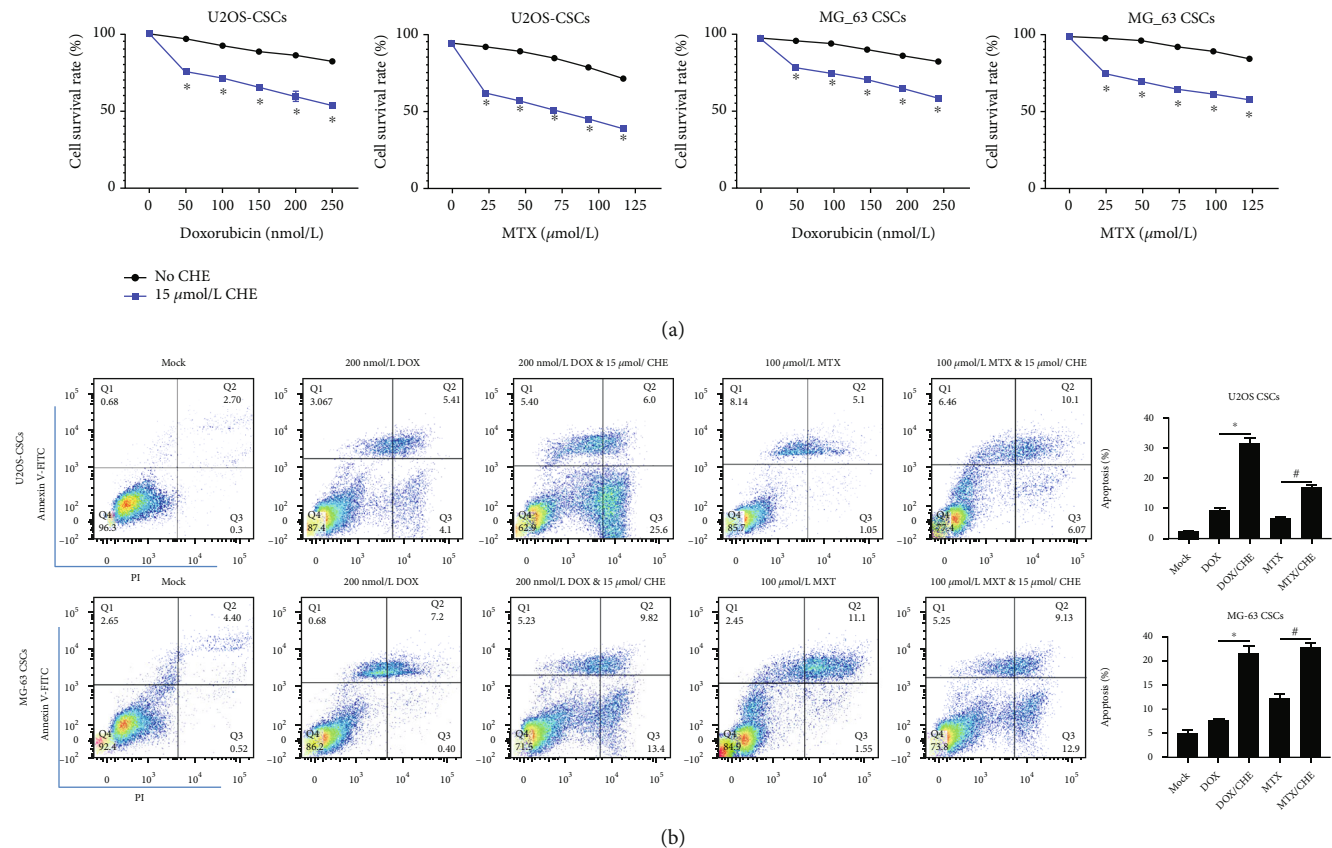
FIGURE 4: CHE enhanced chemoresistance to DOX and MTX in CSCs derived from osteosarcoma cells. (a) After being cultured with or without CHE for 24 h, the cell viability was measured after DOX or MTX treatment. *$P < 0.05$ vs. no CHE group. (b) After being cocultured using CHE with DOX or MTX, apoptosis was measured by performing Annexin V-FITC/PI double staining followed by flow cytometry assay. *$P < 0.05$ vs. DOX group; #$P < 0.05$ vs. MTX group.

(tumor volume $= \pi \times$ lengthdiameter $\times$ short diameter 2/6). The nude mice were sacrificed 30 days later, and tumor growth curve was drawn.

2.8. *Statistical Analysis.* Statistical analysis was conducted using one-way ANOVA, and statistical significance was set at $P < 0.05$.

3. Results

3.1. *CHE Significantly Decreased Colony Formation, Migration, and Invasion in CSCs Derived from Osteosarcoma Cells.* To evaluate the effects of CHE on CSCs, we firstly enriched CSCs from osteosarcoma cells U2OS and MG-63 by being cultured in serum-free medium for 14 days. As it is shown in Figure 1(a), formation of spheres was morphologically observed, which is considered as a character of stemness [5]. In addition, as expected, these cells presented a relative higher level of stemness markers (e.g., Oct4, Nanog, and Nestin) [10].

Spheres derived from U2OS or MG-63 were trypsinized and single-cell suspension was collected to evaluate the effects of CHE. By being cultured in different concentration of CHE (ranged from 5-30 μmol/L) for 24 h, cell viability was detected and IC$_{30}$ of U2OS-CSCs is approximately 15 μmol/L, and that of MG-63-CSCs is approximately 10 μmol/L (Figure 2(a)). Notably, osteosarcoma cells present a similar IC$_{30}$ concentra-

tion, indicated that osteosarcoma cells present similar sensitivity to CHE after 24-h treatment compared with corresponding CSCs. Then, we treated CSCs derived from U2OS or MG-63 with 15 μmol/L or 10 μmol/L of CHE, respectively, and colony formation, tumor formation in soft agar, migration, and invasion were further analyzed. As it is shown in Figures 2(b)– 2(e), addition of CHE obviously inhibited all these malignant behaviors, respectively.

3.2. *CHE Decreased Stemness of Osteosarcoma Cells.* CHE was reported to induce apoptosis and reverse chemoresistance in osteosarcoma cell [11], which promoted us to evaluate the effects of CHE on stemness of osteosarcoma. Single-cell suspension of CSCs were seeded with 5-15 μmol/L of CHE and cultured for 14 days. Added CHE obviously decreased number of spheres (Figure 3(a)), potentially via inhibiting sphere formation, but not proliferation. To further confirm the inhibitory effect of CHE on stemness, 48-hour after CHE treatment, stemness markers, including Oct4, Nanog, and Nestin, were detected and results demonstrated that CHE treatment significantly decreased all these stemness markers (Figures 3(b) and 3(c)). Added CHE failed to affect the number of formed spheres (data not shown), which further indicated that CHE affects stemness, but not exert cytotoxicity.

(a)

(b)

FIGURE 5: CHE decreased MMP-2 and MMP-9. After being treated with CHE for 48 h, total protein was extracted from single-cell suspension of CSCs and analyzed by performing western blot to detect MMP-2 and MMP-9 protein levels (a and b). $*P < 0.05$ vs. mock group.

3.3. CHE Induces Chemosensitivity in CSCs.

Presence of CSCs was believed to contribute to chemoresistance in osteosarcoma [12]. By considering that CHE treatment significantly decreased stemness without affecting cell viability, the effects of CHE on Doxorubicin (DOX) or Methotrexate (MTX)-induced cell death, which are the first choice of treatment for osteosarcoma clinically [13]. Although addition of CHE failed to obviously increased cell death induced by DOX or MTX in osteosarcoma cells (data not shown), as it is shown in Figure 4(a), addition of CHE significantly increased chemosensitivity to DOX or MTX in CSCs and decreased cell survival rate. To further evaluate the promoting effects of CHE on chemoagent-induced apoptosis, Annexin V-FITC/PI double staining was performed followed by flow cytometric assay. As it is shown in Figure 4(b), expectedly, both DOX and MTX treatments significantly increased proportion of Annexin V+/PI− and Annexin V+/PI+. Addition of CHE significantly increased proportion of both Annexin V+/PI− and Annexin V+/PI+, demonstrated the promoting effects of CHE on chemosensitivity. By considering that CHE slightly affects cell viability, the promoting effects of CHE on apoptosis is mainly via decreasing stemness.

3.4. CHE Decreased the Expression Level of MMP-2 and MMP-9 in CSCs Derived from Osteosarcoma Cells.

MMP-2 and MMP-9 are two important members of the MMP family. They are highly expressed in many malignant tumors, and they participate in the degradation and destruction of the ECM and BM and promote tumor metastasis [13]. Moreover, CHE was also demonstrated to be involved in MMP-2 and MMP-9 regulation in hepatocellular carcinoma [14], we then clarified the effect of CHE on MMP-2 and MMP-9 expression. Expectedly, consistent with the effect of CHE on MMP-2 and MMP-9 in hepatocarcinoma cells, 12-h and 24-h CHE treatment significantly decreased MMP-2 and MMP-9 expression levels (Figures 5(a) and 5(b)).

3.5. Effects of CHE on the PI3K/AKT/Mammalian Target of Rapamycin (mTOR) Signaling Pathway.

The phosphatidylinositol 3-kinase (PI3K)/Akt and mitogen-activated protein kinase (MAPK) signal transduction pathways were reported to be tightly involved in regulating metastasis via modulating MMP-2 and MMP-9 [15]. As it is shown in Figure 6, CHE treatment undetectably affected PI3K, AKT, or mTOR total protein levels in CSCs. After CHE treatment, phosphorylation of PI3K, AKT, and mTOR decreased significantly, indicated that, in CSCs derived from osteosarcoma cells, CHE potentially decreased migration and invasion via inhibiting PI3K/AKT/mTOR pathway and inducing MMP-2, MMP-9 inhibition.

3.6. Pretreatment of CHE Suppressed Tumor Growth of CSCs Derived from U2OS.

To further evaluate the effects of CHE on tumor growth in mice, single-cell suspension of CSCs derived from U2OS was pretreated with 15 μmol/L of CHE for 24 h

(a)

(b)

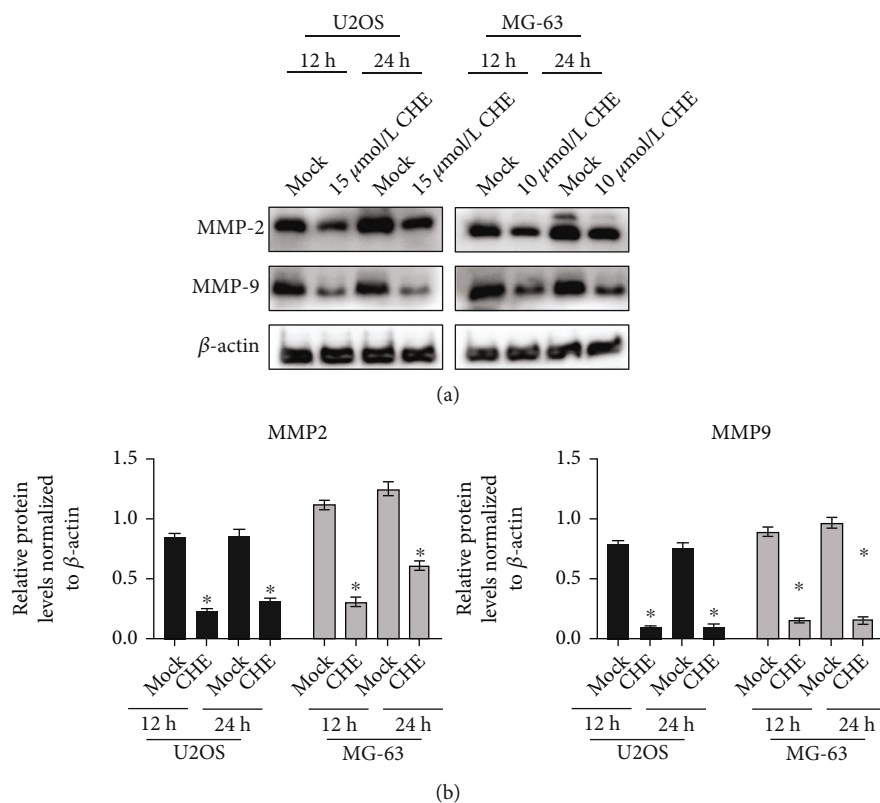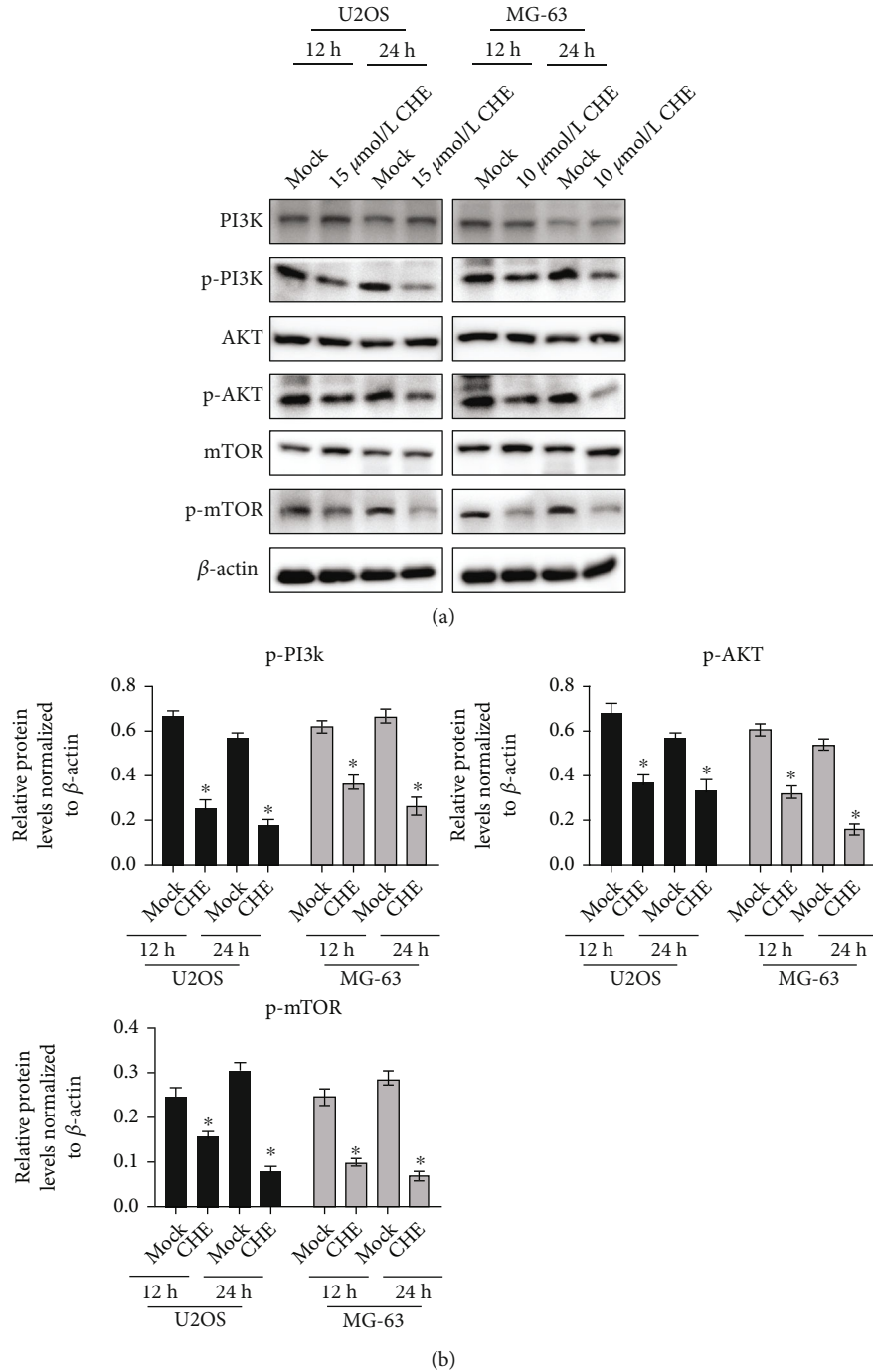FIGURE 6: CHE inhibited PI3K/AKT/mTOR signaling pathway. After being treated with CHE for 48 h, total protein was extracted from single-cell suspension of CSCs and analyzed by performing western blot to detect PI3K/AKT/mTOR protein levels (a and b). $*P < 0.05$ vs. mock group.

and then injected intraperitoneally (I.P.). As it is shown in Figures 7(a), 7(b), and 7(c), CHE pretreatment significantly decreased tumor growth in nude mice. This indicates that, CHE treatment decreased stemness irreversibly in CSCs and suppressed tumor growth. We then also detected stemness markers, including Oct4, Nanog, and Nestin, in burdened tumors. However, no significant difference between these two groups (Figure 7(d)), potentially due to lose of stemness of CSCs after 4-week's growth in mice.

4. Discussion

CHE is known to exert antitumor effects in numerous cancers. Considering that the therapeutic-resistant effects of cancers are mainly due to heterogeneity, it is worth investigating whether CHE exerts antitumor effects on CSCs, which is considered a main cause of recurrence. The present study showed that CHE decreased malignant behaviors, including colony formation, tumor formation in soft agar,
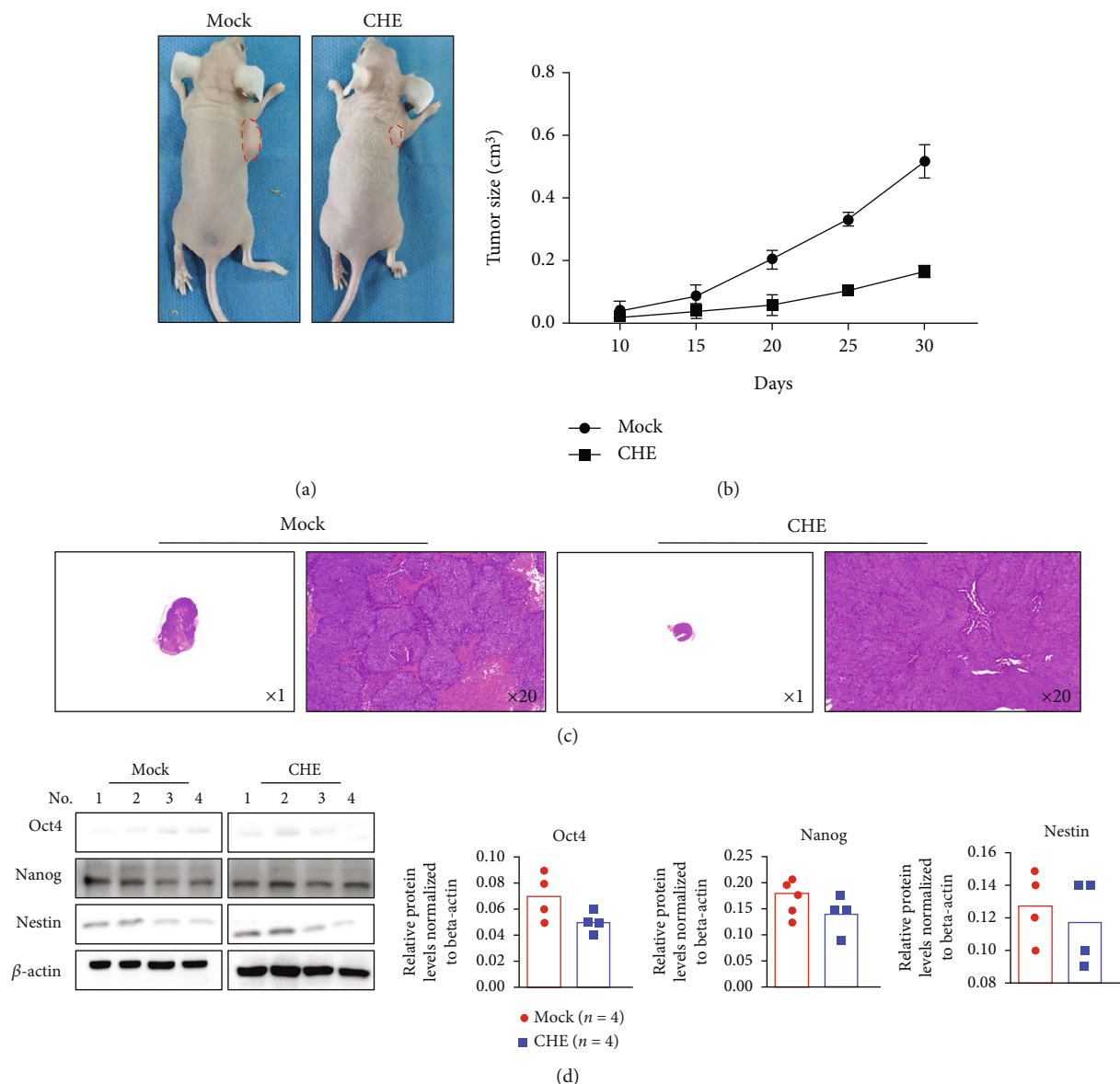
FIGURE 7: Tumor growth inhibition in xenograft mice. (a) After being pretreated with or without CHE for 48 h, CSCs were seeded in mice. $N = 4$ for each group. After 30 days, mice were imaged. (b) 10 days after injection, tumor size was measured every five days, and growth curve was drawn. (c) After 30-day growth, tumors were obtained and physiologically analyzed by performing H&E staining. Samples were observed at amplification of 1× or 20×. (d) After 30-day growth, freshly obtained tumors were lysed and expression levels of Oct4, Nanog, and Nestin were analyzed by performing western blot.

migration, and invasion, potentially by inhibiting the stemness of CSCs. Additionally, the effect of CHE was at least partially dependent on the PI3K/AKT/mTOR signaling pathway. Differences were observed in chemoresistance between CHE-treated and CHE-untreated CSCs. These differences in chemosensitivity might be linked to the maintenance of CSC stemness. Furthermore, CHE pretreatment delayed tumor regrowth in mice transplanted with CSCs.

Based on current research findings, CHE may induce cell apoptosis through a variety of pathways and mechanisms. In addition to acting on Bcl-2 and Bcl-XL factors in the apoptosis pathway, promoting the release of mitochondrial cytochrome C, inhibiting the activity of protein kinase C as well as the polymerization of tubulin (prevent-

ing the progression of mitosis), and rapidly inducing apoptosis through the production of reactive oxygen species, CHE can also induce cell cycle arrest and mitochondria-mediated apoptosis through the caspase-8-dependent KG1a cell pathway [16], balance antiapoptotic and proapoptotic signaling pathways [17], activate P38 and amino-terminal protein kinase pathways [18], and induce cell cycle arrest and mitochondria-mediated apoptosis [19]. Surprisingly, CHE did not exert extra cytotoxicity against CSCs compared to its parental cells in this study. Without inducing obvious cytotoxicity, CHE regulates the PI3K/AKT/mTOR signaling pathway and stemness in CSCs. Subsequently, CHE suppresses malignancies in CSCs in a prosurvival manner.

Doxorubicin is widely used to treat malignant tumors, including osteosarcoma [20, 21]. The toxic effects of doxorubicin on malignant cells are as follows: (i) DNA base-pair intercalation; (ii) drug molecules interact with topoisomerase II to form DNA-cleavable complexes; (iii) drug molecules interact with the electron transport chain, which may cause cells to produce superoxide anion radicals [22]. The chemoresistance mechanisms of tumor cells to doxorubicin include: (1) overexpression of membrane-associated efflux pumps and P glycoproteins mediating multidrug resistance; (2) altered expression of topoisomerase II and integrin; (3) altered glutathione levels [23]. MTX is another cancer drug widely used in osteosarcoma chemotherapy. Some evidence suggests that DHFR is critical in regulating chemoresistance to MTX in human osteosarcoma cells [24, 25]. In this study, these two chemo agents were employed to evaluate the effects of CHE treatment on the chemosensitivity of CSCs. Remarkably, CHE treatment significantly decreased cell viability and promoted apoptosis induced by both DOX and MTX. Although the promoting effects of CHE on chemotreatment have been confirmed, the exact molecular mechanism of its promoting effects on chemosensitivity is still largely unknown and is worthy of further investigation.

5. Conclusion

The findings of the present study demonstrate that CHE treatment significantly decreased the stemness of CSCs derived from osteosarcoma cells, including U2OS and MG-63 cells. CHE significantly decreased stemness markers, including Oct4, Nanog, and Nestin, and thus suppressed malignant behaviors. The present study also demonstrated that CHE treatment decreased MMP-2/9 protein expression and the PI3K/AKT/mTOR signaling pathway, which might contribute to a decrease in the stemness of CSCs. Moreover, CHE treatment also increased chemosensitivity to DOX and MTX, which are two first-choice chemo agents, in CSCs. These findings may be beneficial to the development of novel antitumor therapeutics by targeting CSCs, which critically contribute to recurrence.

Moreover, CHE treatment also increased chemosensitivity to DOX and MTX, which of them are two first-choice chemo agents, in CSCs. These findings may be beneficial to the development of novel antitumor therapeutic strategies by targeting to CSCs, which contributes to recurrence critically.

Data Availability

All data generated or analyzed during this study are included in this published article.

Ethical Approval

All the animal experiments were conducted according to the ethics committee. All are approved by the Institutional Animal Care and Use Committee of Institute of Chengdu University of Traditional Chinese Medicine (No. 2020QKL-001).

Conflicts of Interest

The authors declare that the research was conducted in the absence of any commercial or financial relationships that could be construed as a potential conflict of interest.

Authors' Contributions

ZYZ and QYH both designed the experiments. ZXC, HY, and QLZ performed most of the experiments included in this study. ZXC and QLZ collected and statistically analyzed the data. HY, ZYZ, and QYH wrote the manuscript. ZYZ and QYH revised the manuscript. All authors read and approved the final manuscript. Zhixing Chen, Hui Yang, and Qianlu Zhang contributed equally to this work.

Acknowledgments

References

[1] K. Honoki, "Do stem-like cells play a role in drug resistance of sarcomas?," *Expert Review of Anticancer Therapy*, vol. 10, no. 2, pp. 261–270, 2010.

[2] C. P. Gibbs, V. G. Kukekov, J. D. Reith et al., "Stem-like cells in bone sarcomas: implications for tumorigenesis," *Neoplasia*, vol. 7, no. 11, pp. 967–976, 2005.

[3] G. Gatta, R. Capocaccia, C. Stiller et al., "Childhood cancer survival trends in Europe: a EUROCARE working group study," *Journal of Clinical Oncology*, vol. 23, no. 16, pp. 3742–3751, 2005.

[4] S. Wang, H. Hu, B. Zhong et al., "Bruceine D inhibits tumor growth and stem cell-like traits of osteosarcoma through inhibition of STAT3 signaling pathway," *Cancer Medicine*, vol. 8, no. 17, pp. 7345–7358, 2019.

[5] P. Koka, R. S. Mundre, R. Rangarajan, Y. Chandramohan, R. K. Subramanian, and A. Dhanasekaran, "Uncoupling Warburg effect and stemness in CD133+ve cancer stem cells from Saos-2 (osteosarcoma) cell line under hypoxia," *Molecular Biology Reports*, vol. 45, no. 6, pp. 1653–1662, 2018.

[6] G. Mesiano, G. Grignani, E. Fiorino et al., "Cytokine induced killer cells are effective against sarcoma cancer stem cells spared by chemotherapy and target therapy," *Oncoimmunology*, vol. 7, no. 11, article e1465161, 2018.

[7] Z. Zhao, J. Zeng, Q. Guo et al., "Berberine suppresses stemness and tumorigenicity of colorectal cancer stem-like cells by inhibiting m6A methylation," *Frontiers in Oncology*, vol. 11, p. 775418, 2021.

[8] S. J. Chmura, M. E. Dolan, A. Cha, H. J. Mauceri, D. W. Kufe, and R. R. Weichselbaum, "In vitro and in vivo activity of protein kinase C inhibitor chelerythrine chloride induces tumor

cell toxicity and growth delay in vivo," *Clinical Cancer Research*, vol. 6, no. 2, pp. 737–742, 2000.

[9] X. Wang, M. Tanaka, S. Krstin, H. S. Peixoto, and M. Wink, "The interference of selected cytotoxic alkaloids with the cytoskeleton: an insight into their modes of action," *Molecules*, vol. 21, no. 7, p. 906, 2016.

[10] R. Yang, S. Piperdi, and R. Gorlick, "Activation of the RAF/mitogen-activated protein/extracellular signal-regulated kinase kinase/extracellular signal-regulated kinase pathway mediates apoptosis induced by chelerythrine in osteosarcoma," *Clinical Cancer Research*, vol. 14, no. 20, pp. 6396–6404, 2008.

[11] B. Liu, W. Ma, R. K. Jha, and K. Gurung, "Cancer Stem Cells in Osteosarcoma: Recent Progress and Perspective," *Acta Oncologica*, vol. 50, no. 8, pp. 1142–1150, 2011.

[12] V. H. Bramwell, "Osteosarcomas and other cancers of bone," *Current Opinion in Oncology*, vol. 12, no. 4, pp. 330–336, 2000.

[13] B. Bauvois, "New facets of matrix metalloproteinases MMP-2 and MMP-9 as cell surface transducers: outside-in signaling and relationship to tumor progression," *Biochimica et Biophysica Acta*, vol. 1825, no. 1, pp. 29–36, 2012.

[14] Y. Zhu, Y. Pan, G. Zhang et al., "Chelerythrine inhibits human hepatocellular carcinoma metastasis in vitro," *Biological & Pharmaceutical Bulletin*, vol. 41, no. 1, pp. 36–46, 2018.

[15] T. Tian, K. J. Nan, H. Guo et al., "PTEN inhibits the migration and invasion of HepG2 cells by coordinately decreasing MMP expression via the PI3K/Akt pathway," *Oncology Reports*, vol. 23, no. 6, pp. 1593–1600, 2010.

[16] U. Platzbecker, J. L. Ward, and H. J. Deeg, "Chelerythrin activates caspase-8, downregulates FLIP long and short, and overcomes resistance to tumour necrosis factor-related apoptosis-inducing ligand in KG1a cells," *British Journal of Haematology*, vol. 122, no. 3, pp. 489–497, 2003.

[17] G. Simonis, S. Wiedemann, K. Schwarz et al., "Chelerythrine treatment influences the balance of pro- and anti-apoptotic signaling pathways in the remote myocardium after infarction," *Molecular and Cellular Biochemistry*, vol. 310, no. 1-2, pp. 119–128, 2008.

[18] R. Yu, S. Mandlekar, T. H. Tan, and A. N. Kong, "Activation of p38 and c-Jun N-terminal kinase pathways and induction of apoptosis by chelerythrine do not require inhibition of protein kinase C," *The Journal of Biological Chemistry*, vol. 275, no. 13, pp. 9612–9619, 2000.

[19] J. Vrba, P. Dolezel, J. Vicar, M. Modrianský, and J. Ulrichová, "Chelerythrine and dihydrochelerythrine induce G1 phase arrest and bimodal cell death in human leukemia HL-60 cells," *Toxicology In Vitro*, vol. 22, no. 4, pp. 1008–1017, 2008.

[20] M. Serra, K. Scotlandi, M. C. Manara et al., "Establishment and characterization of multidrug-resistant human osteosarcoma cell lines," *Anticancer Research*, vol. 13, no. 2, pp. 323–329, 1993.

[21] K. Scotlandi, M. Serra, M. C. Manara et al., "Pre-treatment of human osteosarcoma cells with N-methylformamide enhances P-glycoprotein expression and resistance to doxorubicin," *International Journal of Cancer*, vol. 58, no. 1, pp. 95–101, 1994.

[22] C. W. Taylor, W. S. Dalton, P. R. Parrish et al., "Different mechanisms of decreased drug accumulation in doxorubicin and mitoxantrone resistant variants of the MCF7 human breast cancer cell line," *British Journal of Cancer*, vol. 63, no. 6, pp. 923–929, 1991.

[23] T. Rajkumar and M. Yamuna, "Multiple pathways are involved in drug resistance to doxorubicin in an osteosarcoma cell line," *Anti-Cancer Drugs*, vol. 19, no. 3, pp. 257–265, 2008.

[24] C. M. Hattinger, G. Reverter-Branchat, D. Remondini et al., "Genomic imbalances associated with methotrexate resistance in human osteosarcoma cell lines detected by comparative genomic hybridization-based techniques," *European Journal of Cell Biology*, vol. 82, no. 9, pp. 483–493, 2003.

[25] M. Serra, G. Reverter-Branchat, D. Maurici et al., "Analysis of dihydrofolate reductase and reduced folate carrier gene status in relation to methotrexate resistance in osteosarcoma cells," *Annals of Oncology*, vol. 15, no. 1, pp. 151–160, 2004.

Research Article

Synergistic Lethality Effects of Apatinib and Homoharringtonine in Acute Myeloid Leukemia

Yuanfei Shi [iD],[1] **Dandan Xu,**[2] **Yi Xu,**[1] **Huafei Shen,**[1] **Yan Zhang,**[1] **Xiujin Ye,**[1] **Jie Jin,**[1] **Dawei Cui** [iD],[2] **and Wanzhuo Xie** [iD][1]

[1]*Department of Hematology, The First Affiliated Hospital, College of Medicine, Zhejiang University, Hangzhou, Zhejiang, China*
[2]*Department of Blood Transfusion, The First Affiliated Hospital, College of Medicine, Zhejiang University, Hangzhou, Zhejiang, China*

Correspondence should be addressed to Dawei Cui; daweicui@zju.edu.cn and Wanzhuo Xie; xiewanzhuo@zju.edu.cn

Purpose. The significance of vascular endothelial growth factor receptor (VEGFR)-2 in numerous solid tumors and acute myeloid leukemia (AML) has been demonstrated, but Apatinib remains largely unexplored. In this study, whether Apatinib combined with homoharringtonine (HHT) kills AML cell lines and its possible mechanisms have been explored. *Methods*. AML cell lines were treated with Apatinib and HHT in different concentrations with control, Apatinib alone, HHT alone, and Apatinib combined with HHT. The changes of IC_{50} were measured by CCK8 assay, and apoptosis rate, cell cycle, and the mitochondrial membrane potential in each group were measured by flow cytometry. Finally, the possible cytotoxicity mechanism was analyzed by Western blotting. *Results*. Our results noted that Apatinib combined with HHT remarkably inhibited cell proliferation, reduced the capacity of colony-forming, and induced apoptosis and cell cycle arrest in AML cells. Mechanistically, Apatinib and HHT play a role as a suppressor in the expression of VEGFR-2 and the downstream signaling cascades, such as the PI3K, MAPK, and STAT3 pathways. *Conclusion*. Our preclinical data demonstrate that Apatinib combined with HHT exerts a better antileukemia effect than Apatinib alone by inhibiting the VEGFR-2 signaling pathway, suggesting the potential role of Apatinib and HHT in the treatment of AML. This study provides clinicians with innovative combination therapies and new therapeutic targets for the treatment of AML.

1. Introduction

Acute myeloid leukemia (AML) is derived from leukemia stem cells or progenitor cells. The American Cancer Society found that there are about 19, 940 new cases of AML per annum with 11,180 deaths [1]. Although it has significantly improved the molecular biology of this disease and over the last forty years treatment has changed, the outcome remains poor for most patients [2]. Cytogenetic abnormalities are closely associated with clinical features and therapeutic responses in AML [3]. Therefore, there is a crying need for novel AML therapies, ranging from drugs targeting specific vascular endothelial growth factors (VEGF), and oncogenic proteins to immunotherapies. In the last few years, a large number of studies have shown that angiogenesis is involved

not only in leukemogenesis but also in leukemia progression [4]. An increased angiogenesis in the bone marrow niche relates to acute myeloid leukemia progression and resistance to treatment [5–9]. In consideration of the important role of angiogenic activity in different kinds of tumor-like hematological malignancies, targeting vasculogenesis signaling has gained more and more attention as a new therapy to avoid cancer metastasis and resistance. Therefore, antiangiogenic drugs or VEGFR inhibitors may provide a novel innovative approach for AML treatments [10–12].

Apatinib (also known as YN968D1), a small-molecule receptor tyrosine kinase inhibitor, can target VEGFR-2 selectively [13], which has been approved in China as a subsequent treatment for advanced gastric cancer [14]. Moreover, it has also been tested in phase II/III clinical trials

of other cancers, including non-small-cell lung cancer and breast cancer [15]. In this case, we are intrigued to explore whether Apatinib can be used for AML treatment and its relevant mechanisms. Homoharringtonine (HHT) (also known as omacetaxine mepesuccinate), a classical antileukemia drug, has been applied for about forty years in China. HHT has a variety of antitumor effects, including AML [16] and CML [17]. The researchers found that HHT is a protein synthesis inhibitor affecting leukemic cells, which potentiates the therapeutic efficacy of anthracycline and cytarabine [18]. In China, HHT has been widely used in the treatment of AML for more than 30 years because of its good curative effect and low treatment cost [19]. Although HHT has been used for the treatment of a variety of tumors, the specific targets are still unknown [18, 20]. In this paper, we studied whether HHT would strengthen the antileukemic effect when combined with Apatinib. Besides, we also studied the underlying mechanisms of the cooperative effect of both two drugs.

2. Materials and Methods of Drugs

Apatinib (Houston, TX, USA). HHT (Zhejiang Minsheng Pharmaceutical, Zhejiang, China) was dissolved in dimethyl sulfoxide (DMSO) at 1 mg/mL and stored at $-20°$C. HHT was diluted with a culture medium in subsequent experiments.

2.1. Cell Culture.
MV4-11, MOLM-13, OCI-AML2, and OCI-AML3 were purchased from the American Type Culture Collection (ATCC, Manassas, VA, USA). MV4-11 and MOLM-13 expressed MLL fusion oncoprotein with FLT3-ITD. OCI-AML2 and OCI-AML3 expressed mutant NPM1c+ THP1 without FLT3-ITD or NPM1c + mutant, all cells were cultured in RPMI 1640 with 20% fetal bovine serum (Gibco).

2.2. Cell Viability Assay.
AML cell lines (2×10^4 cells/well) were plated in 96-well plates and then treated with different concentrations of Apatinib and HHT for 24 h and 48 h. The cytotoxic effect was determined by cell counting kit-8 (CCK8; Dojindo, Japan) assay. IC_{50} (half-maximal inhibitory concentration) values were determined using a microplate reader (BIO-TEK EPOCH, USA).

2.3. Apoptosis Assay.
To assess apoptosis, MV4-11, MOLM-13, OCI-AML2, and OCI-AML3 cells were cultured and presented with different doses of Apatinib or HHT alone or in combination for 24 h or 48 h then double-labeled with Annexin V/DAPI (eBioscience). However, the same concentration did not work in non-FLT3-ITD mutations in AML cell lines, for example, THP1. The stained cells were analyzed with a NovoCyte flow cytometer (ACEA Biosciences, Inc.) with NovoExpress software. Annexin V-positive cells were defined as apoptotic cells.

2.4. In Vitro Clonogenicity Assay.
MV4-11, MOLM-13, OCI-AML2, and OCI-AML3 cells (2×10^5/well) were used to test colony-forming abilities. AML cells were seeded in 24-well plates and then, treated with 20 μM Apatinib or 16 nM HHT alone or both molecules. After 24 h, cells were washed and then cultured in a complete methylcellulose medium at a cell density of 500 cells/well in 3.5 cm dishes for 10–14 days. The percentage of CFU was determined by counting colonies ($\geq$50 cells). Data were presented as the mean ± SD of three independent experiments.

2.5. Cell Cycle Analysis.
AML cells were treated for 24 h, then cells were fixed overnight with 75% ethanol, washed with PBS three times, and then incubated in buffer containing 50 μg/mL PI and 100 μg/mL RNase A for 30 min at room temperature. Cells were resuspended with DAPI saline solution and subjected to flow cytometry (NovoCyte™).

2.6. Analysis of the Mitochondrial Membrane Potential.
AML cells (2×10^5/ml) were plated in 24-well plates treated with various concentrations of Apatinib and HHT. After 24 h, cells were stained with 2 μM Rhodamine 123 (Beyotime) for 30 min. Then, after washing, mitochondrial membrane potential (MMP) was presented by flow cytometry (FACS Fortessa).

2.7. Western Blot Analysis.
Cell protein was extracted with RIPA protein lysis buffer (Beyotime). MOLM-13 cells (2×10^5/mL) were cultured with 20 μM Apatinib or 16 nM HHT alone or combined for 24 h and 48 h. Related antibodies included $β$-actin, VEGFR-2, p-VEGFR-2, PI3K, Akt, CyclinA2, CyclinD1, P21, and BCL-2 (rabbit, 1 : 1000, Cell Signaling Technology). Blots were tested by the addition of a horseradish peroxidase (HRP)-conjugated secondary antibody. Signals were visualized using the ECL Western blotting detection kit (Gene-Flow, Staffordshire, UK).

2.8. Statistical Analysis.
We used GraphPad Prism software v7.0 to analyze the data. All experiments performed at least three independent experiments. Multigroup comparisons were using a one-way test of variance (ANOVA). Statistical analyses were presented using SPSS 20.0 software (La Jolla, CA).

3. Results

3.1. The Cytotoxic Effect of Apatinib and HHT on FLT3-ITD Mutations AML Cell Lines.
We used the CCK8 assay to test the activity of Apatinib and HHT alone and in combination to verify the synergistic effect in inhibition of FLT3-ITD mutations AML cell viability. The concentrations of Apatinib and HHT are shown in Figures 1(a)–1(d). We found that AML cell lines treated with both Apatinib and HHT showed a much better inhibitory effect, especially in the FLT3-ITD group than those treated with each reagent alone in a time-dependent manner. However, Apatinib and HHT displayed no effect on the THP1 cell line without FLT3-ITD mutations in cell proliferation (Supplemental Figure 1). The IC_{50} values for Apatinib and HHT were calculated using

(a)

(b)
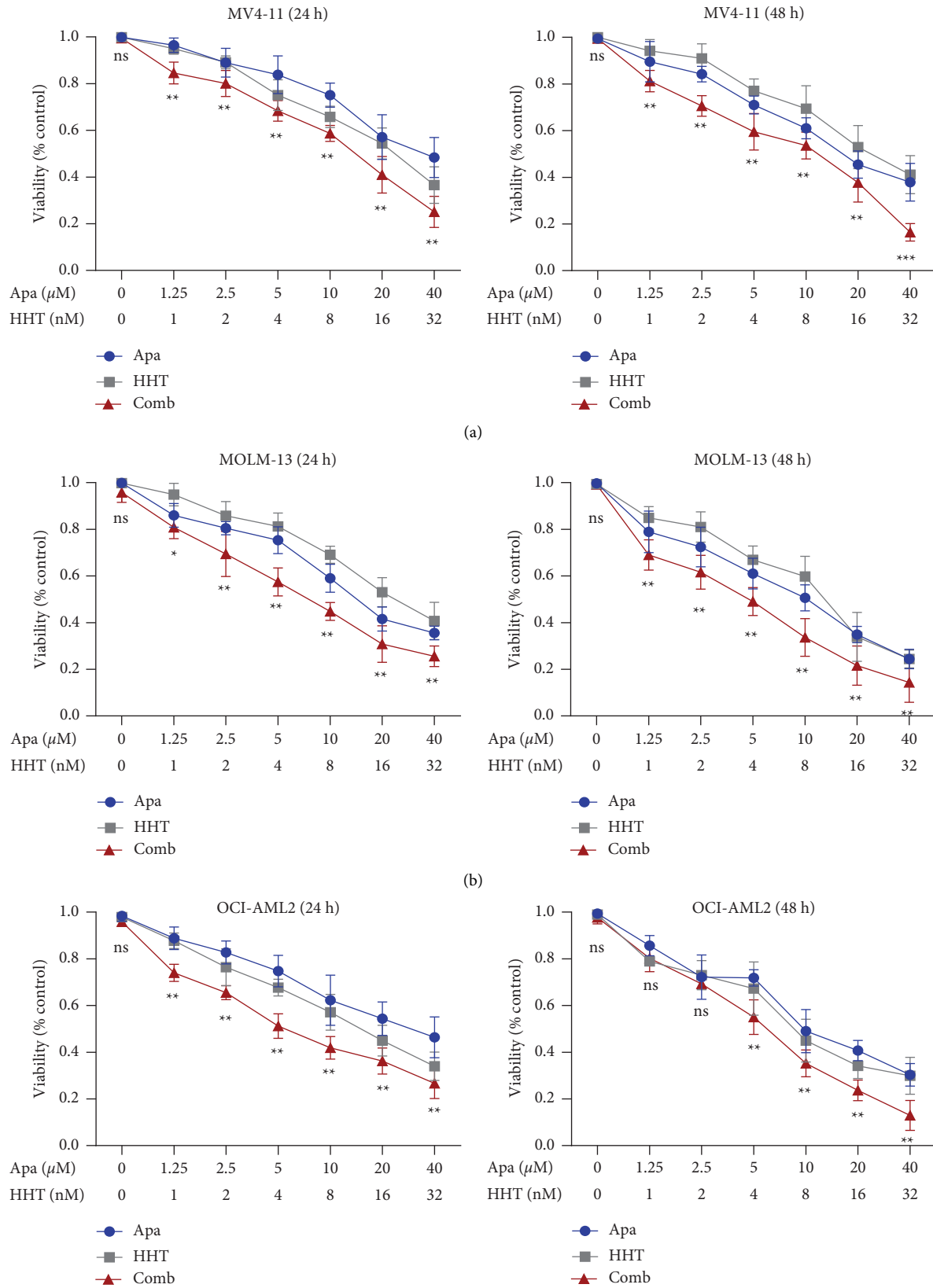
(c)

Figure 1: Continued.
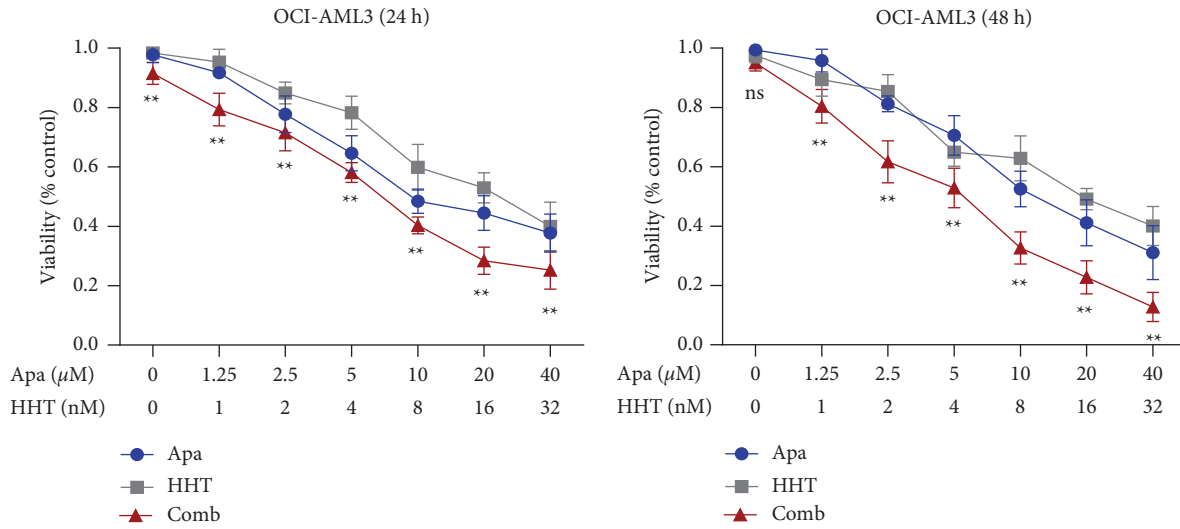
(d)

FIGURE 1: Cell viability after treatment with various doses of Apatinib or HHT alone or in combination for 24 h or 48 h. (a–d) The percent viability is normalized to the percent viability of the DMSO-treated control. Values are expressed as the mean ± SD of three independent experiments. The half-maximal inhibitory concentration (IC_{50}) values of Apatinib and HHT in a time-dependent manner on FLT3-ITD mutations AML cells. $^*p < 0.05$; $^{**}p < 0.01$; $^{***}p < 0.001$.

TABLE 1: IC_{50} values of Apatinib and HHT as single agent in AML cells.

AML cell lines	IC_{50} at 24 h		IC_{50} at 48 h	
	Apa (μM)	HHT (nM)	Apa (μM)	HHT (nM)
MV4-11	6.76 ± 1.14	15.2 ± 1.80	4.67 ± 0.81	6.05 ± 1.31
MOLM-13	4.11 ± 0.81	12.2 ± 2.83	2.25 ± 1.22	5.30 ± 1.04
OCI-AML2	101.1 ± 11	16.2 ± 0.89	31.2 ± 15.8	7.69 ± 1.28
OCI-AML3	4.97 ± 1.30	15.93 ± 1.17	3.23 ± 0.56	5.51 ± 0.91
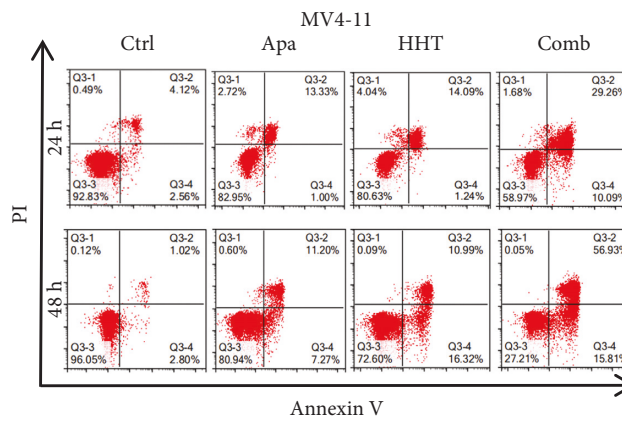
(a)

FIGURE 2: Continued.
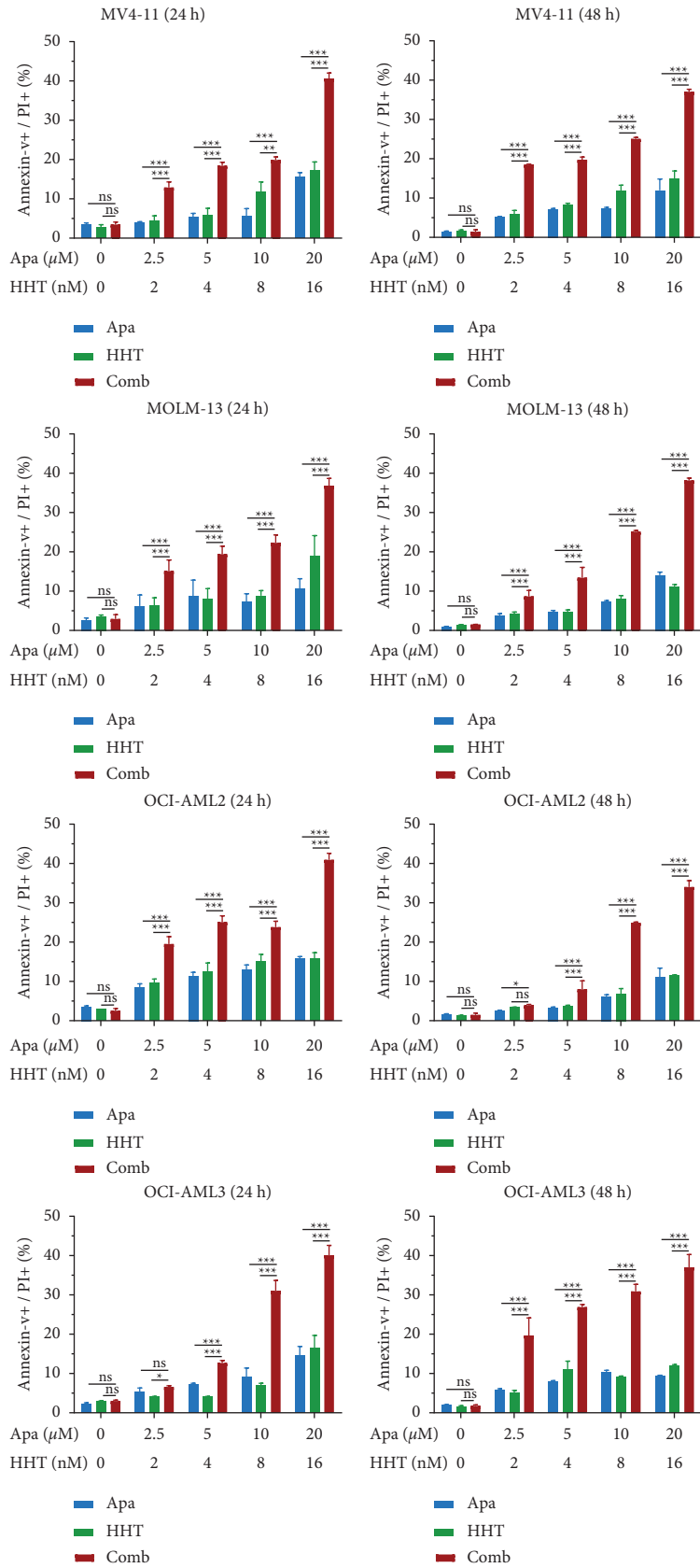
(b)

FIGURE 2: Continued.

(c)

(d)
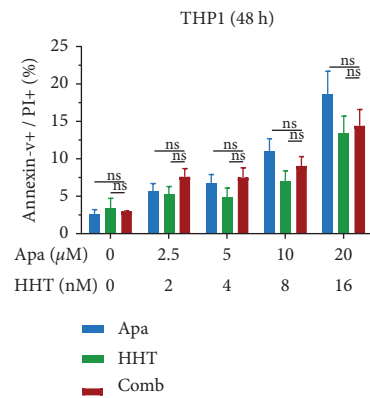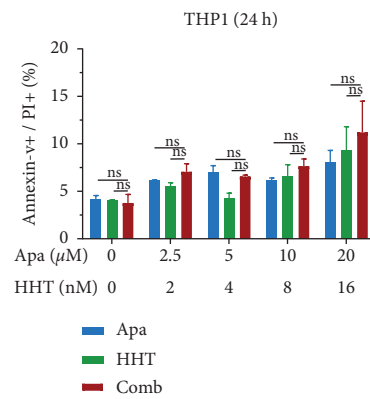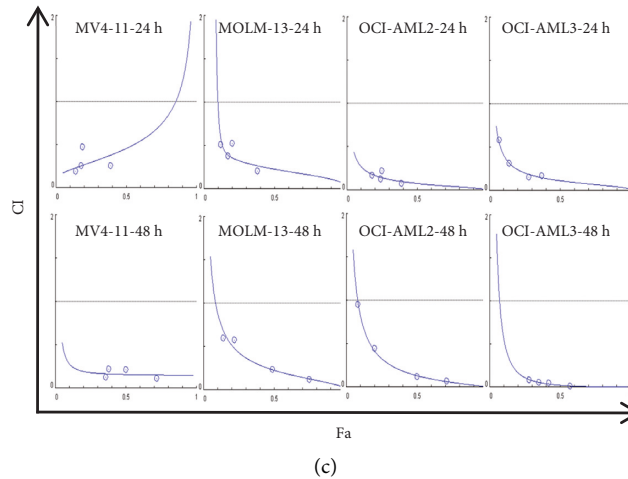
Figure 2: Coexposure to Apatinib and HHT induces apoptosis of AML cells. (a) The percentage of apoptotic cells was examined with a NovoCyte flow cytometer. (b) Cells were treated with the indicated concentrations of Apatinib ± HHT for 24 and 48 h after which the percentage of Annexin-V + apoptotic cells was determined by flow cytometry after annexin V and DAPI double staining. (c) Combination index (CI) values were calculated according to the median effect method of Chou and Talala. (d) The combination of Apatinib and HHT displayed no effect on the THP1 cell line without FLT3-ITD mutations. $^{*}p < 0.05$; $^{**}p < 0.01$; $^{***}p < 0.001$.

GraphPad Prism software v7.0 in AML cells, respectively (Table 1). Together, these results indicate that Apatinib synergistically interacts with HHT to reduce the viability of AML cells.

3.2. Combination Treatment with Apatinib and HHT Plays a Synergistic and Lethal Role in AML Cell Lines Especially in FLT3-ITD Mutations in AML Cells. To explore the synergistic effect of Apatinib and HHT on FLT3-ITD AML cells. Annexin V/DAPI staining was then performed to examine whether Apatinib would enhance HHT to induce apoptosis in FLT3-ITD AML cells. MV4-11, MOLM-13, OCI-AML2, and OCI-AML3 cells were exposed to the defined concentrations of Apatinib and HHT for 24 h or 48 h. As shown in Figures 2(a) and 2(b), Apatinib or HHT alone was unable to induce apoptosis, while the combination could significantly increase apoptosis in all FLT3-ITD AML cell lines. Combination index (CI) values were calculated using the Chou and Talala software (Figure 2(c)) and (Table 2). A CI value of less than 1.0 means a synergistic effect. In contrast, the combination of Apatinib and HHT displayed no effect on the THP1 cell line without FLT3-ITD mutations (Figure 2(d)). These findings suggested that the combination of Apatinib and HHT might be a hopeful therapy for AML with FLT3-ITD mutation cells.

3.3. The Synergistic Effects of Apatinib Combined with HHT on the Formation of Colonies. Next, we studied the effects of Apatinib, HHT, or the combination of these two drugs on the cell colony formation of FLT3-ITD mutation cells. MV4-11, MOLM-13, OCI-AML2, and OCI-AML3 cells were treated with different concentrations of Apatinib or HHT alone or in combination for 48 h. Neither Apatinib ($20 \mu M$) nor HHT (16 nM) alone diminished the colony formation abilities of FLT3-ITD mutations in AML cells. However, when Apatinib was combined with HHT, the colony-forming units significantly decreased ($p < 0.001$ vs. control, Apatinib alone, or HHT alone) (Figures 3(a)–3(d)).

3.4. Apatinib and HHT Induce Cell Cycle Arrest in FLT3-ITD Mutations AML Cells. Cell cycle assays were carried out to investigate whether Apatinib combined with HHT affects the cell cycle capacity in FLT3-ITD mutation cells. MV4-11 and MOLM-13 cells were treated with different concentrations of Apatinib alone or combined with HHT for 24 hours. As shown in Figures 4(a) and 4(b), cells treated with Apatinib at $20 \mu M$ or HHT at 16 nM, these concentrations did not affect G0/G1 or S phase cells notably. However, Apatinib and HHT exerted a prominent G0/G1 phase arrest and the S phase decreased. Then, we used Western blots to explore the cycle-relevant proteins, such as cyclin A2, cyclin D1, and P21, and the results were consistent with the former (Figure 4(c)). Consistent with the cell cycle assays, cell cycle-relevant proteins of Apatinib plus HHT induced a reduction of cyclin D1 and a rising of P21. Also, we found cyclin A2 was increased, which was a relation to the fewer cycling cells in the S phase.

3.5. Apatinib Combined with HHT Dose-Dependent Manner Reduces the Mitochondrial Membrane Potential. We used the JC-1 probe to test the mitochondrial membrane potential (MMP, $\Delta\Psi m$) to validate the joint effects of Apatinib and HHT. As we expected, compared with each reagent alone, co-treatment with Apatinib and HHT remarkably reduced the MMP in MV4-11 and MOLM-13 cells after 24 h treatment (Figures 5(a) and 5(b)). Apatinib combined with HHT downregulates the VEGFR-2 and its downstream signaling pathways in AML cells. As we mentioned above, Apatinib was a selective target to the VEGFR-2 pathway. What surprises us was that when Apatinib was combined with HHT the VEGFR-2 expression was affected. Apatinib and HHT treatment markedly inhibited the downstream signals, PI3K and p-Akt, as well as antiapoptotic proteins like BCL-2 and MCL-1 (Figure 5(c)). We can summarize the mechanism through a brief schematic mechanism as follows: on FLT3-ITD mutations AML cells Apatinib combined with HHT induced cell apoptosis by decreasing the mitochondrial membrane potential, inhibiting cell cycle, and regulating vascular endothelial growth factor as well as its downstream signaling pathways (Figure 5(d)).

4. Discussion

The evidence is overwhelming that the poor prognosis and higher disease relapse rate of AML accompanied by FLT3-ITD mutations make FLT3-ITD a perfect therapeutic target in individualized treatment [21–23]. Through our experimental results, we found that on FLT3-ITD (+) AML cell lines, compared to the monotherapy group, Apatinib and HHT could significantly inhibit cell proliferation, promote cell apoptosis, and regulate Apatinib-relevant protein VEGFR-2. However, these results were not found on the FLT3-ITD (-) THP1 cell line. Hence, we proposed and proved for the first that the combination of Apatinib and HHT exerted a significant antileukemic action. Mechanistically, the combination of Apatinib and HHT synergistically decreases phosphorylated forms of VEGFR-2 protein and its downstream PI3K, BCL-2, Akt, and MCL-1, resulting in cell arresting at G1 and apoptosis. As we know, approximately 30% of AML with normal karyotype will have FLT3 (FMS-like tyrosine kinase 3) gene with mutations of internal tandem duplications (ITD) in the juxtamembrane domain [24]. Meanwhile, AML with FLT3-ITD mutations is concerned with poor overall survival (OS) and decreased disease-free survival (DFS) [25]. Although FLT3-mutant AML patients can be treated with FLT3 tyrosine kinase inhibitors (TKI), the relapse and rapid drug resistance limit its use [26]. Lately, several studies have found that HHT exerted a sensitive cytotoxic function on FLT3-ITD (+) AML cells [27].

The key role of angiogenesis is the process of forming blood vessels in the growth and maintenance of solid tumors. In the last few decades, a large number of studies show the involvement of angiogenesis in leukemogenesis as well as leukemia progression [28]. An increase in angiogenesis in the bone marrow niche is related to both acute lymphoblastic leukemia and acute myeloid leukemia [5–9]. Therefore, targeting angiogenesis with antiangiogenic agents

Table 2: The effect of synergistic inhibition in AML cell lines.

	MV4-11				
Concentration		24 h		48 h	
Apa	HHT	Fa	CI	Fa	CI
2.5	2	0.14	0.1927	0.36	0.1244
5	4	0.18	0.2579	0.38	0.2191
10	8	0.19	0.4723	0.50	0.2153
20	16	0.39	0.2584	0.72	0.1136
	MOLM-13				
Concentration		24 h		48 h	
Apa	HHT	Fa	CI	Fa	CI
2.5	2	0.12	0.5103	0.14	0.5988
5	4	0.17	0.3835	0.22	0.5731
10	8	0.20	0.5256	0.49	0.2373
20	16	0.38	0.2088	0.75	0.1181
	OCI-AML2				
Concentration		24 h		48 h	
Apa	HHT	Fa	CI	Fa	CI
2.5	2	0.18	0.1715	0.08	0.9547
5	4	0.24	0.128	0.20	0.4447
10	8	0.25	0.2212	0.50	0.1198
20	16	0.39	0.0764	0.71	0.0660
	OCI-AML3				
Concentration		24 h		48 h	
Apa	HHT	Fa	CI	Fa	CI
2.5	2	0.07	0.5814	0.28	0.080
5	4	0.14	0.3159	0.35	0.0563
10	8	0.28	0.1578	0.42	0.0435
20	16	0.37	0.1682	0.57	0.0126

Fa: fraction affected.

or VEGFR inhibitors is likely to be a new method for AML treatment. Apatinib is a novel small-molecule tyrosine kinase inhibitor, which inhibits the phosphorylation of vascular endothelial growth factor receptors selectively, with a binding affinity ten times that of sorafenib. Besides, compared with Apatinib sorafenib with only one-tenth of the anti-VEGFR-2 efficacy, it is insufficient for antitumor angiogenesis [10, 14, 29]. Its antitumor activity in all kinds of tumors has been proved in many studies [20, 30, 31]. Results of those clinical trials indicated the antitumor role of Apatinib across a large scale of advanced cancers, but the specific function of tumor angiogenesis in AML pathogenesis remains unknown. Furthermore, our research has found that Apatinib combined with a variety of antitumor drugs can improve the curative effect [32, 33]. It was interesting to note that accompanied FLT3-ITD mutant AML cells presented a significant synergistic effect after being treated with Apatinib and HHT. Nevertheless, it makes no difference to the AML cell line, which was without FLT3-ITD mutant (Figure 2(d)). It has been well reported that the important role of PI3K signaling in the progression of all kinds of tumors, including leukemia [34, 35]. The evasion of apoptosis was an important characteristic of cancer, which was caused by the activation of antiapoptotic molecules of the BCL-2 protein family [36–38]. Aberrant activation of BCL-2 members such as BCL-2 and MCL-1 were related to antiapoptosis and drug resistance in FLT3-ITD mutant AML [39–41].

VEGF is considered a target in leukemia treatment and a variety of strategies have been applied to downregulate or inhibit the VEGF signaling pathway. The new strategy which inhibits the VEGF signaling pathway could be able to block the autocrine VEGF pathway in AML cells or the typical vessel development by the vascular endothelial cells [42]. We and other researchers found that Apatinib-induced cytotoxicity was related to inhibition of the VEGFR-2 and PI3K/Akt pathways, and induction of mitochondrial membrane protein (MMP)-mediated apoptosis. To our surprise, Apatinib and HHT could significantly enhance this phenomenon. As everyone knows that FLT3-ITD mutations result in missing the auto-inhibitory function for FLT3 kinase, which next leads to activation of its downstream signaling pathways, such as PI3K/Akt and JAK/STAT5 [43, 44], our results indicated that Apatinib combined with HHT synergistically suppressed the growth and induced apoptosis of FLT3-ITD mutations AML cells by synergistically downregulating the expression of phosphorylated forms of VEGFR-2 and PI3K/Akt signaling pathways as well as affecting the expression level of cell cycle regulatory protein, upregulating the expressions of cyclin A2 and P21 and downregulating the expression of cyclin D1 in FLT3- ITD (+) AML cell lines. Nevertheless, mechanisms of combined application of Apatinib and HHT in regulating P21, cyclin A2, and cyclin D1 proteins remain unclear and need further study.

(a)

(b)

(c)

(d)
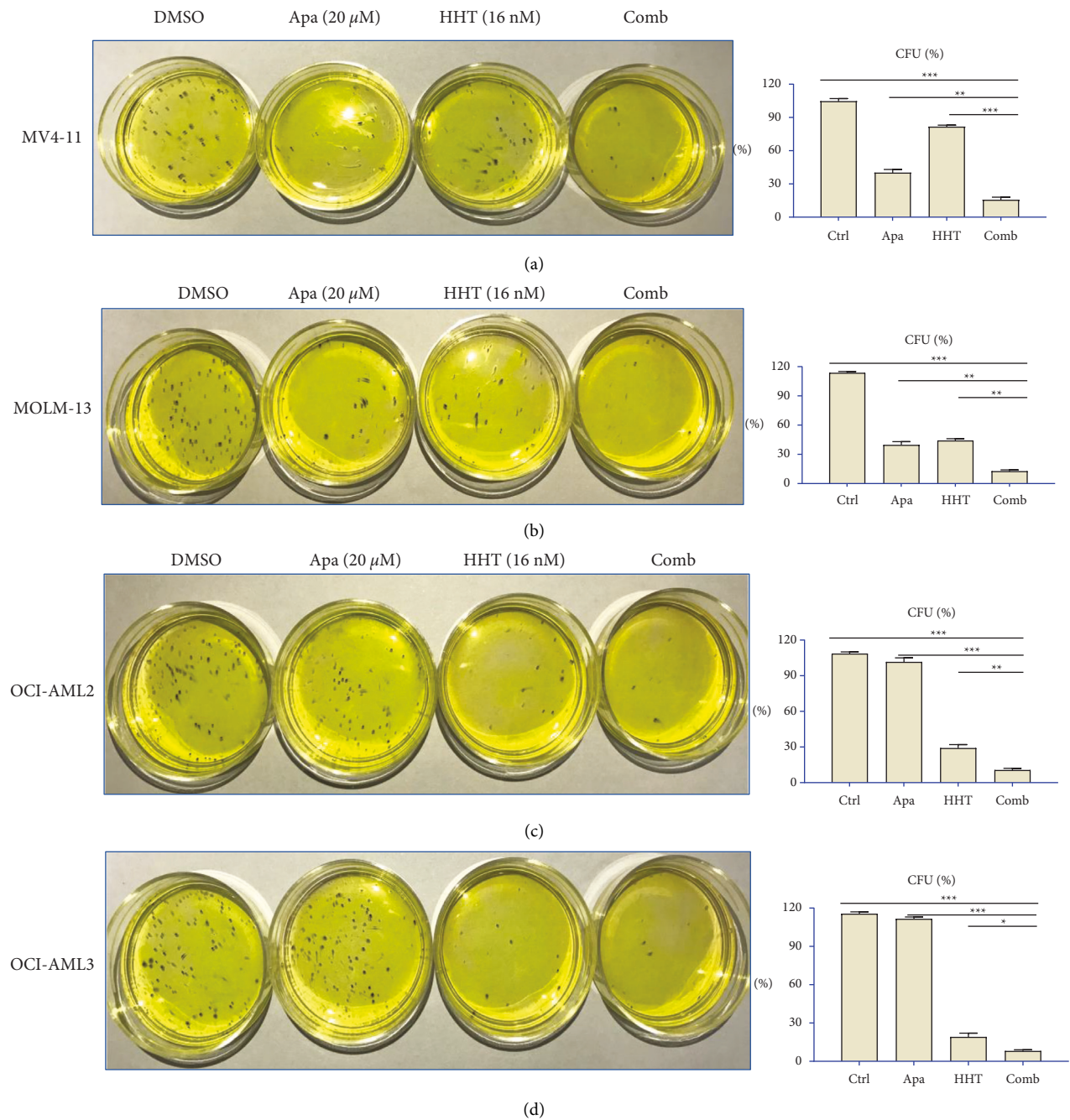
FIGURE 3: Orming abilities. (a–d) AML cells were seeded in 24-well plates and then treated with 20 μM Apatinib or 16 nM HHT alone or both molecules. After 24 h, cells were washed and then cultured in a complete methylcellulose medium at a cell density of 500 cells/well in 3.5 cm dishes for 10–14 days. The percentage of CFU was determined by counting colonies ($\geq$50 cells). Data are presented as the mean $\pm$ SD of three independent experiments. $^{*}p < 0.05$; $^{**}p < 0.01$; $^{***}p < 0.001$.
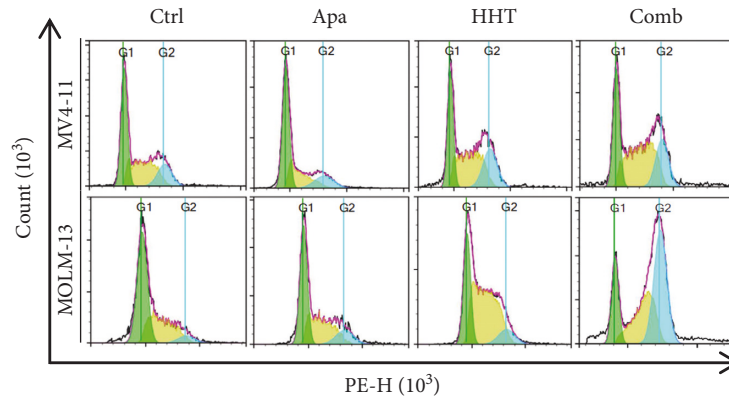
(a)
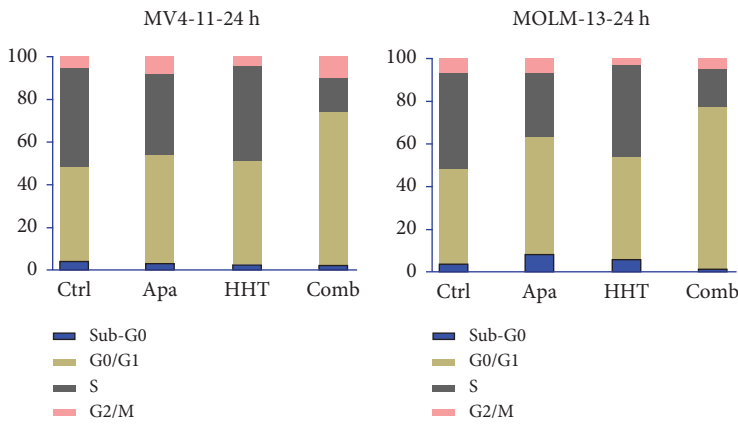
(b)
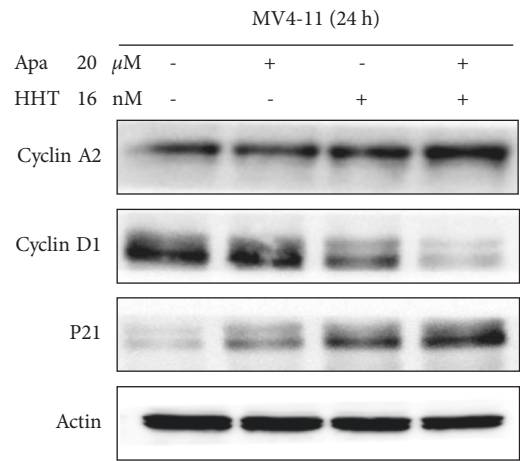
(c)

Figure 4: In MV4-11 and MOLM-13 cells, G0/G1 phase arrest and S phase decrease were observed after treatment with Apatinib and HHT. (a, b) After drug treatment for 24 h, cell cycle distribution was analyzed using flow cytometry ($*p < 0.05$, one-way ANOVA, combination treatments versus control, and single treatments). (c) Western blot analysis showed an increase in cell cycle regulator CyclinA2, CyclinD1, and P21 in cells treated with Apatinib and HHT compared to a single agent. actin served as a loading control.
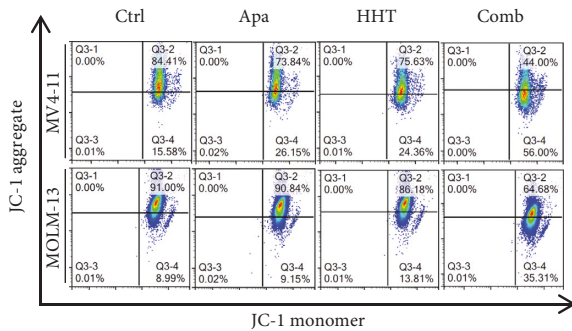
(a)
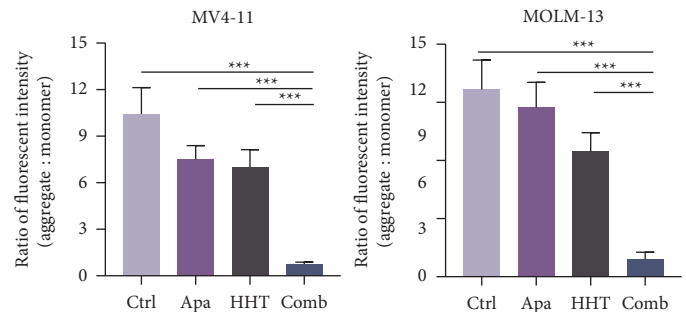
(b)

Figure 5: Continued.

(c)

(d)
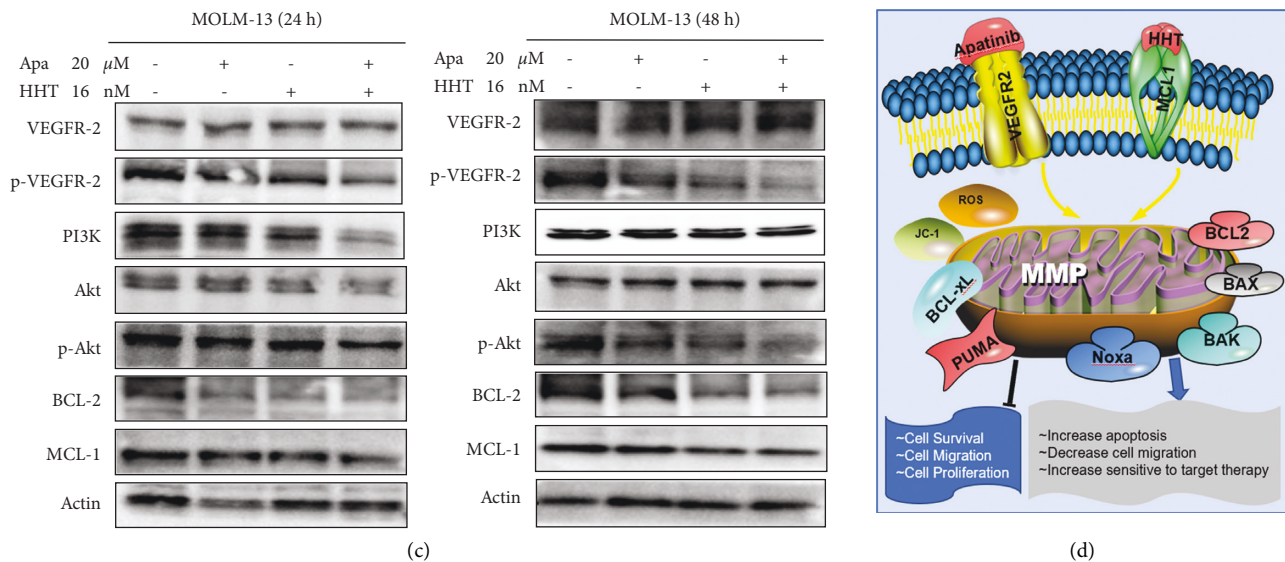
FIGURE 5: In AML cell lines, Apatinib and HHT decreased mitochondrial membrane potential and altered p-VEGFR-2, PI3K/Akt pathway associated proteins. (a, b) MV4-11 and MOLM-13 cells with loss of mitochondrial membrane potential. (c) MOLM-13 cells were exposed to the indicated concentrations of Apatinib ± HHT for 24 h and 48 h after which western blot analysis was shown to monitor the expression of p-VEGFR-2, PI3K/Akt pathway associated proteins, anti-apoptotic proteins BCL-2 and MCL-1. (d) pharmacologic targeting VEGFR-2 and MCL-1 induces mitochondrial dysfunction, decreased intracellular MMP levels, and apoptosis in AML.

5. Conclusions

All in all, our research first reveals the synergistic antileukemic effect between Apatinib and HHT on FLT3-ITD mutant AML cells, likely through inhibiting VEGFR-2-mediated signaling pathways, and suggests potential benefits and clinical application of Apatinib combined with HHT in the treatment of AML patients.

Abbreviations

AML: Acute myeloid leukemia
HHT: Homoharringtonine
VEGFR-2: Vascular endothelial growth factor receptor-2 (VEGFR-2)
CI: Combination index.

Data Availability

The datasets used and/or analyzed during the current study are available from the corresponding author on reasonable request.

Ethical Approval

This article does not contain any studies with human participants or animals performed by any of the authors.

Disclosure

A preprint has previously been published [45].

Conflicts of Interest

The authors declare that they have no potential conflicts of interest.

Authors' Contributions

YFS and YX performed in vitro experiments and animal studies. DDX, HFS, and YZ carried out the statistical analysis. XJY, JJ, and DWC designed the study. WZX wrote the manuscript. All authors read and approved the final manuscript. YFS, DDX, and YX contributed equally to this work.

Acknowledgments

Supplementary Materials

Supplemental Figure 1: Apatinib and HHT displayed no effect on the THP1 cell line without FLT3-ITD mutations in cell proliferation. (*Supplementary Materials*)

References

[1] H. S. Chen, K. Portier, K. Ghosh et al., "Predicting US- and state-level cancer counts for the current calendar year: part I: evaluation of temporal projection methods for mortality," *Cancer*, vol. 118, no. 4, pp. 1091–1099, 2012.

[2] A. E. Perl, "The role of targeted therapy in the management of patients with AML," *Blood Advances*, vol. 1, no. 24, pp. 2281–2294, 2017.

[3] R. B. Walter and E. H. Estey, "Management of older or unfit patients with acute myeloid leukemia," *Leukemia*, vol. 29, no. 4, pp. 770–775, 2015.

[4] A. Kuykendall, N. Duployez, N. Boissel, J. E. Lancet, and J. S. Welch, "Acute myeloid leukemia: the good, the bad, and the ugly," *American Society of Clinical Oncology Educational book. American Society of Clinical Oncology. Annual Meeting*, vol. 38, pp. 555–573, 2018.

[5] R. Shirzad, S. Shahrabi, A. Ahmadzadeh, K. R. Kampen, M. Shahjahani, and N. Saki, "Signaling and molecular basis of bone marrow niche angiogenesis in leukemia," *Clinical and Translational Oncology*, vol. 18, no. 10, pp. 957–971, 2016.

[6] M. Todorovic, Z. Radisavljevic, B. Balint et al., "Increased angiogenesis-associated poor outcome in acute lymphoblastic leukemia: a single center study," *Applied Immunohistochemistry & Molecular Morphology*, vol. 20, no. 5, pp. 488–493, 2012.

[7] K. R. Kampen, A. Ter Elst, and E. S. J. M. de Bont, "Vascular endothelial growth factor signaling in acute myeloid leukemia," *Cellular and Molecular Life Sciences*, vol. 70, no. 8, pp. 1307–1317, 2013.

[8] A. A. AbdElAal, R. A. A. Afify, A. E. Zaher, M. M. ElGammal, and A. M. Atef, "Study of prognostic significance of marrow angiogenesis assessment in patients with de novo acute leukemia," *Hematology*, vol. 20, no. 9, pp. 504–510, 2015.

[9] N. Karakurt, T. Aksu, Y. Koksal et al., "Angiopoietins in the bone marrow microenvironment of acute lymphoblastic leukemia," *Hematology*, vol. 21, no. 6, pp. 325–331, 2016.

[10] D. Passaro, A. Di Tullio, A. Abarrategi et al., "Increased vascular permeability in the bone marrow microenvironment contributes to disease progression and drug response in acute myeloid leukemia," *Cancer Cell*, vol. 32, no. 3, pp. 324–341, 2017.

[11] S. Chatterjee, L. C. Heukamp, M. Siobal et al., "Tumor VEGF: VEGFR2 autocrine feed-forward loop triggers angiogenesis in lung cancer," *Journal of Clinical Investigation*, vol. 123, no. 4, pp. 1732–1740, 2013.

[12] J. Xie, J. Liu, H. Liu et al., "The antitumor effect of tanshinone IIA on anti-proliferation and decreasing VEGF/VEGFR2 expression on the human non-small cell lung cancer A549 cell line," *Acta Pharmaceutica Sinica B*, vol. 5, no. 6, pp. 554–563, 2015.

[13] A. B. C. Brito, G. J. Lourenco, G. B. Oliveira, C. A. de Souza, J. Vassallo, and C. S. P. Lima, "Associations of VEGF and VEGFR2 polymorphisms with increased risk and aggressiveness of multiple myeloma," *Annals of Hematology*, vol. 93, no. 8, pp. 1363–1369, 2014.

[14] S. Tian, H. Quan, C. Xie et al., "YN968D1 is a novel and selective inhibitor of vascular endothelial growth factor receptor-2 tyrosine kinase with potent activity in vitro and in vivo," *Cancer Science*, vol. 102, no. 7, pp. 1374–1380, 2011.

[15] J. Li, S. Qin, J. Xu et al., "Apatinib for chemotherapy-refractory advanced metastatic gastric cancer: results from a randomized, placebo-controlled, parallel-arm, phase II trial," *Journal of Clinical Oncology*, vol. 31, no. 26, pp. 3219–3225, 2013.

[16] H. Kantarjian, S. O'Brien, E. Jabbour, G. Barnes, A. Pathak, and J. Cortes, "Effectiveness of homoharringtonine (omacetaxine mepesuccinate) for treatment of acute myeloid leukemia: a meta-analysis of Chinese studies," *Clinical Lymphoma, Myeloma & Leukemia*, vol. 15, no. 1, pp. 13–21, 2015.

[17] F. E. Nicolini, H. J. Khoury, L. Akard et al., "Omacetaxine mepesuccinate for patients with accelerated phase chronic myeloid leukemia with resistance or intolerance to two or more tyrosine kinase inhibitors," *Haematologica*, vol. 98, no. 7, pp. e78–e79, 2013.

[18] S. Lu and J. Wang, "Homoharringtonine and omacetaxine for myeloid hematological malignancies," *Journal of Hematology & Oncology*, vol. 7, no. 1, 2014.

[19] H. M. Kantarjian, M. Talpaz, V. Santini, A. Murgo, B. Cheson, and S. M. O'Brien, "Homoharringtonine: history, current research, and future direction," *Cancer*, vol. 92, no. 6, pp. 1591–1605, 2001.

[20] H. Zhang, "Apatinib for molecular targeted therapy in tumor," *Drug Design, Development and Therapy*, vol. 9, pp. 6075–6081, 2015.

[21] E. Feldman, Z. Arlin, T. Ahmed et al., "Homoharringtonine is safe and effective for patients with acute myelogenous leukemia," *Leukemia*, vol. 6, no. 11, pp. 1185–1188, 1992.

[22] C. Thiede, C. Steudel, B. Mohr et al., "Analysis of FLT3-activating mutations in 979 patients with acute myelogenous leukemia: association with FAB subtypes and identification of subgroups with poor prognosis," *Blood*, vol. 99, no. 12, pp. 4326–4335, 2002.

[23] Y. Kuwatsuka, D. Tomizawa, R. Kihara et al., "Prognostic value of genetic mutations in adolescent and young adults with acute myeloid leukemia," *International Journal of Hematology*, vol. 107, no. 2, pp. 201–210, 2018.

[24] F. Ravandi, H. Kantarjian, S. Faderl et al., "Outcome of patients with FLT3-mutated acute myeloid leukemia in first relapse," *Leukemia Research*, vol. 34, no. 6, pp. 752–756, 2010.

[25] S. Meshinchi and F. R. Appelbaum, "Structural and functional alterations of FLT3 in acute myeloid leukemia," *Clinical Cancer Research*, vol. 15, no. 13, pp. 4263–4269, 2009.

[26] D. G. Gilliland and J. D. Griffin, "The roles of FLT3 in hematopoiesis and leukemia," *Blood*, vol. 100, no. 5, pp. 1532–1542, 2002.

[27] S. Kayser and M. J. Levis, "FLT3 tyrosine kinase inhibitors in acute myeloid leukemia: clinical implications and limitations," *Leukemia and Lymphoma*, vol. 55, no. 2, pp. 243–255, 2014.

[28] B. Nasilowska-Adamska, I. Solarska, M. Paluszewska, I. Malinowska, W. W. Jedrzejczak, and K. Warzocha, "FLT3-ITD and MLL-PTD influence the expression of MDR-1, MRP-1, and BCRP mRNA but not LRP mRNA assessed with RQ-PCR method in adult acute myeloid leukemia," *Annals of Hematology*, vol. 93, no. 4, pp. 577–593, 2014.

[29] C. Yang and S. Qin, "Apatinib targets both tumor and endothelial cells in hepatocellular carcinoma," *Cancer Medicine*, vol. 7, no. 9, pp. 4570–4583, 2018.

[30] Y. Zhang, W. Fan, Y. Wang, G. Huang, and J. Li, "Apatinib for patients with sorafenib-refractory advanced hepatitis B virus related hepatocellular carcinoma: results of a pilot study," *Cancer Control*, vol. 26, no. 1, Article ID 107327481987221, 2019.

[31] S. Liang, X. Z. Tong, and L. W. Fu, "Inhibitory effect of apatinib on HL-60 cell proliferation and its mechanism," *Nan Fang Yi Ke Da Xue Xue Bao*, vol. 31, no. 5, pp. 871–874, 2011.

[32] Q. Pan, J. Wang, X. Jiang, E. Yang, L. Dong, and K. Gu, "Apatinib enhances chemosensitivity of acute myeloid leukemia hl60 cells to cytarabine by inducing apoptosis," *Journal of the Balkan Union of Oncology*, vol. 24, no. 1, pp. 374–381, 2019.

[33] X. Z. Tong, F. Wang, S. Liang et al., "Apatinib (YN968D1) enhances the efficacy of conventional chemotherapeutical drugs in side population cells and ABCB1-overexpressing leukemia cells," *Biochemical Pharmacology*, vol. 83, no. 5, pp. 586–597, 2012.

[34] Y. J. Mi, Y. J. Liang, H. B. Huang et al., "Apatinib (YN968D1) reverses multidrug resistance by inhibiting the efflux function of multiple ATP-binding cassette transporters," *Cancer Research*, vol. 70, no. 20, pp. 7981–7991, 2010.

[35] R. Pei, T. Si, Y. Lu, J. X. Zhou, and L. Jiang, "Salvianolic acid A, a novel PI3K/Akt inhibitor, induces cell apoptosis and suppresses tumor growth in acute myeloid leukemia," *Leukemia and Lymphoma*, vol. 59, no. 8, pp. 1959–1967, 2018.

[36] I. Nepstad, H. Reikvam, A. K. Brenner, O. Bruserud, and K. J. Hatfield, "Resistance to the antiproliferative in vitro effect of PI3K-Akt-mTOR inhibition in primary human acute myeloid leukemia cells is associated with altered cell metabolism," *International Journal of Molecular Sciences*, vol. 19, no. 2, 2018.

[37] K. W. Yip and J. C. Reed, "Bcl-2 family proteins and cancer," *Oncogene*, vol. 27, no. 50, pp. 6398–6406, 2008.

[38] D. Hanahan and R. A. Weinberg, "The hallmarks of cancer," *Cell*, vol. 100, no. 1, pp. 57–70, 2000.

[39] D. Hanahan and R. A. Weinberg, "Hallmarks of cancer: the next generation," *Cell*, vol. 144, no. 5, pp. 646–674, 2011.

[40] Y. Minami, K. Yamamoto, H. Kiyoi, R. Ueda, H. Saito, and T. Naoe, "Different antiapoptotic pathways between wild-type and mutated FLT3: insights into therapeutic targets in leukemia," *Blood*, vol. 102, no. 8, pp. 2969–2975, 2003.

[41] M. Rahmani, M. M. Aust, E. Hawkins et al., "Co-administration of the mTORC1/TORC2 inhibitor INK128 and the Bcl-2/Bcl-xL antagonist ABT-737 kills human myeloid leukemia cells through Mcl-1 down-regulation and AKT inactivation," *Haematologica*, vol. 100, no. 12, pp. 1553–1563, 2015.

[42] A. Rapisarda and G. Melillo, "Role of the VEGF/VEGFR axis in cancer biology and therapy," *Advances in Cancer Research*, vol. 114, pp. 237–267, 2012.

[43] S. Takahashi, "Downstream molecular pathways of FLT3 in the pathogenesis of acute myeloid leukemia: biology and therapeutic implications," *Journal of Hematology & Oncology*, vol. 4, no. 1, 2011.

[44] L. S. Steelman, S. L. Abrams, J. Whelan et al., "Contributions of the Raf/MEK/ERK, PI3K/PTEN/Akt/mTOR and Jak/STAT pathways to leukemia," *Leukemia*, vol. 22, no. 4, pp. 686–707, 2008.

[45] Y. Shi, Y. Zhang, H. Shen, X. Ye, J. Jin, and W. Xie, "Apatinib enhances chemosensitivity of FLT3-ITD mutations acute myeloid leukemia cells to homoharringtonine via VEGFR2 pathway," *Journal of Oncology*, 2021.

Hindawi

Review Article

The Regulatory Role of Lipid Metabolism in Endometrial Cancer

Shuyang Zhang [ID] **and Xingyu Han**

Medical College, China Three Gorges University, Yichang 443002, China

Correspondence should be addressed to Shuyang Zhang; 2020128103@ctgu.edu.cn

Endometrial cancer is the 6th most common carcinoma as well as the 2nd most common malignancy worldwide in women. It is closely related to fat content, and dyslipidemia is among the most significant metabolic changes in this cancer. Therefore, further understanding of the regulation mechanism in lipid metabolism of endometrial cancer is conducive to the development of better therapeutic strategies and methods. Here, we systematically review the signaling pathways that regulate lipid metabolism in endometrial cancer and the research progress of drugs and targeted therapies that act on lipid metabolism by retrieving relevant articles. The underlying mechanism of occurrence and development of endometrial cancer is relatively clear and comprehensively reviewed here. But following more research studies will help to illuminate more specific regulatory roles of lipid metabolism in endometrial cancer and explore new possible mechanisms, prognostic and therapeutic targets, and subsequent drugs. Our review will provide a full view for the following investigation of lipid metabolism in endometrial cancer.

1. Introduction

Endometrial cancer (EC) ranks 2nd among gynecological malignancies worldwide. In the United States, there were approximately 66,570 new cases in 2021, with 12,940 patient deaths [1]. In recent years, the incidence of endometrial cancer in our country has increased significantly. In 2020, about 81,964 new cases of endometrial carcinoma appeared in China, with 16,607 patient deaths [2, 3]. Associated risk factors include continued estrogen exposure (ovarian anovulatory dysfunction and estrogen-secreting ovarian tumors (estrogen replacement therapy without progesterone protection and selective estrogen receptor modulator therapy, such as tamoxifen)), metabolic abnormalities (such as obesity and diabetes), early menarche, infertility, delayed menopause, carrying genetic susceptibility genes for endometrial cancer, such as Lynch syndrome, Cowden syndrome, and polymerase proofreading-associated polyposis (PPAP), and advanced age [4, 5]. More than 90% of patients are in their 50s, with a median age of 63 at diagnosis, while 4% of patients were younger than 40 years old at diagnosis, and some patients have the will to preserve fertility [4, 6]. 80% of patients with endometrial cancer can be diagnosed at an early stage, with the tumor confined to the uterus, and the 5-year survival rate is greater than 95% [4]; if there is local spread or distant metastasis, the 5-year survival rate drops to 68% or 17%, respectively [7]. Factors associated with preventing endometrial cancer include parity and the use of oral contraceptives. Parity was inversely proportional to the risk of endometrial carcinoma [8]. The use of oral contraceptives can reduce the hazard of developing cancer in the womb by 30 to 40%, and the protective effect is longer lasting over time. Protection can even last decades after it is stopped [9].

The prognosis of endometrial cancer depends on the patient's age at diagnosis, the pathological stage and type, and the degree of tumor differentiation. The prognosis of patients with advanced age, advanced stage, and poor differentiation is worse [10, 11]. Clinically, endometrial cancer can be classified into type I/II (Bokhman classification) [12], and the former is hormone-dependent with mainly endometrioid carcinoma of the pathological type, accompanied with better prognosis, while type II is non-invasive and hormone-dependent type, mainly including serous carcinoma, clear cell carcinoma, carcinosarcoma, and so on, which have a poor prognosis. Currently, endometrial cancer is mainly treated by surgery, with radiotherapy and

chemotherapy as the commonly used adjuvant therapy. The treatment plan should be made in consideration of the patient's age, pathological type and molecular type, clinical staging, and physical performance status. In recent years, with the development of clinical studies, targeted therapy and immunotherapy have also shown good curative effects on endometrial cancer. In addition, the widespread application of genetic testing not only provides a basis for the diagnosis of hereditary endometrial cancers such as Lynch syndrome but also guides molecular typing of endometrial cancer and the selection of targeted drugs.

Endometrial cancer has been on the rise in recent years, owing to the influence of a high-fat, high-calorie diet and a sedentary lifestyle. Compared with all other malignancies, the strongest association with obesity was endometrial cancer. According to the American Cancer Society's 2019 report, 57% of endometrial cancer patients are obese, and a significant correlation exists between BMI and endometage group. Obese postmenopausal women are 1.56 times more likely than non-obese women to suffer endometrial cancer. Perimenopausal obese women are twice as probably as norial cancer [13]. Women with a normal body mass index (BMI) have a 3% increased lifetime risk of endometrial cancer, and each 5-unit rise in BMI increases the risk by 50% [14, 15]. The association between obesity and the incidence of endometrial cancer varies by n-obese women to acquire endometrial cancer [16, 17]. According to research, deliberate weight loss or maintaining a healthy weight can considerably lower the incidence of endometrial cancer or improve the prognosis of endometrial cancer patients [18]. Endometrial cancer was 1.34 and 1.65 times more common in patients with raised total cholesterol and high-density lipoprotein, respectively, than in normolipidemic patients [19]. In conclusion, aberrant lipid metabolism is an important cause of endometrial cancer. Abnormal fat metabolism is one of the most significant metabolic changes in tumors. Through fat metabolism, cells obtain energy, signaling molecules and biofilm components to gain the microstructure for proliferation, survival, invasion, metastasis and influence of tumors and the treatment of cancer [20]. As one of the most common female reproductive system tumors, endometrial cancer deserves further in-depth understanding. Therefore, more in-depth and effective disease prevention measures and better therapeutic drugs need to be developed. Here, based on the new research progress on lipid metabolism-regulating endometrial cancer, we will comprehensively review the research progress on lipid metabolism and endometrial cancer signaling pathway, small molecule drugs, and targeted therapy, to provide information for subsequent research and provide a reference for clinical diagnosis and treatment.

2. Signaling Pathways in the Lipid Metabolism of Endometrial Cancer

2.1. MAPK Family Signaling Pathway. The signaling pathway of mitogen-activated protein kinase (MAPK) is diffusely expressed in many important cellular physiological and pathological processes (Figure 1). At the same time, it is one of the most frequently mutated oncogenic channels in malignant tumors. A large number of research studies have shown that the state of the MAPK pathway is frequently activated or altered in most cancers. MAPK signaling is triggered by the activation of a family consisting of small guanine triphosphatases (GTPases), which include RAS proteins (KRAS, NRAS, and HRAS) that integrate signaling from upstream to activate guanosine exchange factors (GEFs), causing downstream changes [21]. The MAPK which is mitogen-activated protein kinase pathways include MAPK, MAPK kinases (MKK and MEK) and MAPK kinase kinases (MKKK or MEKK). These three kinases can be successively activated and participate in the modulate of cell growth, differentiation, stress, inflammation and many other key physiological or pathological processes. The MAPK pathway has 4 major branching routes: ERK, JNK, p38/MAPK, and ERK5. In endometrial cancer-related studies, adiponectin treatment can downregulate ERK1/2 signaling, that is, through the ERK1/2-MAPK pathway, reducing cell viability and inhibiting cell proliferation in endometrial cancer cell lines [22]. In addition, adiponectin therapy inhibited the phosphorylation of AKT of KLE and HEC-1-A and inhibited the phosphorylation of ERK1/2 by expression and activation of PTEN gene [23]. Gal-3, Gal-3 in the galactocoagulin gene exists in a and concentration dependent form, and gal-3-induced ERK1/2 expression is also associated with calcium and protein kinase C-related activation [24, 25].

2.2. JAK-STAT Signaling Pathway. JAK kinases are a family of signaling molecules linked by intracellular structures of type I/II cytokine receptors and belong to the non-receptor class of tyrosine kinases (Figure 1). Constituents of the signal transducer and activators of transcription (STAT) protein family are pivotal proteins for cytokine signaling and interferon-related antiviral activity. These elements are able to transmit signals from the cell membrane to the nucleus, thus activating gene transcription. The JAK/STAT signaling pathway consists of ligand-receptor complexes, JAKs, and STATs. Through ligand-receptor binding, the receptor is dimerized, and the JAK coupled to the receptor is activated by autophosphorylation. The phosphorylated receptor recruits STAT, and then JAK phosphorylates STAT to form a dimer and enters the nucleus to regulate transcription and export signals. To date, we have identified four members of the JAK family: JAK1, JAK2, JAK3, and TYK2. The major STAT family members that have been discovered include STAT1, STAT2, STAT3, STAT4, STAT5a, STAT5b, and STAT6. Their signaling pathways are related to a variety of common cellular physiological processes, including proliferation, differentiation, apoptosis, angiogenesis, and immune system regulation [26].

In research studies related to lipid metabolism in endometrial cancer, omentin, an adipokine secreted from visceral fat, stimulates apoptosis by activating the JAK signaling pathway and p53 upregulation mechanism [25]. Leptin regulates PI3K/AKT3 and ERK1/2 signaling through the JAK/STAT pathway and increases the expression of anti-apoptotic proteins such as XIAAP and systemic inflammation factors (TNF-α, IL6). Meanwhile, increased expression of angiogenic factor (VEGF) and hypoxia-
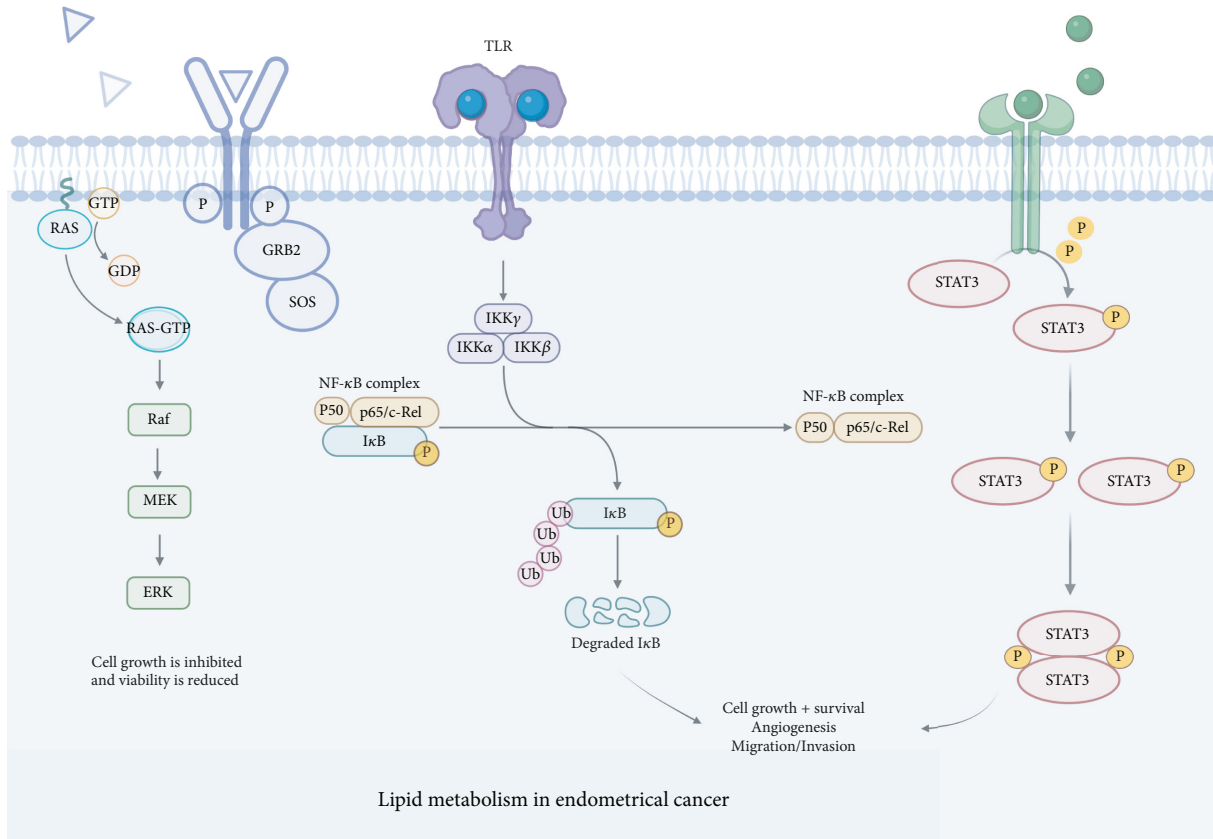
FIGURE 1: Signaling pathways and mechanisms in the lipid metabolism of endometrial cancer.

inducible factor-1a (HIF-1a) promotes endometrial cancer cell survival, proliferation, and migration [27].

2.3. NF-κB/Notch1 Signaling Pathway.

The NF-κB family consists of five members, including p65 (RelA), RelB, c-Rel, p105/p50, and p100/p52 [28]. A number of illnesses and processes, including carcinoma, inflammatory and autoimmune diseases, septic shock, viral infection, and aberrant immunological development, have been linked to NF-B dysregulation. Ingredients of the IκB kinase (IKK) complex, including the canonical heterotrimeric IKKα/IKKβ/IKKγ and the alternative IKKα/IKKα homodimer, determine the activation pathway of NF-κB (Figure 1). The Notch gene produces the Notch1 receptor, a single transmembrane protein. The Notch receptor, which controls cell differentiation, proliferation, and death, transmits signals between nearby cells. Through the NF-B/Notch1 signaling pathway, visfatin drives malignant behavior in the development of endometrial cancer and may stimulate cell proliferation, among other things. Another study found that vaspin reduced cancer cell motility and proliferation by blocking the NF-B/Notch1 signaling pathway [25, 29].

2.4. Reprogramming of Lipid Metabolism in Endometrial Cancer by ERRα.

Under the condition of hypoxia and malnutrition, reprogramming of metabolism is the key to tumor survival. The stronger the metabolic plasticity of surviving tumor cells, the more malignant their biological behavior and the stronger the chemotherapy resistance [30]. HIF-1 regulates a wide variety of genes and proteins involved in cell metabolism, pH, and EMT, increasing the aggressiveness of tumor cells. ERRα expression is linked to both EC cell growth and death. HIF-1 transcriptional activity is increased in cancer cells, which promotes glucose and lipid metabolic remodeling. ERR promotes tumor cell adaptability to hypoxia by increasing glutamine metabolism and lipid de novo synthesis. In conclusion, HIF-1/ERRα interaction can promote tumor cell adaptability to hypoxia, increase cancer cell metabolism, and promote cancer cell resistance to pyrophosphorylation [31].

TFEB promotes EC migration via EMT signaling, regulates wound healing via TFEB-ERR in EK and ECC-1 cells, increases membrane fluidity, and promotes endometrial cancer cell invasion in TFEB-ERR axis-induced lipid reprogramming. Higher TFEB/ERR patients showed deeper myometrial infiltration and lower serum HDL values [32].

3. Other Regulators in the Lipid Metabolism of Endometrial Cancer

3.1. Research Progress of Other Molecules in Lipid Metabolism in Endometrial Cancer.

Upregulation of ATP citrate lyase (ACLY), a sterol biosynthesis pathway enzyme, can encourage EC cell proliferation and colony formation while reducing apoptosis. Concurrent administration of drugs linked

to obesity (estradiol, insulin, and leptin) promotes ACLY nuclear translocation through Akt-mediated phosphorylation of ACLY at Ser455. The nucleus-located ACLY promotes histone acetylation, which activates the DHODH and other pyrimidine metabolism genes. By focusing on the ACLY axis, new EC therapeutic strategies can be created and obesity risk factors can be linked to the control of histone acetylation [33].

The greatly elevated expression of monoacylglycerol lipase is closely connected with an increased risk of EC, and targeting MAGL could be a novel and effective treatment for EC. It is unclear how MAGL promotes tumorigenesis and growth in EC, and the possible mechanism and subsequent drug development need to be confirmed by further experiments in EC [34].

Altered choline phospholipid metabolism in endometrial cancer results from overexpression of choline kinase alpha and an overactivated deacylation pathway. Endometrial cancer has significantly dysregulated lipid metabolism, with increased phosphocholine levels being the most significant lipid-related change. A deacylation pathway that has been triggered, increased expression of the catabolic enzymes LYPLA1, LYPLA2, and GPCPD1, and increased expression of choline kinase alpha (CHKA) are thought to be the causes of the changes. After malignant transformation, CHKA is connected to endometrial hyperplasia, atypical hyperplasia, and adenocarcinoma tissue [35].

Cyclin-dependent kinase 8 (CDK8) is a member of the transcriptionally regulated CDK family, and in an *in vivo* mouse model, ectopic expression of CDK8 in KLE cells in endometrial cancer inhibits cell proliferation and effectively blocks tumor growth. In trans well, CDK8 overexpression in KLE cells inhibited cell migration and invasion. CDK8 deficiency increases lipid gene expression in endometrial cancer cells [36].

3.2. Small Molecule Drugs against Lipid Metabolism for Endometrial Cancer Therapy. Combined therapy with micronized estradiol and progesterone is a safe and effective conservative treatment for early-stage endometrial cancer (stage IA/G1) in patients with polycystic ovary syndrome who wish to preserve fertility. Simultaneous use of antidiabetic, antioxidant, antidopaminergic, and anti-serotonergic drugs helps restore female sex hormone concentrations and normal endometrium [37].

Silibinin reduces endometrial cancer cell growth, produces cell cycle arrest, and promotes cell death through reducing STAT3 phosphorylation expression. It may also control the expression of downstream genes engaged in cell cycle and death in EC cells, such as endogenous SREBP1, which reduces lipid buildup in EC cells [38].

Raloxifene, a selective estrogen receptor modulator, exerts estrogenic antagonism on bone and lipid metabolism, which helps to protect the endometrium and prevent endometrial cancer [39].

3.3. Other Targeted Therapies for Endometrial Cancer. Stearoyl-CoA desaturase 1 (SCD1) is a molecular target of many primary tumors. Studies have demonstrated that targeted knockdown of SCD1 can significantly inhibit endometrial cancer cell growth and induce cellular apoptosis *via* affecting the process of lipid metabolism. Targeted knockdown of short hairpin RNA and chemical inhibitors of SCD1 both inhibited foci formation in the metastatic endometrial cell line AN3CA. It can be seen that SCD1 is a potential therapeutic target for endometrial cancer and achieves the effect of anti-cancer therapy by inhibiting lipid metabolism in cancer cells [40].

4. Conclusion

The signaling pathways that regulate lipid metabolism in endometrial cancer include MAPK, JAK/STAT, NF-kB/Notch1, ERRα involved in lipid metabolism reprogramming, and other molecules including ATP citrate lyase (ACLY), monoacylglycerol lipase (MAGL), choline kinase alpha (CHKA), cyclin-dependent kinase 8 (CDK8), and so on. Specifically, adiponectin downregulated ERK1/2-MAPK signaling, decreased ERK1/2 phosphorylation in RL95-2 cells, and inhibited cell proliferation and migration. Leptin promotes cell proliferation and migration through the JAK/STAT pathway. Omentin activates the JAK signaling pathway to stimulate apoptosis. Vaspin inhibits cancer cell proliferation and chemotaxis by inhibiting NF-κB/Notch1 signaling pathway. HIF-1/ERR connection can accelerate tumor cell tolerance to hypoxia and improve metabolism, whereas TFEB-ERR axis-induced lipid reprogramming improves membrane fluidity and promotes cell invasion. Upregulation of ATP citrate lyase promotes cancer cell proliferation and colony formation, and increased monoacylglycerol lipase could increase cancer risk. Moreover, enhanced expression of choline kinase alpha (CHKA) promotes endometrial hyperplasia and deterioration.

In the treatment of lipid metabolism in endometrial cancer, micronized estradiol and progesterone are combined to treat early endometrial cancer (IA/G1 stage), and silibinin can effectively inhibit the proliferation of cancer cells by inhibiting the expression of STAT3 phosphorylation. Raloxifene also exerts estrogenic antagonism on bone and lipid metabolism and protects the endometrium. Based on the above studies, therapeutic targets can focus on targeting the knockdown of SCD1, ACLY axis, and MAGL. The underlying mechanism of occurrence and development of endometrial cancer is relatively clear, but further research is needed to illuminate more lipid metabolism-associated targets for future precise therapy.

Data Availability

The data used to support the findings of this study are included within the article.

Conflicts of Interest

The authors declare that they have no conflicts of interest.

Acknowledgments

References

[1] R. L. Siegel, K. D. Miller, H. E. Fuchs, and A. Jemal, "Cancer statistics," *CA: A Cancer Journal for Clinicians*, vol. 71, no. 1, pp. 7–33, 2021.

[2] F. Bray, J. Ferlay, I. Soerjomataram, R. L. Siegel, L. A. Torre, and A. Jemal, "Global cancer statistics 2018: GLOBOCAN estimates of incidence and mortality worldwide for 36 cancers in 185 countries," *CA: A Cancer Journal for Clinicians*, vol. 68, no. 6, pp. 394–424, 2018.

[3] P. Sun, Y. Shen, T. Wang et al., "Distinct clinical and genetic mutation characteristics in sporadic and Lynch syndrome-associated endometrial cancer in a Chinese population," *Cancer Epidemiology*, vol. 73, Article ID 101934, 2021.

[4] K. H. Lu and R. R. Broaddus, "Endometrial Cancer Endometrial cancer," *New England Journal of Medicine*, vol. 383, no. 21, pp. 2053–2064, 2020.

[5] M. E. Urick and D. W. Bell, "Clinical actionability of molecular targets in endometrial cancer," *Nature Reviews Cancer*, vol. 19, no. 9, pp. 510–521, 2019.

[6] R. Nitecki, T. Woodard, and J. A. Rauh-Hain, "Fertility-sparing treatment for early-stage cervical, ovarian, and endometrial malignancies," *Obstetrics & Gynecology*, vol. 136, no. 6, pp. 1157–1169, 2020.

[7] N. Colombo, C. Creutzberg, F. Amant et al., "ESMO-ESGO-ESTRO consensus conference on endometrial cancer: diagnosis, treatment and follow-up," *Annals of Oncology*, vol. 27, no. 1, pp. 16–41, 2016.

[8] L. A. Brinton, M. L. Berman, R. Mortel et al., "Reproductive, menstrual, and medical risk factors for endometrial cancer: results from a case-control study," *American Journal of Obstetrics and Gynecology*, vol. 167, no. 5, pp. 1317–1325, 1992.

[9] Collaborative Group on Epidemiological Studies on Endometrial Cancer, "Endometrial cancer and oral contraceptives: an individual participant meta-analysis of 27 276 women with endometrial cancer from 36 epidemiological studies," *The Lancet Oncology*, vol. 16, no. 9, pp. 1061–1070, 2015.

[10] P. Benedetti Panici, S. Basile, M. G. Salerno et al., "Secondary analyses from a randomized clinical trial: age as the key prognostic factor in endometrial carcinoma," *American Journal of Obstetrics and Gynecology*, vol. 210, no. 4, pp. 363.e1–363.e10, 2014.

[11] K. M. Doll, J. Tseng, S. A. Denslow, A. N. Fader, and P. A Gehrig, "High-grade endometrial cancer: revisiting the impact of tumor size and location on outcomes," *Gynecologic Oncology*, vol. 132, no. 1, pp. 44–49, 2014.

[12] J. V. Bokhman, "Two pathogenetic types of endometrial carcinoma," *Gynecologic Oncology*, vol. 15, no. 1, pp. 10–17, 1983.

[13] E. E. Calle and R. Kaaks, "Overweight, obesity and cancer: epidemiological evidence and proposed mechanisms," *Nature Reviews Cancer*, vol. 4, no. 8, pp. 579–591, 2004.

[14] K. Bhaskaran, I. Douglas, H. Forbes, I. dos-Santos-Silva, D. A. Leon, and L. Smeeth, "Body-mass index and risk of 22 specific cancers: a population-based cohort study of 5·24 million UK adults," *The Lancet*, vol. 384, no. 9945, pp. 755–765, 2014.

[15] A. G. Renehan, M. Tyson, M. Egger, R. F. Heller, and M. Zwahlen, "Body-mass index and incidence of cancer: a systematic review and meta-analysis of prospective observational studies," *The Lancet*, vol. 371, no. 9612, pp. 569–578, 2008.

[16] M. Dougan, "Prospective Study of Body Size throughout the Life-course and the Incidence of Endometrial Cancer Among Premenopausal and Postmenopausal Women," *International journal of cancer*, vol. 137, 2015.

[17] W. H. Xu, Y. B. Xiang, W. Zheng et al., "Weight history and risk of endometrial cancer among Chinese women," *International Journal of Epidemiology*, vol. 35, no. 1, pp. 159–166, 2006.

[18] C. Aubrey, K. Black, S. Campbell, and S. Pin, "Endometrial cancer and bariatric surgery: a scoping review," *Surgery for Obesity and Related Diseases*, vol. 15, no. 3, pp. 497–501, 2019.

[19] R. S. Arthur, G. C. Kabat, M. Y. Kim et al., "Metabolic syndrome and risk of endometrial cancer in postmenopausal women: a prospective study," *Cancer Causes & Control*, vol. 30, no. 4, pp. 355–363, 2019.

[20] X. Bian, R. Liu, Y. Meng, D. Xing, D. Xu, and Z. Lu, "Lipid metabolism and cancer," *Journal of Experimental Medicine*, vol. 218, no. 1, Article ID e20201606, 2021.

[21] R. Yaeger and R. B. Corcoran, "Targeting alterations in the RAF-MEK pathway," *Cancer Discovery*, vol. 9, no. 3, pp. 329–341, 2019.

[22] S. Parida, S. Siddharth, and D. Sharma, "Adiponectin, obesity, and cancer: clash of the bigwigs in health and disease," *International Journal of Molecular Sciences*, vol. 20, no. 10, p. 2519, 2019.

[23] L. Gelsomino, G. D. Naimo, S. Catalano, L. Mauro, and S. Ando, "The emerging role of adiponectin in female malignancies," *International Journal of Molecular Sciences*, vol. 20, no. 9, p. 2127, 2019.

[24] X. Gao, V. Balan, G. Tai, and A. Raz, "Galectin-3 induces cell migration via a calcium-sensitive MAPK/ERK1/2 pathway," *Oncotarget*, vol. 5, no. 8, pp. 2077–2084, 2014.

[25] K. Michalczyk, N. Niklas, M. Rychlicka, and A. Cymbaluk-Ploska, "The influence of biologically active substances secreted by the adipose tissue on endometrial cancer," *Diagnostics*, vol. 11, no. 3, p. 494, 2021.

[26] X. Hu, J. li, M. Fu, X. Zhao, and W. Wang, "The JAK/STAT signaling pathway: from bench to clinic," *Signal Transduction and Targeted Therapy*, vol. 6, no. 1, p. 402, 2021.

[27] S. Ghosh, D. Dutta, K. Pandit, P. Mukhopadhyay, and S. Chowdhury, "Leptin and cancer: pathogenesis and modulation," *Indian Journal of Endocrinology and Metabolism*, vol. 16, no. 9, pp. S596–S600, 2012.

[28] F. Ferrandino, P. Grazioli, D. Bellavia, A. F. Campese, I. Screpanti, and M. P. Felli, "Notch and NF-κB: coach and players of regulatory T-cell response in cancer," *Frontiers in Immunology*, vol. 9, p. 2165, 2018.

[29] H. Li, W. Peng, J. Zhuang et al., "Vaspin attenuates high glucose-induced vascular smooth muscle cells proliferation and chemokinesis by inhibiting the MAPK, PI3K/Akt, and NF-κB signaling pathways," *Atherosclerosis*, vol. 228, no. 1, pp. 61–68, 2013.

[30] L. Ma, Y. Tao, A. Duran et al., "Control of nutrient stress-induced metabolic reprogramming by PKCζ in tumorigenesis," *Cell*, vol. 152, no. 3, pp. 599–611, 2013.

[31] P. Su, L. Yu, X. Mao, and P. Sun, "Role of HIF-1α/ERRα in enhancing cancer cell metabolism and promoting resistance of endometrial cancer cells to pyroptosis," *Frontiers in Oncology*, vol. 12, Article ID 881252, 2022.

[32] X. Mao, H. Lei, T. Yi et al., "Lipid reprogramming induced by the TFEB-ERRα axis enhanced membrane fluidity to promote EC progression," *Journal of Experimental & Clinical Cancer Research*, vol. 41, no. 1, p. 28, 2022.

[33] M. Dai, B. Yang, J. Chen et al., "Nuclear-translocation of ACLY induced by obesity-related factors enhances

pyrimidine metabolism through regulating histone acetylation in endometrial cancer," *Cancer Letters*, vol. 513, pp. 36–49, 2021.

[34] X. Li, S. Gao, W. Li et al., "Effect of monoacylglycerol lipase on the tumor growth in endometrial cancer," *Journal of Obstetrics and Gynaecology Research*, vol. 45, no. 10, pp. 2043–2054, 2019.

[35] S. Trousil, P. Lee, D. J. Pinato et al., "Alterations of choline phospholipid metabolism in endometrial cancer are caused by choline kinase alpha overexpression and a hyperactivated deacylation pathway," *Cancer Research*, vol. 74, no. 23, pp. 6867–6877, 2014.

[36] W. Gu, C. Wang, W. Li et al., "Tumor-suppressive effects of CDK8 in endometrial cancer cells," *Cell Cycle*, vol. 12, no. 6, pp. 987–999, 2013.

[37] S. Stanosz, J. von Mach-Szczypinski, K. Sieja, and J. Koociuszkiewicz, "Micronized estradiol and progesterone therapy in primary, preinvasive endometrial cancer (1A/G1) in young women with polycystic ovarian syndrome," *Journal of Clinical Endocrinology and Metabolism*, vol. 99, no. 12, pp. E2472–E2476, 2014.

[38] Z. Shi, Q. Zhou, S. Gao et al., "Silibinin inhibits endometrial carcinoma via blocking pathways of STAT3 activation and SREBP1-mediated lipid accumulation," *Life Sciences*, vol. 217, pp. 70–80, 2019.

[39] S. Gizzo, C. Saccardi, T. S. Patrelli et al., "Update on raloxifene: mechanism of action, clinical efficacy, adverse effects, and contraindications," *Obstetrical & Gynecological Survey*, vol. 68, no. 6, pp. 467–481, 2013.

[40] W. Li, H. Bai, S. Liu et al., "Targeting stearoyl-CoA desaturase 1 to repress endometrial cancer progression," *Oncotarget*, vol. 9, no. 15, pp. 12064–12078, 2018.